Pre-clinical Changes During Scrapie Disease Progression in Hamsters, Detected by Magnetic Resonance Imaging.

By

Richard Stephen Baydack

A Thesis submitted to the Faculty of Graduate Studies of

The University of Manitoba

In partial fulfillment of the requirements of the degree of

PhD of Science

Department of Medical Microbiology and Infectious Disease

University of Manitoba

Winnipeg

Acknowledgements

During the course of my studies, I have received support and instruction from numerous people. I would first like to thank my Advisor, Tim Booth, for his guidance, instruction, advice and support. I would also like to thank the other members of my examining committee, past and present: Kevin Coombs; Gary Glavin; David Westaway; Mike Jackson; and Marco Gruwel. One other individual in particular has contributed significantly towards my technical training, especially relating to histological techniques: Cathy Robertson. I would also like to thank past and present members of the Biosystems group at NRC-IBD, in particular Eilean McKenzie, Janie Dubois, Eric Pellerin, Janice Baranoski, Stephen Szczerba, Crystal Fulton, Elda Bravo Grimaldo, and Darren Manley. Other NRC-IBD employees who have contributed to this work include John Rendell, Slava Volotovskyy', and Earle Edie (technical aspects of MRI projects, including coil and animal holder development). I would also like to thank the animal care workers at both NRC-IBD and at NML for their contributions.

I would like to thank the University of Manitoba, and the Department of Medical Microbiology and Infectious Disease for providing me with the opportunity to undertake my studies, and for providing a stimulating learning environment. I would also like to thank the TSE Resource Centre, Institute for Animal Health, and Norton Healthcare for providing the PPS free of charge, and for providing the infectious agent.

I would like to express my appreciation for financial support that I have received, including: University of Manitoba Graduate Fellowship; Department of

Medical Microbiology Allan Ronald Scholarship; and financial support from Ian C. P. Smith, and from Tim Booth.

Finally I would like to thank my parents, Len and Luise; my sisters, Natalie and Karina; and my wife, Lydia for their support throughout my studies.

Abstract

Transmissible spongiform encephalopathies (TSEs), or prion diseases, are a group of invariably fatal neurodegenerative diseases of both humans and animals, thought to be caused by the abnormally folded prion protein PrP^{Sc}. Prion disease research continues to be faced by a number of difficult challenges. First, the unequivocal diagnosis of most prion diseases currently requires the post-mortem collection of central nervous system tissue, either for histological examination or Western blot analysis; second, a viable treatment for clinical stage disease has not yet been identified; third, the exact details of disease pathogenesis have not been elucidated; and fourth, the normal function of PrP^{C} is not definitively known.

The primary objective of the studies presented here was to diagnose prion disease in live animals, using Magnetic Resonance Imaging (MRI). Increases in T_2 relaxation time and apparent diffusion coefficient (ADC) were observed very early following the infection of Syrian golden hamsters with the 263K strain of scrapie. These changes were evident well before the appearance of either clinical symptoms or the typical histological changes characteristic of prion disease, suggesting that they are the result of the progressive accumulation of fluid, and that this may constitute a novel early marker of prion disease pathogenesis. Following the establishment of this model system, a secondary objective was composed: to test the viability of a potential treatment (pentosan polysulphate) using a number of different treatment regimens. It was determined that pentosan polysulphate (PPS) was ineffective as a treatment unless it was

administered intra-cerebrally very early in infection, although it was shown to slow the appearance of the histological hallmarks of prion disease. In response to the results of these studies, a potential model was proposed, relating PrP, aquaporin-4 (AQP4) regulation, and oedema. Although speculative, this model may have implications for both normal PrP^{C} function and disease pathogenesis.

Table of Contents

List of Tables

List of Figures

List of Copyrighted Material for which Permission was Obtained

- Figure 16 B: Reprinted from: Journal of Comparative Pathology, Volume 78 Issue 3, Fraser H, Dickinson AG, “The sequential development of the brain lesions of scrapie in three strains of mice”, pages 301-311, Copyright 1968, with permission from Elsevier.

1. Introduction

Transmissible spongiform encephalopathies (TSEs), or prion diseases, are a group of invariably fatal neurodegenerative diseases of both humans and animals. It is now widely accepted that prion diseases are caused, in whole or in part, by an abnormally-folded form of the normal cellular protein PrP [1]. The normal form of this protein, known as PrP^{C} (for Prion Protein, Cellular), undergoes a conformational change during which it acquires a significant amount of β-sheet [2,3], producing the pathological form, PrP^{Sc} (for Prion Protein, Scrapie), which is partially protease resistant and insoluble [2,4]. Prion diseases exist in genetic, sporadic, and acquired forms, all of which are transmissible [5]. The most common human prion disease is Creutzfeld-Jakob Disease (CJD), the variant form (vCJD) of which is likely acquired through ingestion of beef from Bovine Spongiform Encephalopathy (BSE) infected cattle [1,6,7]. Other important prion diseases include scrapie of sheep and goats, and Chronic Wasting Disease (CWD) of deer and elk in North America. Prion diseases are characterized by the deposition of PrP^{Sc}, the appearance of vacuoles, and gliosis in the brain [5]. Different strains can be distinguished by the distributions of these histological markers in a given host. However, the unequivocal diagnosis of most prion diseases requires the post-mortem collection of central nervous system tissue, either for histological examination or Western blot analysis.

Although much progress has been made since the identification of the prion protein in the early 1980's, a number of aspects of prion disease remain unresolved. First, with the notable exception of vCJD, which can be diagnosed

with some success by detection of PrP^{Sc} in tonsil tissue [8], there is no method of unequivocal diagnosis in live subjects. Second, a viable treatment for clinical stage disease has not yet been identified, although some treatments have at least prolonged survival time, usually through treatment before the appearance of clinical symptoms. Third, the exact details of disease pathogenesis have not been elucidated. The precise mechanism of conversion of PrP^{C} to PrP^{Sc} has not been described; and more importantly, it is not yet clear whether disease results from a loss of function of PrP^{C}, a gain of (pathological) function on the part of PrP^{Sc}, the response of the immune system to the presence of PrP^{Sc}, or some combination of all of these. Fourth, the normal function of PrP^{C} is not definitively known, although evidence exists for a number of different functions, and PrP^{C} is highly conserved evolutionarily, indicating its importance.

The primary objective of the studies presented here was to diagnose prion disease in live animals, using Magnetic Resonance Imaging (MRI). For the first time to my knowledge, increases in T_2 relaxation time and apparent diffusion coefficient (ADC) were observed very early following the infection of Syrian golden hamsters with the 263K strain of scrapie. These changes were evident well before the appearance of either clinical symptoms or the typical histological changes characteristic of prion disease, suggesting that they are the result of the progressive accumulation of fluid, and that this may constitute a novel early marker of prion disease pathogenesis. Following the establishment of this model system, a secondary objective was composed: to test the viability of a potential treatment (pentosan polysulphate) using a number of different treatment

regimens. My research, described in this thesis, has shown that pentosan polysulphate (PPS) was ineffective as a treatment unless it was administered intra-cerebrally very early in infection, although it was shown to slow the appearance of the histological hallmarks of prion disease. In response to the results of these studies, a potential model was proposed, relating PrP, aquaporin-4 (AQP4) regulation, and oedema. Although speculative, this model may have implications for normal PrP^{C} function and could explain, at least in part, the disease pathogenesis.

1.1 Prion Disease – An Historical Perspective

1.1.1 From Recognition of a Group of Diseases to Discovery of the Prion Protein

In the early 1950's, TSEs had not yet been recognized as a group of diseases or been associated with a causative agent. CJD and scrapie were being studied entirely independently, and Kuru had not yet been identified. Within this context, Bjorn Sigurdsson described a disease of sheep known in Iceland as rida during a series of Special University Lectures given in the University of London in 1954 [9]. There were marked similarities between the disease he described and scrapie in England (indeed, they would later be found to be one and the same). In his lecture, Sigurdsson reported the experimental transmission of rida to sheep by intra-cerebral injection of brain material from diseased animals, and suggested that the disease was caused by infection with what he termed a "slow virus" [9]. By the end of the decade, English scrapie had been experimentally transmitted to sheep [10,11] and goats [12]; the first reports

of Kuru had surfaced [13,14]; and it had been suggested that Kuru was a similar disease to scrapie [15], and to CJD [16].

While their clinical and pathological similarities caused scrapie, Kuru, CJD and Transmissible Mink Encephalopathy (TME) to be considered together, investigators studying the different diseases had different ideas as to their cause. Possibilities considered for any or all of these diseases included the so-called slow virus; viroids; genetic causes; infectious lipids or carbohydrates; or toxins. The transmission of rida [9] and scrapie [10–12] by injection of brain material; the inability to discern a pattern of inheritance in Kuru; the transmission of Kuru to chimpanzees [17]; and the discovery that it was transmitted through ritualistic cannibalism led many researchers to lean towards the slow virus theory as the cause of these diseases. This opinion persisted despite evidence of the extraordinary resistance of the agents responsible for scrapie [18–20] and CJD and Kuru [21] to ultraviolet and ionizing radiation, which would be expected to destroy any nucleic acid component. Although the possibility that the infectious agent responsible for TSEs could be a protein and devoid of nucleic acid was first raised in the 1960s [22,23], it was only after the discovery that a protein was required for infectivity (and that nucleic acid was not) [24] that this theory was given any real credence. The evidence provided in this study indicated that scrapie infectivity was resistant to five processes that modify nucleic acids, while it was partially sensitive to protease digestion [24]. This data allowed a number of hypotheses regarding the nature of the infectious agent to be eliminated, including: viroids; lipids; carbohydrates; and toxins [24]. At the same time, the

term “prion” was coined to refer to a small proteinaceous infectious particle [24]. Soon afterwards, the prion protein isoform known as PrP27-30 was discovered and found to correlate with infectivity [25,26]. Further studies indicated that PrP27-30 was the protease-resistant core of PrP^{Sc} [27,28]; that it is formed through the NH_2-terminal truncation of PrP^{Sc} [4,27–30]; that PrP^{C} is the normal cellular, protease-sensitive form of PrP^{Sc}/PrP27-30 [4,29]; and that conversion of PrP^{C} to PrP^{Sc} involves the conversion of a significant proportion of the α-helical structure of the protein to β-sheet [2].

1.1.2 Infectious Protein or Slow Virus

Despite significant evidence indicating that the causative agent responsible for TSEs was composed entirely of an abnormally folded, infectious form of a normal cellular protein, this concept remained difficult to accept for many researchers. There were a number of reasons why the so-called “Protein Only Hypothesis” [5,22] was difficult to accept, but most revolve around the fact that it was highly heretical when compared to the central dogma of biology, that genetic information is encoded in DNA, which is transcribed to RNA, which in turn is translated into protein. Despite many examples of viruses with RNA genomes, and the existence of reverse transcriptase, these examples at least maintain that genetic information is encoded in nucleic acid; the idea that a protein can seemingly occupy this role was too much for many to accept. Two aspects of the prion hypothesis were particularly difficult to reconcile. First was the observation that PrP^{C} and PrP^{Sc} had identical amino acid sequences [5], and yet had two very different conformations [2,3], while one of them caused disease

and the other was a normal cellular protein. Second was the existence of different strains of scrapie, which were taken as strong evidence against prions [31,32]. Since the prion hypothesis requires that host PrP^{C} be converted to PrP^{Sc}, it would seem to follow that the "strain" would depend only on the amino acid sequence of the host. However, infection of the same host (e.g. a specific mouse strain) with different scrapie strains results in infection with different characteristics [6,33], that is, the integrity of the infecting strain is maintained. Since these arguments hinge largely on the manner in which strains of TSE are determined, it is worth examining this issue more closely.

Prion strains were initially recognized according to differences in clinical signs, incubation period, and lesion profile, or the distribution of spongiform change in the brain [34–36]. Other characteristics that are now commonly used to differentiate between strains include the electrophoretic mobility of PrP^{Sc} following proteinase K (PK) digestion [7,37,38]; the glycosylation pattern of PrP^{Sc} [7,38,39]; and histological changes [40–43]. Finally, strain specificity has been observed with respect to the following: the extent of resistance to PK digestion, and sedimentation properties of PrP^{Sc} [37]; copper binding affinity [44]; and resistance to denaturation by chaotropic agents [45]. Opponents of the prion theory insist that the only possible explanation for the existence of prion strains is the existence of an as yet unidentified associated genome [46], although there is no evidence for this [47]. Proponents of the prion theory, on the other hand argue that differences between prion strains are determined by alternative conformations of PrP^{Sc} that are capable of propagating themselves [48–52].

Evidence for this argument consists of the identification of strain specific differences in PrP^{Sc} conformation, identified by a number of methods, including Fourier Transform infrared (FTIR) spectroscopy [45,53,54]; conformation-dependent immunoassays [45,55,56]; and atomic force microscopy [57]. Furthermore, different PrP^{Sc} conformations have been shown to have different properties such as their heat stability [45,55]. Despite a number of lines of evidence supporting the theory that prion strains are determined by differences in conformation, this cannot yet be concluded definitively [58].

In fact, another characteristic of prion diseases, the so-called species barrier, may provide indirect evidence that strain specificity is not enciphered in the conformation of individual PrP^{Sc} molecules after all. When infectious material from one species, e.g. a sheep, is used to infect another species, typically a mouse, disease usually results only after a very long incubation period, and in some cases no disease ever develops. If infectious material from that mouse is then used to infect another mouse, the incubation period is greatly reduced, and remains constant upon further passages. The initial, very long incubation period is known as the species barrier, and has been proposed to be dependent on similarities in amino acid sequence between the infecting and host PrP molecules [5]. However, when bank voles were injected with sporadic and genetic strains of CJD, no species barrier was evident, despite little homology between prion protein genes of humans and voles, and despite the existence of a species barrier when voles were infected with prions from sheep, mice, and hamsters [59]. An alternative to PrP sequence similarities as a basis for the

species barrier may be the prevalence of different glycoforms of PrP. During post-translational modifications, PrP^{C} undergoes glycosylation, which can result in mono-, di-, or unglycosylated PrP molecules. It has been shown that different glycoforms of PrP^{Sc}, but not PrP^{C}, co-immunoprecipitate [39], and that the most infectious form of PrP^{Sc} has a mass that is equivalent to between fourteen and twenty-eight PrP molecules [60]. It has also been argued that the structure of PrP seeds may be determined by the relative prevalence of different glycoforms [61]. Taken together, these data support the possibility that prion strains may be dependent on the ratios of different PrP^{Sc} glycoforms that associate in a complex [47].

Although experimental evidence supports at least two different possible mechanisms by which prion strains may be determined by the conformation either of individual PrP^{Sc} molecules or PrP^{Sc} complexes, neither of these mechanisms has been proven definitively. Despite the absence of evidence for the existence of a nucleic acid genome associated with TSEs [5,47], opponents of the “Protein-Only Hypothesis” [5,22] have come up with colourful explanations for this lack of evidence. Among these were suggestions that a TSE-associated virus may incorporate a PrP^{Sc}-like protein, or PrP^{Sc} itself into its structure, or that PrP may be a cell-surface receptor for said virus. Although small virus-like particles have recently been reported in scrapie- and CJD-infected cell cultures [62], these reports have not been duplicated or extended to animal studies, and there have been countless descriptions of natural and experimental TSEs that found no evidence of similar particles. The argument for a viral cause of TSEs

has been adapted in a number of ways to explain particular pieces of experimental evidence. However, there is no single viral hypothesis that can explain all of the results that can be explained by PrP^{Sc} as the causative agent for TSEs [5].

With this in mind, it is useful to consider all of the evidence in support of the prion hypothesis together. Among the lines of evidence that have already been discussed are the resistance of infectivity to UV and ionizing radiation [18–21]; the inability to identify a nucleic acid or other macromolecule that associates with infectivity [5]; the inability to isolate or identify disease-associated viral particles, with the recent exception of virus-like particles in cell cultures infected with scrapie or CJD [62]; the co-purification of PrP^{Sc} with infectivity [25,26], and evidence that PrP27-30 and infectivity have similar properties with respect to inactivation [63–67]; the potential to explain the existence of the species barrier, as a result of sequence non-homology between host and infecting PrP molecules [5]; and the potential to explain the existence of strains, either as a result of conformational differences in PrP^{Sc} molecules [45,48,49,53,54,56,57], or as a result of differences in glycoform ratios in PrP^{Sc} complexes or seeds [47,61]. A number of other lines of evidence also support prions as the causative agent of TSEs. First, mutations in the Prnp gene result in the formation of PrP^{Sc} and in disease. In a related matter, the prion hypothesis satisfies an important requirement: it explains how TSEs can have both genetic and infectious causes [5]. Finally, two pieces of evidence regarding genetically modified mice support PrP^{Sc} as the cause of disease: when PrP^{C} is over-expressed in Tg mice, it

results in more extensive formation of PrP^{Sc} and shortening of the incubation period [68]; and mice lacking the Prnp gene are immune to infection with prion disease and to replication of prions [69–73]. After many years of controversy, perhaps the final hurdle for the prion hypothesis to gain full acceptance is the *de novo* creation of infectivity *in vitro*. This result was approached with the development of a method to convert PrP^{C} to PrP^{Sc} by cyclic amplification of protein misfolding [74]. The resulting PrP^{Sc} was biochemically similar to PrP^{Sc} derived from infected brains, and produced disease when injected into hamsters [74], however other cellular components were present as well, failing to eliminate the possibility that such a component could be part of the infectious agent. This is perhaps not surprising, and the role of cellular components in the process of conformational change producing PrP^{Sc} will be discussed below. Even in view of a body of very convincing data, some researchers continue to distrust the prion hypothesis [62], indicating that it may never be fully accepted.

1.2 The Prion Protein

1.2.1 Structure

PrP^{C} can be divided into two parts: the unstructured, flexible amino-terminal tail; and the carboxy-terminal end, which contains regions of secondary structure, including three α-helices [75,76], a loop that is flexible in most species [75], but rigid in elk and deer [77], and two short strands of anti-parallel β-sheet that flank the first α-helix [78]. Beginning with the amino-terminal end of the protein, there is a short signal peptide that is removed by signal peptidase in the endoplasmic reticulum [76]. Downstream of this are two highly conserved

regions: a region that has been proposed to bind copper [79], consisting of five octapeptide repeats [78]; and a domain that has been called the “hydrophobic core” [75]; these two domains are separated by a hydrophilic domain known as the charge cluster, the carboxy-terminal end of which is also the boundary of the PK-resistant fragment of PrP^{Sc} [75]. The carboxy-terminal end of the protein is home to the regions of secondary structure, as mentioned above. In addition to the α-helices, β-sheets, and loop structure, it also contains a disulfide bridge, between cysteine residues 179 and 214, which stabilizes α-helices two and three [80]. Following cleavage of the carboxy-terminal membrane attachment domain, a glycosyl phosphatidyl inositol (GPI) anchor is added, which allows PrP^{C} to attach to the external side of the plasma membrane [81,82].

The carboxy-terminal end of PrP^{C} also has two glycosylation sites, at asparagine residues 181 and 197 [75,76]. Although di-glycosylated forms of PrP^{C} are most common in all species, un- and mono-glycosylated forms are also observed [83]. While all glycoforms of PrP^{C} can be converted to PrP^{Sc}, there is variation in the ratio of glycotypes between prion strains [83]. In vitro studies of glycosylation mutants in which glycosylation is prevented at one or both sites have indicated that mutant PrP^{C} localizes intracellularly rather than at the cell surface [84], and that glycosylation is not required for PrP^{Sc} formation [85]. A number of research groups have also developed transgenic mice that express glycosylation mutants in which glycosylation at one or both sites is prevented [83,86–89]. Results of infection of these mice with different prion strains proved variable. One group reported that mice expressing only unglycosylated PrP were

resistant to two different prion strains [88], while another found that both monoglycosylated mutants were susceptible to two strains of scrapie as well as BSE [89]. The third group found that while mutants expressing only unglycosylated PrP^C produced PrP^C that was primarily localized intracellularly, this did not result in spontaneous formation of PrP^{Sc} [86]. Furthermore, when all three mutant lines were infected with two different scrapie strains, susceptibility was dependent on both the infecting scrapie strain and on the glycosylation status of the mice, but glycosylation of host PrP^C was not an absolute requirement for disease susceptibility or for transmission of infectivity [87].

1.2.2 Normal Localization and Cycling of PrP^C

On the cell surface, PrP^C can be found mostly in lipid rafts [90–92], although at least some PrP^C is constitutively found on the plasma membrane outside of lipid rafts [76]. It makes sense that PrP^C should be found in lipid rafts when it is on the cell surface, since it has three distinct raft-localization signals: its GPI anchor; a raft-localization signal in the first 28 amino acid residues of the amino-terminus [93,94]; and the disulfide loop between residues 179 and 214, which has the binding properties of a sphingolipid binding domain [95], a major component of lipid rafts. It has been shown that PrP^C molecules leave lipid rafts every few minutes; are endocytosed via clathrin-coated pits; and wind up inside recycling endosomes [96]. The amino-terminus of PrP^C is both necessary and sufficient for endocytosis via clathrin-coated pits [96–98], and has also been identified as a binding site for heparan sulphate and glycosaminoglycans (GAGs) [99,100], which suggests that endocytosis may involve heparan sulphates [95].

Heparan sulphates commonly act as co-receptors for the low density lipoprotein (LDL) receptor-related protein (LRP1), which is constitutively endocytosed [95]. Very recent findings indicate that PrP^C associates with LRP1 during endocytosis, and that this association is required for endocytosis to occur [101,102]. Furthermore, it appears as though LRP1 may also be responsible for trafficking of PrP^C to the cell surface following synthesis [101]. Taken together these results indicate a cycle, summarized largely in [95], consisting of the following steps: unbound PrP^C on the cell surface exists mainly in lipid rafts. PrP^C leaves the rafts in association with LRP1 and possibly a heparan sulphate. This complex is then endocytosed in clathrin-coated pits, and trafficked through sorting endosomes into a recycling endosome, which returns PrP^C to lipid rafts on the cell surface, where the cycle begins anew.

1.2.3 Conversion of PrP^C to PrP^{Sc}

The mechanism by which PrP^C undergoes a conformational change to produce PrP^{Sc} remains unclear. Two theories were proposed in the 1990s to explain this conversion: the template-assisted model [103,104], and the nucleation-polymerization model [105,106]. More recently, a third theory has been proposed, the nucleated-assisted model [76]. The template-assisted model may be summarized as follows [103,104]: PrP^C is capable of taking on an intermediate conformation, PrP*, which may be partially unfolded. While in this alternative conformation, the PrP* molecule binds to some host conversion factor; this has been called Protein X [107], but it is possible that this role could be played by a species other than a protein. Association with Protein X is

proposed to be necessary for PrP* to be bound by a molecule of PrP^{Sc}. PrP^{Sc} then acts as a template to refold PrP*, forming a second molecule of PrP^{Sc}. In comparison, the nucleation-polymerization model [105,106] requires neither an intermediate form of PrP, nor a Protein X or other host factor. Rather, it suggests that PrP^{C} and PrP^{Sc} exist always in equilibrium. However, monomers of PrP^{Sc} are unstable, and require polymerization to become stable. As such, the initial formation of stable PrP^{Sc} requires a number of PrP^{Sc} molecules to become associated and oligomerize. Once a PrP^{Sc} oligomer has been formed, it can recruit PrP^{Sc} monomers and stabilize them, shifting the equilibrium towards the formation of PrP^{Sc}.

In considering these two models of conversion, two clear distinctions can be made: the template-assisted model requires some kind of host factor (such as Protein X), while the nucleation-polymerization model does not; and the nucleation-polymerization model requires PrP^{Sc} aggregates, while the template-assisted model does not [108]. Beginning with the first difference, if no host factor is required for conversion, then it should be possible to replicate PrP^{Sc} in the absence of other biological components. However, to date, even those procedures that have come closest to this, amplifying both PrP^{Sc} [109,110] and infectivity [74], have done so from brain homogenate, indicating that other molecules may be required for conversion [108]. A number of other studies have also provided evidence of a requirement of some kind of cofactor [107,111,112]. On the other hand, the template-assisted model assumes that monomers of PrP^{Sc} represent the infectious form, and that PrP^{Sc} aggregates are not required.

Recent data, however, have revealed that oligomers of fewer than six PrP^{Sc} molecules were non-infectious in hamsters, and oligomers with mass equivalent to between fourteen and twenty-eight PrP^{Sc} molecules corresponded to the most infectious form [60].

In response to the body of data, which refutes aspects of each of the above models, Abid and Soto recently suggested a third theory, which they termed the nucleated-assisted model [76]. This model combines aspects of each of the earlier theories in an attempt to satisfy the available body of evidence, and may be summarized as follows: similarly to the template-assisted model, it requires both an intermediate, partially unfolded conformation PrP* and some host conversion factor, but it states that PrP^{Sc} never exists as a monomer. The first step in the process involves association of PrP* with the conversion factor. In this state, molecules of PrP*, bound to the conversion factor, can associate; if, and only if, some minimum number of PrP* molecules associate in this manner, they can form an intermolecular β-sheet, which corresponds to PrP^{Sc}. The resulting PrP^{Sc} oligomer would then be capable of recruiting further molecules of PrP*, as well as acting as an infectious molecule.

At present none of the above models have been proven, and the mechanism by which PrP^{C} is converted to PrP^{Sc} is unresolved. Clearly, this remains one of the most pressing issues in prion research. Besides the mechanism of conversion, the site of conversion also remains unknown. In order to narrow down the possible sites of initial contact between PrP^{C} and PrP^{Sc}, it is worth revisiting some aspects of PrP^{C} cycling. Since PrP^{C} is endocytosed

through clathrin-coated pits and transported to recycling endosomes [96], and PrP^{Sc} is transported to lysosomes following endocytosis [95], it is unlikely that these two molecules would come into contact inside the cell unless they were endocytosed within the same clathrin-coated pit. If PrP^{C} and PrP^{Sc} are endocytosed within the same clathrin-coated pit, then they likely would come into contact at the cell surface. If this is the case, then initial contact could occur either inside lipid rafts, or outside of them. A number of lines of evidence indicate that lipid rafts may be protective of PrP^{C}: GPI-anchored PrP^{C} has been shown to be resistant to conversion [113]; when recombinant PrP is anchored to a lipid bilayer through a GPI anchor, it adopts the PrP^{C} conformation [114,115]; in a scrapie model, inhibition of sphingomyelin [116] or cholesterol [117,118] production (which would each result in depletion of lipid rafts) increased scrapie infectivity [116] and the amount of misfolded PrP in the endoplasmic reticulum [117,118]. PrP^{Sc} has also been observed to float at a higher density than PrP^{C} in detergent resistant membranes (DRMs) produced from cell culture or brain tissue [91,119]. This may provide a mechanism for a potential protective effect of lipid rafts, by sequestration of PrP^{C} and PrP^{Sc} from each other [95]. Taken together, these data suggest the cell surface, outside of lipid rafts as the most likely site of initial contact between PrP^{C} and PrP^{Sc}.

1.2.4 Function of PrP^{C}

PrP^{C} is highly conserved evolutionarily [120], indicating that it probably has an important function. However, despite the identification in 1986 of the *Prnp* gene that encodes PrP^{C} [28], and the creation of the first PrP knockout

mice in 1992 [121], pinning down the critical function of PrP^C has proven elusive. In fact, PrP-null mice have shown no major developmental or cognitive problems, or neurodegeneration [121,122], even when gene knockout is executed post-natally [123]. Having said that, evidence exists for a wide range of functions of PrP^C, including roles in signal transduction, copper binding, cell adhesion, and various protective effects. Protective effects of PrP^C include protection/rescue of cultured cells from apoptosis induced by Bax [124,125]; serum deprivation [126,127]; and Doppel (Dpl) [128,129]. PrP^C may also protect against oxidative stress, since cell cultures derived from PrP-null mice are more susceptible than cells expressing PrP to oxidative stress [130,131], and brain tissue from PrP-null mice display biochemical changes that are indicative of oxidative stress [132]. There is also evidence that PrP^C inhibits the phagocytic activity of macrophages, indicating that it may limit the inflammatory response to damaged or apoptotic cells, which would be of particular importance in the brain [133]. A number of studies have shown that PrP^C binds copper [134–137], indicating that PrP^C may be a receptor for the cellular uptake or efflux of copper [138]. PrP^C has also been shown to be involved in cell signalling through a number of pathways, including fyn [139–141]; STI-1 [142–144]; p38 MAPK [145]; and PKC, PKA, PI-3 kinase/Akt, and ERK [140,141]. PrP^C may be involved in cell adhesion, since it binds neural cell adhesion molecule (N-CAM) [146] and laminin [147]. Finally, PrP^C may play a role at the synapse, since it has been shown to be involved in the elaboration of axons and dendrites, and it increases synaptic contacts [140].

While the above list is not exhaustive, it nonetheless provides an indication of the many possible functions of PrP^{C}.

1.3 Prion Disease Pathogenesis

The pathogenesis of prion diseases may be broken down into three steps: infection and replication in the periphery; neuroinvasion; and neurodegeneration. Depending on the route of infection, not all of these steps are required. For example, following intra-cerebral infection of experimental animals, the agent is already in the brain and need only to replicate and initiate neurodegeneration.

1.3.1 Infection and Replication of Prions in the Periphery

In describing prion infection and replication of prions outside the central nervous system, the first consideration is the portal of entry into the body. Replication in the periphery is irrelevant to disease pathogenesis when the infectious agent is introduced directly into the central nervous system. This occurs in a number of categories of prion disease, including intra-cerebral infection of experimental animals; iatrogenic infection through dura mater transplant; and presumably in familial and sporadic forms of prion disease when the initial appearance of PrP^{Sc} occurs in the brain. Categories of prion disease that involve entry through the periphery, and therefore require significant replication in the periphery include intra-peritoneal infection of experimental animals; oral infection, including in BSE and vCJD; infection through blood transfusion; and iatrogenic infection resulting from administration of human growth hormone, or through the use of improperly sterilised surgical equipment.

Most peripherally acquired prion diseases require replication in the lymphoreticular system before neuroinvasion can occur [75,148]. A number of lines of evidence indicate that follicular dendritic cells (FDCs) represent the critical cell type for PrP^{Sc} replication in the periphery. FDCs have been shown to accumulate PrP^{Sc} following peripheral infection [149], and dedifferentiation or inactivation of FDCs delays neuroinvasion and reduces susceptibility to peripheral prion infection [150–153]. B-cells are also critical for peripheral spread of prions and neuroinvasion [154,155], but neuroinvasion can occur in the absence of PrP^{C} expression on B-cells [154,156,157]. Prevention of B-cell signalling has also been shown to prevent the maturation of FDCs and inhibits prion replication in the periphery and neuroinvasion [151,158]. Taken together, these data indicate that the requirement of B-cells for neuroinvasion is based on the requirement of B-cell signalling for the formation of mature FDCs. The complement system may be involved in early prion spread and replication, since the absence of some complement components and complement receptors inhibits the accumulation of PrP^{Sc} in the spleen [158,159]. Complement components and receptors are required by FDCs in order to retain immune complexes [160], providing a potential mechanism for the requirement of complement for efficient spread and replication of PrP^{Sc} [148].

If FDCs are the critical cell type for prion replication and neuroinvasion, then transportation of PrP^{Sc} from its portal of entry to FDCs is also critical. When PrP-null mice received wild type bone marrow and were infected with scrapie, there was no neuroinvasion [156], but PrP^{Sc} accumulated in the spleen

[156,161]. These data have been interpreted as an indication that haematopoietic cells transport PrP^{Sc} from its portal of entry to FDCs [162]. Two possible cell types that may be considered for this role are macrophages and dendritic cells (DCs). Some experimental results indicate that macrophages may be involved in clearance of prion infection [163,164]. DCs are responsible for sampling antigens and transporting them to lymphoid tissues [165]. Although antigens presented by DCs may be degraded, some DCs have been shown to retain PrP^{Sc} in its native state during transportation [166,167]. Despite these data, the role of DCs in transportation of PrP^{Sc} to FDCs is not yet conclusive [148]. Even if DCs are responsible for transportation of PrP^{Sc} to FDCs, the mechanism of transfer between cells remains unclear, although it may involve exosomes containing PrP^{Sc} [148].

Prion infection by the oral route represents a special case with respect to pathogenesis, since the infectious agent must somehow move out of the digestive system. A number of studies have found that following oral infection, prion infectivity accumulates in the intestines very early [150,168–171]; in orally infected hamsters, early prion accumulation occurs in the gut-associated lymphoid tissue [172]. In order to be accessed by DCs, or other cells responsible for transport to FDCs, PrP^{Sc} must cross the intestinal epithelium. One study has suggested that this may be accomplished by translocation through M cells [173], although it is also possible that DCs directly acquire PrP^{Sc} by extending their dendrites into the intestinal lumen [148]. Another special case of prion disease pathogenesis involves infection through transfusion with infected blood. This

route of infection has resulted in at least three cases of vCJD [174–176], but the details of pathogenesis, including the blood-borne cells that act as PrP^{Sc} carriers are currently unknown [75].

1.3.2 Neuroinvasion

Following replication in FDCs, PrP^{Sc} is thought to invade the peripheral nervous system, and move to the brain either via the spinal cord or by bypassing the spinal cord altogether. The first step in this process involves translocation of PrP^{Sc} from FDCs to peripheral nerves. The mechanism by which this occurs remains unclear, but the speed of neuroinvasion is affected by the distance between FDCs and splenic nerves [177]. Once inside the nerves, PrP^{Sc} is thought to be transported to the CNS via the autonomic nervous system [178–180]. It has been suggested that innervation of the secondary lymphoid organs represents the rate-limiting step in neuroinvasion, since sympathectomy delays or even prevents scrapie, and hyper-innervation enhances neuroinvasion and reduces incubation time [181]. A number of studies have described the sequential passage of PrP^{Sc} along the spinal cord following peripheral infection [182–184]. However, it appears as though in at least some models, PrP^{Sc} can reach the brain through an alternative pathway that bypasses the spinal cord [182,183,185].

1.3.3 Neurodegeneration

Once PrP^{Sc} arrives in the brain, the resulting pathology has been well documented, and includes deposition of PrP^{Sc}; spongiform change; gliosis, and neuronal loss. However, the reason for the initiation of neurodegeneration

remains unclear. In general terms, potential reasons for neurodegeneration include a toxic function of PrP^{Sc}; a loss of function of PrP^{C}; or modulation of function of PrP^{C}. Although this subject remains one of the major unknown areas of prion research, many hypotheses have been put forward to explain the observed neurodegeneration. Potential toxic functions of PrP^{Sc} that have been suggested include induction of apoptosis, and interference with axonal transport or synaptic function [186]. Alternatively, neurodegeneration may result from a loss of function of PrP^{C}, although the relative health of PrP-null mice [121–123] would seem to argue against this mechanism. Having said that, many different potentially important functions have been proposed for PrP^{C} (and discussed above) including cellular protection from apoptosis and oxidative stress; signal transduction; and synaptic functions. As a loss of any of these functions could presumably lead to cell death, it is not unreasonable to view loss of PrP^{C} function as an important pathogenic mechanism. A potential explanation for the good health of PrP-null mice, could be that the protective function(s) of PrP^{C} are dispensable under normal conditions, and that it is only under conditions of stress that the loss of these functions leads to neurodegeneration [186].

Some experimental results indicate a requirement for both PrP^{Sc} and PrP^{C} for neurodegeneration and neuron toxicity, seemingly supporting the third potential mechanism of neurodegeneration, modulation of PrP^{C} function. PrP-null neurons are resistant to any potential toxic effects of PrP^{Sc} [187,188]. This is more compelling evidence for a modulation of PrP^{C} function than the observation that PrP-null mice are immune to prion disease [69,70,189], since in the latter

case it could be argued that this lack of susceptibility is due to insufficient amounts of PrP^{Sc}, since it cannot replicate without PrP^{C}. In comparison, if PrP^{Sc} were in itself toxic, PrP-null neurons would be expected to be susceptible to this toxicity. The observations in mice expressing PrP^{C} that lacks the GPI anchor provide both further evidence for a modulation of PrP^{C} function as a cause of neurodegeneration and one potential mechanism [190]. When infected with scrapie, these mice exhibited accumulation of PrP^{Sc} amyloid plaques, in the absence of brain pathology and neurological symptoms [190]. These data indicate a requirement of PrP^{C} to be membrane bound in order to transduce a toxic signal as a result of interaction with PrP^{Sc} [186]. Although the available data may be used to argue for any number of mechanisms to explain the initiation of neurodegeneration as a result of prion disease infection, both normal PrP^{C} function and the effects of PrP^{Sc} must be further clarified before all of the details of disease pathogenesis can be described.

1.4 Methods Used to Investigate Prion Disease

Prion diseases are characterized by the deposition of PrP^{Sc}, the appearance of vacuoles, and gliosis in the brain [5]. Different strains can be distinguished by the distributions of these histological markers in a given host. However, the unequivocal diagnosis of most prion diseases requires the post-mortem collection of central nervous system tissue, either for histological examination or Western blot analysis. In addition a number of other methods have been developed to address the particular problems posed by prion diseases.

1.4.1 Histological Techniques

The classical method for the investigation of prion disease is the examination of paraffin-embedded tissue sections for spongiform change. Before the discovery of the prion protein, the most important indicator of prion disease was the presence of vacuoles in the brain. The distribution of vacuoles within different brain regions, known as the lesion profile, is used to distinguish between different strains of prion disease [33,191]. The degree of spongiform change is most often scored on a 0-5 scale, with each number corresponding to a verbal description [191]. Subsequently, imaging techniques were devised in order to remove the subjectivity inherent in this scoring method, as well as the requirement for a very experienced pathologist to score the sections of interest [192–194].

The discovery of the prion protein allowed for the development of immunohistochemical protocols to study the distribution and progressive appearance of PrP^{Sc} in infected brain tissue. The first of these techniques is analogous to the evaluation of spongiform change: monoclonal antibodies that recognize the prion protein are used to visualize the distribution of PrP on paraffin-embedded tissue sections. Two variations on this theme have also been developed: histoblots and paraffin-embedded tissue (PET) blots. The procedure for histoblotting involves the transfer of a frozen tissue section onto a nitrocellulose membrane, followed by limited proteolysis with proteinase K (PK), and finally immunostaining using antibodies that recognize PrP [195]. This technique allows for the visualization of PrP^{Sc} deposition in an entire coronal

tissue section, and proteolysis with PK digests PrP^{C}, so that staining is the result of PrP^{Sc} only. The PET blot technique is very similar to histoblotting, except that it involves transfer of paraffin-embedded tissue sections onto a nitrocellulose membrane; this is followed by proteolysis with PK, and immunostaining [196–198]. PET blotting retains the advantages of histoblotting, has been shown to be more sensitive than immunohistochemistry, Western blotting, and histoblotting with respect to detection of PrP [196], and has even been used as a means of strain typing [198]. All three of these techniques can also be applied to the evaluation of gliosis by immunostaining for glial fibrillary acidic protein (GFAP), although only traditional immunohistochemistry is commonly used for this application.

1.4.2 Immunoassays Involving Brain Homogenates

The most frequently used immunoassay is the Western blot of infected tissue. It is carried out in the same manner as any other Western blot, except that each sample is divided into two aliquots, one of which is treated with PK. Infected and uninfected samples are indistinguishable when their untreated (without PK) aliquots are compared, with a band in the range of 33 kilodaltons (kDa). Since PrP^{Sc} is partially resistant to PK digestion, running the PK-digested aliquot results in a band of 27-30 kDa, while the lane with uninfected tissue is empty, because of the sensitivity of PrP^{C} to PK digestion.

The conformation-dependent immunoassay (CDI) makes use of the fact that the immunoreactivity of PrP^{Sc} is increased through denaturation, while that of PrP^{C} is not [45]. CDI is an adaptation of ELISA, in which samples are divided

into two aliquots, one of which is denatured by treatment with guanidine hydrochloride [45,199]. Binding is then quantified using dissociation-enhanced time-resolved fluorescence spectroscopy, and the ratio of PrP detected in the denatured and native states is determined [45,199]. This method has been shown to differentiate between different prion strains, since this ratio is characteristic of different strains [45,55,200,201].

Homogenates of brain or other tissues can be enhanced for prion content by the process of precipitation with sodium phosphotungstic acid [45,202]. Beginning with the brain homogenate, gross cellular debris is removed by centrifugation, and the supernatant is incubated with sarkosyl before the addition of sodium phosphotungstic acid and magnesium chloride [45,202]. Following centrifugation, the pellet is resuspended in either water [45] or phosphate buffered saline containing sarkosyl [202].

1.4.3 Proteomics and Microarrays

Proteomics and microarrays provide means to study the host response to infection by examining protein and gene expression, respectively. Proteomics involves the comparison of protein expression between infected and uninfected animals [203] or cells [204], or human tissues [205], and can be carried out at different stages of disease pathogenesis. Three steps are generally involved: separation of proteins according to size and charge by two dimensional gel electrophoresis; identification of these proteins by mass spectrometry; and comparison of the characteristics of the proteins in the samples to information obtained from protein databases [203–205]. Information that can be obtained

includes differences in the amount of protein expressed between infected and uninfected tissues, as well as any changes in the proteins themselves. Applications of this technique include the identification of differences in protein expression that can be used as markers of disease state [205]; mechanisms underlying the mode of action of anti-prion drugs [204]; and preclinical changes that may shed light on the processes behind disease pathogenesis [203], among others.

Microarray analysis explores gene expression in tissues, allowing high-throughput evaluation of huge datasets. RNA is isolated and purified, and used as a template to produce cDNA [206–209]. Depending on the microarray chip being used, either labelled cDNA is hybridized to a DNA chip [208,209], or cDNA is used as a template to produce antisense cRNA which is in turn labelled and hybridized to an RNA chip [206,207]. Microarray software is then used to identify genes that are either up- or down-regulated in infected tissues [206–209]. This technique has been used to identify differences in gene expression in humans [206], and in animals at different stages of disease progression [207,209], and to classify scrapie strains according to expression profiles [208].

1.5 Prion Diseases of Animals

1.5.1 Scrapie

Scrapie, which naturally affects sheep and goats, is the prototypical TSE, and has been recognised at least since the 18th century [210]; a complete listing of all currently known prion diseases can be found in Table 1. Scrapie got its name because a common behavioural manifestation of the disease is that sheep

Table 1. Prion Diseases of Humans and Animals.	
Host	Disease
Sheep, goats, moufflon	Scrapie
Cattle	Bovine Spongiform Encephalopathy (BSE) Bovine Amyloidotic Spongiform Encephalopathy (BASE)
Elk, whitetail and mule deer	Chronic Wasting Disease (CWD)
Exotic ungulates (greater kudu, nyala, oryx)	Exotic ungulate encephalopathy
Mink	Transmissible Mink Encephalopathy (TME)
Cats, including some Big Cats	Feline Spongiform Encephalopathy (FSE)
Humans	Kuru Gerstmann-Sträussler-Scheinker Syndrome (GSS) Fatal Familial Insomnia (FFI) Fatal Sporadic Insomnia (FSI) Creutzfeld-Jakob Disease (CJD) Sporadic CJD (sCJD) Familial CJD (fCJD) Iatrogenic CJD (iCJD) Variant CJD (vCJD)

rub their bodies against the fence posts and wires of their pasture. Scrapie can be transmitted through contaminated feed; however, it can also be transmitted to sheep sharing a pasture with an affected animal. It is not yet clear how this horizontal transmission occurs, but recent data indicate that prion-contaminated soil retains infectivity [211–213], and may even enhance it [213].

There are approximately twenty known scrapie strains, none of which have been shown to cross the species barrier to humans, although it has been suggested that some cases of sCJD in humans are caused by a scrapie strain [214]; this assertion remains unconvincing based on the current data. Scrapie has historically been the prion disease of choice for animal research because of the development of many rodent-adapted strains that result in highly reproducible disease in inbred mice. However, most scrapie strains have incubation periods of at least 150 days in mice. In comparison, the 263K strain of scrapie has an incubation period of 68-71 days following intra-cerebral infection of Syrian golden hamsters [215,216]. The 263K strain was developed by serially passaging the Chandler strain of scrapie in hamsters [215,217]. In these experiments, incubation time only became stable as of the fifth passage [217], and it was determined that there were at least two different strains present even as late as the third passage [217]. One of these strains was highly pathogenic in mice, while the other, 263K, was not [217]. Following the fifth passage, only the latter strain remained in brain homogenates, providing some evidence that the process of adaptation of a strain to a particular host may involve selection of a single strain from a mixture [217].

Most of the characterization of the 263K strain of scrapie was carried out in the labs of Liberski, and of Kimberlin and Walker, who developed the strain. Besides its short incubation time, 263K scrapie is most remarkable for its high infectivity titres in the brains of clinically diseased hamsters, compared to most strains of murine scrapie [215]. 263K scrapie shares with other prion diseases the characteristic hallmarks of spongiform change, PrP^{Sc} deposition, and gliosis. Much of the characterization of 263K scrapie was carried out either before the identification of the prion protein, or very soon after; for this reason, the most systematic studies deal mainly with spongiform change and gliosis. Compared to other scrapie strains, vacuolation in 263K scrapie develops relatively late in the incubation period [218]. With respect to both spongiform change [219] and gliosis [219,220], at the end stage of disease, the regions of the brain that are most affected are the brain stem, the thalamus, the hypothalamus and the hippocampus. In addition, gliocytosis (the combination of hypertrophy and hyperplasia of astrocytes, along with the proliferation of rod-like microglial cells), which is a rare phenomenon in murine scrapie, has been described in hamsters infected with 263K scrapie [220]. Two studies have sequentially evaluated spongiform change and gliosis following i.c. infection in 263K scrapie-infected hamsters [219,221], allowing for comparison with the data collected during the experiments described in this volume.

A number of studies describe pathology in Syrian golden hamsters following infection with the Sc237 strain of scrapie, and can be used as a basis for comparison of the sequential appearance of PrP^{Sc} with the data collected in

this experiment. Sc237 was the agent that produced 263K following multiple passages in hamsters [217], and it is likely that upon multiple passages in the hands of other researchers, the same strain was produced [222]. Studies using Sc237 indicate that PrP^{Sc} deposition correlates with vacuolation and gliosis [222,223]; that PrP^{Sc} appears one to two weeks before gliosis in a given brain region [223]; and that the thalamus and the septum are the two regions affected first, as early as 14 to 21 and 28 days post infection, respectively [222,223].

1.5.2 BSE

BSE, or mad cow disease, as it is sometimes known, became epidemic through the use of meat and bone meal (MBM) as a protein supplement in cattle feed. MBM was composed of the offal of cattle and sheep, as well as chickens and pigs. It is widely accepted that the cause of the epidemic was a change in rendering practices in the late 1970s, which resulted in a higher fat content in MBM [224]. As a result, it is believed that scrapie prions were no longer eliminated in the rendering process, and that they were subsequently able to cross the species barrier and cause disease in cattle [210]. Another possibility is that bovine prions already existed at a low level, and that the change in rendering procedures allowed their presence to be greatly amplified in the population. The latter hypothesis is perhaps more attractive since all mammals express PrP [103]. It is thus conceivable that a sporadic prion disease could exist with a low level of incidence in any mammal. The presence of the disease could easily go undetected if the incubation period for the disease in that species is longer than, or almost as long as, the normal lifespan of that species. Support for this

explanation as the origin of BSE comes from recent data regarding atypical BSE. During the course of surveillance for BSE in Europe and Japan, cases of BSE exhibiting unusual characteristics have been identified [225–228]. These potential new strains have since been transmitted to mice [225,229–231], and a haplotype of the *Prnp* gene appears to associate with atypical BSE [232]. Most strikingly, when the BASE (bovine "amyloidotic" spongiform encephalopathy) strain of atypical BSE was serially passaged in mice, the molecular and neuropathological disease phenotype was identical to that caused by BSE, possibly suggesting the origin of BSE [229].

1.6 Prion Disease of Humans

1.6.1 CJD

CJD is the most common human TSE, with sCJD representing 90% of CJD cases [233]. All forms of classical CJD are characterized by progressive dementia, myoclonus, ataxia and a characteristic electroencephalogram (EEG) [234]. The familial prion diseases, including fCJD, are caused by mutations to the *Prnp* gene that follow the pattern of autosomal dominant inheritance [5]. At least twenty mutations to *Prnp* have been found so far [235]. Genetic linkage has been documented in a number of these mutations [236–240], and all cases of inherited prion diseases have proven to have a mutation in the *Prnp* gene [235]. Iatrogenic CJD (iCJD) is acquired through surgical procedures, or through the administration of human products as a treatment. The most common sources of infectivity are dura mater grafts and cadaveric human growth hormone (hGH) [241], but other cases have arisen after corneal transplants [242], through

the use of contaminated neurosurgical instruments [243], electroencephalogram (EEG) depth probes [244], and from pituitary-derived gonadotropin [245,246].

It is unclear how sporadic prion diseases are acquired, but three hypotheses have been put forward. The first states that somatic mutations to *Prnp* are responsible. If this is the case, the same mutations that cause familial TSEs in germ line cells cause sporadic TSEs when they occur in somatic cells. The second hypothesis is that PrP^{C} is spontaneously converted to PrP^{Sc} by some unknown mechanism [247], perhaps due to random protein misfolding. The third and final hypothesis states that sporadic prion diseases are transmitted horizontally between humans, or between humans and animals [248]. In support of this hypothesis, Lasmézas *et. al*. suggest that some sCJD cases may share a causative agent with certain scrapie strains [214]. They found that the shape of the lesion profiles that resulted when C57BL/6 mice were injected with either scrapie from a French experimental flock, or sCJD or iCJD from two French patients were similar, although the intensities differed. In addition, the incubation times were similar, although not identical [214]. For a more convincing case, incubation times upon serial passage, which have not been reported, should be identical. It is not impossible that a proportion of sCJD patients could represent transmission to humans of animal TSEs, but evidence of this has not been convincing.

1.6.2 vCJD

The epidemic of Bovine Spongiform Encephalopathy (BSE) in the United Kingdom, which began with the first recognized case in 1986 [249], is also a very

real threat to human health, due to the emergence of variant Creutzfeld-Jakob disease (vCJD) in the mid-1990s [250,251], and the discovery that it was caused by ingesting BSE-infected beef [6,252,253]. Several lines of evidence now suggest that vCJD is caused by eating beef from cattle infected with BSE, including similarities in lesion profiles, incubation times and PrP^{Sc} glycoform patterns of BSE and vCJD in mice, and infection of non-human primates with both BSE and vCJD. Lasmézas *et. al.* [254] inoculated cynomolgus macaques intra-cerebrally with BSE, and compared the clinical and pathological features of the resulting disease to the existing descriptions of vCJD in humans [255,256]. The authors found that the morphology of the florid plaques, the distribution of spongiform change, and the deposition pattern of PrP^{Sc} were strikingly similar to vCJD [254]; the macaques even presented with behavioural abnormalities before the onset of cerebellar signs [254]. In another study [214], Lasmézas *et. al.* infected cynomolgus macaques intra-cerebrally with vCJD and macaque-passaged BSE. In both cases, the clinical and pathological features were the same as in the previous study; the incubation time of the disease was decreased in macaque-adapted BSE, and was shorter than that of vCJD in macaques, due to the absence of a species barrier [214].

Two studies have used different strategies to show that BSE and vCJD share a common causative agent. Bruce *et. al.* [6] compared the lesion profiles and incubation times in mice of vCJD from three sources, BSE, and sCJD from six sources. Based on the “signature” formed by the combination of the lesion profile and the incubation time, they concluded that the prion strain causing vCJD

was distinct from that causing sCJD, but that it was indistinguishable from that causing BSE. In the second study [252], Hill *et. al.* inoculated both transgenic mice expressing the human *Prnp* gene but not the murine *Prnp* gene, and non-transgenic mice with BSE, vCJD, sCJD, and iCJD. In transgenic mice, BSE and vCJD were much less efficient than sCJD and iCJD in causing disease. BSE had the longest incubation time, as it was the only inoculum that faced a species barrier. In the non-transgenic mice, vCJD and BSE caused disease much more efficiently than either sCJD or iCJD. Most importantly, on Western blots, sCJD and iCJD produced glycoform patterns of types-1-3 when digested with proteinase K, while BSE and vCJD produced only the type-4 glycoform pattern. When taken together, the evidence provided by the identical glycoform patterns [252], the indistinguishable "signatures" composed of the lesion profiles and incubation times in inbred mice [6], as well as the clinical and pathological similarities in non-human primates [214,254] provide solid evidence that vCJD and BSE share a common causative agent.

Since the first cases of vCJD were identified in the mid-1990s [250,251,255], more than two hundred cases have been reported to date, mainly in the United Kingdom [257]. The median age of onset of vCJD cases as of December 2007 is 28.5 years, with a range of 14 to 74 years [138], much lower than traditional sCJD. The median time from onset of illness to death is 413 days [138]. Both the clinical symptoms and the pathology of vCJD are distinct from those of classical CJD. Dementia and other signs of cognitive decline are only evident in the late stages of vCJD; early on, depression, apathy, withdrawal, and

other psychiatric features, as well as sensory symptoms are the most common signs of illness [258]. The typical EEG pattern often observed in classical CJD is absent in vCJD [258,259]. Like classical CJD, the affected brain shows spongiform change, astrocytic gliosis, and neuronal loss; in addition to these signs, large florid Kuru-type plaques can be widespread [260]. Finally, unlike classical CJD, vCJD is characterized by the presence of PrP^{Sc} in the lymphoreticular system [8]. In addition to infection through ingestion of BSE-infected beef, secondary, human-to-human transmission of vCJD has also been reported as a result of blood transfusion [175,261–264]. From an epidemiological standpoint, 166 of a total of 207 cases of vCJD reported as of April 2008 have occurred in residents of the United Kingdom [257]. Estimates of the incubation time of vCJD are difficult to make because the exact time of exposure to the agent cannot be pinpointed. It has been suggested that the highest risk of infection of the human population of the UK from BSE was around 1989-90 [265], although a broader estimate has described the most likely period for ingestion of BSE-tainted material as between 1984 and 1989 [266]. Based on the incubation time of BSE, and the timing of the identification of the first cases (the mid-1980's), it was suggested that the first cases of vCJD would have had incubation periods on the order of eleven years or more [265]. This agrees with findings for other human prion diseases acquired orally or through peripheral inoculation. Incubation times for Kuru ranged from four to forty years [266], while the mean incubation period for iCJD acquired through injection of hGH was estimated at about twelve years [267].

The minimum dose requirement is unknown, and it is unclear whether infection occurs through cumulative low doses or one high dose of infective material. Furthermore, as in other acquired human TSEs, a genetic aspect is at work as well. All vCJD patients that developed clinical disease as of 2006 have been homozygous for methionine at codon 129 [266]. Similarly, most of the iCJD cases related to hGH were valine homozygotes at codon 129 [268], and methionine homozygosity resulted in increased susceptibility to Kuru [269–271], suggesting that the codon 129 genotype affects susceptibility to, and incubation time of human prion diseases.

1.7 Challenges Facing Prion Disease Research

Great advances have been made in prion research since the initial recognition that these disparate diseases shared a common cause, and since the discovery of the prion protein. Nevertheless, a number of very important problems remain unresolved. There continues to be no reliable means of prion disease diagnosis, particularly in the pre-clinical stages, and no effective treatment exists. Furthermore, the precise function(s) of PrP^{C} remain unclear, although it seems as though it is likely responsible for a number of important functions. Finally, details of disease pathogenesis require clarification, specifically whether disease occurs as a result of a loss or modulation of PrP^{C} function or gain of toxic function of PrP^{Sc}; the steps in disease pathogenesis following peripheral infection, especially following infection through blood transfusion; and the mechanistic details of neuroinvasion, and of conversion of PrP^{C} to PrP^{Sc}.

Issues relating to disease pathogenesis and PrP^C function have been outlined above, and will not be revisited here. With respect to prion disease diagnosis, there is currently no means of unequivocal diagnosis in live subjects, with the exception of vCJD, which can sometimes be diagnosed by detection of PrP^{Sc} in tonsil tissue [8]. When cases present, a suspected diagnosis of TSE is made based on patient history, electroencephalogram (EEG), and neurological findings [272]. High levels of 14-3-3 proteins in the cerebrospinal fluid provide further support for a diagnosis of prion disease [272]. However, unambiguous diagnosis requires post-mortem detection of PrP^{Sc} in the brain. Exacerbating the absence of a means of definitive diagnosis is the lack of an effective treatment in the clinical stage of disease. If disease could be diagnosed before the appearance of clinical symptoms, the effectiveness of any potential treatments would likely be increased. For this reason, the efficacy of magnetic resonance imaging (MRI) as a means of diagnosing prion disease in live animals was investigated (see below).

The final major issue remaining in prion disease research is also the most important: a viable treatment for clinical stage disease has not yet been identified. Many different classes of compounds and treatment strategies have been tested for anti-prion effects. A recent publication provided an exhaustive review of compounds with anti-prion properties [273]. Among the compounds and strategies that have shown promise are polyanions like pentosan polysulphate (PPS); polycations like polyamidoamide (PAMAM); amyloid binding compounds like congo red; suramin; tetrapyrroles like porphyrin; compounds that

are relevant to cholesterol metabolism, like polyene antibiotics; tricyclic compounds like quinacrine; cell signalling inhibitors, including inhibitors of tyrosine kinase; gene silencing therapy, including through the use of siRNAs; immunotherapy, including through the use of anti-PrP antibodies; and neuroprotective compounds like flupirtine [273]. Three of these compounds have been used to treat human patients: PPS [274–277]; quinacrine [278]; and flupirtine [279]. A double-blind, placebo-controlled study of flupirtine treatment did not identify any effect on survival time, but patients receiving flupirtine performed better on dementia tests [279]. Quinacrine treatment resulted in short term improvements in cognitive function and mood [278]. Success of PPS treatment has been variable, with reports of both extended survival time [276], and no effect [277]. Taking all twenty-six patients who have received intra-ventricular PPS into account, beneficial effects could not be proven due to a lack of objective criteria for their evaluation [274]. In the study presented here, PPS was chosen to treat scrapie-infected hamsters.

1.8 Magnetic Resonance Imaging

Magnetic Resonance Imaging (MRI) uses radio frequency (RF) pulses and a strong magnetic field to detect changes in soft tissues like the brain. The concepts discussed in this section come largely from the book “MRI Made Easy (…Well Almost”) [280], but similar basic MRI background information may be found in any MRI textbook. When a subject is placed within a strong magnetic field (like an MRI scanner), the initial random magnetization of individual protons inside the subject now aligns with that of the strong external magnet. The

magnetization of the subject is made up of the net magnetic moment of individual protons (mainly from water) within the subject. When placed within a strong external magnetic field, the magnetic moments of individual protons move around the axis of the external magnetic field, in a manner that can be likened to the spinning of a top (this is called precession); for this reason, the magnetic moments of individual protons are known as spins. These spins take on either a parallel or an anti-parallel alignment compared to the external magnetic field within which they are placed. The parallel alignment requires less energy, and therefore more spins are always found in this alignment, resulting in a net magnetic field of the subject that is parallel to that of the external magnetic field.

The net magnetization of a subject is made up of its longitudinal magnetization (parallel to the external magnetic field) and its transversal magnetization (perpendicular to the external magnetic field). After placement in a large magnetic field the longitudinal magnetization of individual spins is constant within a typical time constant T_1. At any one moment these spins are scattered around the axis of the external magnetic field, the transversal magnetizations of individual spins cancel each other out with a typical time constant T_2 and the subject has a net transversal magnetization of zero. When an RF pulse is applied to the system, the base situation described so far is altered in two ways: the RF pulse supplies energy, which is absorbed by the spins, allowing them to take on the anti-parallel alignment, and therefore reducing the net longitudinal magnetization; and the RF pulse causes spins to move in phase, which results in a net transversal magnetization that spins

around the axis of the external magnetic field. Conversely, when the RF pulse is switched off, the system gradually returns to its previous state, allowing for the measurement of two effects: Longitudinal, or T_1, Relaxation; and Transversal, or T_2, Relaxation.

Longitudinal Relaxation is the phenomenon by which the net longitudinal magnetization returns to normal. This process involves the release of energy by individual spins to the surroundings, or lattice; for this reason, it is also known as Spin-Lattice Relaxation. T_1 relaxation is influenced by the similarity in frequency of the precession of the spins of interest, compared to those in the lattice: the closer these frequencies, the shorter the T_1 relaxation time. In comparison, Transversal Relaxation is the phenomenon by which the net transversal magnetization returns to zero. This occurs as spins gradually exchange polarization, not affecting the net polarization, and by doing so obtaining a random phase factor. As a result the net transversal magnetization decays without affecting the longitudinal magnetization. This process of parallel and anti-parallel spins exchanging energy, without losing any energy to the surrounding lattice, is also known as Spin-Spin Relaxation. T_2 relaxation is influenced by the homogeneity of the magnetic field, such that decreased homogeneity results in a decrease in the T_2 relaxation time. This effect is often referred to as the T_2* effect.

In practice, a sequence of RF pulses rather than a single pulse is used to optimize measurement of the effect of interest in order to create contrast in soft tissue. By applying a sequence of pulses of different strengths and at different

times, the resulting images can be altered such that their appearance is determined by one phenomenon or another: for example, images can be T_2-weighted, meaning that they reflect mainly T_2 effects. MR images are influenced by the experimental conditions, including factors such as temperature, under which they are collected. In the clinical setting, images of interest are not typically compared to other images; instead, relative signal strength (intensity) is compared within the image of interest. In order to compare images collected at different times, under different conditions, it is necessary to account for these different conditions. Including a reference sample will facilitate the comparison between images obtained in different scanning sessions. Any observed differences in measurements of this reference sample can then be attributed to differences in experimental conditions, and measurements of interest can be normalized using the reference. Addition of copper sulphate shortens the T_2 value of water, allowing for the observation of complete T_2 relaxation, resulting in a consistent high intensity signal. For this reason, a copper sulphate solution is commonly used as a reference sample, either as described above, as a so-called phantom for testing purposes, or as a geometrical marker.

1.9 Pre-Clinical Detection of Scrapie in Hamsters by MRI, and Evaluation of PPS as a Treatment for Scrapie

The lack of a means to diagnose prion disease in live subjects is a problem not only because it inhibits effective treatment of human patients, but also because it creates a requirement for a large number of experimental animals in order to conduct longitudinal studies. As such, the first objective of this study

was to not only detect disease in live animals, but relate it to known physical changes that occur in the brain during disease pathogenesis as well. By achieving this objective, it would be possible to use this system to follow disease progression in individual animals. For the purpose of research, prion diseases have been adapted to rodent hosts that develop disease much more rapidly than would the natural hosts. One of the most rapid models of disease is the 263K strain of scrapie in Syrian golden hamsters, which has an incubation period of 68-71 days following intra-cerebral infection [215,216].

Magnetic Resonance Imaging (MRI) uses a radio frequency pulse and a strong magnetic field to detect changes in soft tissues like the brain. This method has been used to examine patients suspected of having CJD or other prion diseases. MR image abnormalities that have been reported include: increased signal intensity in T_2-weighted images of the basal ganglia [281,282], caudate nuclei and putamina [283], and cerebral cortex [281]; increased signal intensity in T_1-weighted images of the globus pallidus [284]; and increased signal intensity in diffusion-weighted images in the cerebral cortex [285,286], basal ganglia [286], and striatum [285]. In some cases, MR image abnormalities were compared to histological changes evident in tissues collected upon death. High signal intensity in diffusion-weighted [281,287], and T_2-weighted [281] images correlated with a high degree of spongiform change determined through histological examination. In experimentally-infected rodents, increased signal intensity on T_2-weighted images correlated with gliosis [288,289] or PrP^{Sc} deposition [289], while vacuolation correlated with decreased signal intensity

[288]. Only one of these reports described pre-clinical MR image abnormalities, and they occurred late in the pre-clinical stage of disease [289].

In the study reported here, Syrian golden hamsters were injected intra-cerebrally with the 263K strain of scrapie or phosphate buffered saline (PBS), or were not injected with anything. Beginning at 19 days post injection (dpi), hamsters underwent MRI every two weeks until 61 dpi. Since prion disease progression involves progressive physical changes in the brain, it was hypothesized that the diseased state could be identified using MRI. In a second study, corresponding groups of Syrian golden hamsters were examined histologically for the typical hallmarks of prion disease. Beginning at 19 dpi, hamsters were euthanized every two weeks until 61 dpi, and examined for spongiform change, PrP^{Sc} deposition and gliosis. It was hypothesized that any MR image abnormalities observed would correlate with the progressive appearance of histological hallmarks of prion disease.

This MRI model system was subsequently used as a method to evaluate the efficacy of a number of pentosan polysulphate (PPS) treatment regimens. Syrian golden hamsters were injected intra-cerebrally either with the 263K strain of scrapie or with control brain homogenate. The hamsters received PPS treatment regimens that were chosen with two objectives in mind: to compare the effectiveness of intra-cerebral (i.c.) and intra-peritoneal (i.p.) PPS treatment, and to compare the effectiveness of treatments administered at different time points. The first of these objectives was important to address because intra-cerebral treatment is highly invasive, so it would be desirable if prion disease

could be successfully treated by a less invasive method. Previous reports of PPS treatment of scrapie-infected rodents have used arbitrary treatment time points; the objective here was to use a meaningful time point for PPS treatment: the time at which MRI could detect scrapie infection. The hamsters were imaged by MRI every two weeks beginning at 19 dpi, until they exhibited severe signs of disease, or until 150 dpi in the case of mock-infected hamsters, and the brains of hamsters were removed and examined for histological changes. It was hypothesized that intra-cerebral PPS treatment would be more effective than intra-peritoneal treatment in prolonging survival time of scrapie-infected hamsters; that treatments administered at the earliest time points would be most effective; and that PPS treatment would slow the appearance of histological changes in scrapie-infected hamsters.

In order to explain some of the unexpected results of this study, a speculative model was proposed, relating PrP^{Sc} replication, aquaporin-4 (AQP4) expression, and oedema. Briefly, it was suggested that conversion of PrP^{C} to PrP^{Sc} alters signalling through PKC and p38 MAPK, resulting in dysregulation of AQP4 expression and activity, and that this could be significant for disease pathogenesis.

2. Materials and Methods

2.1 Initial Magnetic Resonance Imaging Study

2.1.1 Experimental Design

Five-week-old Syrian golden hamsters (Charles River) were divided into scrapie-infected; mock-infected; and control groups, with six hamsters/group. Hamsters were maintained according to approved animal use protocols. Beginning at 19 days post injection (dpi), hamsters underwent MRI every two weeks until 61 dpi. Three hamsters in each group were euthanized at 48 dpi, and the remaining hamsters at 62 dpi.

2.1.2 Infections

Five-week-old Syrian golden hamsters were injected with 50 microlitres of 1% (w/v) 263 K scrapie brain homogenate in phosphate buffered saline (PBS) into the right parietal region of the brain under isoflurane anaesthetic. Injections were performed using a 26-gauge needle fitted with a guard to prevent it from penetrating too deeply; a 2.25 mm length of needle was left exposed. The 263 K scrapie brain homogenate used in the initial MRI study and the histology study was obtained from the TSE Resource Centre, Institute for Animal Health (Compton, Newbury, Berkshire, UK) as a stock 10% suspension in PBS. Mock-infected hamsters were injected with 50 microlitres of PBS only, and controls received no injection.

2.1.3 Magnetic Resonance Imaging

Beginning at 19 days post injection (dpi), hamsters underwent magnetic resonance imaging (MRI) every two weeks until either 47 or 61 dpi. Imaging was

performed using a Bruker 7 Tesla scanner. Hamsters were enclosed in a custom-made holder, and breathing and temperature were monitored throughout imaging under isoflurane anaesthetic (Figure 1). A custom-made quadrature coil was used, and T_2-weighted and diffusion weighted images were acquired using respiratory gating as a trigger for the Radio Frequency (RF) sequence. Nine coronal slices were collected, 1.7 mm thick and 2 mm apart (Figure 2). T_2 parameters: TR=1450 ms; TE=15 ms; 6 echoes (at multiple times of TE); field of view 3 x 3 cm; data matrix 256 x 128; 1 average. Diffusion-weighted imaging parameters (spin-echo sequence): TR=1200 ms; TE=40 ms; 1 echo; field of view 3 x 3 cm; data matrix 256 x 64. T_2-maps were produced from T_2-weighted data; apparent diffusion coefficient (ADC) maps were produced from diffusion-weighted data.

2.1.4 Statistical Analysis of MRI Data

MR images were processed using in-house developed software (Marevisi). Contour plots of T_2 relaxation time were created from the multi-echo data sets in order to identify regions that were consistently affected in infected hamsters. In order to compare the mean T_2 relaxation time in the region identified (the hippocampus in two consecutive brain slices), in images collected at different times, this measurement was expressed as a percentage of the mean T_2 relaxation time in the thalamus in Slice 5. This region was chosen following the evaluation of all nine brain slices for regions in which minimal differences were observed between hamster groups at any of the four time points studied. By using the ratio of T_2 relaxation time in the regions of interest to that in the

Figure 1. Custom-made hamster holder for MRI.

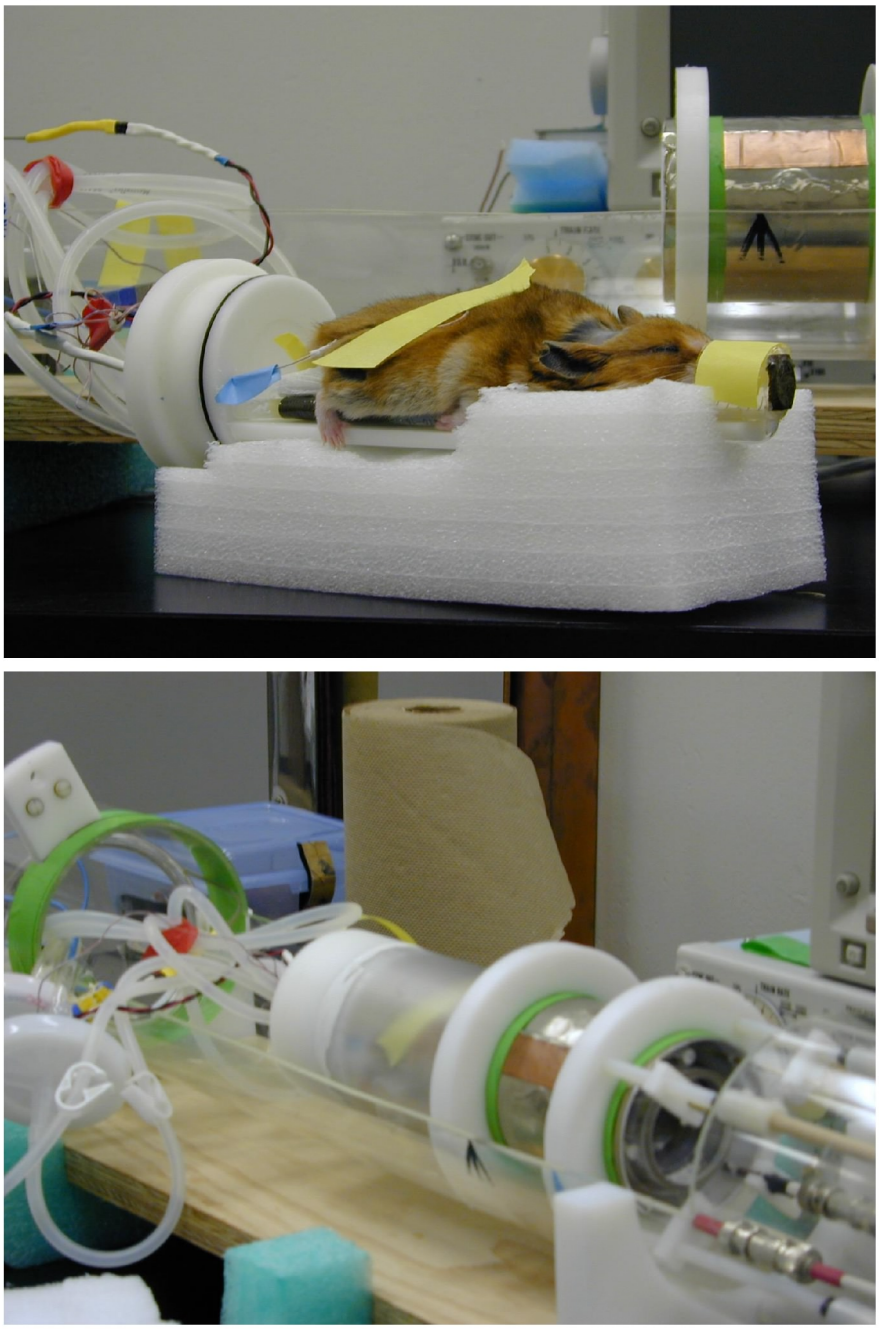

A hamster is shown being prepared for Magnetic Resonance Imaging. The anaesthetized hamster is placed in the custom-made holder and the appropriate monitoring probes are attached, including respiratory and temperature probes (top). The holder is closed and placed inside the custom-made quadrature coil, before being placed in the MRI scanner (bottom).

Figure 2. Images collected by Magnetic Resonance Imaging (MRI).

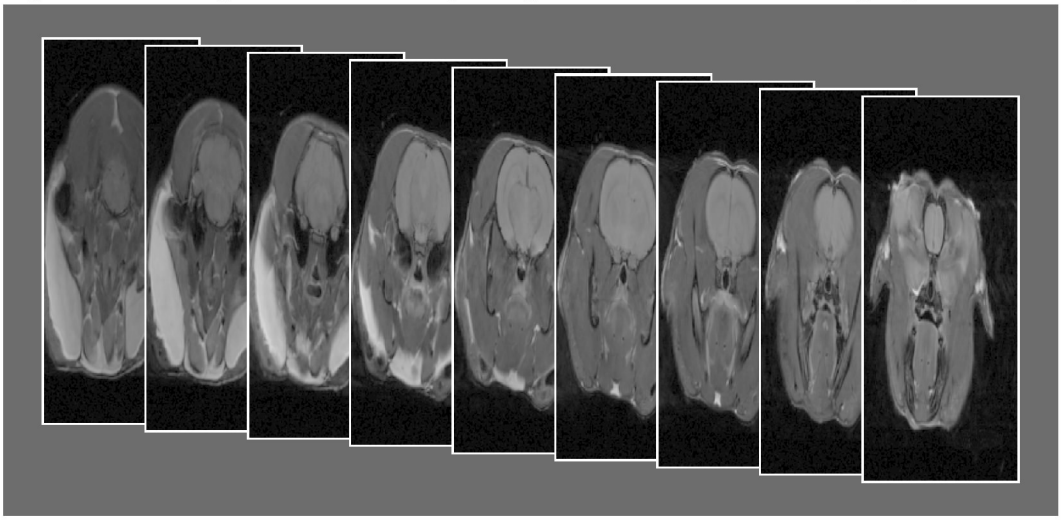

Nine coronal slices were numbered from posterior to anterior (left to right).

thalamus in Slice 5, the measurements being compared were corrected for differences in experimental conditions during MR image collection. At each of the four time points, an ANOVA was carried out to compare the corrected T_2 values in the hippocampus in the three hamster groups. In certain instances, comparison by ANOVA was not possible due to heterogeneity of variances between groups. In these cases, groups were compared using the Kruskall-Wallis test. The mock-infected and control hamster groups were also combined into a group named "Uninfected" and compared to the scrapie-infected hamsters. These two groups were compared by t-Test, or by Mann-Whitney u-Test when the assumptions of the t-Test were not met. ADC images were processed in the same manner.

2.1.5 Collection of Tissues

Hamsters were euthanized at 48 or 62 dpi by intra-cardiac injection of Euthanol. Each hamster brain was removed and flash-frozen in liquid nitrogen, and then stored at -80°C for infrared microspectroscopic analysis, and for production of brain homogenate for subsequent infections.

2.1.6 SDS-PAGE and Western Blotting

Samples were prepared by homogenizing brain tissue in brain lysis buffer (10% N-lauroylsarcosine in 0.01M sodium phosphate buffer), and incubated at room temperature for 30 minutes. Proteinase K (PK) positive aliquots were incubated with PK (at a final concentration of 50 μg/ml) at 50°C for 40 minutes, and phenylmethylsulfonylfluoride (PMSF) was added to a final concentration of 2 mM to stop digestion; PK negative aliquots did not undergo these steps.

Samples were diluted with 6x sample buffer (Tris-Cl, glycerol, SDS, bromophenol blue, and DTT in H_2O), heated at 98°C for 10 minutes, loaded on NuPage 4-12% SDS-PAGE pre-cast gels, and run at 110 volts for 2 hours. Proteins were transferred to PVDF membrane using a Bio-Rad semi-dry transfer apparatus, run at 15 volts for 15 minutes, with transfer buffer (48 mM Tris, 39 mM glycine, 0.04% SDS, pH 9.2). Membranes were blocked overnight in blocking solution composed of 5% skim milk powder in TBST wash buffer (100 mM Tris, 150 mM NaCl, 0.05% Tween-20) at 4°C with shaking. The membranes were then incubated at room temperature for one hour with primary antibody 3F4 diluted in TBST wash buffer; washed three times in TBST wash buffer; incubated for 45 minutes at room temperature with secondary antibody diluted in TBST wash buffer; washed a further three times; and incubated for 1-2 hours in TBST wash buffer to reduce background. Finally, the membranes were incubated for 2 minutes with Pierce's SuperSignal West Femto Maximum Sensitivity Substrate, exposed to X-ray films for 20 seconds or one minute, and the films were developed.

2.2 Histology Study

2.2.1 Experimental Design

Twenty five-week-old Syrian golden hamsters were infected with 263K scrapie for the purpose of histological examination. Beginning at 19 days post injection (dpi), five hamsters were euthanized every two weeks until 61 dpi. At each time point, one each of control and mock-infected hamsters were

euthanized for comparison, and the brains were removed, fixed in formalin, and embedded in paraffin.

2.2.2 Infections

Infections were carried out exactly as described above.

2.2.3 Collection of Tissues

Five scrapie-infected and one each of mock-infected and control hamsters were euthanized at each of 19, 33, 47, and 61 dpi by intra-cardiac injection of Euthanol. Upon removal, brains were fixed in formalin.

2.2.4 Tissue Processing and Paraffin Embedding

Hamster brains were cut into 3-5 mm thick slices to expose different planes for sectioning. Tissues were kept in individual cassettes in 10% formalin until tissue processing was initiated. Tissues were soaked for one hour with gentle shaking in 98% formic acid to decrease infectivity before being placed in a Leica TP1050 tissue processor. The tissue-processing program consisted of a series of ethanol baths ranging from 70-100%, followed by xylene, and finally molten paraffin. Upon completion of the processing program, the brain tissue was placed in moulds, which were then filled with molten paraffin from a Leica EG1160 embedding machine, and the moulds were placed on a cold plate for the paraffin to harden.

2.2.5 Sectioning From Paraffin Blocks and Preparation of Slides for Staining

Paraffin-embedded hamster brains were cut into 5-6 micron thick sections using a microtome. Sections were draped across the surface of a 41-45°C water

bath, and a slide was used to lift the section of interest off the surface of the water from underneath. For sections to be stained with haematoxylin and eosin, regular glass slides were used; sections to be examined immunohistochemically were placed on Probe-On slides. Sections were air-dried before further manipulation.

In preparation for staining, slides were heat fixed for forty-five minutes at 60°C before being placed in two successive xylene washes for five minutes each. The slides were then hydrated by washing in two successive 100% ethanol baths, followed by one each of 90% and 70% ethanol, and were then left in water until ready for further staining.

2.2.6 Haematoxylin and Eosin Staining

After being hydrated, slides were stained in haematoxylin for three minutes; rinsed in water; destained in 1% acid alcohol; rinsed in water; blued in Scott's Tap Water Substitute; and rinsed in water again. After checking slides under a microscope for sufficient staining, they were stained in eosin for three minutes; rinsed in water; and checked again for sufficient staining before dehydration.

2.2.7 Immunostaining for PrP

Hydrated slides were rinsed in TBS-Tween before soaking in 98% formic acid for ten minutes to reduce infectivity, and were rinsed again in TBS-Tween. They were then soaked twice in 3% H_2O_2 in methanol; rinsed in distilled water; and autoclaved for ten minutes at 121°C in 2 mM HCl in water to expose the epitopes recognized by monoclonal antibody 3F4. The slides were rinsed in

TBS-Tween; blocked in normal goat serum (diluted one drop in 10 ml of TBS-Tween) at 45°C for twenty minutes; rinsed again in TBS-Tween; and incubated overnight with monoclonal antibody 3F4 (diluted 1:50 in TBS-Tween) at 4°C. After rinsing with TBS-Tween, slides were incubated for twenty minutes at 45°C with biotinylated goat anti-mouse secondary antibody (diluted 1:1000 in TBS-Tween), and rinsed again in TBS-Tween. The slides were then incubated with Strept-ABComplex (Dako) for twenty minutes at 45°C; rinsed in TBS-Tween; incubated with DAB Substrated for approximately three minutes; and rinsed in distilled water. The slides were then counterstained with haematoxylin as described above.

2.2.8 Immunostaining for GFAP

Slides were immunostained for GFAP according to the protocol described above with the following changes: slides were not autoclaved; slides were incubated with proteinase K (Dako) for thirty minutes at room temperature; the primary antibody was a polyclonal anti-GFAP antibody raised in rabbit (diluted 1:1000, thirty minute incubation at room temperature); secondary antibody was a biotinylated goat anti-rabbit antibody, diluted 1:1000.

2.2.9 Slide Dehydration and Covering

Stained slides were dehydrated by washes in 70% and 90% ethanol, and two successive 100% ethanol washes, and were then washed twice in xylene. Finally, slides were covered with coverslips using a drop of Krystalon™ for sealing.

2.2.10 Quantification of Histological Changes

Images of stained sections were acquired using Leica FireCam 1.2.0 software and a Leica DMLD light microscope fitted with a DFC 300 digital camera. ImagePro software was used to quantify spongiform change, PrP^{Sc} deposition and glial cell staining in four selected regions of the brain: the hippocampus; the cortex at the level of the hippocampus; the thalamus; and the hypothalamus. In each of these regions, images were collected in all sub-regions, such that most of the region of interest was included in the images. For images of sections stained immunohistochemically, the software was used to create a template of the colour range identifiable as being immunostained. This template was then applied to all images, and a measurement, consisting of the percentage of the total image area that was covered by immunostaining, was produced (Figure 3). In the case of gliosis, the measurement was expressed as the raw percentage, whereas PrP^{Sc} deposition was expressed as 100 x % area covered.

In order to measure spongiform change, ImagePro software was used to evaluate potential vacuoles based on their size and shape. The size and shape restrictions were based on those set out by Sutherland *et. al.* [192,193], except that vacuoles of a smaller size were included in this analysis (minimum of 8 square microns compared to 69). Potential vacuoles whose aspect ratios exceeded 3, or whose convex hull area to object area ratios exceeded 1.7 were eliminated. Before any measurements were collected or potential vacuoles were excluded, a series of image processing steps was applied to precisely define the

Figure 3. Quantification of immunohistochemistry using ImagePro software.

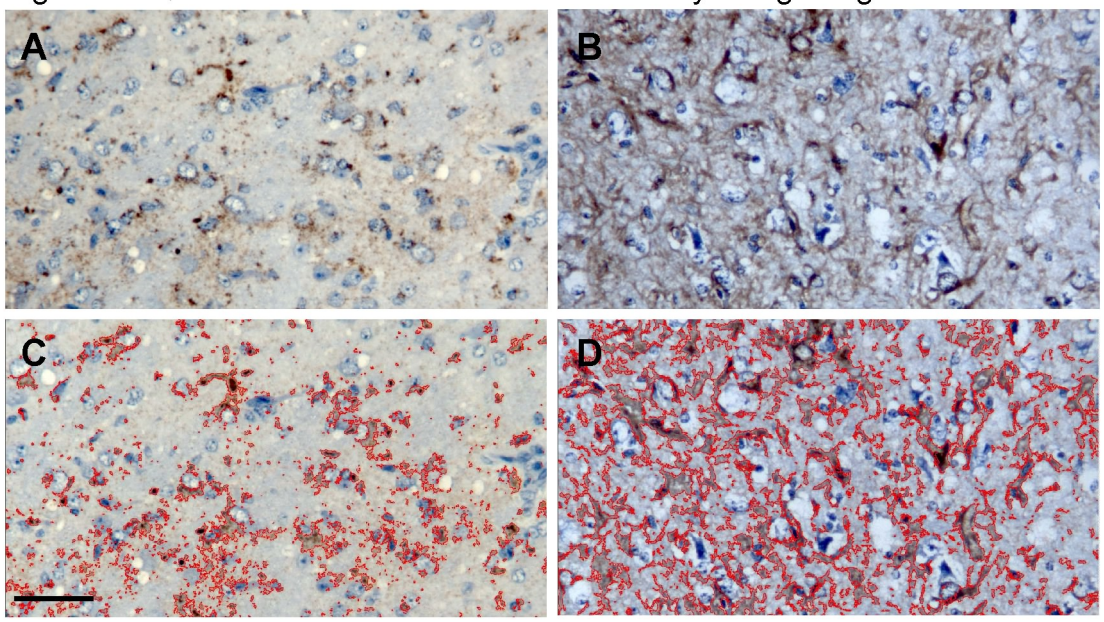

ImagePro software was used to quantify immunostaining for PrP^{Sc} (A and C) and glial fibrillary acidic protein (B and D). Raw images (A and B); immunostaining recognized by ImagePro outlined in red (C and D). Scale bar 50 microns.

boundaries of each object (Figure 4). The image was converted to greyscale and a Fast Fourier Transform was performed. A low-pass filter was then applied using Hanning filtering to attenuate high frequency information in the image, and an inverse Fourier Transform was executed. Finally, an intensity threshold was applied, eliminating lower intensity areas of the image, and leaving only potential vacuoles. This thresholded image was copied, and two object counts were carried out using the size and aspect restrictions outlined above: one calculating the object area, and the other the convex hull area of each object. The resulting ratio was then used to further exclude potential objects based on shape. Summing the percentage of the image area covered by each vacuole produced a final vacuolation score for each image. For each region of interest, the vacuolation score in each hamster was produced by multiplying the mean percentage of image area covered by vacuoles in all images of that given region of interest by 100. These individual hamster scores were then used to produce a mean score for spongiform change at each time point, for both infected and uninfected hamsters.

2.2.11 Statistical Analysis of Histological Data

For the purpose of comparison of histological hallmarks of prion disease, mock-infected and control hamsters were grouped together as a single group, called Uninfected, since MRI results were similar for both groups, and since neither were expected to show significant spongiform change or PrP^{Sc} deposition. At each time point, and for each histological characteristic being studied, two analyses were conducted: a series of t-tests comparing infected and

Figure 4. Improved method for quantification of spongiform change using ImagePro.

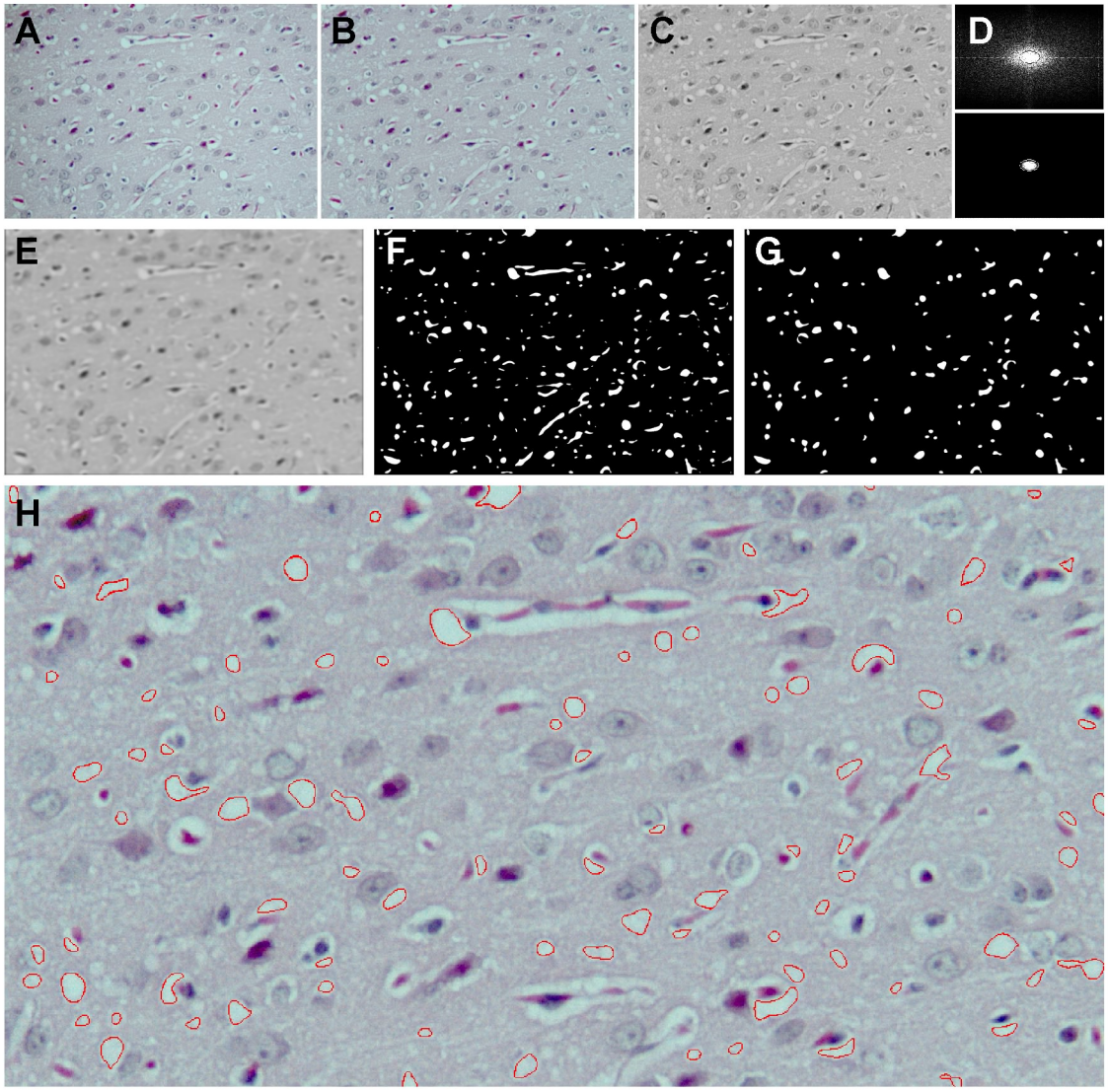

Image procession and vacuole measurement steps are shown. A detailed explanation of these steps may be found in section 2.2.10. Briefly, a raw digital image (A) undergoes background correction (B) and is converted to greyscale (C). A Fast Fourier Transform is performed, followed by a low-pass Hanning filter (D) and an inverse Fourier Transform (E). The resulting image is thresholded, and objects are excluded based on size and shape (F and G). The remaining objects are measured, and the outlines can be placed back on the original image (H).

uninfected groups in each of the four regions of interest; and an one way ANOVA comparing the four regions of interest in infected animals only.

2.3 Pentosan Polysulphate Drug Study

2.3.1 Experimental Design

Eighteen five-week-old Syrian golden hamsters were infected intra-cerebrally with 1% 263K scrapie brain homogenate, and an equal number were mock-infected with 1% control brain homogenate. The hamsters were divided into groups of three that received either no treatment, or one of the following five pentosan polysulphate (PPS) drug regimens: intra-cerebral (i.c.) injection of 2 mg/kg PPS at the time of infection; i.c. injection of 1 mg/kg twenty-six days post infection (dpi); intra-peritoneal (i.p.) injection of 100 mg/kg PPS at the time of infection; i.p. injection of 100 mg/kg PPS at twenty-six dpi; i.p. injection of 100 mg/kg PPS at twenty-six, forty, and fifty-four dpi. The hamsters were imaged by MRI every two weeks beginning at 19 dpi, until they exhibited severe signs of disease, or until 150 dpi in the case of mock-infected hamsters. Upon euthanasia, the brains of the hamsters were removed, and two brains from each group were fixed in formalin for paraffin embedding while the other was frozen.

2.3.2 Injections

Hamsters in the drug study were injected in the manner described above, either with 263K scrapie or control brain homogenate. The infectious inoculum used was produced from brain tissue collected at 62 days post injection (dpi) in the initial MRI study; control inoculum was produced from a single uninfected hamster.

2.3.3 Drug Treatment

PPS was supplied by the TSE Resource Centre, Institute for Animal Health, and Norton Healthcare; a Certificate of Analysis can be found in Appendix 4. All PPS injections were administered under isoflurane anaesthetic. Intra-peritoneal injections were administered at a dose of 100 mg/kg PPS, using a 23-gauge needle into the lower right-hand quadrant of the abdomen. Intra-cerebral injections were administered at a dose of 2 mg/kg for treatments at 0 dpi, and 1 mg/kg for treatments at 26 dpi, using a 26 gauge needle; the reasons for the differential doses will be discussed below in the PPS toxicity section and in the Results section. For the injections at 0 dpi, the PPS was mixed with the brain homogenate immediately prior to injection so that only one injection could be performed. The i.c. injections at 26 dpi required a more complex protocol since the skulls of the hamsters at that age had hardened sufficiently to prevent a simple injection with a 26-gauge needle. First, the hamster's head was shaved, and a short incision was made in the skin on top of the head. This incision was then held open while a bowl-shaped impression was made in the skull using a dental drill, being careful not to penetrate through the entire skull. Next, the injection was made using a 26-gauge needle fitted with a double guard (one with a wider diameter to rest outside the impression made by the drill, and a narrower internal one to give the outer one strength and integrity). Following the injection, the impression was filled with bone wax, and the skin incision was sealed with skin glue. The hamsters were then monitored for one hour or more to ensure that they recovered fully from the manipulation.

2.3.4 Magnetic Resonance Imaging

Beginning at 19 days post injection (dpi), hamsters underwent magnetic resonance imaging (MRI) every two weeks until they were euthanized due to severe symptoms of scrapie, or 150 dpi in the case of mock-infected hamsters. Imaging was performed as described above, with a few changes. A new custom-made quadrature coil was used, due to the use of a new, larger hamster holder, and T_2-weighted images only were acquired without the use of respiratory gating as a trigger for the Radio Frequency (RF) sequence. A tube of copper sulphate was included on the bed of the hamster holder as a reference sample to facilitate the comparison between images obtained in different scanning sessions. Any observed differences in measurements of this reference sample could then be attributed to differences in experimental conditions, and measurements of interest could be normalized using the reference. Copper sulphate shortens the T_2 value of water, allowing for the observation of complete T_2 relaxation, resulting in a consistent high intensity signal. Nine coronal slices were collected, 1.8 mm thick and 2 mm apart. T_2 parameters were as follows: TR=1450 ms; TE=15 ms; 6 echoes (at multiple times of TE); field of view 3 x 3 cm; data matrix 256 x 128; 4 averages. T_2-maps were produced from T_2-weighted data. Figure 5 demonstrates how the experiment was set up: first, an axial (coronal) scout image was acquired; next, the pink rectangle was placed on the image, indicating where the sagittal scout image would be acquired. In the same manner, a block of nine pink rectangles was placed on the sagittal scout image to determine where the final nine axial (coronal) images would be collected. Finally, scout

Figure 5. Set-up of magnetic resonance image collection.

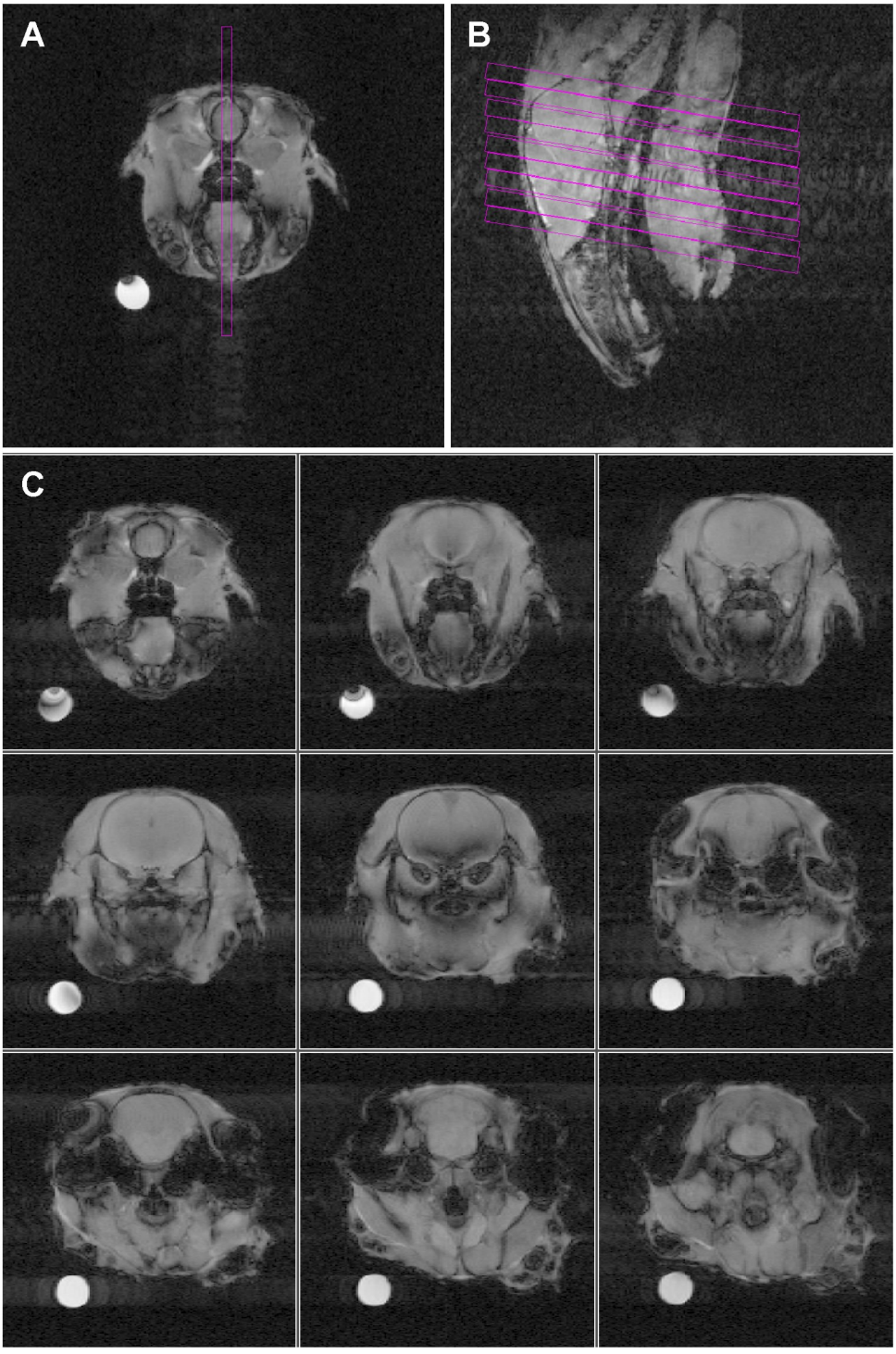

A. Coronal scout image; rectangle indicates slice chosen for sagittal scout image collection. B. Sagittal scout image; rectangles indicate slices chosen for nine coronal scout images (shown in C).

images of the nine axial images were collected to ensure that they were in the proper location before collection of the T_2-weighted images.

2.3.5 Statistical Analysis of MRI Data

MR images were again processed using in-house developed software (Marevisi). Contour plots of T_2 relaxation time were created as before from the multi-echo data sets in order to confirm that the hippocampus remained consistently affected in infected hamsters. In addition, since the presence of a copper sulphate standard allowed for a more reliable method to compare images collected under slightly different experimental conditions, other regions of the brain, corresponding to those examined histologically in the previous study, were evaluated using standard ROIs applied to all images. More specifically, in each of MRI slices 5 and 6, the following regions were identified: the cerebral cortex at the level of the thalamus; the hippocampus; the thalamus; and the hypothalamus. In MRI Slice 7, the lateral ventricles and surrounding area, the septum, and the cerebral cortex at the level of the septum were evaluated. For each MRI slice, a standard set of ROIs was constructed, saved, and applied to all of the images of that slice, in all hamsters and at all time points; these standard ROIs are shown in Figure 6. In order to compare the mean T_2 relaxation time in these regions of interest, this measurement was expressed as a percentage of the mean T_2 relaxation time in the copper sulphate standard in the same image set. For all ROIs other than the hippocampus, the measurements from the standard ROIs were used; however, for comparison of the hippocampus, ROIs identified on the contour plots were used instead.

Figure 6. Regions of interest evaluated by MRI.

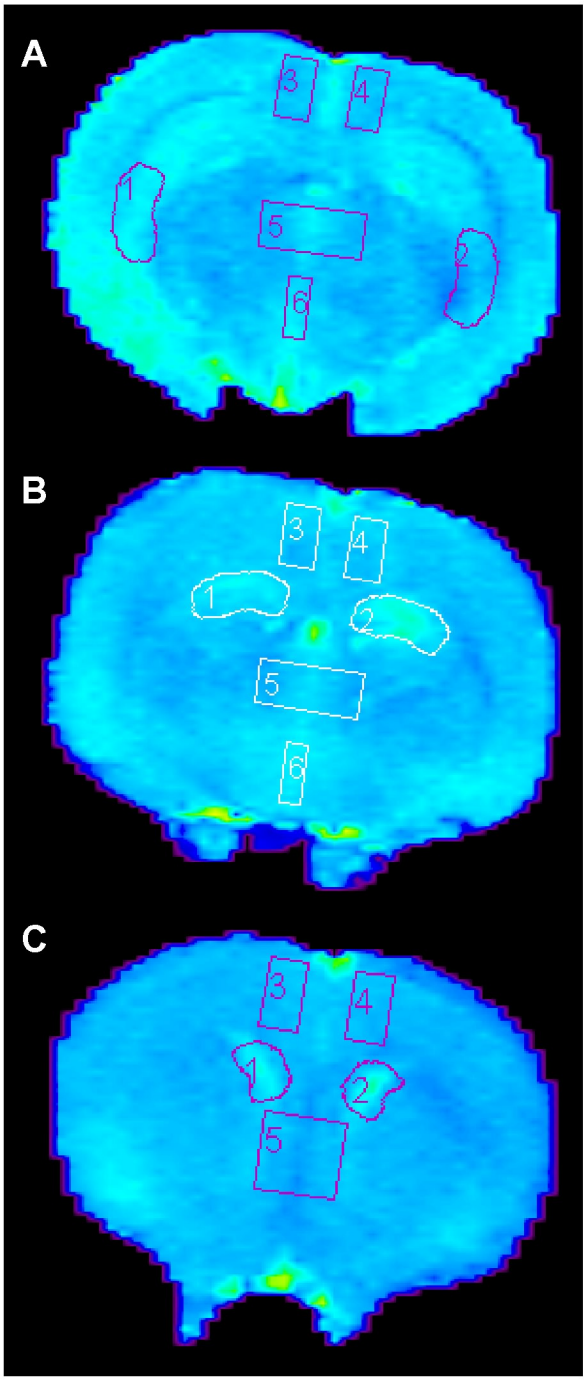

MRI slices 5 (A), 6 (B), and 7 (C) evaluated in pentosan polysulphate treatment study. Hippocampus: 1 and 2 in A and B; cortex: 3 and 4 in A, B, and C; thalamus: 5 in A and B; hypothalamus: 6 in A and B; ventricles and surrounding area: 1 and 2 in C; septum: 5 in C.

At each time point, a multi-way, or factorial, ANOVA with treatment group and brain region as the independent variables, was carried out to compare the corrected T_2 values in each of the regions of interest in all of the treatment groups. In certain instances, comparison by ANOVA was not possible due to heterogeneity of variances between groups. In these cases, groups were compared using the Kruskall-Wallis test. Since it quickly became apparent that i.c. treatment with PPS was confusing the results, by producing hyperintensities in the hippocampus of mock-infected hamsters (see Results section), it was necessary to combine some of the treatment groups in order to produce a more meaningful analysis. As such, scrapie-infected and mock-infected hamsters were each grouped into the following two groups, summarized in Table 2: those that received an i.c. injection of PPS (original i.c. 0 dpi and i.c. 26 dpi treatment groups); and those that did not receive an i.c. injection of PPS (original i.p. 0 dpi; i.p. 26 dpi; i.p. multiple treatments; and no treatment groups). These new groups were not, however, constant; hamsters in the initial i.c. 26 dpi treatment groups were grouped with those that did not receive an i.c. injection of PPS for the first MRI session (19 dpi), and with those that did receive an i.c. injection of PPS from the second MRI session (33 dpi) onward.

2.3.6 Collection of Tissues

Hamsters were euthanized either at about 150 dpi for mock-infected hamsters, or when infected hamsters began to show severe symptoms of scrapie. A cardiac blood draw was carried out using a 12-gauge needle under isoflurane anaesthetic; in cases where enough blood to euthanize the hamster

Table 2. Regrouping of PPS Treatment Groups		
New Groups	19 dpi	33 dpi and later
Scrapie-Infected i.c. PPS	Scrapie-Infected i.c. 0 dpi	Scrapie-Infected i.c. 0 dpi Scrapie-Infected i.c. 26 dpi
Scrapie-Infected No i.c. PPS	Scrapie-Infected i.c. 26 dpi Scrapie-Infected i.p. 0 dpi Scrapie-Infected i.p. 26 dpi Scrapie-Infected i.p. Multiple Scrapie-Infected No Treatment	Scrapie-Infected i.p. 0 dpi Scrapie-Infected i.p. 26 dpi Scrapie-Infected i.p. Multiple Scrapie-Infected No Treatment
Mock-Infected i.c. PPS	Mock-Infected i.c. 0 dpi	Mock-Infected i.c. 0 dpi Mock-Infected i.c. 26 dpi
Mock-Infected No i.c. PPS	Mock-Infected i.c. 26 dpi Mock-Infected i.p. 0 dpi Mock-Infected i.p. 26 dpi Mock-Infected i.p. Multiple Mock-Infected No Treatment	Mock-Infected i.p. 0 dpi Mock-Infected i.p. 26 dpi Mock-Infected i.p. Multiple Mock-Infected No Treatment

PPS: pentosan polysulphate; dpi: days post injection; i.c.: intra-cerebral; i.p.: intra-peritoneal.

was not drawn, an intra-cardiac injection of Euthanol was used. Upon removal, the brain of one hamster from each group was frozen, and stored at -80°C; the brains of the other two hamsters in each group were fixed in formalin and embedded in paraffin for histological examination.

2.3.7 Histological Analysis

Formalin fixed hamster brains were embedded in paraffin; sectioned; and stained as described above. Images of stained slides were also analyzed in the manner described previously in order to quantify histological changes; the method of statistical analysis used was also the same as that described earlier.

2.4 Supplemental Work

2.4.1 Histology Involving C57Bl Mice Infected With ME7 Scrapie

Forty-two-day-old female C57Bl mice were infected intra-cerebrally with 50 μl of 1% brain homogenate from ME7 scrapie-infected mice, and were euthanized when they began to show severe symptoms of scrapie infection around 168 dpi. Age-matched female control mice were not injected, and were euthanized at 170 dpi. Upon removal, brains were either frozen, or fixed in formalin. Formalin-fixed mouse brains were cut, processed, embedded in paraffin, sectioned from paraffin-embedded blocks, stained with haematoxylin and eosin, and photographed as described above.

2.4.2 Evaluation of Spongiform Change

Images of slides of C57Bl mouse brains were used to evaluate the ability of ImagePro software to measure spongiform change. Similarly to the description above, ImagePro was used to evaluate potential vacuoles based on

their size and shape in order to produce a so-called lesion profile; this lesion profile was compared to those reported by Bruce *et. al.* [33] and Fraser and Dickinson [191] in the same mouse strain, with the same infectious agent. The nine brain regions commonly used in lesion profiles [33,191] were examined in a total of seven mice: the cerebral cortex at the levels of the septum and the thalamus; the septum; the hippocampus; the thalamus; the hypothalamus, the superior colliculus; the cerebellum; and the medulla. The size and shape restrictions applied to potential vacuoles were based on those set out by Sutherland *et. al.* [192,193], except that the vacuole size restrictions were based on pixel size, not actual size since this was only a proof-of-concept exercise. Potential vacuoles whose areas fell outside the arbitrary range of 80-5000 pixels, whose aspect ratios exceeded 3, or whose convex hull area to object area ratios exceeded 1.7 were eliminated. Before any measurements were collected or potential vacuoles were excluded, a series of image processing steps was applied to precisely define the boundaries of each object; these image processing steps and the following measurement steps are outlined in Figure 7. The image was converted to greyscale and an intensity threshold was applied, eliminating lower intensity areas of the image, and leaving only potential vacuoles. This thresholded image was copied, and two object counts were carried out using the size and aspect restrictions outlined above: one calculating the object area, and the other the convex hull area of each object. The resulting ratio was then used to further exclude potential objects based on shape. A final score for each region of the brain in each mouse was produced by reporting the

Figure 7. Quantification of spongiform change using ImagePro.

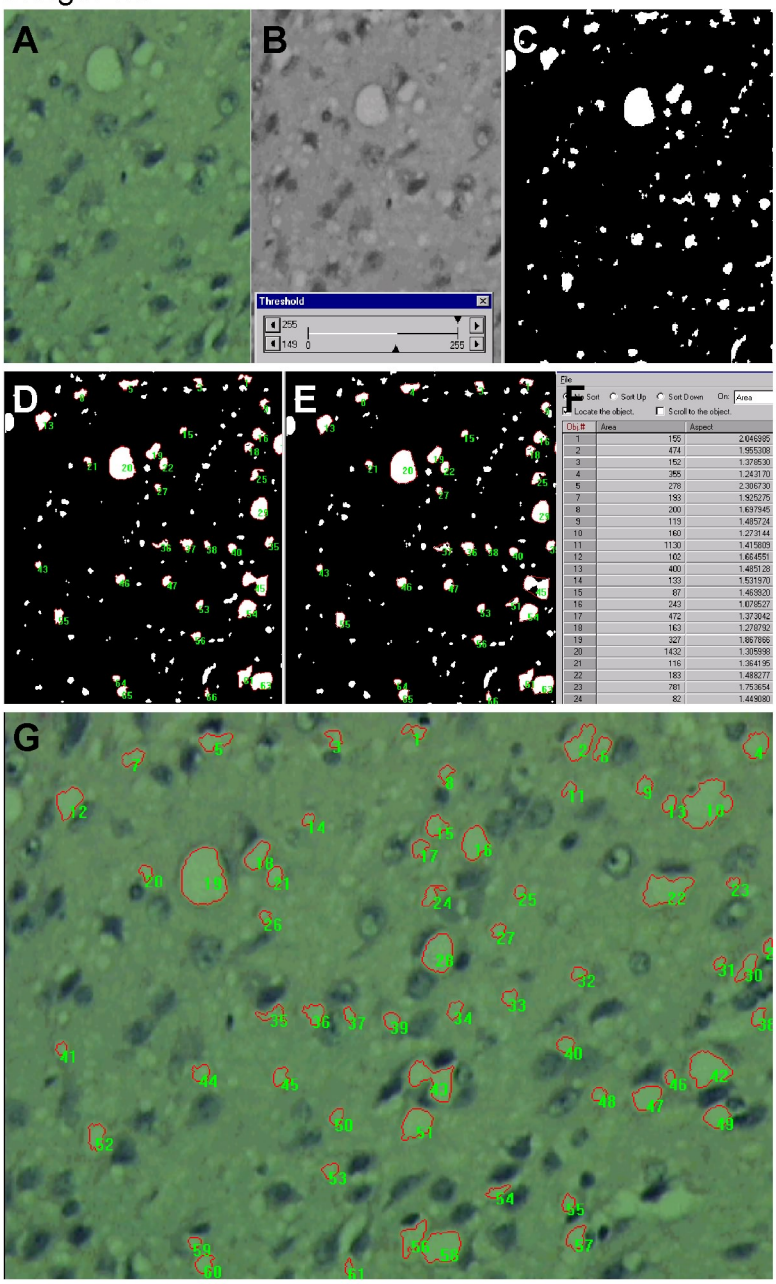

Digital images of haematoxylin and eosin stained sections (A) were converted to greyscale (B), and thresholded for intensity (C). The area of objects (D) and convex hulls of objects (E) were measured, and tabulated (F); the ratio of these measurements was used to exclude some objects from the analysis. Outlines of all of the objects that satisfied the criteria were placed on the original image (G).

total vacuole area, in pixels, from three images from that region of interest. Finally, a lesion profile was produced by taking the mean vacuolation score in each region of interest in the seven mice evaluated, and dividing by 5000; this yielded a set of scores on a scale of 1-5, which is the scale most often used in reporting lesion profiles. It was not always possible to identify all nine regions of interest in each mouse, meaning that the number of mice represented by the mean vacuolation score of a given region was variable, with a maximum of seven.

2.4.3 Pentosan Polysulphate Toxicity Screen

The effects of intra-cerebral pentosan polysulphate injection of rodents have not been reported in great detail. As a result, the initial dose of 20 mg/kg PPS used for i.c. treatment was chosen as essentially an educated guess. Upon injection of the first six mock-infected hamsters at this dose, it was clear that a lower dose would be necessary (see Results). To determine the proper dose, a short experiment was designed in which four different doses of PPS were given to three hamsters each. Hamsters were injected intra-cerebrally as described earlier, with control brain homogenate mixed with PPS at a dose of 0.5 mg/kg; 1 mg/kg; 2 mg/kg; or 5 mg/kg. Following injections, hamsters were monitored for signs of adverse effects for a minimum of one hour; hamsters showing adverse effects were euthanized and dissected to determine the cause of their distress. In order to reduce the number of animals used, the hamsters receiving the dose of PPS chosen as the proper dose were shunted into the main

PPS drug treatment study, becoming the mock-infected group receiving i.c. PPS treatment at 0 dpi.

3. Results

3.1 Magnetic Resonance Imaging - T_2 Changes in Scrapie-Infected Hamsters

Syrian golden hamsters were infected intra-cerebrally with 263K scrapie brain homogenate. Magnetic Resonance Images were collected at 19; 33; 47; and 61 days post injection (dpi), and hamsters were euthanized at 48 or 62 dpi, and hamster brains were removed and frozen. At each imaging time point, a series of nine coronal images was collected (Figure 2). Differences were visually evident between infected hamsters and mock-infected or uninfected controls in slices five and six as early as the first time point studied. Symptoms of disease were not yet evident at the time of euthanasia.

Upon initial visual examination of T_2 maps, hyperintensities were apparent in the hippocampus in slices 5 and 6 in scrapie-infected hamsters. The pixel intensity of T_2-maps reflects the T_2 relaxation time, which varies with specific experimental conditions (e.g. temperature). In order to compare images collected at different times, it was necessary to express the T_2 relaxation time in the region of interest (ROI) in relative terms. It was therefore necessary to find a region or regions of the brain that had broadly consistent T_2 relaxation times across both time and hamster group. This region could then be used to remove some of the variation due to differences in experimental conditions. T_2 relaxation times were measured in different regions in all nine brain slices collected, and compared between hamster groups at all four time points. No single brain region met the ideal criteria of no significant differences between any groups at any of

the four time points. The region that came closest to this ideal was the thalamus in Slice 5. Figure 8 A and B show comparisons of the mean T_2 relation time in the thalami of scrapie-infected, mock-infected, and control hamsters in slices 5 and 6, respectively; in Figure 8 C and D, the thalami in infected and uninfected hamsters are compared. Summaries of the statistical significance of these comparisons at each time point are found in Tables 3 and 4, respectively. Briefly, when all three hamster groups were considered, significant differences were found in the thalamus in Slice 5 only at 47 dpi, when the mock-infected group was significantly different from the other two groups. In Slice 6, significant differences were observed between two or more groups at 33, 47, and 61 dpi. When mock-infected and control hamsters were combined into a single Uninfected group, significant differences were observed in the thalamus in Slice 5 at 61 dpi only; in Slice 6, significant differences were observed at both 33 and 61 dpi, and the differences were more pronounced. As a result, the thalamus in Slice 5 was chosen as the region to be used to produce a relative measurement of T_2 relaxation time in the regions of interest.

Increases in T_2 relaxation time were observed in the hippocampus of infected animals in MRI slices 5 and 6 (Figures 9 and 10, respectively). Contour plots were used to define the ROIs in individual animals, by identifying areas where the T_2 relaxation time changed rapidly. In this way, regions of interest were defined according to the boundaries of the damage observed on the images rather than by simply using some regular shape to artificially define the ROI; this ensured that the ROI would reflect the damage as fully as possible. In control

Figure 8. T_2 relaxation time in the thalamus in MRI slices 5 and 6.

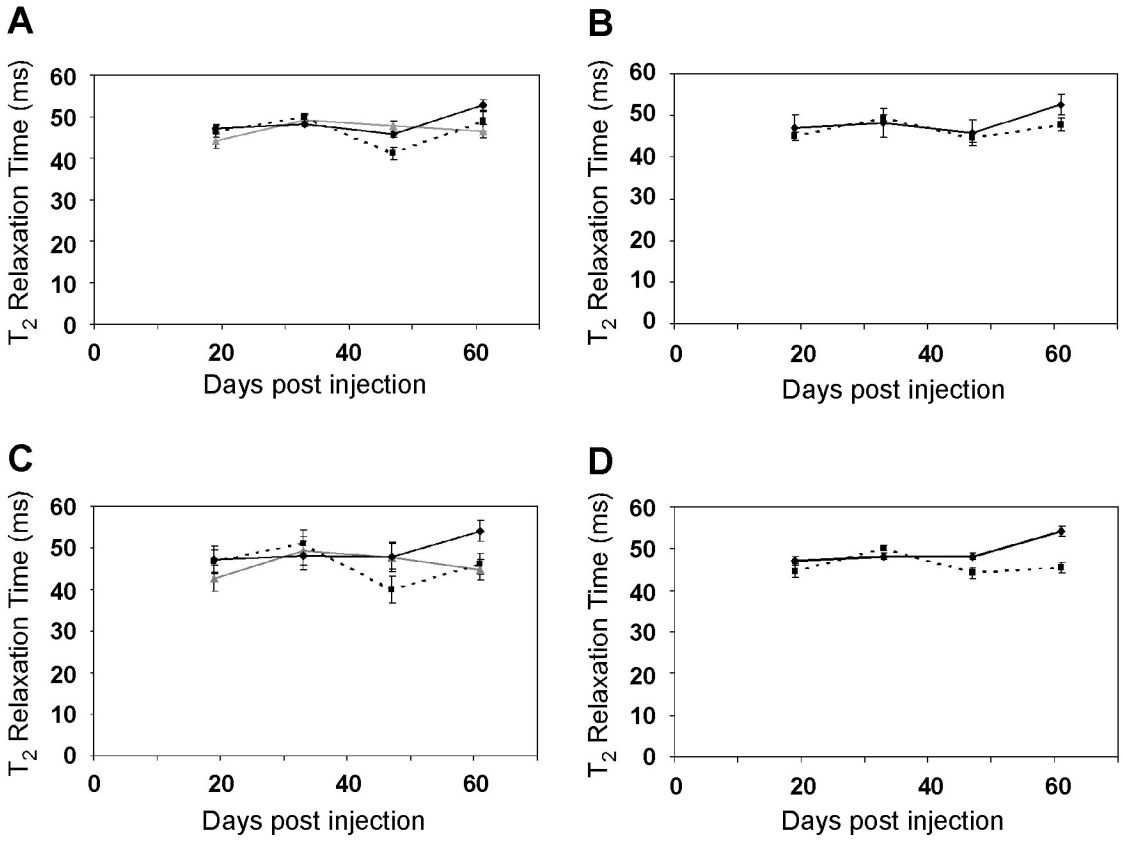

Comparison of T_2 relaxation time in the thalamus in MRI slice 5 (A and B) and slice 6 (C and D). A and C: solid black line: scrapie-infected hamsters; broken black line: mock-infected hamsters; solid grey line: control hamsters. B and D: solid black line: scrapie-infected hamsters; broken black line: uninfected hamsters.

Table 3. T_2 in the Thalamus of Scrapie- and Mock-Infected and Control Hamsters in Slices 5 and 6.					
			p values		
Slice	Dpi	Statistical Test	Scrapie/Control	Scrapie/Mock	Mock/Control
5	19	Kruskall-Wallis	NS	NS	NS
	33	ANOVA	NS	NS	NS
	47	ANOVA	NS	<0.03	<0.002
	61	ANOVA	NS	NS	NS
6	19	Kruskall-Wallis	NS	NS	NS
	33	ANOVA	NS	<0.025	NS
	47	Kruskall-Wallis	NS	<0.025	<0.01
	61	ANOVA	<0.005	<0.015	NS

Dpi: days post injection; NS: no significant differences.

Table 4. T_2 in the Thalamus of Scrapie-Infected and Uninfected Hamsters in Slices 5 and 6.			
			p values
Slice	Dpi	Statistical Test	Scrapie/Control
5	19	t-Test	NS
	33	t-Test	NS
	47	Mann-Whitney u-test	NS
	61	t-Test	<0.05
6	19	t-Test	NS
	33	t-Test	<0.05
	47	Mann-Whitney u-test	NS
	61	t-Test	<0.001

Dpi: days post injection; NS: no significant differences.

Figure 9. T_2 relaxation time in the hippocampus in MRI Slice 5.

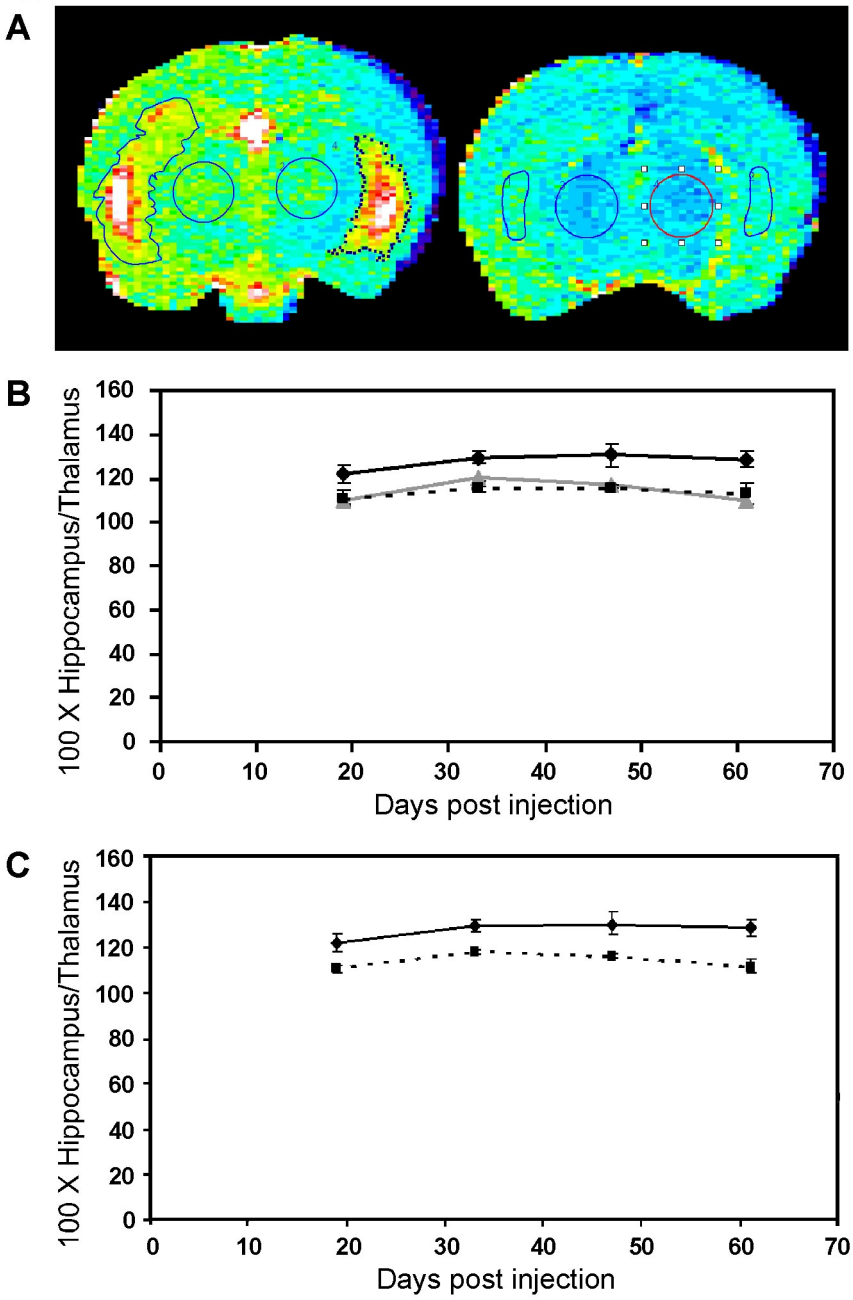

A. False colour T_2 maps of scrapie-infected (left) and uninfected (right) hamsters collected at 61 days post injection (dpi). B. Mean relative T_2 relaxation time in the hippocampus expressed as a percentage of the mean T_2 relaxation time in the thalamus, +/- standard error of the mean (s.e.m.). Solid black line: infected hamsters; broken black line: mock-infected hamsters; solid grey line: control hamsters. C. Mean relative T_2 relaxation time in the hippocampus expressed as a percentage of the mean T_2 relaxation time in the thalamus, +/- standard error of the mean (s.e.m.). Solid black line: scrapie-infected hamsters; broken black line: uninfected hamsters.

Figure 10. T_2 relaxation time in the hippocampus in MRI Slice 6.

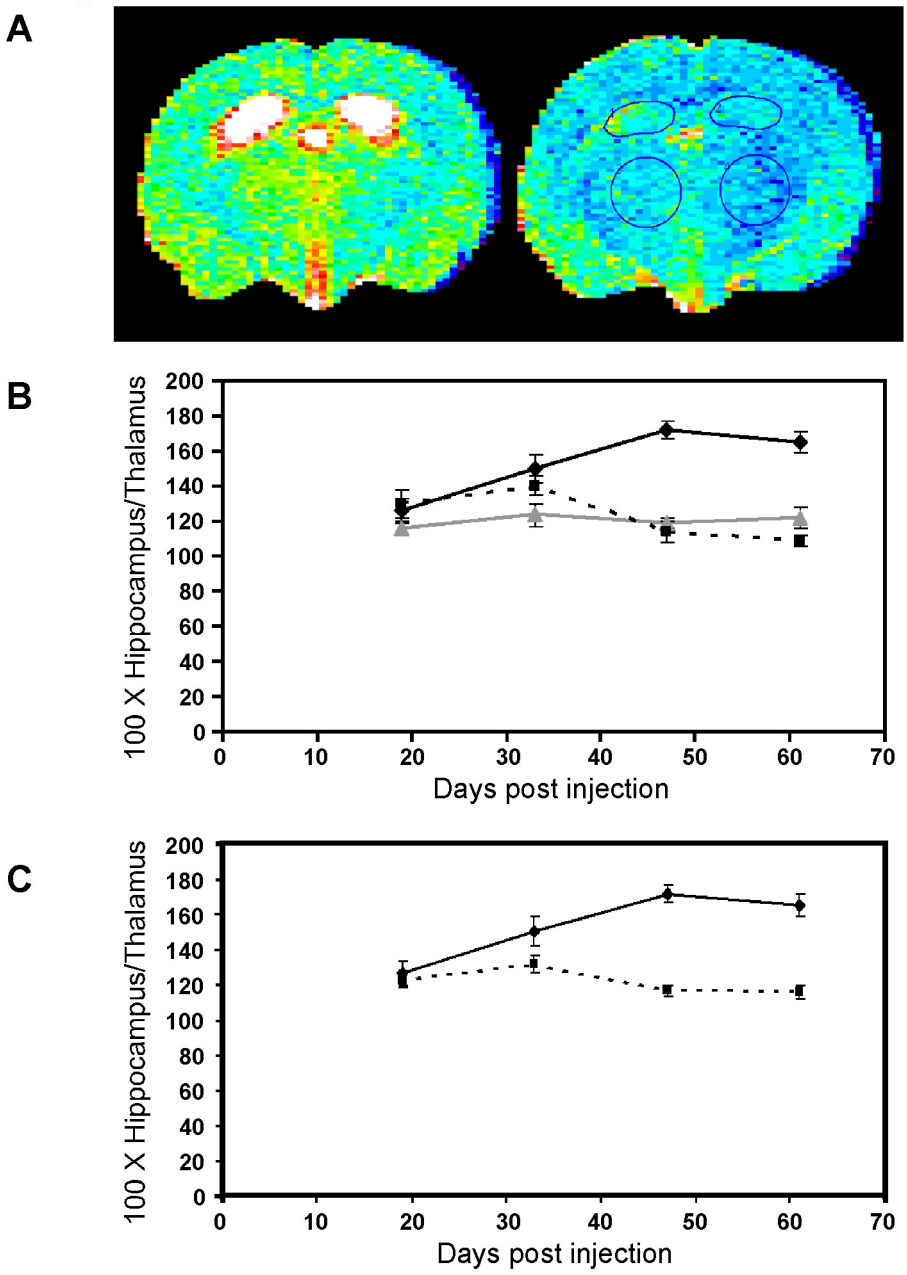

A. False colour T_2 maps of scrapie-infected (left) and uninfected (right) hamsters collected at 61 days post injection (dpi). B. Mean relative T_2 relaxation time in the hippocampus expressed as a percentage of the mean T_2 relaxation time in the thalamus, +/- standard error of the mean (s.e.m.). Solid black line: infected hamsters; broken black line: mock-infected hamsters; solid grey line: control hamsters. C. Mean relative T_2 relaxation time in the hippocampus expressed as a percentage of the mean T_2 relaxation time in the thalamus, +/- standard error of the mean (s.e.m.). Solid black line: scrapie-infected hamsters; broken black line: uninfected hamsters.

and mock-infected hamsters, where contour plots did not identify affected regions, standard ROIs of a smaller size were used for comparison. Since minimal differences were observed in the thalamus in Slice 5 between groups of hamsters at any time point, the T_2 relaxation time in that region of the brain was used as a correction factor to account for differences in experimental conditions during the collection of MR images: the mean T_2 relaxation time in the ROI was expressed as a percentage of that in the thalamus. Actual T_2 relaxation times in affected regions at 61 dpi were on the order of 70 ms in Slice 5 and 90 ms in Slice 6; in the thalamus, T_2 relaxation times measured in the low- to mid-fifties. Increases in T_2 relaxation times are indicative of increased levels of bio-fluid or water in the tissue.

Similarly to the evaluation of T_2 relaxation time in the thalamus, the ROIs in slices 5 and 6 were evaluated by two separate comparisons: first, scrapie-infected hamsters were compared to mock-infected and control hamsters (Figures 9 B and 10 B; Table 5); and second, scrapie-infected hamsters were compared to all uninfected hamsters (Figures 9 C and 10 C; Table 6). The three-way comparison will be considered here first, beginning with the hippocampus in Slice 5. At 19 days post injection (dpi), the difference between the scrapie-infected and control groups was significant ($p<0.03$), although increased variability in infected and mock-infected hamsters resulted in no other significant differences being found. At 33 dpi, the T_2 values of all three groups increased in comparison to those measured at 19 dpi. At this time point the T_2 values of scrapie-infected hamsters were significantly higher than those of mock-infected

Table 5. T_2 in the Hippocampus of Scrapie- and Mock-Infected and Control Hamsters in Slices 5 and 6.					
			p values		
Slice	Dpi	Statistical Test	Scrapie/Control	Scrapie/Mock	Mock/Control
5	19	ANOVA	<0.03	NS	NS
	33	Kruskall-Wallis	NS	<0.001	NS
	47	Kruskall-Wallis	NS	NS	NS
	61	ANOVA	<0.02	<0.03	NS
6	19	ANOVA	NS	NS	NS
	33	ANOVA	<0.03	NS	NS
	47	ANOVA	<0.001	<0.001	NS
	61	ANOVA	<0.001	<0.001	NS

Dpi: days post injection; NS: no significant differences.

Table 6. T_2 in the Hippocampus of Scrapie-Infected and Uninfected Hamsters in Slices 5 and 6.			
			p values
Slice	Dpi	Statistical Test	Scrapie/Control
5	19	t-Test	<0.005
	33	t-Test	<0.001
	47	Mann-Whitney u-test	NS
	61	t-Test	<0.005
6	19	t-Test	NS
	33	t-Test	<0.05
	47	t-Test	<0.001
	61	t-Test	<0.001

Dpi: days post injection; NS: no significant differences.

hamsters ($p<0.001$); there were no other significant differences between groups. No significant differences were observed at 47 dpi, although the separation between the mean T_2 value of infected hamsters (130.59% +/- 5.14, mean +/- standard error of the mean), and those of mock-infected (115.55% +/- 1.94) and control (117.06% +/- 1.14) hamsters remained large. The absence of statistically significant differences in some instances at 33 and 47 dpi could be partially explained by the use of the less sensitive Kruskall-Wallis test for comparison purposes, and by increased variability within some hamster groups. At 61 dpi, the relative T_2 values in infected hamsters were significantly greater than those in mock-infected ($p<0.03$) and control ($p<0.02$) hamsters, while there were no significant differences between control and mock-infected hamsters.

The differences between scrapie-infected and the other two hamster groups were more pronounced in MRI Slice 6 at 47 and 61 dpi. At these time points, infected hamsters had significantly higher relative T_2 values than both mock-infected and control hamsters ($p<0.001$ in all cases), while there were no significant differences between the latter two groups at either time point. At 33 dpi, the only significant differences were between scrapie-infected hamsters and un-injected controls ($p<0.03$); mock-infected hamsters yielded T_2 scores of intermediate value. No significant differences were observed at 19 dpi.

Taking MRI slices 5 and 6 into consideration together, differences between scrapie-infected hamsters and both uninfected controls and mock-infected hamsters were statistically significant at 33, 47, and 61 dpi; at 19 dpi, scrapie-infected hamsters could be distinguished from controls only. At 19 dpi,

significant differences between scrapie-infected and control hamsters were observed in Slice 5, while no differences were found in Slice 6. At 33 dpi, scrapie-infected hamsters could be distinguished from mock-infected hamsters in Slice 5, and from control hamsters in Slice 6. The hippocampus in scrapie-infected hamsters was significantly different from both mock-infected and control hamsters in Slice 6 at 47 dpi, while no significant differences were observed in Slice 5. At 61 dpi, scrapie-infected hamsters could be differentiated from the other two hamster groups in both slices 5 and 6. No significant differences were ever observed between mock-infected and control hamsters in either slice at any time point.

Because differences between the T_2 measurements in the hippocampus of mock-infected and control hamsters in slices 5 and 6 were never significant, a second evaluation was made in which these two groups were combined to form a group named “Uninfected”. At 19 dpi, significant differences existed between scrapie-infected and uninfected hamsters in Slice 5 ($p<0.005$), but not Slice 6. At 47 dpi, these differences were significant in Slice 6 ($p<0.001$) but not in Slice 5. Significant differences were observed between the two groups at 33 and 61 dpi in both Slice 5 ($p<0.001$ at 33 dpi; $p<0.005$ at 61 dpi) and Slice 6 ($p<0.05$ at 33 dpi; $p<0.001$ at 61 dpi). It was possible to distinguish between scrapie-infected and uninfected hamsters at each of the four time points studied in one or both of slices 5 and 6.

3.2 Apparent Diffusion Coefficient Magnetic Resonance Imaging

Diffusion-weighted MR images were also collected, and the resulting apparent diffusion coefficient (ADC) MR maps were compared to T_2-maps (Figure 11). It was determined that regions with increased relative T_2 values (hyper-intensities in the hippocampus in slices 5 and 6) corresponded to increased ADC values, supporting the assertion that image abnormalities are the result of fluid accumulation in the hippocampus. In infected hamsters at 61 dpi, ADC values in the hippocampus were in the range of 1×10^{-3} mm^2/s with a high of 1.21×10^{-3} mm^2/s in Slice 5; and 1.45×10^{-3} mm^2/s with a high of 1.71×10^{-3} mm^2/s in Slice 6. In control and mock-infected hamsters, the highest single ADC value in the hippocampus at 61 dpi was 8.85×10^{-4} mm^2/s in Slice 5 and 1.20×10^{-3} mm^2/s in Slice 6.

Despite these apparent differences, it was necessary to compare relative values in the same manner as the comparison of T_2 relaxation time. As before, the regions of interest in the thalamus in MR slices 5 and 6 were evaluated for their suitability to produce relative scores for apparent diffusion coefficient. Figure 12 shows comparisons of raw ADC scores in the thalamus in slices 5 and 6, either as a three-way comparison involving scrapie-infected, mock-infected and control hamsters, or as a two-way comparison of infected and all uninfected hamsters. Summaries of statistical significance of these two comparisons are found in Tables 7 and 8, respectively. Briefly, in each comparison, there were an equal number of instances in which statistically significant differences were found between infected and other hamsters in each of slices 5 and 6. Because the

Figure 11. T_2 relaxation time and apparent diffusion coefficient over time in a scrapie-infected hamster.

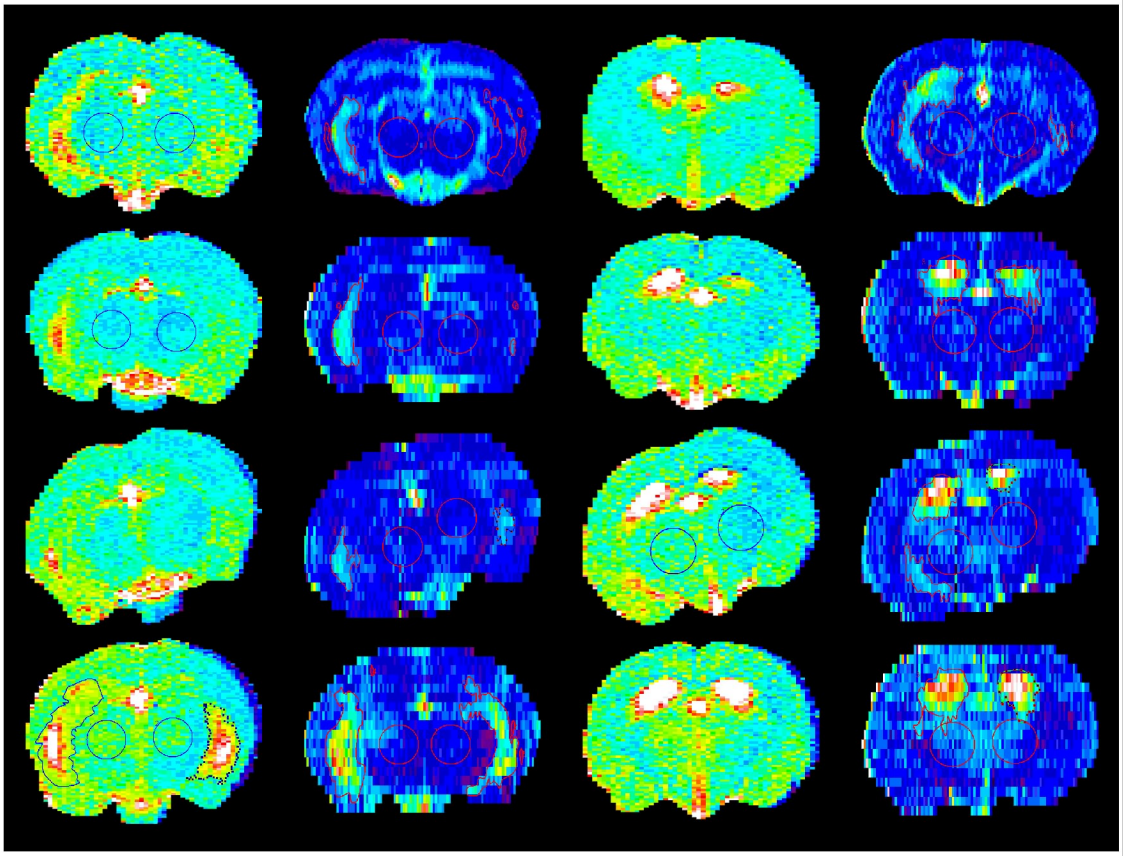

First column: slice 5 false colour T_2 maps; second column: slice 5 false colour ADC maps; third column: slice 6 false colour T_2 maps; fourth column: slice 6 false colour ADC maps. Rows 1-4: images collected at 19, 33, 47, and 61 days post injection, respectively. Circles represent regions of interest in the thalamus used to produce relative values.

Figure 12. Apparent diffusion coefficient in the thalamus in MRI slices 5 and 6.

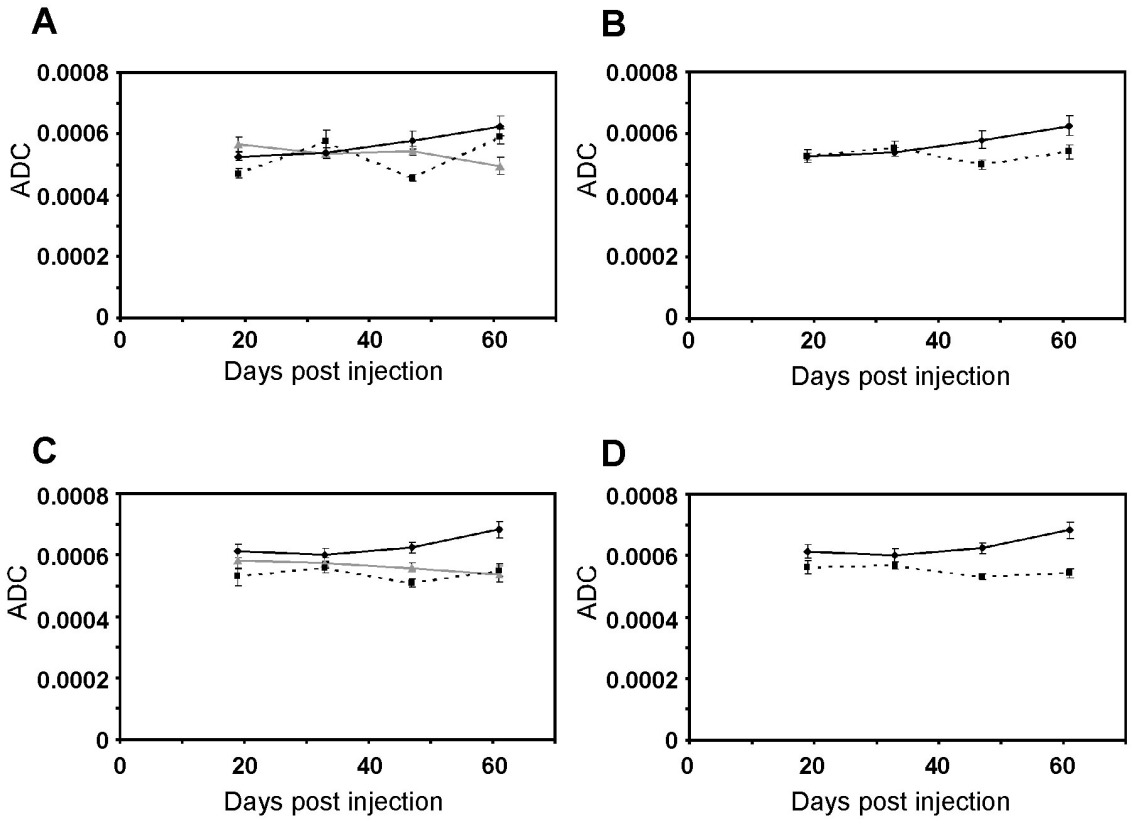

Comparison of apparent diffusion coefficient (ADC) in the thalamus in MRI slice 5 (A and B) and slice 6 (C and D). A and C: solid black line: scrapie-infected hamsters; broken black line: mock-infected hamsters; solid grey line: control hamsters. B and D: solid black line: scrapie-infected hamsters; broken black line: uninfected hamsters.

Table 7. ADC in the Thalamus of Scrapie- and Mock-Infected and Control Hamsters in Slices 5 and 6.					
			p values		
Slice	Dpi	Statistical Test	Scrapie/Control	Scrapie/Mock	Mock/Control
5	19	ANOVA	NS	NS	<0.01
	33	ANOVA	NS	NS	NS
	47	ANOVA	NS	<0.002	<0.03
	61	ANOVA	<0.015	NS	NS
6	19	ANOVA	NS	NS	NS
	33	ANOVA	NS	NS	NS
	47	ANOVA	<0.015	<0.001	NS
	61	ANOVA	<0.005	<0.01	NS

Dpi: days post injection; NS: no significant differences.

Table 8. ADC in the Thalamus of Scrapie-Infected and Uninfected Hamsters in Slices 5 and 6.			
			p values
Slice	Dpi	Statistical Test	Scrapie/Control
5	19	Mann-Whitney u-test	NS
	33	Mann-Whitney u-test	NS
	47	t-test	<0.015
	61	t-test	<0.05
6	19	t-test	NS
	33	t-test	NS
	47	t-test	<0.001
	61	t-test	<0.001

Dpi: days post injection; NS: no significant differences.

thalamus in neither slice was clearly better suited to produce relative ADC scores, it was determined that for the regions of interest (the hippocampus in slices 5 and 6), the score would be produced by dividing by the measurement in the thalamus on the same side of the brain in the same slice.

When all three groups of hamsters were compared very few significant differences were found (Figure 13 A and B, Table 9). In fact, the only statistical differences were between scrapie-infected and mock-infected hamsters at 33 and 47 dpi in Slice 5, and at 61 dpi in Slice 6. However, when the graphs are examined more closely, certain trends become evident, even if significant differences were not observed. In both of slices 5 and 6, the relative ADC scores in the hippocampus of scrapie-infected hamsters increased over the course of the experiment. The slope of the curve was greater in Slice 6 between 19 and 47 dpi, before reaching a plateau, which was maintained between 47 and 61 dpi. The increase in ADC scores was more gradual in Slice 5, although it was maintained over the entire time period. In comparison, both mock-infected and control scores in Slice 5 remained essentially constant over the course of study, with a slight decrease being the general trend. In Slice 6, control hamsters maintained constant ADC scores from 19-47 dpi before dipping at 61 dpi. The scores from mock-infected hamsters in Slice 6 were the most variable, fluctuating up and down over the course of the study.

When scrapie-infected hamsters were compared to all uninfected hamsters, there were significant differences at all four time points studied (Figure 13 C and D, Table 10). In Slice 5, the relative ADC scores in the hippocampus of

Figure 13. Apparent diffusion coefficient in the hippocampus in MRI slices 5 and 6.

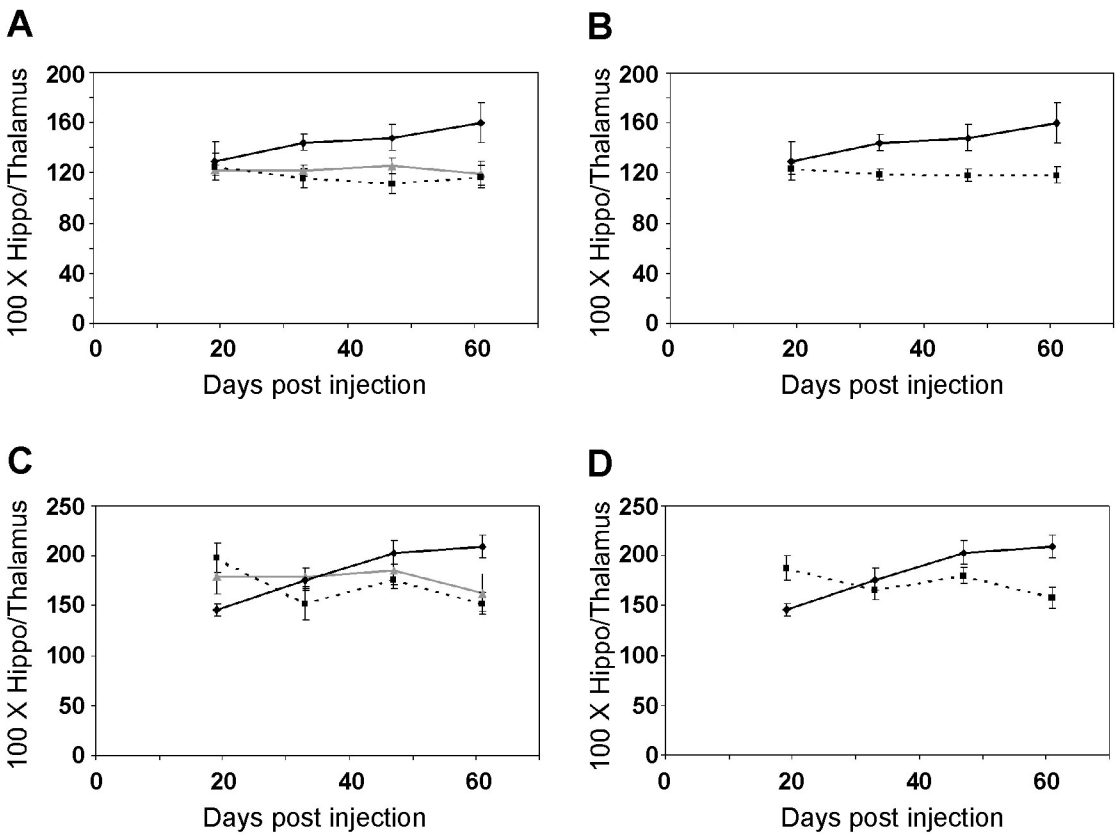

Comparison of relative apparent diffusion coefficient (ADC) values in the hippocampus, expressed as a percentage of ADC in the thalamus, in MRI slice 5 (A and B) and slice 6 (C and D). A and C: solid black line: scrapie-infected hamsters; broken black line: mock-infected hamsters; solid grey line: control hamsters. B and D: solid black line: scrapie-infected hamsters; broken black line: uninfected hamsters. Hippo: Hippocampus.

Table 9. ADC in the Hippocampus of Scrapie- and Mock-Infected and Control Hamsters in Slices 5 and 6.					
			p values		
Slice	Dpi	Statistical Test	Scrapie/Control	Scrapie/Mock	Mock/Control
5	19	ANOVA	NS	NS	NS
	33	ANOVA	NS	<0.02	NS
	47	ANOVA	NS	<0.02	NS
	61	ANOVA	NS	NS	NS
6	19	ANOVA	NS	NS	NS
	33	ANOVA	NS	NS	NS
	47	Kruskall-Wallis	NS	NS	NS
	61	ANOVA	NS	<0.05	NS

Dpi: days post injection; NS: no significant differences.

Table 10. ADC in the Hippocampus of Scrapie-Infected and Uninfected Hamsters in Slices 5 and 6.			
			p values
Slice	Dpi	Statistical Test	Scrapie/Control
5	19	Mann-Whitney u-test	NS
	33	t-test	<0.01
	47	t-test	<0.01
	61	t-test	<0.01
6	19	t-test	<0.03
	33	t-test	NS
	47	t-test	NS
	61	t-test	<0.01

Dpi: days post injection; NS: no significant differences.

infected hamsters were significantly greater than those of uninfected hamsters at 33 ($p<0.001$), 47 ($p<0.001$), and 61 dpi ($p<0.03$). In Slice 6, the hippocampus of infected hamsters had a significantly higher ADC score than in uninfected hamsters at 61 dpi ($p<0.01$), but a significantly lower ADC score at 19 dpi ($p<0.03$).

The differences in relative ADC values between hamster groups were not as pronounced as in the case of relative T_2 values. However, this may not tell the whole story. When the relative T_2 and ADC values in the hippocampus of scrapie-infected hamsters were compared in each of Slices 5 and 6, the curves exhibited striking similarities (Figure 14). At 19, 33, and 47 dpi relative ADC values in infected hamsters closely mirror the corresponding T_2 values. At 61 dpi, T_2 values in both MRI slices dip slightly; at the same time, the slope of the ADC curve increases in Slice 5, and decreases in Slice 6, although the ADC values continue to rise in both slices. This observed close agreement between relative T_2 and ADC values in scrapie-infected hamsters supports a common cause for the two effects. In order to confirm the diseased state of scrapie-infected hamsters, brain tissue from some infected and control hamsters was collected for Western blotting. As seen in Figure 15, PrP from individual scrapie-infected hamsters (including Slices 5 and 6) was partially resistant to proteinase K (PK) digestion, confirming the presence of PrP^{Sc}.

3.3 Measuring Histological Changes

In order to explore the causes of scrapie-induced changes on MR images of hamster brains, different brain regions were examined at each time point for

Figure 14. Comparison of T_2 relaxation time and apparent diffusion coefficient in scrapie-infected hamsters.

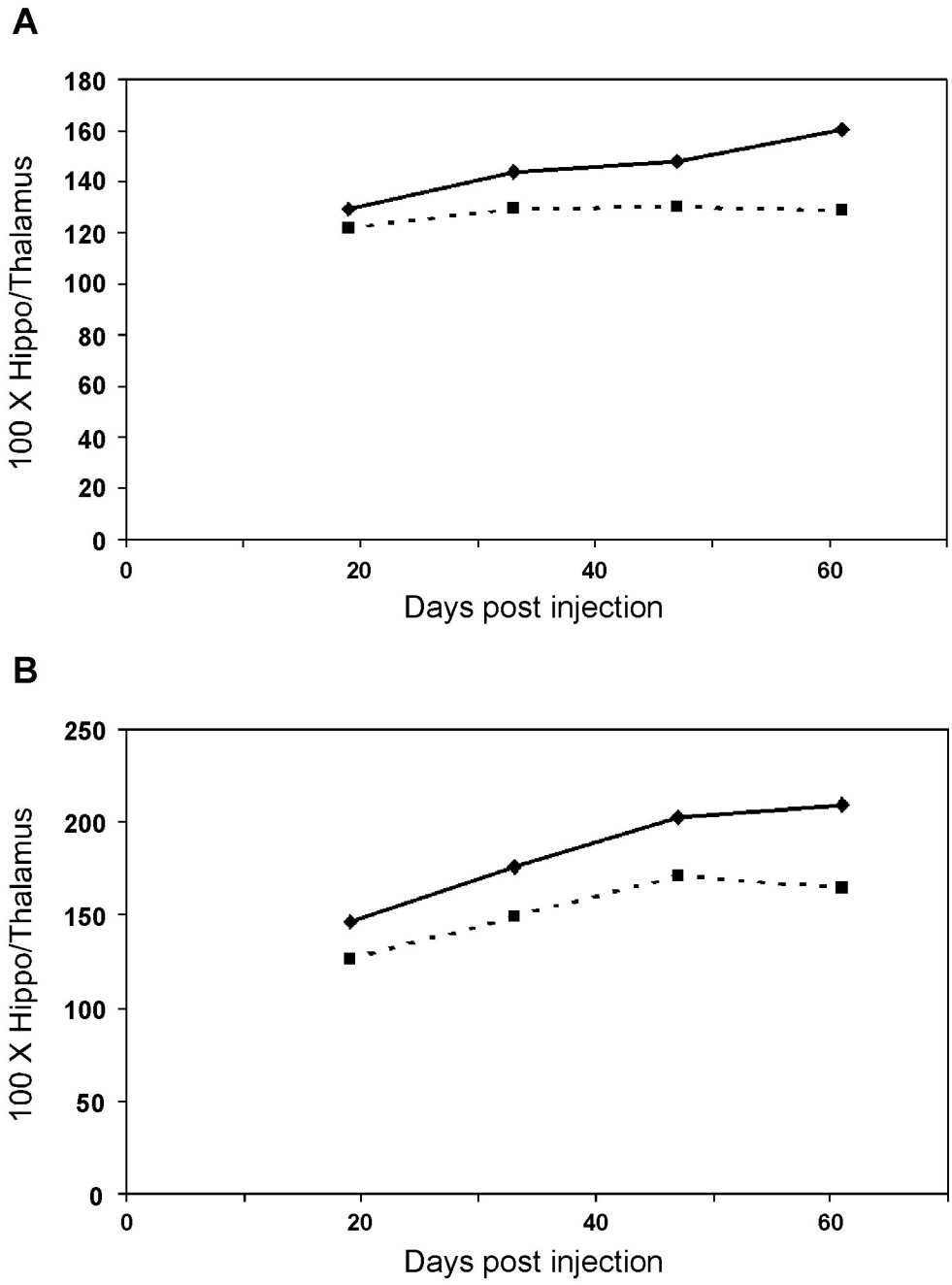

Relative T_2 and apparent diffusion coefficient (ADC) values are compared in MRI slice 5 (A) and slice 6 (B). Solid black line: ADC; broken black line: T_2. Hippo: hippocampus.

Figure 15. Western blot of scrapie-infected and uninfected hamster brain tissue at 62 dpi.

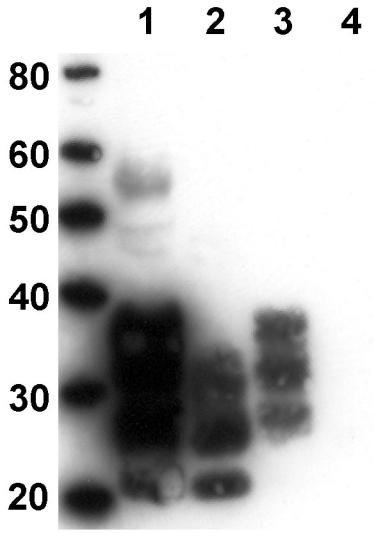

Lanes 1 and 2: scrapie-infected brain tissue; lanes 3 and 4: uninfected brain tissue; lanes 2 and 4: samples have been digested with proteinase K. Left-most lane: standard, band sizes marked in kDa.

three histological hallmarks of prion disease: spongiform change; accumulation of PrP^{Sc}; and gliosis (Figure 16). The hippocampus was one region chosen, along with three regions where no obvious differences were observed between infected, mock-infected, and control hamsters on MR images: the cerebral cortex at the level of the thalamus; the thalamus; and the hypothalamus. All four of these regions are part of the lesion profile commonly used to evaluate spongiform change in rodents with prion disease. Qualitatively, it appeared that the thalamus was the region most affected histologically, particularly by spongiform change and PrP^{Sc} deposition. In order to make a quantitative assessment, images of histological slides were evaluated using imaging software, allowing measurements of vacuolation, accumulation of PrP^{Sc}, and gliosis to be collected. Since mock-infected and control hamsters yielded similar results on MRI, they were assembled into a single "Uninfected" group for the purpose of histological examination.

3.3.1 Evaluation of ImagePro Software as a Means of Measuring Spongiform Change

Before it could be used for the purpose of measuring the hallmarks of prion disease in hamsters, it was necessary to evaluate the imaging software to determine its suitability to the task. In order to do this, it was used to measure spongiform change only in the nine regions of grey matter that typically make up the lesion profile in C57Bl mice infected with the ME7 strain of scrapie. This is a well-established rodent model of prion disease, with published lesion profiles that could be compared to the results produced using ImagePro software.

Figure 16. Histology in scrapie-infected and uninfected hamsters at 61 dpi.

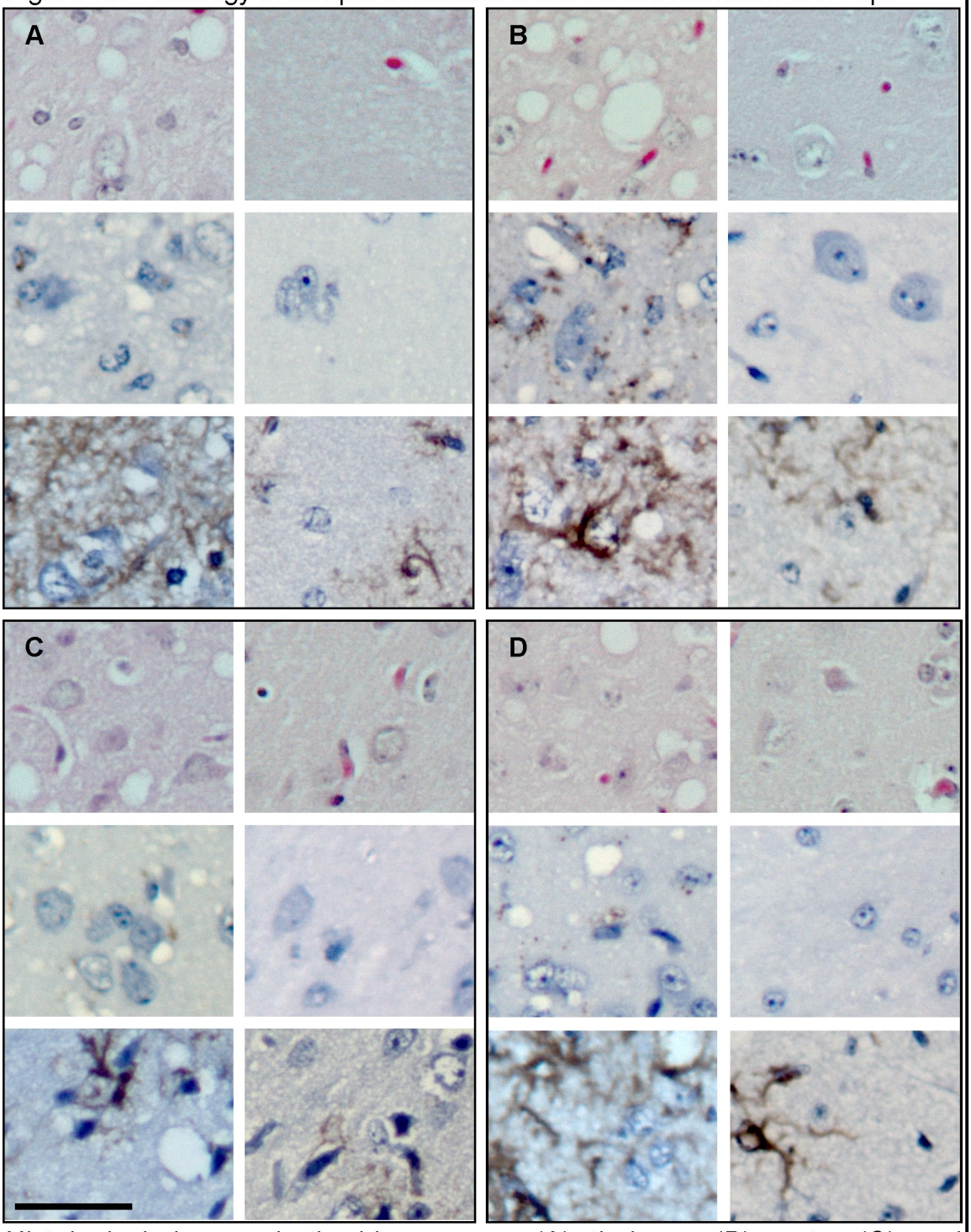

Histological changes in the hippocampus (A), thalamus (B), cortex (C), and hypothalamus (D) of scrapie-infected (first and third columns) and uninfected (second and fourth columns) hamsters at 61 days post injection (dpi). Haematoxylin and eosin staining for vacuoles: first and fourth rows; immunohistochemistry for PrP (second and fifth rows), and GFAP (third and sixth rows). Size bar = 50 microns.

Figure 17 B, taken with permission from Fraser and Dickinson [191], shows the nine regions of the lesion profile: the medulla; the cerebellum; the superior colliculus; the hypothalamus; the thalamus; the hippocampus; the septum; the medial cerebral cortex at the level of the thalamus; and the medial cerebral cortex at the level of the septum. In Figure 17 A, the lesion profile measured using ImagePro is compared to a composite lesion profile produced by taking the mean value in each region of the profile of those reported by Fraser and Dickinson [191] and by Bruce *et. al.* [33]. In both of these papers, a subjective score of 0-5 was used, with each value corresponding to a verbal description. In contrast, the results presented here measured vacuoles in pixels, producing a total vacuole area score/image for each mouse, which was used in turn to produce a mean score for each region. These scores ranged to a maximum of about 23000 pixels, which allowed them to be easily converted to a 0-5 scale by dividing each score by 5000.

The general shape of the measured lesion profile agrees broadly with the composite profile from the literature, however, the literature values in the middle of the profile in particular are lower. These regions also represent the areas with the highest vacuolation scores, both in the literature and in the measured values. Given that the two profiles have been artificially placed on the same scale, it is possible that differences in the true scales could account for some of the differences in value. As such, the actual scores in the different brain regions are of somewhat less importance than the shape of the profile.

Figure 17. Evaluation of ImagePro software as a means to quantify spongiform change.

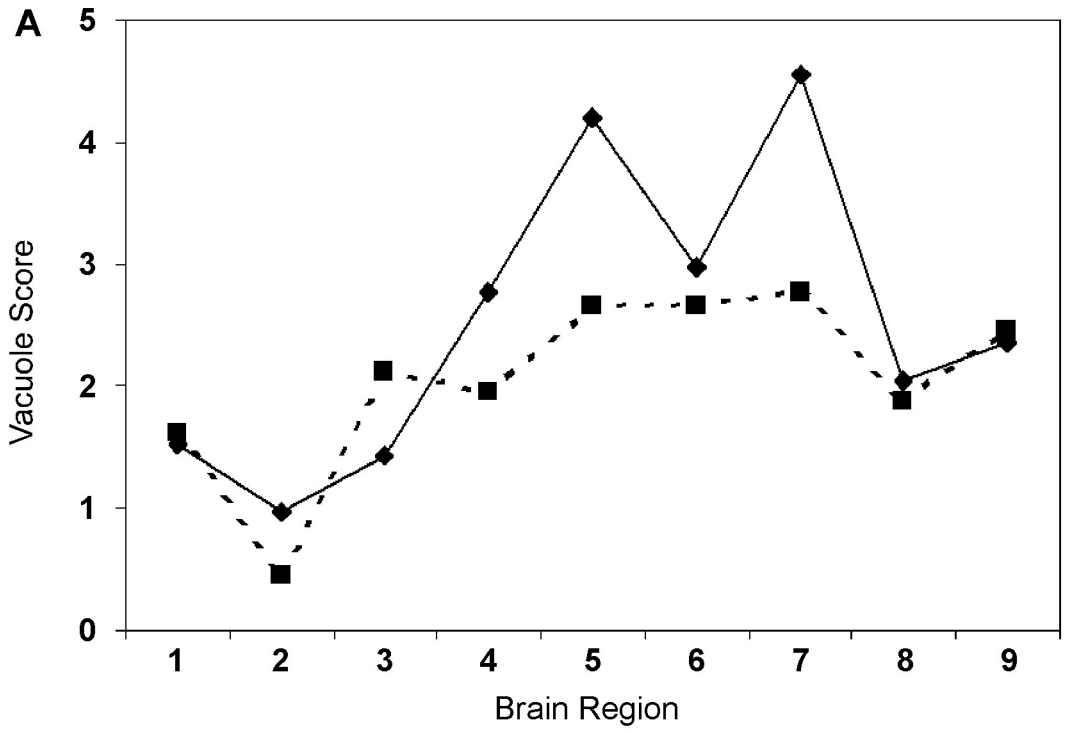

A. Lesion profiles of C57Bl mice infected with ME7 scrapie produced using ImagePro software (solid line) and by averaging two lesion profiles in the literature (broken black line) [33,270] are compared. Scale: subjective 0-5 scale used for literature profiles; total vacuole area per image/5000 for ImagePro profile. B. Illustration of the brain regions that compose the lesion profile, used with permission [270]. Brain Regions: 1: medulla; 2: cerebellum; 3: superior colliculus; 4: hypothalamus; 5: thalamus; 6: hippocampus; 7: septum; 8: cortex at the level of the thalamus; 9: cortex at the level of the septum.

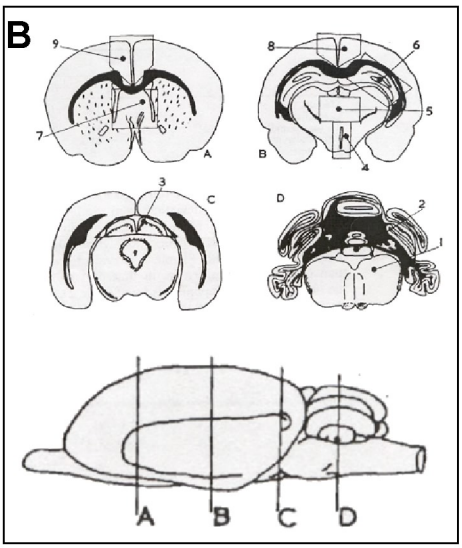

The first segment of the measured lesion profile, spanning regions one to four, matches the shape of the literature profile closely. The one exception is the transition from region three (the superior colliculus) to four (the hypothalamus), where, rather than decreasing, the vacuolation score increases. In the second segment of the lesion profile, spanning regions four to seven, the only difference in shape between the two curves is the significant dip in region six (the hippocampus) in the ImagePro lesion profile. In the final segment, spanning regions seven to nine, agreement between the two lesion profiles is very good. Overall, the shape of the ImagePro lesion profile agrees very well with that of the profile found in the literature, with the exception of an apparent under-valuation of spongiform change in regions three and six (the superior colliculus and the hippocampus). Given these minor differences, it was determined that the ImagePro system, with further refinement, would be a good means of evaluating the histological hallmarks of prion disease in hamsters.

3.3.2 Histological Changes in Scrapie-Infected Hamsters

The procedure for measuring spongiform change using ImagePro was improved as described in the Materials and Methods section, and corresponding protocols for measuring PrP^{Sc} deposition and gliosis were developed. Measurements of these three histological characteristics were collected, and comparisons between infected and uninfected hamsters in the four regions of interest at 19, 33, 47, and 61 dpi, are shown in Figure 18. Instances of statistical significance are summarized in Table 11. At the first two time points, the only comparison that was statistically significant was the measurement of GFAP in the

Figure 18. Histological changes in scrapie-infected and uninfected hamsters at 19, 33, 47, and 61 days post infection.

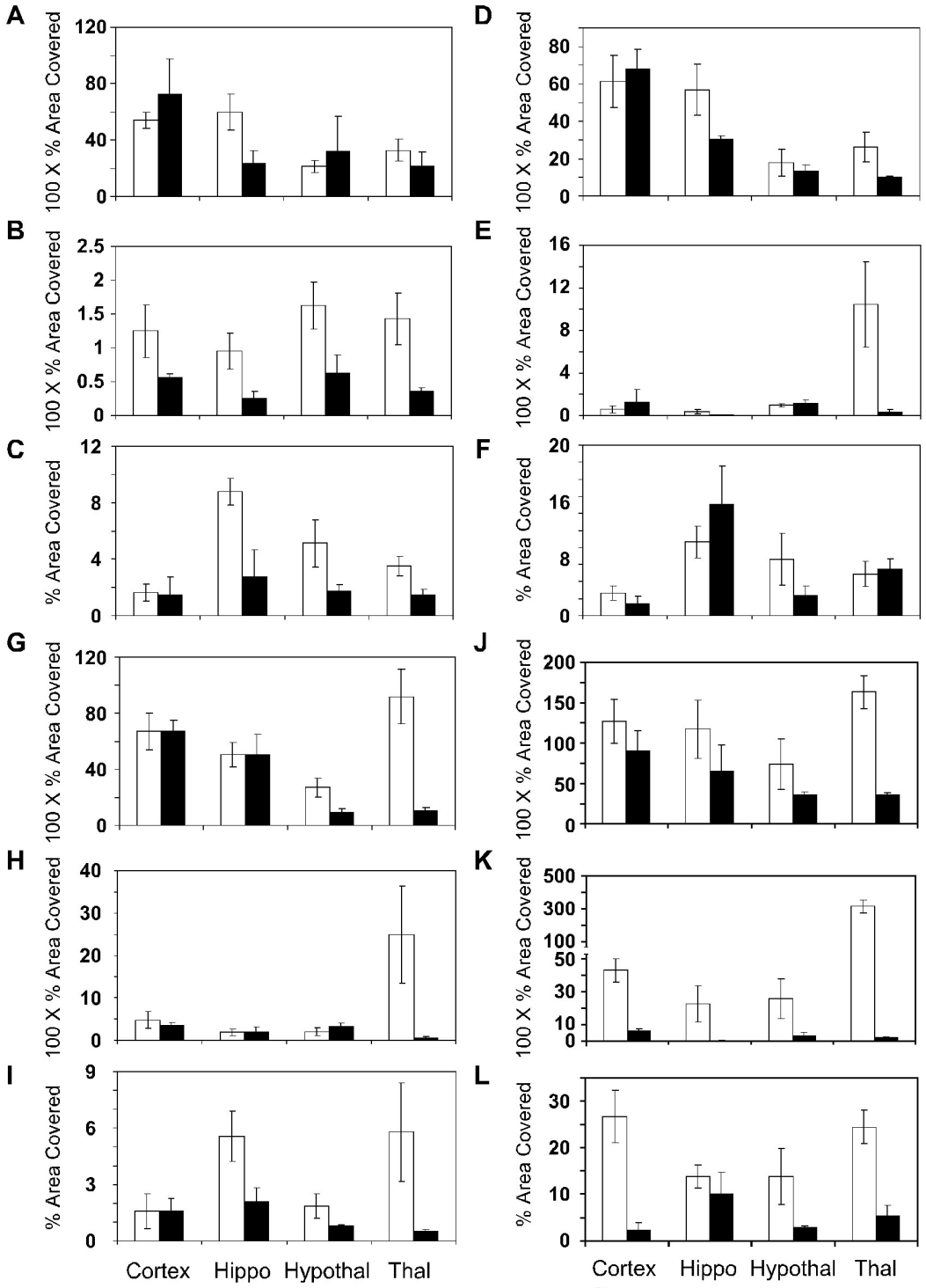

Comparison of levels of total vacuole area (A,D,G,J), PrP^{Sc} deposition (B,E,H,K), and gliosis (C,F,I,L) at 19 (A-C), 33 (D-F), 47 (G-I), and 61 (J-L) days post infection. Scrapie-infected hamsters: white bars; uninfected hamsters: black bars. Mean +/- standard error of the mean (s.e.m). Hippo: Hippocampus; hypothal: hypothalamus; thal: thalamus.

Table 11. Comparison of Histology in Scrapie-Infected and Uninfected Hamsters.				
	19 days post injection			
	p values			
	Cortex	Hippocampus	Hypothalamus	Thalamus
Vacuole Area	NS	NS	NS	NS
# of Vacuoles	NS	NS	NS	NS
PrP^{Sc}	NS	NS	NS	NS
Gliosis	NS	<0.025	NS	NS
	33 days post injection			
	p values			
	Cortex	Hippocampus	Hypothalamus	Thalamus
Vacuole Area	NS	NS	NS	NS
# of Vacuoles	NS	NS	NS	NS
PrP^{Sc}	NS	NS	NS	NS
Gliosis	NS	NS	NS	NS
	47 days post injection			
	p values			
	Cortex	Hippocampus	Hypothalamus	Thalamus
Vacuole Area	NS	NS	NS	NS (<0.06)
# of Vacuoles	NS	NS	NS	NS (<0.07)
PrP^{Sc}	NS	NS	NS	<0.01
Gliosis	NS	NS	NS	NS (<0.08)
	61 days post injection			
	p values			
	Cortex	Hippocampus	Hypothalamus	Thalamus
Vacuole Area	NS	NS	NS	<0.015
# of Vacuoles	NS	NS	NS	<0.02
PrP^{Sc}	0.03	0.0399	NS	<0.001
Gliosis	0.0497	NS	NS	<0.03

NS: no significant differences.

hippocampus at 19 dpi ($p<0.025$). This is indicative that at this stage, the levels of each histological characteristic measured represent essentially the background levels inherent to the system. Having said that, at 19 dpi, infected hamsters had consistently higher levels of PrP^{Sc} deposition across all brain regions studied, although these differences were not statistically significant. There was a sizable difference in PrP^{Sc} deposition in the thalamus of infected, compared to uninfected hamsters at 33 dpi, although this difference was not significant, due to the high degree of variability in the infected group. At 47 dpi, the only statistically significant difference between infected and uninfected hamsters was once again observed in PrP^{Sc} deposition in the thalamus ($p<0.01$). However, differences in the other histological hallmarks approached statistical significance in the thalamus ($p<0.06$ for vacuole area; $p<0.07$ for vacuole number; and $p<0.08$ for GFAP). At 61 dpi, the thalamus was once again the region most affected, but by this time point significant differences were observed in all histological characteristics: $p<0.015$ for percentage of tissue covered by vacuoles; $p<0.02$ for number of vacuoles; $p<0.03$ for GFAP; and $p<0.001$ for PrP^{Sc} deposition. Other significant differences were observed in gliosis in the cortex ($p<0.05$) and in PrP^{Sc} deposition in the cortex and the hippocampus ($p<0.05$ in both cases). These data suggest that the thalamus is the first of the brain regions studied to experience all of the histological hallmarks of prion disease, and that PrP^{Sc} deposition precedes both spongiform change and gliosis. Under this supposition, the cortex appears to be slightly ahead of the

hippocampus in terms of the progression of hallmarks of disease, and that the hypothalamus lags further behind.

When the four brain regions of interest were compared in infected hamsters only, at least some significant differences were observed between brain regions at all time points. At 19 dpi, GFAP staining was significantly higher in the hippocampus than in the cortex ($p<0.002$) and the thalamus ($p<0.015$). The number of vacuoles in the cortex was significantly greater than in the hypothalamus and the thalamus ($p<0.05$ in both cases), while the area covered by vacuoles in the hippocampus was significantly greater than in the hypothalamus ($p<0.025$).

Beginning at 33 dpi, no further differences were observed in GFAP staining, although PrP^{Sc} deposition in the thalamus was significantly greater than in all other brain regions studied ($p<0.005$ cortex; $p<0.03$ hippocampus; $p<0.05$ hypothalamus). The area covered by vacuoles in the hypothalamus was significantly lower than in the cortex ($p<0.05$) and the hippocampus ($p<0.03$), although no significant differences were observed in the number of vacuoles in different brain regions. At 47 dpi, PrP^{Sc} deposition in the thalamus was significantly greater than in the hippocampus ($p<0.01$) and the hypothalamus (p0.015). Vacuole number was significantly lower in the hypothalamus than in the thalamus ($p<0.05$), while vacuole area in the hypothalamus was significantly lower than in both the cortex ($p<0.05$) and the thalamus ($p<0.01$). At 61 dpi, PrP^{Sc} deposition was significantly greater in the thalamus than in all other brain

regions ($p<0.001$ in all cases), while no significant differences were observed with respect to spongiform change or gliosis.

3.3.3 Progression of Histological Changes in Scrapie-Infected Hamsters

Initial evaluation of histological data at each time point was unable to explain the differences observed on MR images, so the patterns of onset of histological hallmarks of prion disease were examined. Beginning with spongiform change (Figure 19 A), three of the regions of interest present similar curves: the cortex; the hippocampus; and the hypothalamus. In each case, the percentage of the area covered by vacuoles remains at an essentially constant level through 47 dpi before a spike at 61 dpi; the levels observed in the hypothalamus remain lower than the other two regions throughout. In comparison, the percentage of the thalamus covered by vacuoles begins on the order of that in the hypothalamus before a linear increase through the final two time points, making the thalamus the most highly vacuolated region at both 47 and 61 dpi. The curves of all four regions effectively parallel each other in the increasing stage; this seems to indicate that once spongiform change begins to occur, it appears at the same pace, regardless of brain region. Spongiform change cannot, however, be evaluated solely on the basis of the fraction of a brain section that is covered by vacuoles; the number of vacuoles present is also important. In the four brain regions studied, the curves representing area covered by vacuoles were effectively mirrored by those representing the number of vacuoles in a given area of tissue (Figure 20). In each case the increase in vacuole area, once initiated, was more rapid than that in number of vacuoles.

Figure 19. Progressive histological changes in scrapie-infected hamsters.

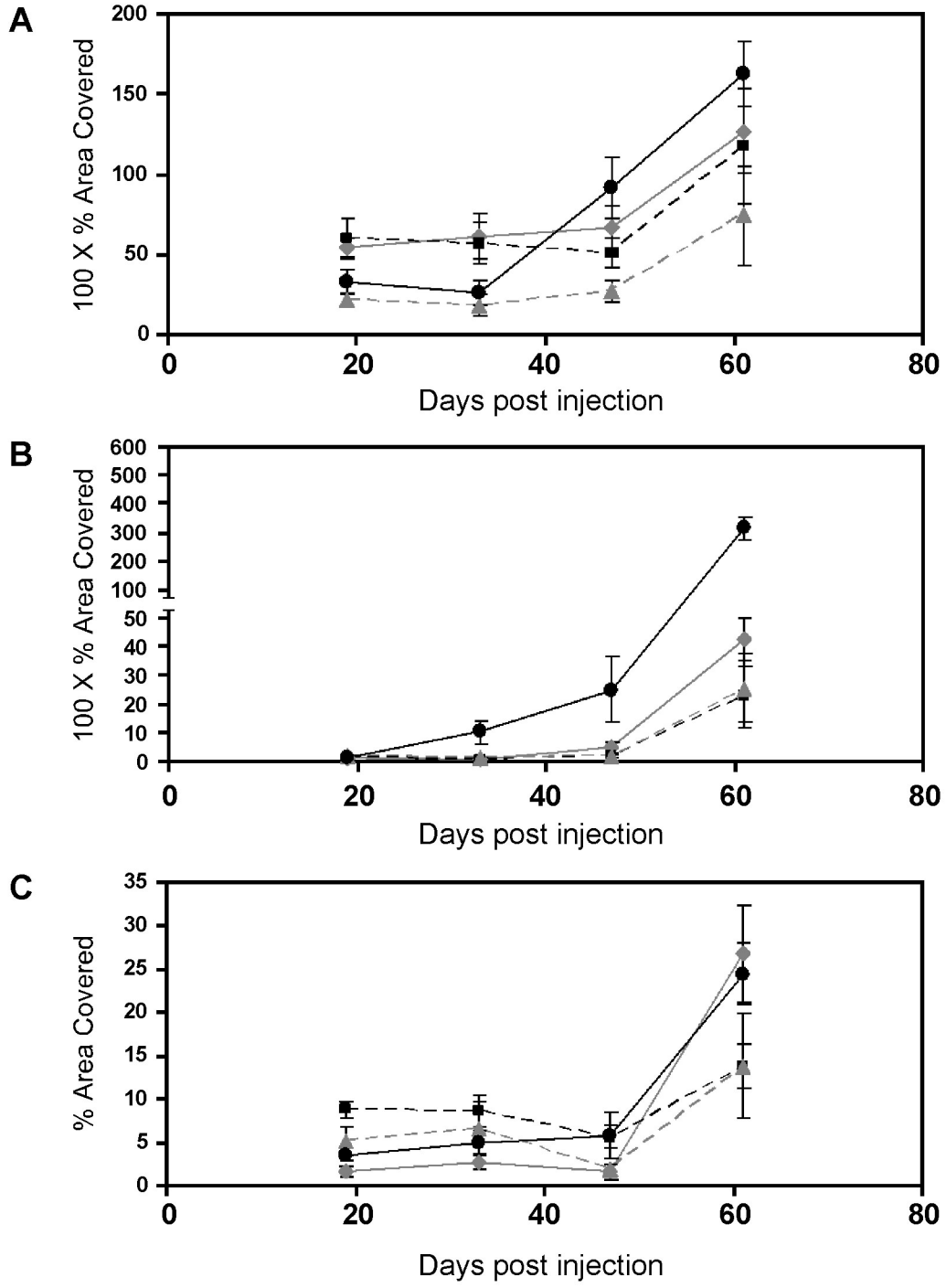

Solid grey line: cortex; broken black line: hippocampus; broken grey line: hypothalamus; solid black line: thalamus. Measurements represent the proportion of slide area covered by vacuoles (A), PrP deposition (B), and gliosis (C).

Figure 20. Total vacuole area and number of vacuoles in scrapie-infected hamsters.

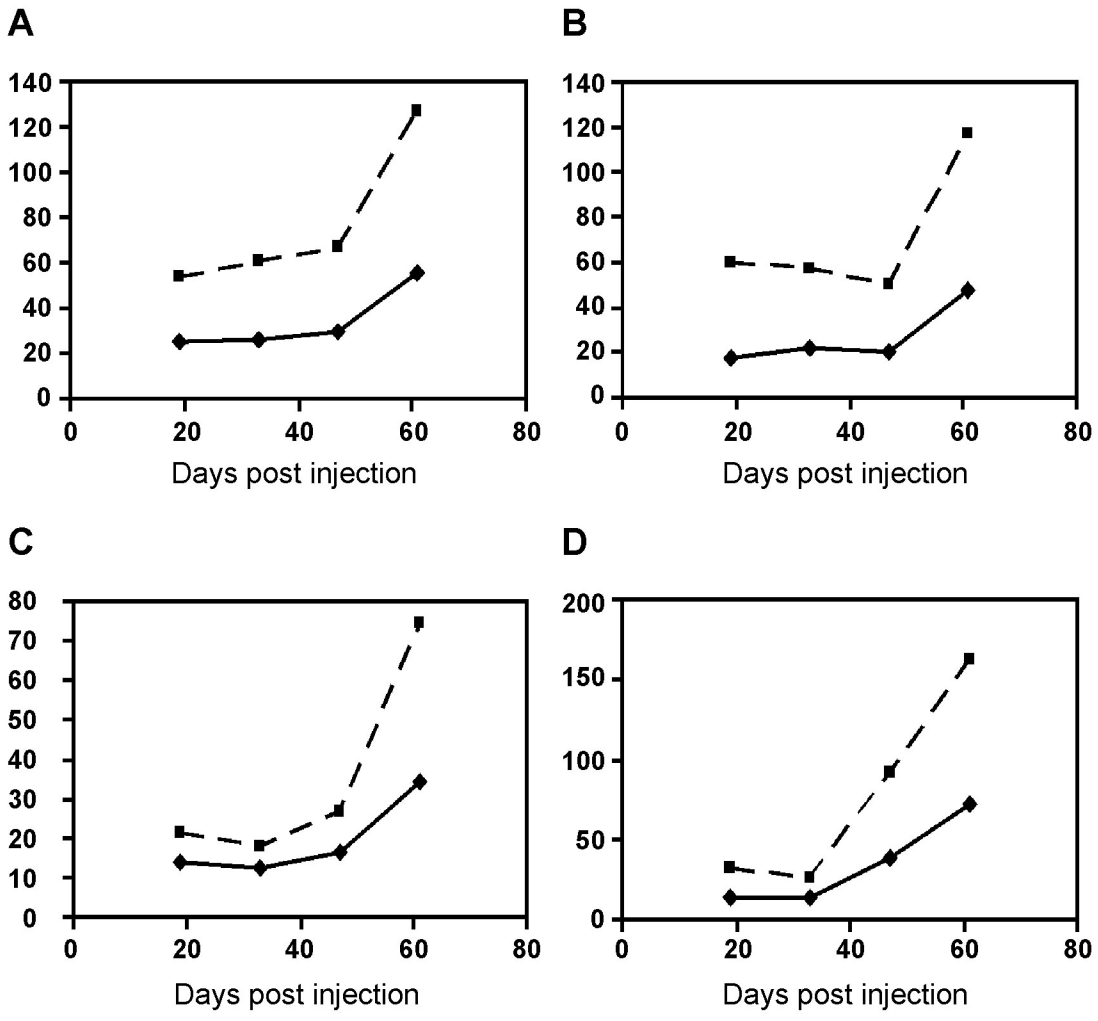

Relationship between total vacuole area and the number of vacuoles in the cortex (A); hippocampus (B); hypothalamus (C); and thalamus (D) of scrapie-infected hamsters. Scale: number of vacuoles/digital image (solid black line); 100 x percentage of image area covered by vacuoles (broken black line).

This is intuitive, since the total vacuole area increases not only with the addition of new vacuoles, but with the expansion of those vacuoles that were already present.

Although PrP^{Sc} deposition follows a similar pattern to that of spongiform change, it is not identical (Figure 19 B). Once again, the cortex, hippocampus, and hypothalamus share almost identical curves, with no real change over the first three time points before an increase at 61 dpi. In this case, the level of PrP^{Sc} in the cortex at 61 dpi is clearly higher than those in either the hippocampus or the hypothalamus. Contrary to any observations regarding spongiform change, PrP^{Sc} levels in the thalamus begin to increase at the first opportunity, and continue to do so throughout the time course studied. This increase accelerates over time, with the curve becoming almost exponential (take note of the scale break in Figure 19 B).

When gliosis levels were examined, all four brain regions showed similar results: gliosis levels were constant in each brain region between 19 and 47 dpi, with an increase of varying degree at 61 dpi. The cortex and thalamus, which began with slightly lower glial cell levels than the hippocampus and the hypothalamus, experienced a greater increase at the end of the time period studied, producing higher final gliosis measurements.

Contrary to expectations, when histological characteristics were examined as a function of time, the thalamus was the only region of the brain that significantly distanced itself from the other regions studied. This observation was confirmed when patterns of spongiform change (total vacuole area and number

of vacuoles), PrP^{Sc} deposition and gliosis were compared within individual brain regions (Figure 21). In general terms, the results in the cortex, hippocampus, and hypothalamus were extremely similar (Figure 21 A-C). In each case, the degree of each histological hallmark remained essentially constant between 19 and 47 dpi, before increasing at 61 dpi. Considering the rate of increase of each histological characteristic between 47 and 61 dpi, total vacuole area > PrP^{Sc} deposition > gliosis in all three regions of the brain discussed here.

The thalamus is the only region of interest where there appears to be an order of onset of the different histological changes (Figure 21 D). Specifically, an increase in PrP^{Sc} levels is evident as of 33 dpi; vacuole levels increase as of 47 dpi; and proliferation of glial cells materializes at 61 dpi only. In fact, gliosis levels in the thalamus share the same pattern as all of the histological changes in the other three regions of interest. While PrP^{Sc} deposition is the first characteristic to experience an increase, the rate of increase in spongiform change is greater during the period from 33 to 47 dpi. It is only during the period between 47 and 61 dpi that the rate of PrP^{Sc} deposition increases beyond that of spongiform change, which undergoes a constant increase (again note the scale break in Figure 21 D). This observation highlights the second difference between the thalamus and the other regions of interest: while vacuoles appear at a constant rate in the thalamus, PrP^{Sc} reproduction seems to be exponential in nature. It was impossible to detect changes in the rate of appearance of any histological hallmarks of prion disease in the cortex, hippocampus, or

Figure 21. Evolution of histological changes in scrapie-infected hamsters.

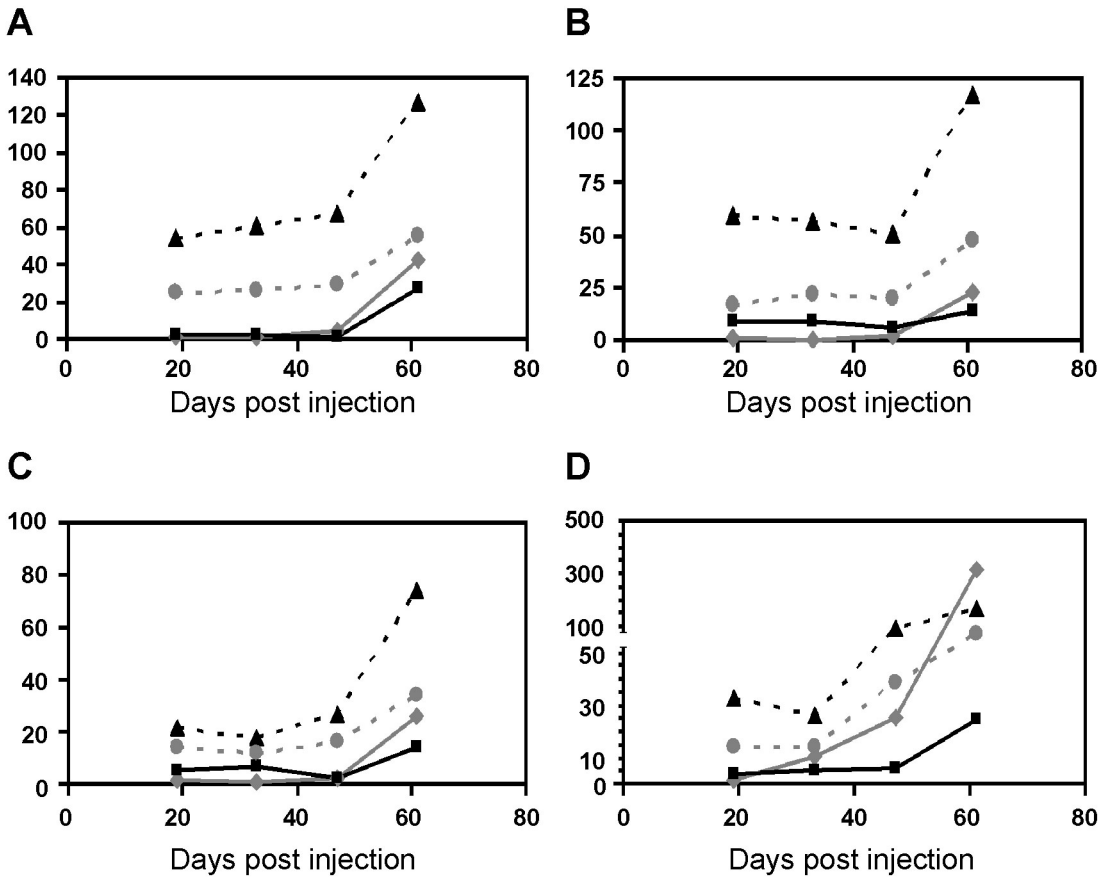

Patterns of histological changes in the cortex (A); hippocampus (B); hypothalamus (C); and thalamus (D) of scrapie-infected hamsters. Scale: 100 x percentage of image area covered by PrP (solid grey line) or vacuoles (broken black line); percentage of image area covered by gliosis (solid black line); number of vacuoles/digital image (broken grey line).

hypothalamus since no increases occur until the last time point studied; the use of additional time points may have allowed these observations.

3.4 Pentosan Polysulphate Treatment Study

3.4.1 Progression of Symptoms in Scrapie-Infected Hamsters

Unlike in the initial MRI study described above, scrapie-infected hamsters in the pentosan polysulphate treatment study were allowed to progress to the clinical stage of disease. Scrapie-infected hamsters were euthanized once it was deemed that symptoms had progressed to a point where the hamsters could no longer function on their own. Indications of this state included loss of interest in food, or difficulty feeding or drinking water; extreme lethargy; difficulty moving as a result of severe ataxia; and significant weight loss. The duration of symptoms, from their first appearance until the time at which hamsters were euthanized, was on the order of ten to fourteen days. The first indication of disease was invariably slight bobbing of the head during walking. In the initial stages, this head bobbing was very difficult to distinguish from normal, slight motion, which occurs regularly as hamsters walk. Over the course of a day or so, the bobbing motion progressed to the point that it was clearly evident as a symptom. From then on, the head bobbing was the most immediately obvious symptom of disease, and it was not restricted to times when the hamster was walking.

Over the course of the next several days, most hamsters began to exhibit periods of hyperactivity of varying extent and duration. At later stages, these were sometimes interspersed cyclically with periods of no activity. Progressive ataxia of the limbs was another symptom, although it was not consistent in terms

of affecting primarily the front or hind limbs, or the limbs on one side of the body or the other. As ataxia progressed, it resulted in problems with mobility, which could take several forms. Common forms in late stages included: dragging of the hind limbs; using the hind limbs to propel the body forward, with the front end snow-ploughing due to front limb ataxia; frequent falling on one side, due to ataxia in both limbs on that side of the body; and moving in a circular motion, due to ataxia in one front limb. Less frequently, hamsters would spontaneously roll onto their back, typically during periods of hyperactivity. Initially, they would immediately right themselves and carry on, but as disease progressed, hamsters that continued these back rolls would have more difficulty righting themselves, and would sometimes remain on their back for several seconds.

In the final stages of disease, hamsters would lose interest in food, or else would be unable to successfully feed themselves, in some cases because of violent head bobbing that prevented them from biting the food pellet. As a result of failing to eat, sometimes in combination with continued hyperactivity, hamsters often lost significant body weight in the last few days before they were euthanized. Hamsters that did not remain hyperactive through the final stages of disease often became extremely lethargic; this likely resulted at least in part from vastly decreased mobility due to severe ataxia, and in turn contributed to the inability of those hamsters to feed themselves.

Disease progression in scrapie-infected hamsters had several symptoms common to all affected hamsters. While there were variations in many of these symptoms that resulted in a range of patterns of disease progression, these

patterns did not correlate with particular PPS treatment regimens. Thus, while PPS treatment altered survival time in scrapie-infected hamsters (see below), it did not obviously alter disease progression, with respect to quality of life, or duration of disease as measured from the first appearance of symptoms to the time at which hamsters were euthanized.

3.4.2 Effects of Pentosan Polysulphate Treatment on Survival Time in Scrapie-Infected Hamsters

The survival times of scrapie-infected hamsters receiving different PPS treatment regimens were compared (Table 12). Figure 22 A and B show the survival curves and the mean survival times of the six treatment groups, respectively. Hamsters receiving intra-cerebral PPS at the time of infection had significantly longer survival times than any other group (Table 13, $p<0.03$ in all cases); and there was more variability in survival time within the two treatment groups receiving intra-cerebral PPS than in the other four treatment groups. Since some large differences in survival time between PPS treatment groups were not found to be statistically significant, and because there was a small number of animals in each group, the power of the comparison was tested (Table 14). When the observed population standard deviation of 13.2468 was used in the calculation, the power was only 0.6149, providing a potential reason why apparent differences between treatment groups were not found to be significant. However, when the standard deviation of the incubation period from the literature [215] was used to produce a standard error of 4.4721, the resulting power was 1.0. This indicates that while the observed data did not provide for an ideally

Table 12. Survival Time in Hamsters Receiving Different PPS Treatment Regimens.	
Treatment Group	Mean Survival Time (+/-s.e)
No Treatment	82 +/- 0
I.p. PPS at 0 dpi	93+/- 1.528
I.p. PPS at 26 dpi	80.333 +/- 1.333
I.p. PPS at 26, 40, and 54 dpi	86.667 +/- 1.856
I.c. PPS at 0 dpi	115 +/- 8.185
I.c. PPS at 26 dpi	93.667 +/- 4.91
No I.c. PPS (first 4 groups)	85.5 +/- 1.593
I.c. PPS (last 2 groups)	104.333 +/- 6.401

PPS: pentosan polysulphate; i.p.: intra-peritoneal; i.c.: intra-cerebral; dpi: days post injection; s.e.: standard error of the mean.

Table 13. Differences in Survival Time in Hamsters Receiving Different PPS Treatment Regimens.							
		p values					
Group ID		1	2	3	4	5	6
1	No treatment		0.437	1	0.959	0.379	<0.002
2	I.p. 0 dpi	0.437		0.301	0.871	1	<0.025
3	I.p. 27 dpi	1	0.301		0.871	0.256	<0.001
4	I.p. multiple	0.959	0.871	0.871		0.819	<0.005
5	I.c. 27 dpi	0.379	1	0.256	0.819		<0.03
6	I.c. 0 dpi	<0.002	<0.025	<0.001	<0.005	<0.03	

PPS: pentosan polysulphate; i.p.: intra-peritoneal; i.c.: intra-cerebral; dpi: days post injection.

Table 14. Power of Survival Time Comparison.		
Analysis	Power	
	Standard Deviation Used in Calculation	
	Literature	Measured
ANOVA - 6 Treatment Groups	1	0.6149
t-test - i.c. PPS/No i.c. PPS	1	0.7610

i.c. PPS: intra-cerebral pentosan polysulphate treatment.

Figure 22. Survival time of scrapie-infected hamsters receiving different PPS treatments.

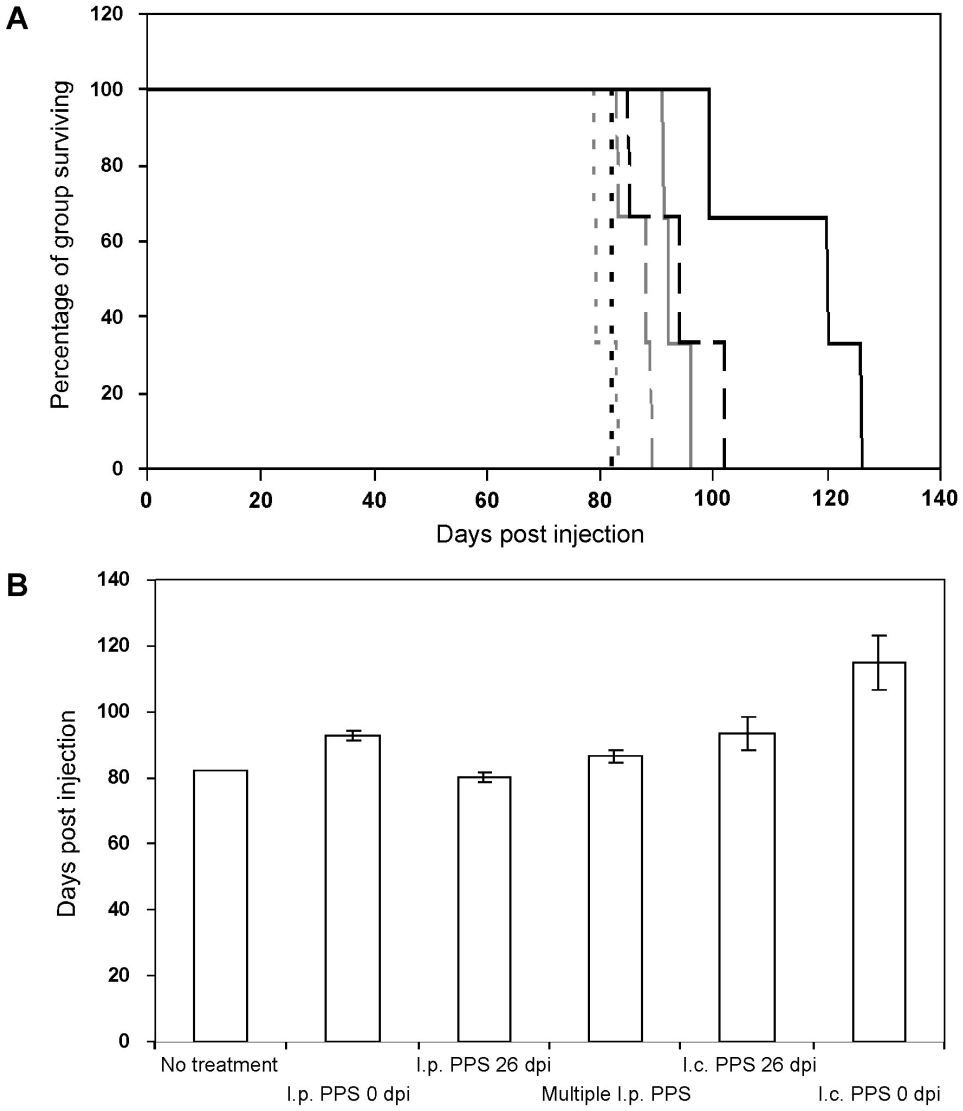

A. Survival curve of scrapie-infected hamsters receiving the following pentosan polysulphate (PPS) treatments: solid black line: intra-cerebral (i.c.) PPS treatment at 0 days post injection (dpi); broken black line: i.c. PPS treatment at 26 dpi; dotted black line: no treatment; solid grey line: i.p. PPS treatment at 0 dpi; broken grey line: i.p. treatments at 26, 40, and 54 dpi; dotted grey line: i.p. treatment at 0 dpi. B. Mean survival time of different treatment groups, +/- standard error of the mean (s.e.m).

powerful study, this was unexpected given the literature. The difference between the observed and literature standard errors can be attributed to the different treatment regimens.

Because of the increased variability within the intra-cerebral treatment groups, and because of their subsequent grouping for the purpose of MRI comparison (see below), all of the infected hamsters were divided into two groups: those that received intra-cerebral PPS injection, and those that did not. The mean survival times of these two new groups are shown in Figure 23 and Table 12; hamsters that received intra-cerebral PPS treatment had significantly longer survival times than those that did not ($p<0.005$). Examination of the power of this comparison yields similar results to the comparison of all treatment groups. When the literature standard deviation is used, the resulting power is 1.0, but when the measured standard deviation is applied, the power is reduced, this time to 0.7610. In this case it did not matter, as the only possible difference was observed to be significant.

3.4.3 Effects of Pentosan Polysulphate Treatment on Magnetic Resonance Images of Scrapie-Infected Hamsters

Scrapie-infected and mock-infected hamsters were divided into groups that received either no treatment, or one of five PPS drug regimens. The hamsters were imaged by MRI every two weeks beginning at 19 dpi, until they exhibited severe signs of disease, or until 150 dpi in the case of mock-infected hamsters. T_2 relaxation times in the following regions were compared: the cerebral cortex at the level of the thalamus, the hippocampus, the thalamus, and

Figure 23. Survival time of scrapie-infected hamsters that were or were not treated intra-cerebrally with PPS.

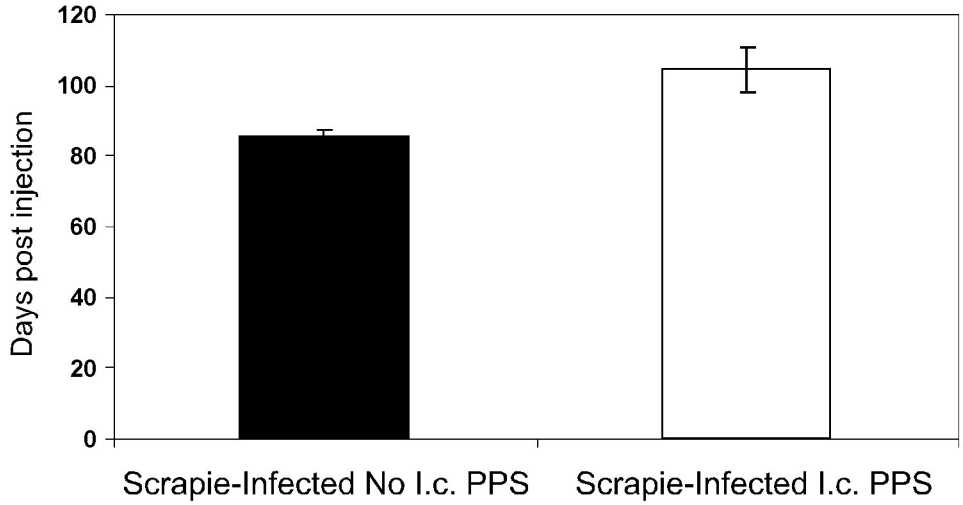

No i.c. PPS: hamsters that were not treated intra-cerebrally with PPS; i.c. PPS: hamsters that were treated intra-cerebrally with PPS.

the hypothalamus in each of Slices 5 and 6; the lateral ventricles and surrounding region, septum, and cerebral cortex at the level of the septum in Slice 7. In order to compare the mean T_2 relaxation time in these regions of interest, this measurement was expressed as a percentage of the mean T_2 relaxation time in the copper sulphate standard in the same image set. Including a tube of copper sulphate as a reference sample facilitates the comparison of images obtained in different scanning sessions. Any observed differences in measurements of this reference sample can then be attributed to differences in experimental conditions, and measurements of interest can be normalized using the reference. Addition of copper sulphate shortens the T_2 value of water, allowing for the observation of complete T_2 relaxation, resulting in a consistent high intensity signal.

3.4.3.1 Confounding Effects of Intra-cerebral Pentosan Polysulphate Treatment Require Consolidation of Hamster Groups

Since previous MRI results indicated that hyperintensities, indicative of increased T_2 relaxation time, appeared in the hippocampus in Slices 5 and 6 of scrapie-infected hamsters, this was the region of greatest initial interest. Unexpectedly, it quickly became apparent that intra-cerebral treatment with PPS resulted in hyperintensities in the hippocampus of mock-infected hamsters. Figure 24 compares T_2 maps of Slice 6 in a mock-infected hamster that was treated intra-cerebrally with PPS, and a scrapie-infected hamster that did not receive intra-cerebral treatment. Since intra-cerebral PPS treatment on its own drastically influenced T_2 maps, the resulting temporal patterns of T_2 relaxation

Figure 24. Effects of scrapie-infection and i.c. PPS treatment on MRI slice 6.

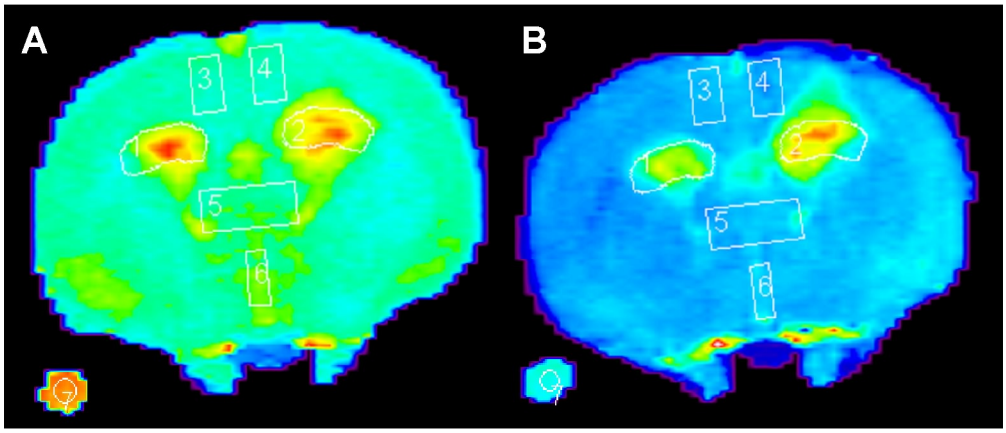

False colour T_2 maps of a scrapie-infected hamster that was not treated intra-cerebrally (i.c.) with pentosan polysulphate (PPS) at 89 days post injection (A), and a mock-infected hamster that received i.c. PPS, at 75 days post injection (B).

times in different hamster treatment groups were extremely complex. In order to simplify the analysis, different treatment groups were examined for similar patterns.

In Figure 25, temporal patterns of relative T_2 values in the hippocampus in Slice 6 of mock-infected hamsters that did not receive intra-cerebral treatment with PPS are examined. In parts A-D of the figure, the mean values for each of the four treatment groups are compared to the individual animals making up the group. These figures demonstrate that while there is a certain amount of expected variation in pattern within each of these groups, all of the individual animals in a given group share the same overall pattern. Figure 25 E compares the mean relative T_2 values of each of the four treatment groups that were not treated intra-cerebrally with PPS to a new overall mean comprising all four of these groups. Each of these four treatment groups share the same temporal pattern of relative T_2 value in the hippocampus in Slice 6. As a result, the new overall mean can be considered an accurate representation of the temporal pattern in all mock-infected hamsters that were not treated intra-cerebrally with PPS. This new group will be known as Mock-Infected Hamsters Without I.c. PPS Treatment, or more briefly Mock-Infected No I.c. PPS; the composition of this group can be found in Table 2.

In order to determine the effects of intra-cerebral treatment with PPS alone on T_2 maps, the two groups of mock-infected hamsters that received this treatment were compared. In Figure 26 A and B, the mean values for these two treatment groups are compared to the individual animals making up the group.

Figure 25. Relative T_2 values in mock-infected hamsters that did not receive i.c. PPS treatment.

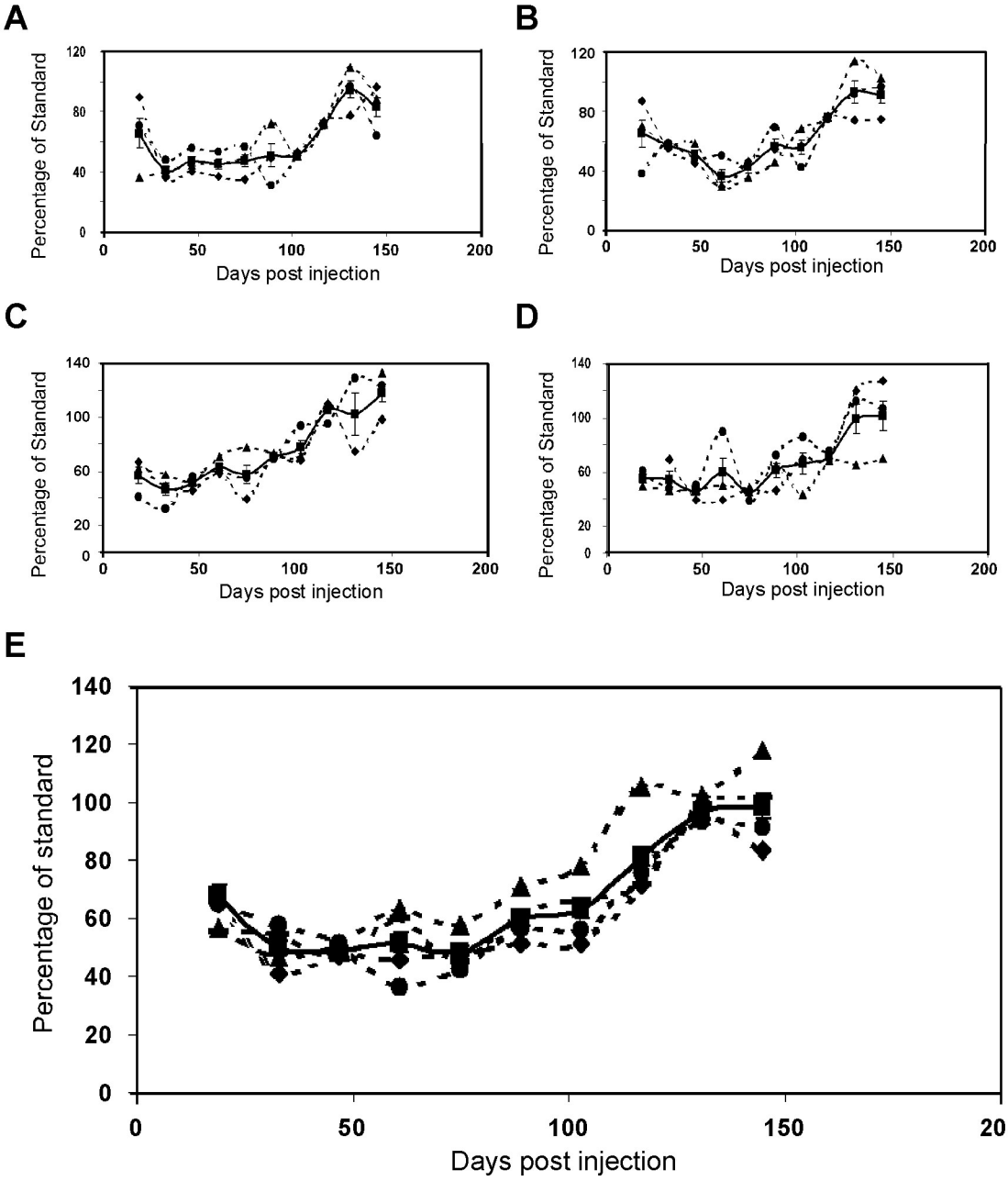

Relative T_2 values of individual mock-infected hamsters are compared to their respective group means in A-D. A. Intra-peritoneal (i.p.) pentosan polysulphate (PPS) treatment at 0 days post injection (dpi). B. i.p. PPS treatment at 26 dpi. C. i.p. PPS treatment at 26, 40, and 54 dpi. D. No treatment. E. Mock-infected hamster group means are compared to the new Mock-Infected No i.c. PPS treatment group mean.

Figure 26. Relative T_2 values in mock-infected hamsters that received i.c. PPS treatment.

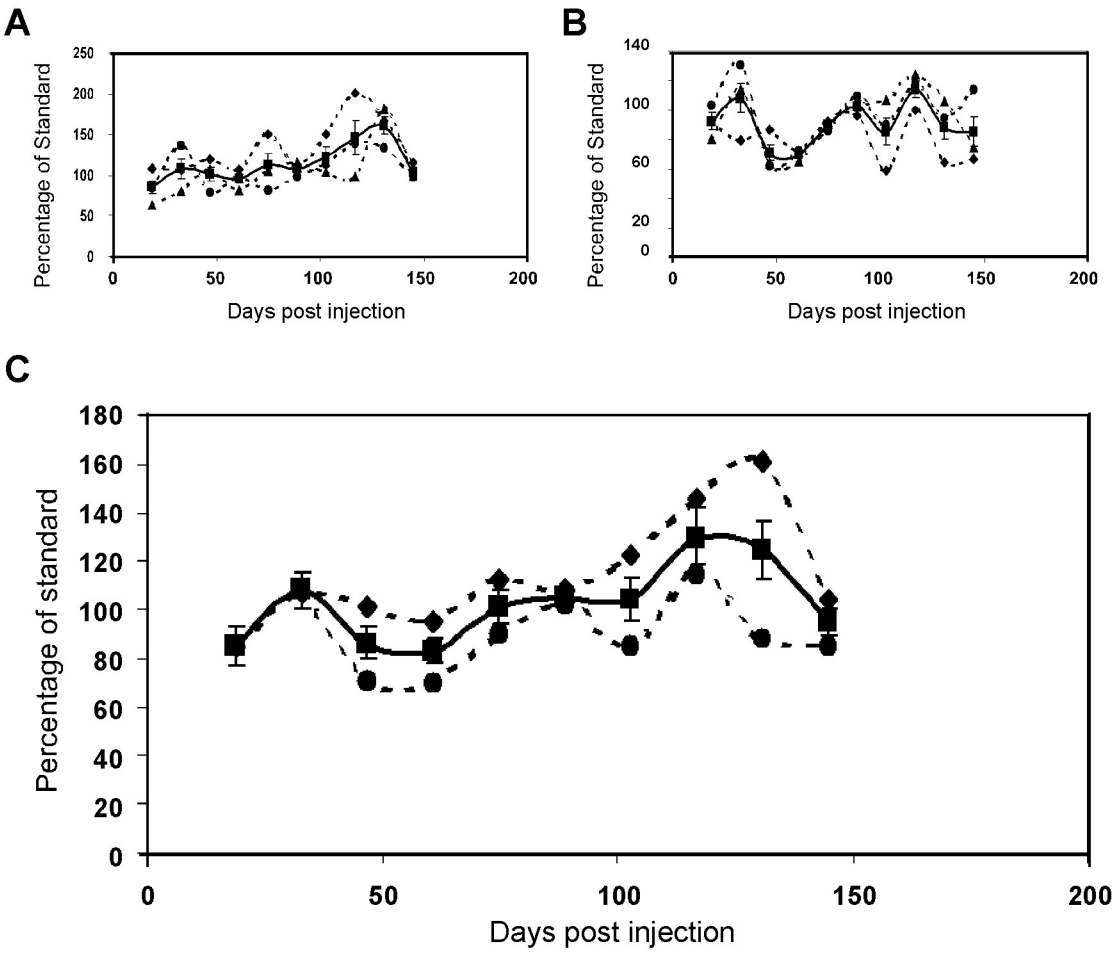

Relative T_2 values of individual mock-infected hamsters are compared to their respective group means in A and B. A. Intra-cerebral (i.c.) pentosan polysulphate (PPS) treatment at 0 days post injection (dpi). B. i.c. PPS treatment at 26 dpi. C. Mock-infected hamster group means are compared to the new Mock-Infected i.c. PPS treatment group mean.

While the overall degree of variation within each of these groups seems to be greater than in any of the four groups examined above, the patterns exhibited by individual animals within each of the groups remain broadly consistent. Figure 26 C compares the mean relative T_2 values in the hippocampus in Slice 6 in the two groups of mock-infected hamsters that received intra-cerebral PPS treatment, and establishes a new Mock-Infected I.c. PPS treatment group. The temporal pattern of mean relative T_2 values of this new group can again be considered an accurate representation of all mock-infected hamsters that received intra-cerebral PPS.

Figure 27 compares the groups of scrapie-infected hamsters that did not receive intra-cerebral PPS treatment in the same manner as above. Parts A-D of the figure compare the temporal patterns of relative T_2 values in the hippocampus of Slice 6 in individual hamsters to the respective group means, while part E compares each of the group curves to a newly-produced mean curve of Scrapie-Infected No I.c. PPS hamsters. In this case, there are enough differences between the groups of scrapie-infected hamsters that did not receive intra-cerebral PPS to merit closer examination of the individual groups. Scrapie-infected hamsters that received no treatment had constant relative T_2 values between 19 and 61 dpi, before a steep increase at 75 dpi. Individual scrapie-infected hamsters that received a single PPS treatment intra-peritoneally at 26 dpi also exhibited a consistent temporal pattern of relative T_2 values: a steep increase at 33 dpi was followed by an equally steep decrease at 47 dpi, with a return to high values for the final two time points (Figure 27 B). For the most

Figure 27. Relative T_2 values in scrapie-infected hamsters that did not receive i.c. PPS treatment.

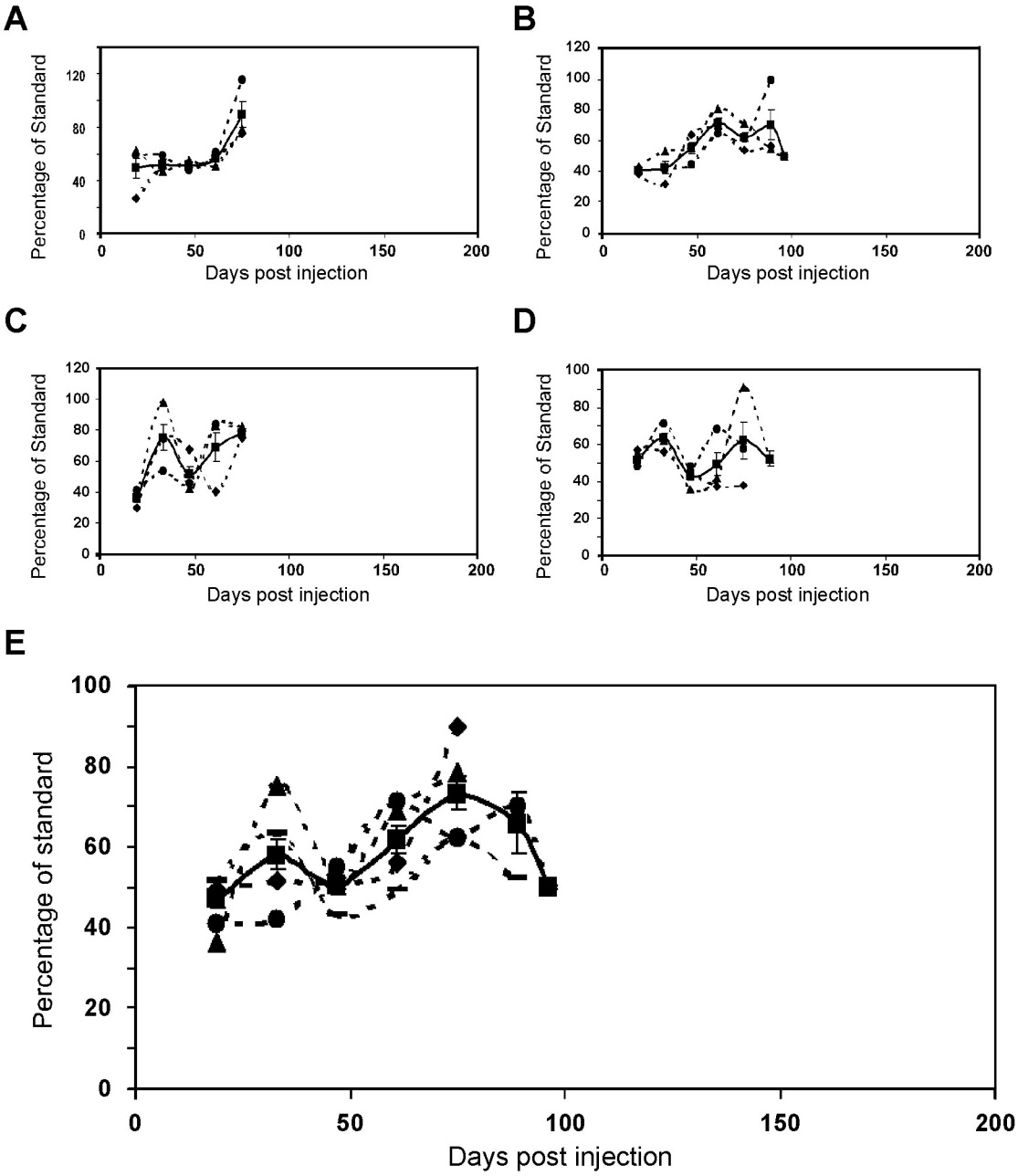

Relative T_2 values of individual scrapie-infected hamsters are compared to their respective group means in A-D. A. No treatment. B. Intra-peritoneal (i.p.) pentosan polysulphate (PPS) treatment at 26 days post injection (dpi). C. i.p. PPS treatment at 0 dpi. D. i.p. PPS treatment at 26, 40, and 54 dpi. E. Scrapie-infected hamster group means are compared to the new Scrapie-Infected No i.c. PPS treatment group mean.

part, individual scrapie-infected hamsters that received a single PPS treatment intra-peritoneally at the time of infection shared a common temporal pattern of relative T_2 values until 75 dpi, after which some divergence occurred (Figure 27 C). The patterns of relative T_2 values in individual scrapie-infected hamsters that received multiple intra-peritoneal PPS treatments were the most divergent in this group (Figure 27 D), but they retained enough similarities that the mean curve remained an acceptable representation of all individual hamsters.

When all four scrapie-infected groups that did not receive intra-cerebral PPS treatment are considered together (Figure 27 E), the resulting curve for the new Scrapie-Infected No I.c. PPS hamster group is an acceptable, if not ideal representation of these hamsters. It is important to note that towards the end of the curve, the number of hamsters that were being imaged was decreasing as hamsters were euthanized. This meant that the data from individual hamsters gained a greater weighting in the mean representation, so that unusual data would not be hidden as much by the remaining, normal data.

The remaining groups of scrapie-infected hamsters were those that were treated intra-cerebrally with PPS, either at the time of infection, or at 26 dpi. Temporal patterns of relative T_2 values in the hippocampus in Slice 6 are compared in Figure 28: individuals are compared to their respective group means in A and B, while the group means are compared to the curve for a new Scrapie-Infected I.c. PPS group in C. Beginning with the group that received i.c. treatment at 26 dpi (between the first and second imaging sessions), it is apparent that PPS treatment elicited an immediate response in the form of a

Figure 28. Relative T_2 values in scrapie-infected hamsters that received i.c. PPS treatment.

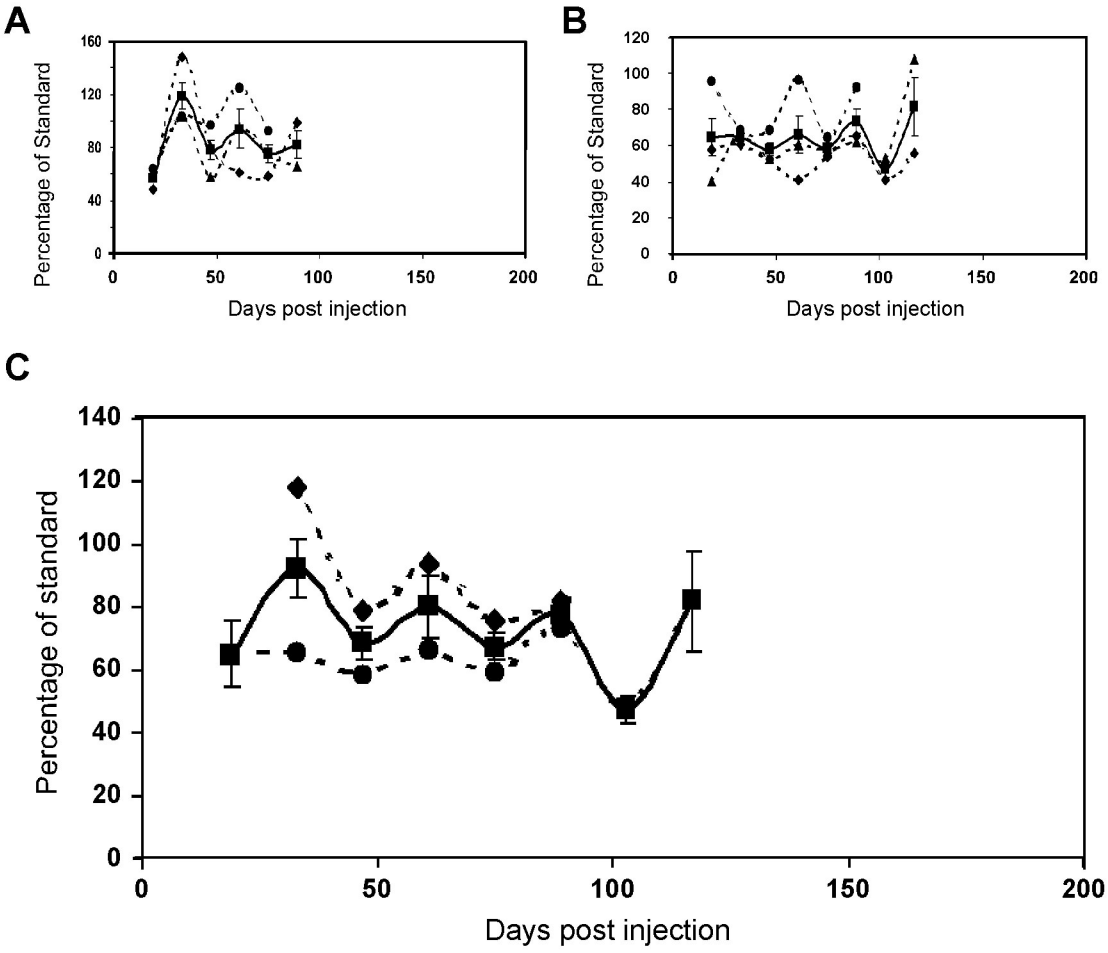

Relative T_2 values of individual scrapie-infected hamsters are compared to their respective group means in A and B. A. Intra-cerebral (i.c.) pentosan polysulphate (PPS) treatment at 26 days post injection (dpi). B. i.c. PPS treatment at 0 dpi. C. Scrapie-infected hamster group means are compared to the new Mock-Infected i.c. PPS treatment group mean.

steep increase in relative T_2 values at 33 dpi. Beyond this, there was some variation within the group, but the group mean curve was observed to be an acceptable representation of all individuals within the group. The group of scrapie-infected hamsters that were treated intra-cerebrally with PPS at the time of infection is not only the group with the most in-group variation, but it is also the group whose individuals varied the most in survival time, resulting in individuals that were at different stages of disease progression at a given time point. While the three individuals in this group represent three different patterns of relative T_2 values in the hippocampus in Slice 6, these differences exemplify the role of the different pace of disease progression in individual animals in the production of varying temporal curves of relative T_2 value.

When the two groups of scrapie-infected hamsters are combined to form a single Scrapie-Infected I.c. PPS group, the resulting curve is once again acceptable, if not ideal (Figure 28 C). While the two group means diverge significantly from the newly produced mean curve between 33 and 61 dpi, the most important features of the curves are maintained.

Given the results of the examination of relative T_2 values in the hippocampus in Slice 6 of all hamsters in the study, it was concluded that the regrouping of hamsters as described above would be the best way to simplify the analysis. The composition of the four new groups of hamsters is detailed in Table 2 (note that this changes between 19 and 33 dpi). Although the representations provided by these new mean curves are not always ideally

accurate, particularly in the case of scrapie-infected hamsters that received intra-cerebral PPS treatment, they do provide the best opportunity to execute a meaningful analysis. Equivalent comparisons were also conducted in all of the regions of interest, in each of MRI Slices 5, 6, and 7 (data not shown), in order to confirm the validity of the regrouping.

3.4.3.2 Effects of Pentosan Polysulphate Treatment on MRI Slice 6

In Figure 29, the temporal patterns of relative T_2 values in the hippocampus in scrapie-infected and mock-infected hamsters that either received or did not receive intra-cerebral PPS are compared. By initially considering the two groups of mock-infected hamsters only, the effects of intra-cerebral PPS treatment alone on relative T_2 values in the hippocampus in Slice 6 can be ascertained. The differences between these two groups are clear from the outset of the experiment: relative T_2 values in mock-infected hamsters that received i.c. PPS were considerably higher than those in hamsters that were not treated in that manner. This difference was maintained until the late stages of the experiment, when the two curves began to converge, culminating at 145 dpi, when the difference disappeared completely.

When the two groups of scrapie-infected hamsters are considered, it is not possible to isolate the cause of changes in relative T_2 values. While the Scrapie-Infected No I.c. PPS group can be thought of as being influenced by scrapie infection only, this is an oversimplification. Some members of this group that received intra-peritoneal PPS treatment had longer survival times than others.

Figure 29. Comparison of relative T_2 values in the hippocampus in MRI slice 6.

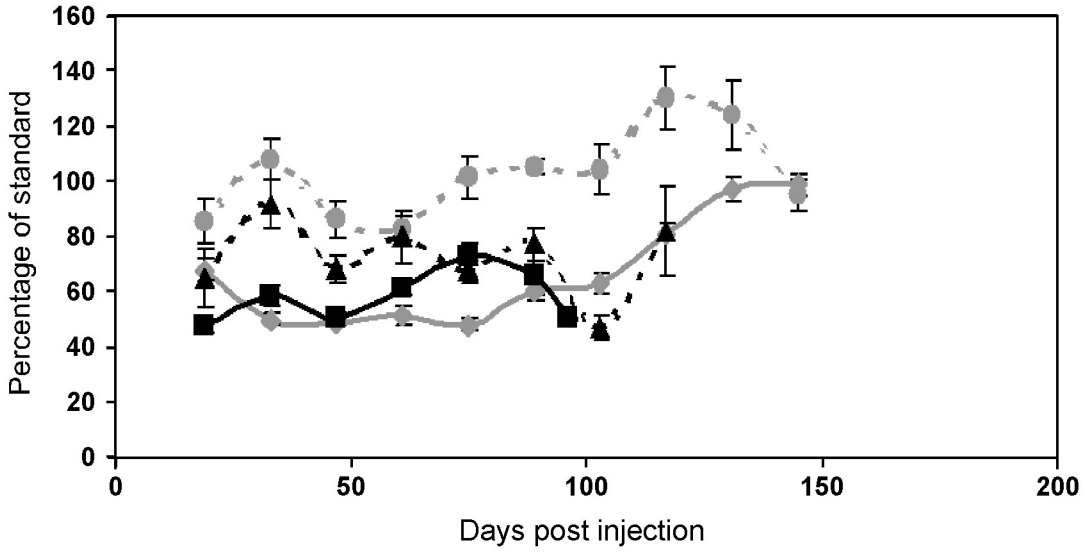

Solid black line: Scrapie-infected hamsters that did not receive intra-cerebral (i.c.) pentosan polysulphate (PPS) treatment (Scrapie-Infected No I.c. PPS); broken black line: scrapie-infected hamsters that received i.c. PPS treatment (Scrapie-Infected I.c. PPS); solid grey line: mock-infected hamsters that did not receive i.c. PPS treatment (Mock-Infected No I.c. PPS); broken grey line: mock-infected hamsters that received i.c. PPS treatment (Mock-Infected I.c. PPS).

Since this is evidence of an alteration in disease progression, it follows that this could also have an effect on relative T_2 values at specific time points. Having said that, when Scrapie-Infected No I.c. PPS hamsters are compared to Mock-Infected No I.c. PPS hamsters, the curves diverge at 61 and 75 dpi, with the scrapie-infected hamsters registering higher relative T_2 values at these timepoints. In comparison, scrapie-infected hamsters that received i.c. PPS treatment maintain higher relative T_2 values than those that did not between 19 and 61 dpi. Beyond this point, the curves converge and maintain similar values for the duration of the experiment. While the Scrapie-Infected I.c. PPS group has higher relative T_2 values than the two No I.c. PPS groups, these values do not approach those attained by the Mock-Infected I.c. PPS group. These data seem to indicate that while both intra-cerebral PPS treatment and scrapie infection lead to increased relative T_2 values in the hippocampus in Slice 6, when these two modulations are exercised on the same hamsters, their effects begin to oppose one another.

Although the hippocampus was the brain region of greatest interest in MRI Slice 6 because of previous results, three other regions were tracked as well: the cortex, the thalamus, and the hypothalamus. All four of these regions are compared in each of the four hamster groups in Figure 30. Two broad observations regarding these graphs are sufficient for the time being. First, in each hamster group, the relative T_2 value curves of the cortex, the thalamus, and the hypothalamus all closely follow that of the hippocampus. Second, the relative T_2 values in the hippocampus and the hypothalamus are consistently higher than

Figure 30. Comparison of relative T_2 values in four regions in MRI slice 6.

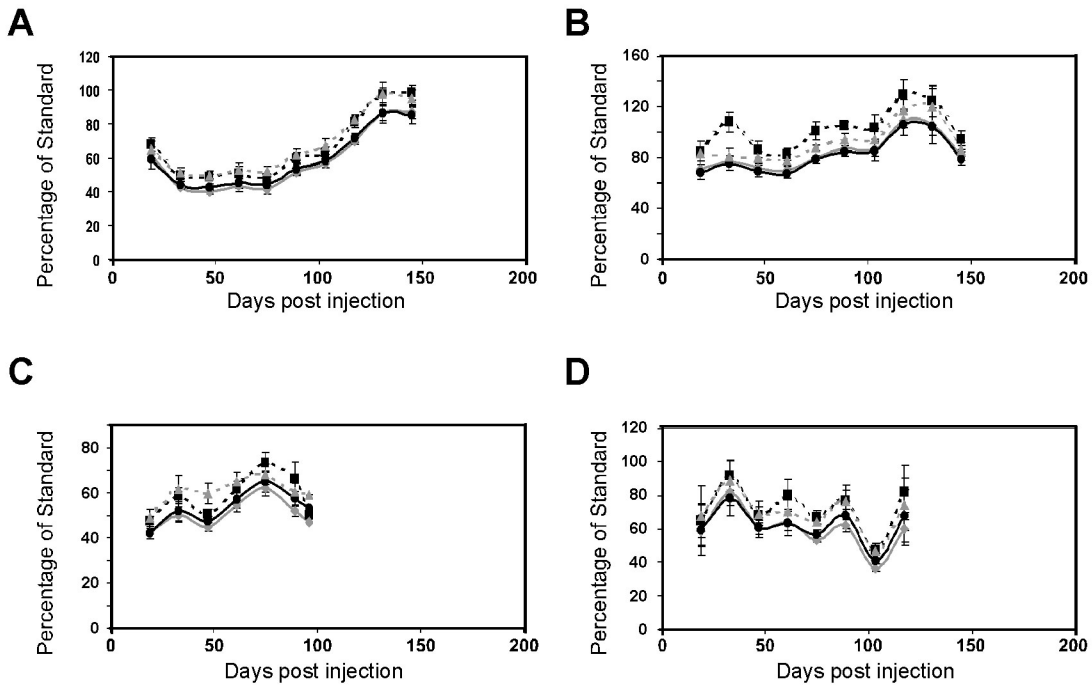

Relative T_2 values are compared in four regions of interest. A: mock-infected hamsters that did not receive intra-cerebral (i.c.) pentosan polysulphate (PPS) treatment (Scrapie-Infected No I.c. PPS); B: mock-infected hamsters that received i.c. PPS treatment (Scrapie-Infected I.c. PPS); C: scrapie-infected hamsters that did not receive i.c. PPS treatment (Mock-Infected No I.c. PPS); D: scrapie-infected hamsters that received i.c. PPS treatment (Mock-Infected I.c. PPS). Solid black line: thalamus; broken black line: hippocampus; solid grey line: cortex; broken grey line: hypothalamus.

those in the cortex and the thalamus in a given hamster group. In Figure 31, each of the four brain regions of interest is compared between hamster groups. There are no obvious differences in the patterns of any of the four brain regions.

In order to compare the relative T_2 values in all regions of interest in scrapie- or mock-infected hamsters that did or did not receive intra-cerebral PPS treatment, a multi-way, or factorial, analysis of variance was conducted at each time point with treatment group and brain region as the independent variables. When this was impossible due to heterogeneity of variances, the equivalent non-parametric analyses were conducted. Instances of statistically significant differences are summarized in Tables 15 and 20 to 27 (the latter can be found in Appendix 2). Beginning with the comparison of hamster groups, including pooled data from all brain regions, a number of observations can be noted. At 19 dpi, Scrapie-Infected No I.c. PPS hamsters recorded significantly lower relative T_2 values than the other three groups. This result was influenced in part by the absence of a copper sulphate standard when three of the hamsters were imaged, resulting in relative values produced in another manner (see Materials and Methods); these values were lower than they likely would have been if they had been produced in the usual manner. Between 33 and 61 dpi, and at 89 dpi, relative T_2 values maintained the following order: Mock-Infected I.c. PPS > Scrapie-Infected I.c. PPS > Scrapie-Infected No I.c. PPS > Mock-Infected No I.c. PPS. At 33 and 61 dpi relative T_2 values in the two groups that did not receive i.c. PPS treatment were significantly lower than in the other two groups, while differences between all groups were statistically significant at 47 dpi. At 75 dpi,

Figure 31. Relative T_2 values in four regions of MRI slice 6 compared by hamster group.

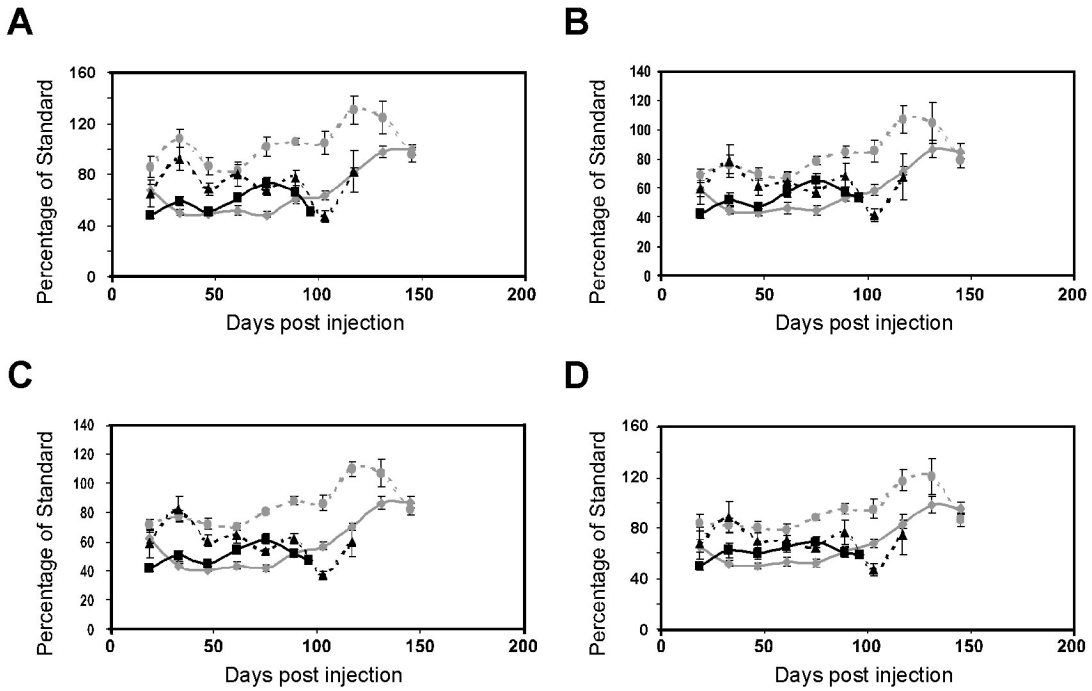

Relative T_2 values are compared in the hippocampus (A), thalamus (B), cortex (C), and hypothalamus (D) in MRI slice 6. Solid black line: Scrapie-infected hamsters that did not receive intra-cerebral (i.c.) pentosan polysulphate (PPS) treatment (Scrapie-Infected No I.c. PPS); broken black line: scrapie-infected hamsters that received i.c. PPS treatment (Scrapie-Infected I.c. PPS); solid grey line: mock-infected hamsters that did not receive i.c. PPS treatment (Mock-Infected No I.c. PPS); broken grey line: mock-infected hamsters that received i.c. PPS treatment (Mock-Infected I.c. PPS).

Table 15. Summary of all Slice 6 MRI Comparisons.			
dpi	Group Comparison	Region Comparison	Groups x Region
19	D<A,B,C (p<0.025)	NS	Table 20, Appendix 2
33	B and D<A and C (p<0.001)	Hippo>Cortex,Thalamus (p<0.02) Hypothal>Cortex (p<0.015)	Table 21, Appendix 2
47	Significant Differences between all groups (p<0.03)	Hippo and Hypothal>Cortex and Thalamus (p<0.015)	Table 22, Appendix 2
61	B and D<A and C (p<0.001)	Cortex<Hippo and Hypothal (p<0.05)	Table 23, Appendix 2
75	NS between C and D; all other differences significant (p<0.001)	Hippo>Cortex, Thalamus; Hypothal>Cortex (p<0.04)	Table 24, Appendix 2
89	NS between B and D; all other differences significant (p<0.01)	Hippo>Cortex, Thalamus; Hypothal>Cortex (p<0.0055)	Table 25, Appendix 2
103	Significant Differences between all groups (p<0.001)	Hippo>Cortex (p=0.04687)	Table 26, Appendix 2
117	A>B,C (p<0.001)	Hippo>Cortex, Thalamus (p<0.05)	Table 27, Appendix 2
131	A>B (p=0.01)	NS	Mock I.c. PPS Hippo>Mock no I.c. Cortex (p<0.025)
145	NS	Hippo>Cortex,Thalamus (p<0.05)	NS

Statistically significant results indicated in black. A: Mock-infected i.c. PPS; B: Mock-infected No i.c. PPS; C: Scrapie-Infected i.c. PPS; D: Scrapie-Infected No i.c. PPS. Hippo: Hippocampus; Hypothal: Hypothalamus. Dpi: days post injection; NS: no significant differences.

Scrapie-Infected No I.c. PPS hamsters had greater relative T_2 values than Scrapie-Infected I.c. PPS hamsters, although differences were not significant. Other than that change, the order of groups noted above remained the same, and differences between all other groups were statistically significant. At 89 dpi, the last time point at which all four groups remained in the study, differences between all groups except those that did not receive intra-cerebral PPS treatment were statistically significant. At 103 and 117 dpi (the last two time points at which scrapie-infected hamsters were imaged), the following order of groups was maintained: Mock-Infected I.c. PPS > Mock-Infected No I.c. PPS > Scrapie-Infected I.c. PPS. Differences between all groups were significant at 103 dpi, while relative T_2 values in Mock-infected I.c. PPS hamsters were significantly greater than the other two groups at 117 dpi. Mock-Infected I.c. PPS hamsters retained significantly greater relative T_2 values than Mock-Infected No I.c. PPS hamsters at 131 dpi, while there were no significant differences at 145 dpi.

When data from all four hamster groups were pooled and the four regions of interest in the brain were compared, the situation was much simpler than the previously discussed comparison: relative T_2 values in the hippocampus and the hypothalamus were consistently higher than in the thalamus and the cortex. Instances when these differences were statistically significant are listed in Table 15.

Differences between brain regions in different hamster groups (Group x Region) were also compared; Tables 20-27 in Appendix 2 summarize significant differences in these comparisons. At 19 dpi, most regions in Scrapie-Infected No

I.c. PPS hamsters had significantly lower relative T_2 values than most regions in the two groups that received i.c. PPS treatment. At 33 and 47 dpi, significant differences were frequent between regions in hamsters that received i.c. PPS treatment compared to hamsters that did not receive i.c. PPS. Conversely, significant differences between regions in a given hamster group were rare, not only at 33 and 47 dpi, but throughout the experiment. In fact the only instances of significant differences were the following at 47 dpi: relative T_2 values in the hippocampus were greater than in the cortex in Mock-Infected No I.c. PPS hamsters; and values in the hypothalamus were greater than in the cortex in Scrapie-Infected No I.c. PPS hamsters. Between 61 and 89 dpi, and at 117 dpi, significant differences were less frequent than at earlier time points. When they did occur, they were predominantly between regions in Mock-Infected I.c. PPS and Mock-Infected No I.c. PPS hamsters. At 103 dpi, relative T_2 values in most regions in Mock-Infected I.c. PPS hamsters were greater than in most regions in Scrapie-Infected I.c. PPS and Mock-Infected No I.c. PPS hamsters. At the final two time points, significant differences were rare.

3.4.3.3 Effects of Pentosan Polysulphate Treatment on MRI Slice 5

Having established that intra-cerebral PPS treatment induced changes on T_2 maps of MRI Slice 6 that were similar to those induced by scrapie infection, two more MRI slices of interest were examined to determine whether this was a common phenomenon. In MRI Slice 5, the other slice where hyperintensities had previously been observed in the hippocampus, this was indeed the case (Figure 32). The Slice 5 data were evaluated in the same manner as the Slice 6 data in

Figure 32. Effects of scrapie-infection and i.c. PPS treatment on MRI slice 5.

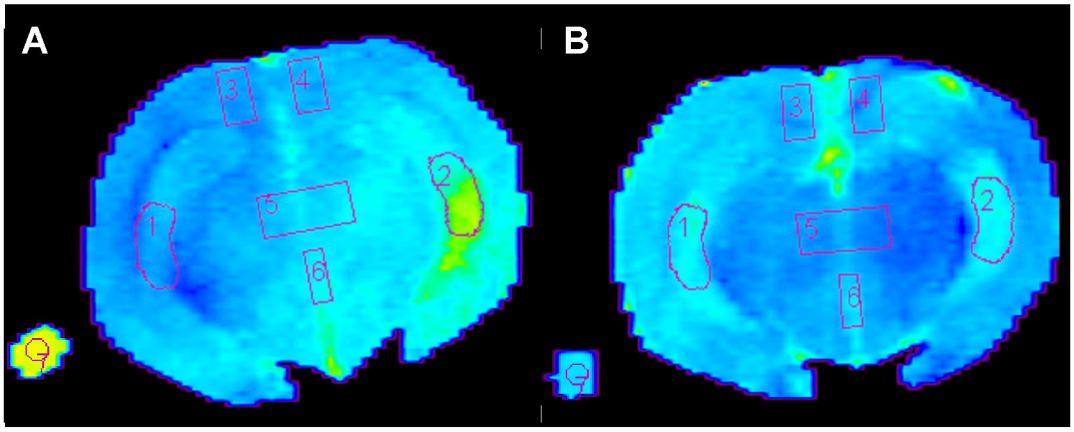

False colour T_2 maps of a scrapie-infected hamster that was not treated intra-cerebrally (i.c.) with pentosan polysulphate (PPS) at 75 days post injection (A), and a mock-infected hamster that received i.c. PPS, at 75 days post injection (B).

order to confirm that reducing the number of hamster groups was an acceptable means of reducing complexity. These data will not be presented here, but they did conform to the requirements.

The regions of interest in MRI Slice 5 were the following: the hippocampus, the thalamus, the hypothalamus, and the cortex at the level of the thalamus. Relative T_2 values in all four of these regions are compared in each of the four hamster groups in Figure 33. As in Slice 6, it was apparent that the temporal patterns of relative T_2 values in different brain regions were very similar in a given hamster group. The relative T_2 values of the four hamster groups were also compared in each of the four regions of interest (Figure 34), and these four graphs were very similar as well. As a general rule, the curves of Mock-Infected I.c. PPS and Mock-Infected No I.c. PPS hamsters marked the boundaries of the range of relative T_2 values over most of the time course, while the curves of Scrapie-Infected I.c. PPS and Scrapie-Infected No I.c. PPS hamsters were both intermediate in value, and less linear than their counterparts.

As described earlier, a multi-way analysis of variance was used to compare hamster groups, brain regions, and Group x Region with regards to relative T_2 value. Statistically significant differences are tabulated in Tables 16 and 28 to 35 (the latter can be found in Appendix 2). Data from all four brain regions were pooled to compare values in the four different hamster groups. At 19 dpi, relative T_2 values in Scrapie-Infected No I.c. PPS hamsters were significantly lower than in the other three groups, as they had been in Slice 6.

Figure 33. Comparison of relative T_2 values in four regions in MRI slice 5.

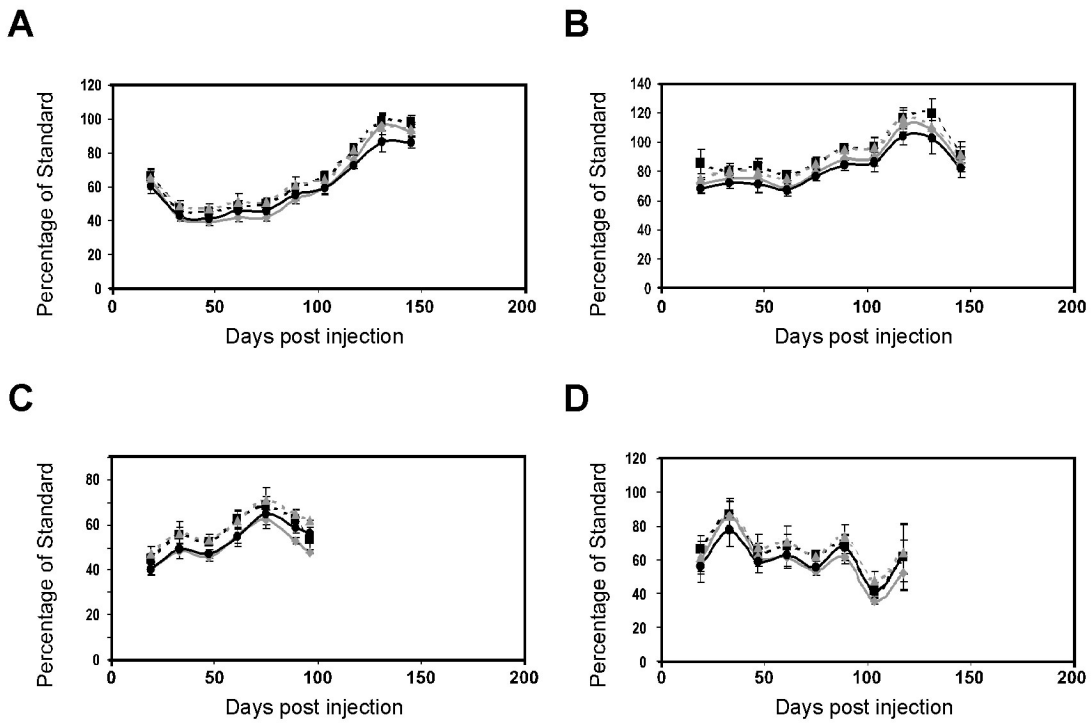

Relative T_2 values are compared in four regions of interest. A: mock-infected hamsters that did not receive intra-cerebral (i.c.) pentosan polysulphate (PPS) treatment (Scrapie-Infected No I.c. PPS); B: mock-infected hamsters that received i.c. PPS treatment (Scrapie-Infected I.c. PPS); C: scrapie-infected hamsters that did not receive i.c. PPS treatment (Mock-Infected No I.c. PPS); D: scrapie-infected hamsters that received i.c. PPS treatment (Mock-Infected I.c. PPS). Solid black line: thalamus; broken black line: hippocampus; solid grey line: cortex; broken grey line: hypothalamus.

Figure 34. Relative T_2 values in four regions of MRI slice 5 compared by hamster group.

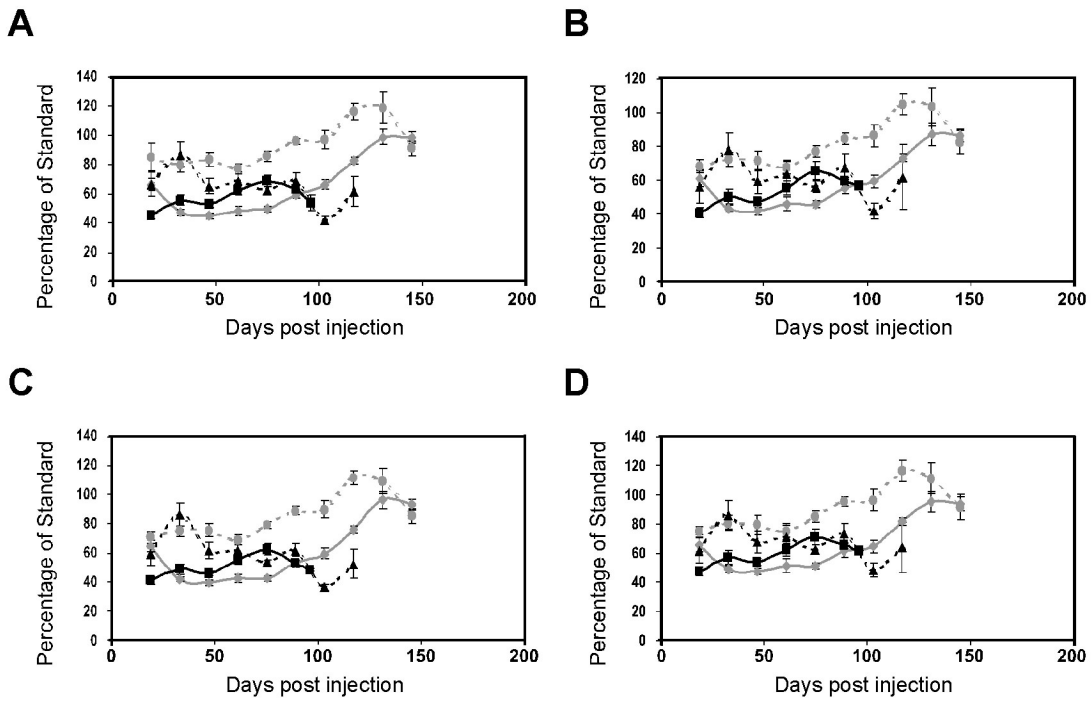

Relative T_2 values are compared in the hippocampus (A), thalamus (B), cortex (C), and hypothalamus (D) in MRI slice 5. Solid black line: Scrapie-infected hamsters that did not receive intra-cerebral (i.c.) pentosan polysulphate (PPS) treatment (Scrapie-Infected No I.c. PPS); broken black line: scrapie-infected hamsters that received i.c. PPS treatment (Scrapie-Infected I.c. PPS); solid grey line: mock-infected hamsters that did not receive i.c. PPS treatment (Mock-Infected No I.c. PPS); broken grey line: mock-infected hamsters that received i.c. PPS treatment (Mock-Infected I.c. PPS).

Table 16. Summary of all MRI Slice 5 Comparisons			
dpi	Group Comparison	Region Comparison	Groups x Region
19	D<A,B,C (p<0.002)	NS	Table 28, Appendix 2
33	B and D<A and C (p<0.001)	NS	Table 29, Appendix 2
47	Significant differences between all groups (p<0.001)	Hypothal>Cortex, Thalamus; Hippo>Cortex (p<0.05)	Table 30, Appendix 2
61	NS between A and C; all other differences significant (p<0.0015)	Cortex<Hippo, Hypothal (p<0.05)	Table 31, Appendix 2
75	NS between C and D; all other differences significant (p<0.002)	Cortex<Hippo, Hypothal (p<0.01)	Table 32, Appendix 2
89	A>B,C,D (p<0.001)	Cortex<Hippo, Hypothal (p<0.01)	Table 33, Appendix 2
103	Significant differences between all groups (p<0.002)	NS	Table 34, Appendix 2
117	A>B,C (p<0.001)	NS	Table 35, Appendix 2
131	A>B (p<0.01)	NS	NS
145	NS	NS	NS

Statistically significant results indicated in black. A: Mock-infected i.c. PPS; B: Mock-infected No i.c. PPS; C: Scrapie-Infected i.c. PPS; D: Scrapie-Infected No i.c. PPS. Hippo: Hippocampus; Hypothal: Hypothalamus. Dpi: days post injection; NS: no significant differences.

At 33 dpi, relative T_2 values in the two groups that received intra-cerebral PPS treatment were significantly greater than those in hamsters that did not receive i.c. PPS. The order of mean relative T_2 values between 47 and 89 dpi was Mock-Infected I.c. PPS > Scrapie-Infected I.c. PPS> Scrapie-Infected No I.c. PPS > Mock-Infected No I.c. PPS, with the following exception: at 75 dpi, relative T_2 values in Scrapie-Infected No I.c. PPS hamsters were greater than in Scrapie-Infected I.c. PPS hamsters. At 47 dpi, differences between all groups were significant, while at 61 dpi differences between all groups except Mock-Infected I.c. PPS and Scrapie-Infected I.c. PPS were significant. At 75 dpi, differences between all groups other than the two scrapie-infected groups were significant, while Mock-Infected I.c. PPS hamsters had significantly higher relative T_2 values than all other groups at 89 dpi. At 103 and 117 dpi, the order of relative T_2 values in hamster groups changed such that Mock-Infected I.c. PPS > Mock-Infected No I.c. PPS > Scrapie-Infected I.c. PPS. Differences between all groups were significant at 103 dpi, while Mock-Infected I.c. PPS hamsters had significantly greater relative T_2 values than both other remaining groups at 117 dpi. At 131 and 145 dpi, only the two groups of mock-infected hamsters remained; at 131 dpi, those that received intra-cerebral PPS retained significantly greater relative T_2 values, while there were no significant differences at 145 dpi.

When pooled data from all four hamster groups were used to compare the four brain regions of interest, relative T_2 values were generally greater in the hippocampus and the hypothalamus than in the cortex and the thalamus, although significant differences were observed only between 47 and 89 dpi. At

all of these time points, relative T_2 values in the hippocampus and the hypothalamus were significantly greater than those in the cortex, while values in the hypothalamus were also significantly greater than those in the thalamus at 47 dpi.

As expected, the most complex assessment to decipher was the Group x Region comparison, where all regions of interest in all hamster groups were compared (Tables 28-35, Appendix 2). However, it was possible to identify trends in instances of statistically significant differences. For example, at 19 dpi, Scrapie-Infected No I.c. PPS hamsters were involved in all statistically significant comparisons; this result was not unexpected, as this group had significantly lower relative T_2 values than all other groups when data from all brain regions were pooled. At 33 dpi, significant differences were restricted to comparisons between regions in hamsters that received intra-cerebral PPS with regions in hamsters that did not. The 47 dpi time point saw the largest number of significant differences, including between Scrapie-Infected No I.c. PPS and Mock-Infected No I.c. PPS hamsters. These differences persisted at 61 and 75 dpi, while differences between the two groups of scrapie-infected hamsters disappeared. At 103 and 117 dpi, nearly all observed significant differences occurred between Mock-Infected I.c. PPS hamsters and the other remaining groups, while no significant differences were observed at 131 and 145 dpi. At no time point were there significant differences between different brain regions in a given hamster group.

3.4.3.4 Effects of Pentosan Polysulphate Treatment on MRI Slice 7

The last brain slice to be evaluated for differences in relative T_2 values was MRI Slice 7. As in the two brain slices discussed previously, it was observed that intra-cerebral PPS treatment resulted in similar changes on T_2 maps as scrapie infection (Figure 35). In this slice, the regions of interest were the cortex at the level of the septum; the septum; and the area surrounding the lateral ventricles, including the ventricles (Figure 6 C). Relative T_2 values in these regions are compared in each of the four hamster groups in Figure 36. As in Slices 5 and 6, it was apparent that the temporal patterns of relative T_2 values in different brain regions were very similar in a given hamster group. In particular, the patterns of relative T_2 values in the septum and the cortex are very nearly identical in all four hamster groups. In comparison, while the curves of the lateral ventricles agree largely with those of the other two regions, there are some notable differences. In the two mock-infected groups, increases in relative T_2 values that are observed in both the septum and the cortex are much more evident in the lateral ventricles, resulting in divergence between their curves. Perhaps of greater importance is that both scrapie-infected groups as well as Mock-Infected I.c. PPS hamsters show a clear difference between relative T_2 values in the lateral ventricles and those in the cortex and septum from the outset of the experiment. In comparison, Mock-Infected No I.c. PPS hamsters, which did not receive either of the manipulations that resulted in MR image abnormalities, do not exhibit a large difference between the lateral ventricles and the other regions of interest until late in the time course.

Figure 35. Effects of scrapie-infection and i.c. PPS treatment on MRI slice 7.

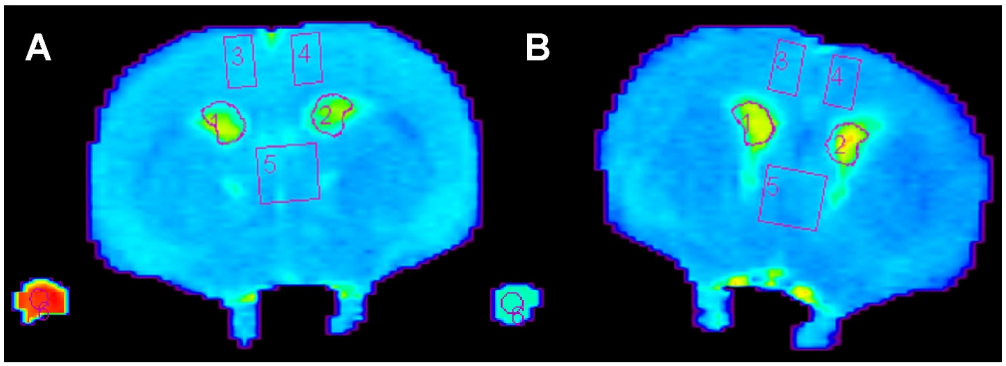

False colour T_2 maps of a scrapie-infected hamster that was not treated intra-cerebrally (i.c.) with pentosan polysulphate (PPS) at 61 days post injection (A), and a mock-infected hamster that received i.c. PPS, at 19 days post injection (B).

Figure 36. Comparison of relative T_2 values in three regions in MRI slice 7.

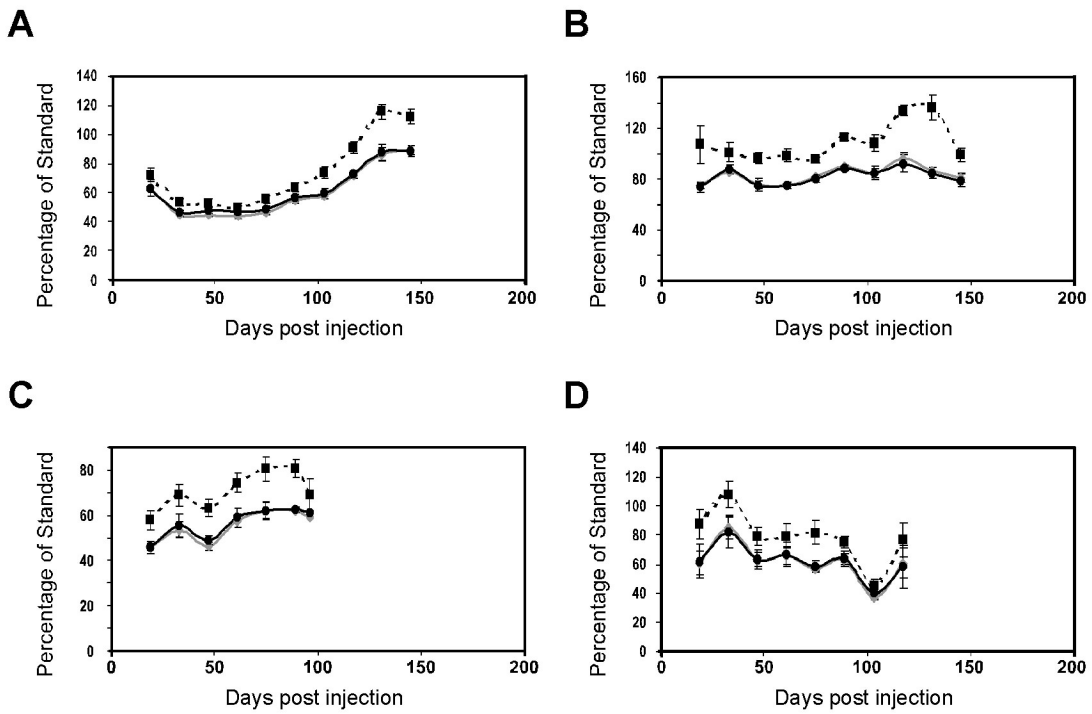

Relative T_2 values are compared in three regions of interest. A: mock-infected hamsters that did not receive intra-cerebral (i.c.) pentosan polysulphate (PPS) treatment (Scrapie-Infected No I.c. PPS); B: mock-infected hamsters that received i.c. PPS treatment (Scrapie-Infected I.c. PPS); C: scrapie-infected hamsters that did not receive i.c. PPS treatment (Mock-Infected No I.c. PPS); D: scrapie-infected hamsters that received i.c. PPS treatment (Mock-Infected I.c. PPS). Solid black line: septum; broken black line: ventricles and surrounding area; solid grey line: cortex.

The relative T_2 values of the four hamster groups were also compared in each of the three regions of interest (Figure 37). As in the other slices, the curves of Mock-Infected I.c. PPS and Mock-Infected No I.c. PPS hamsters marked the boundaries of the range of relative T_2 values over most of the time course, while the curves of Scrapie-Infected I.c. PPS and Scrapie-Infected No I.c. PPS hamsters were intermediate in value. It is notable that during the period between 47 dpi and 89 dpi, the separation between the curves of the two scrapie-infected hamster groups and the Mock-Infected No I.c. PPS group is greater in the lateral ventricles than in the cortex and the septum.

As discussed previously, three evaluations were carried out, based on hamster group, brain region, and Group x Region; results are tabulated in Tables 17 and 36 to 44 (the latter can be found in Appendix 2). Beginning with the comparison of hamster groups using data pooled from all brain regions of interest, results were similar to those observed in the other slices. At 19 dpi, relative T_2 values in Scrapie-Infected No I.c. PPS hamsters were significantly lower than in all other groups, while those in Mock-Infected No I.c. PPS hamsters were significantly lower than in Mock-Infected I.c. PPS hamsters. At 33 dpi, there were no significant differences between the two groups that received intracerebral PPS treatment, while differences between all other groups were significant. At 47 and 61 dpi, the order of relative T_2 values was Mock-Infected I.c. PPS > Scrapie-Infected I.c. PPS > Scrapie-Infected No I.c. PPS > Mock-Infected No I.c. PPS, while the two scrapie-infected groups switched places at 75 and 89 dpi.

Figure 37. Relative T_2 values in three regions of MRI slice 7 compared by hamster group.

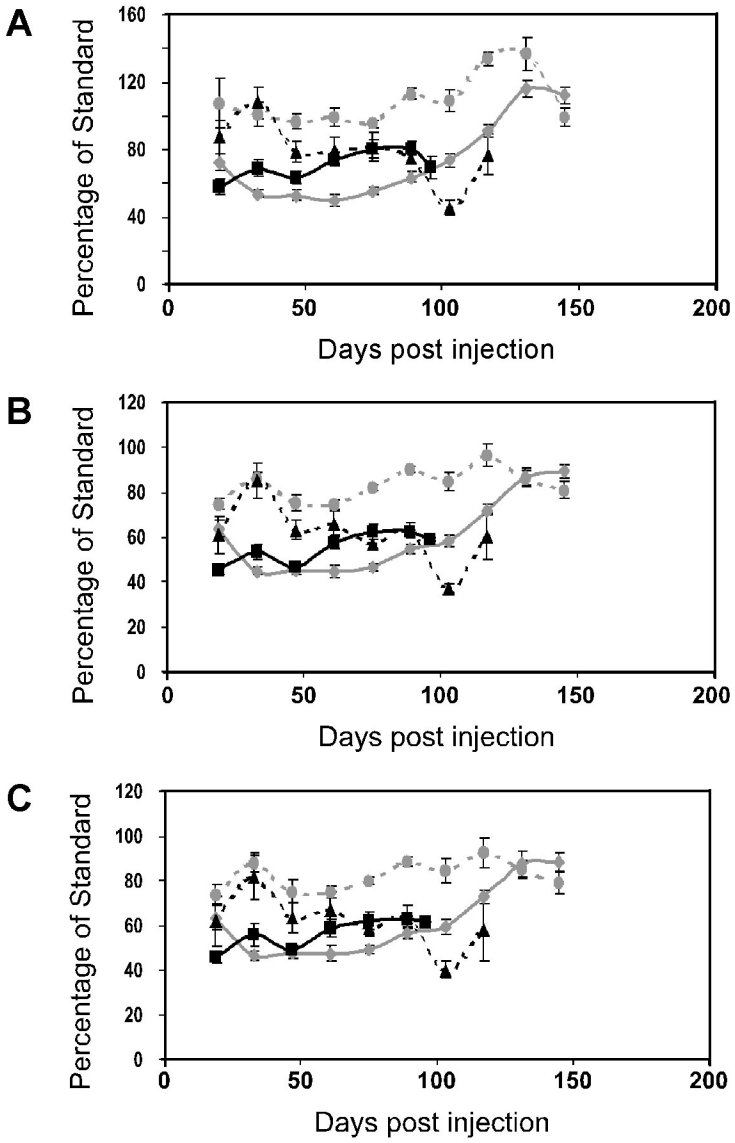

Relative T_2 values are compared in the ventricles and surrounding area (A), cortex (B), and the septum (C), in MRI slice 7. Solid black line: Scrapie-infected hamsters that did not receive intra-cerebral (i.c.) pentosan polysulphate (PPS) treatment (Scrapie-Infected No I.c. PPS); broken black line: scrapie-infected hamsters that received i.c. PPS treatment (Scrapie-Infected I.c. PPS); solid grey line: mock-infected hamsters that did not receive i.c. PPS treatment (Mock-Infected No I.c. PPS); broken grey line: mock-infected hamsters that received i.c. PPS treatment (Mock-Infected I.c. PPS).

Table 17. Summary of all MRI Slice 7 Comparisons.			
dpi	Group Comparison	Region Comparison	Groups x Region
19	D<all others; B<A (p<0.005)	Ventricles>Cortex, Septum (p<0.05)	Table 36, Appendix 2
33	NS between A and C; all other differences significant (p<0.02)	Ventricles>Cortex, Septum (p<0.01)	Table 37, Appendix 2
47	NS between B and D; all other differences significant (p<0.001)	Ventricles>Cortex, Septum (p<0.01)	Table 38, Appendix 2
61	NS between C and D; all other differences significant (p<0.002)	Ventricles>Cortex (p=0.002)	Table 39, Appendix 2
75	NS between C and D; all other differences significant (p<0.002)	Ventricles>Cortex, Septum (p<0.001)	Table 40, Appendix 2
89	NS between C and D; all other differences significant (p<0.002)	Ventricles>Cortex, Septum (p<0.001)	Table 41, Appendix 2
103	A>B>C (p<0.001)	Ventricles>Cortex, Septum (p<0.01)	Table 42, Appendix 2
117	A>B and C (p<0.001)	Ventricles>Cortex, Septum (p<0.001)	Table 43, Appendix 2
131	NS	Ventricles>Cortex, Septum (p<0.001)	Table 44, Appendix 2
145	A<B (p<0.015)	Ventricles>Cortex, Septum (p<0.001)	Mock No I.c. Hippo>all others except Mock I.c. Hippo(p<0.005)

Statistically significant results indicated in black. A: Mock-infected i.c. PPS; B: Mock-infected No i.c. PPS; C: Scrapie-Infected i.c. PPS; D: Scrapie-Infected No i.c. PPS. Dpi: days post injection; NS: no significant differences.

At all of these time points, differences between all groups were statistically significant, with the following exceptions: Scrapie-Infected No I.c. PPS and Mock-Infected No I.c. PPS hamsters at 47 dpi; and Scrapie-Infected I.c. PPS and Scrapie-Infected No I.c. PPS hamsters at 61, 75 and 89 dpi. At 103 and 117 dpi, the order of relative T_2 values was Mock-Infected I.c. PPS > Mock-Infected No I.c. PPS > Scrapie-Infected I.c. PPS, with significant differences observed between all groups with the exception of Mock-Infected No I.c. PPS and Scrapie-Infected I.c. PPS at 117 dpi. There were no significant differences at 131 dpi, while relative T_2 values in Mock-Infected No I.c. hamsters were greater than those in Mock-Infected I.c. hamsters at 145 dpi.

When pooled data from all hamster groups were used to compare relative T_2 values in the regions of interest, values in the lateral ventricles were significantly greater than those in both the cortex and the septum at all time points studied, except for at 61 dpi, when they were significantly greater than those in the cortex only. It is easiest to address the complex Group x Region comparison by first making any broad observations that are possible. As observed in the other two MRI slices, significant differences between regions in a given hamster group were rare. In this case, there were several instances: at 47 dpi, values in the lateral ventricles were significantly greater than in the cortex in Scrapie-Infected No I.c. PPS hamsters; at both 117 and 131 dpi, values in the lateral ventricles were significantly greater than in both the cortex and the septum in each of the two mock-infected hamster groups. With regards to significant differences in general, results were very similar to the two MRI slices discussed

above. At 19 dpi, most of the significant differences involved regions in Scrapie-Infected No I.c. PPS hamsters. At subsequent time points, most significant differences occurred between hamsters that received intra-cerebral PPS treatment and those that did not. This emphasis gradually shifted such that regions in Mock-Infected No I.c. PPS hamsters progressively became the common denominator in most occurrences of significant differences up until 75 dpi. At 89 and 117 dpi, the group most commonly involved in significant differences was Mock-Infected I.c. PPS, while regions in each hamster group were significantly different from each other group most of the time at 103 dpi. At 131 dpi, relative T_2 values in the lateral ventricles in both remaining hamster groups were significantly greater than those in the cortex and the septum in both hamster groups. At 145 dpi, relative T_2 values in the ventricles in Mock-Infected No I.c. PPS hamsters were significantly greater than those in the cortex and septum in both remaining hamster groups.

3.4.4 Effects of Pentosan Polysulphate Treatment on Histology in Scrapie-Infected Hamsters

Intra-cerebral treatment of hamsters with pentosan polysulphate resulted in drastic changes on MR images. In scrapie-infected hamsters, images were altered even by intra-peritoneal PPS treatment compared to scrapie-infected hamsters that received no PPS treatment whatsoever. In order to explore the causes of scrapie-induced changes on MR images of hamster brains, different brain regions were previously examined at two week intervals between 19 and 61 dpi for three histological hallmarks of prion disease: spongiform change;

accumulation of PrP^{Sc}; and gliosis. Although it was determined that abnormalities on MR images caused by scrapie infection could not be explained by histological changes, they remain the gold standard indicators of prion disease progression. As such, it was important to determine whether PPS treatment could influence the progression of histological changes in scrapie-infected hamsters, and whether it caused any changes in mock-infected hamsters.

In order to accomplish this, hamsters from all groups were evaluated for these histological hallmarks after they were euthanized. Initially, hamsters remained in the four groups used in the comparison of MRI results, and the following four regions were evaluated: the hippocampus; the cortex at the level of the thalamus; the thalamus; and the hypothalamus. When data from all regions were pooled and hamster groups were compared, the two scrapie-infected groups had significantly greater measurements than mock-infected groups with respect to all three histological hallmarks ($p<0.001$ for gliosis, PrP^{Sc} deposition and vacuolation area). Since this confirmed that mock-infection of hamsters did not result in the appearance of any histological changes typical of prion disease, the evaluation was adjusted such that mock-infected hamsters were excluded.

3.4.4.1 Influence of Intra-cerebral PPS Treatment on Histology in Scrapie-Infected Hamsters

In this new evaluation, the two remaining hamster groups, namely Scrapie-Infected I.c. PPS and Scrapie-Infected No I.c. PPS were evaluated with respect to hamster group, brain region, and Group x Region comparisons. When data from all regions of interest were pooled, no significant differences were found between Scrapie-Infected I.c. PPS and Scrapie-Infected No I.c. PPS hamsters with respect to any of the histological hallmarks of prion disease. Considering PrP^{Sc} deposition, the difference approached statistical significance ($p<0.08$), with levels in hamsters that received I.c. PPS greater than in those that did not. When different regions of the brain were compared for levels of PrP^{Sc} deposition, the following order was observed between regions: thalamus >>> cortex > hypothalamus > hippocampus. Differences between all regions except the cortex and the hypothalamus were statistically significant (Table 18). Total vacuole area in the thalamus was significantly greater than in the hippocampus and the hypothalamus ($p<0.025$); although differences between the thalamus and the cortex approached statistical significance ($p<0.07$), there were no significant differences between other regions. Similarly, no significant differences were observed in gliosis levels between any regions of the brain.

When groups and regions were evaluated together, no significant differences were observed between any Group x Region combinations with respect to gliosis levels. Total vacuole levels in the hypothalamus of Scrapie-

Table 18. Region Comparison of PrP^{Sc} Deposition in Scrapie-Infected Hamsters.				
	p values			
	Hippocampus	Cortex	Thalamus	Hypothalamus
Hippocampus		<0.001	<0.001	<0.05
Cortex	<0.001		<0.001	0.36
Thalamus	<0.001	<0.001		<0.001
Hypothalamus	<0.05	0.36	<0.001	

Statistically significant results indicated in black.

Infected No I.c. PPS hamsters were significantly lower than those in the thalamus ($p<0.005$) and hypothalamus ($p<0.05$) in Scrapie-Infected I.c. PPS hamsters and the thalamus ($p<0.002$) of Scrapie-Infected No I.c. PPS hamsters. When PrP^{Sc} deposition was compared in Group x Region combinations, a large number of instances of statistical significance were observed (Table 19). The order of brain regions remained the same as in the comparison of brain regions only, and measurements from the same brain region were invariably close between the two hamster groups. With respect to a given brain region, measurements in Scrapie-Infected I.c. PPS hamsters were invariably greater than those in Scrapie-Infected No I.c. PPS hamsters. However, differences between hamster groups in a given brain region were never statistically significant.

3.4.4.2 Pentosan Polysulphate Slows the Appearance of Histological Hallmarks of 263K Scrapie in Hamsters

In order to evaluate the effects of PPS treatment on the appearance of histological hallmarks of prion disease, each of the six treatment groups were compared with respect to these hallmarks in each of the four regions of interest. In Figure 38 A, vacuolation levels are compared, with the treatment groups arranged based loosely on increasing survival time. Comparing levels in a given brain region, a common pattern is observed, of increasing values in the first four treatment groups (in some cases, values increase only through the first three groups). This increase did not hold in the two treatment groups that received

Table 19. Group x Region Comparison of PrP^{Sc} Deposition in Scrapie-Infected Hamsters.

Group/Region ID			p values							
	Group	Region	1	2	3	4	5	6	7	8
1	A	Hippo		0.437	<0.001	0.531	0.868	0.584	<0.001	1
2		Cortex	0.437		0.06	1	<0.015	0.999	0.314	0.418
3		Thal	<0.001	0.06		<0.05	<0.001	<0.005	0.896	<0.001
4		Hypo	0.531	1	<0.05		<0.02	1	0.232	0.526
5	B	Hippo	0.868	<0.015	<0.001	<0.02		<0.01	<0.001	0.476
6		Cortex	0.584	0.999	.005	1	<0.01		<0.025	0.545
7		Thal	<0.001	0.314	0.896	0.232	<0.001	<0.025		<0.001
8		Hypo	1	0.418	<0.001	0.526	0.476	0.545	<0.001	

Statistically significant results indicated in black. A: Scrapie-Infected i.c. PPS; B: Scrapie-Infected No i.c. PPS. Hippo: Hippocampus; Thal: Thalamus; Hypo: Hypothalamus.

Figure 38. Effect of PPS treatment on histological change in scrapie-infected hamsters.

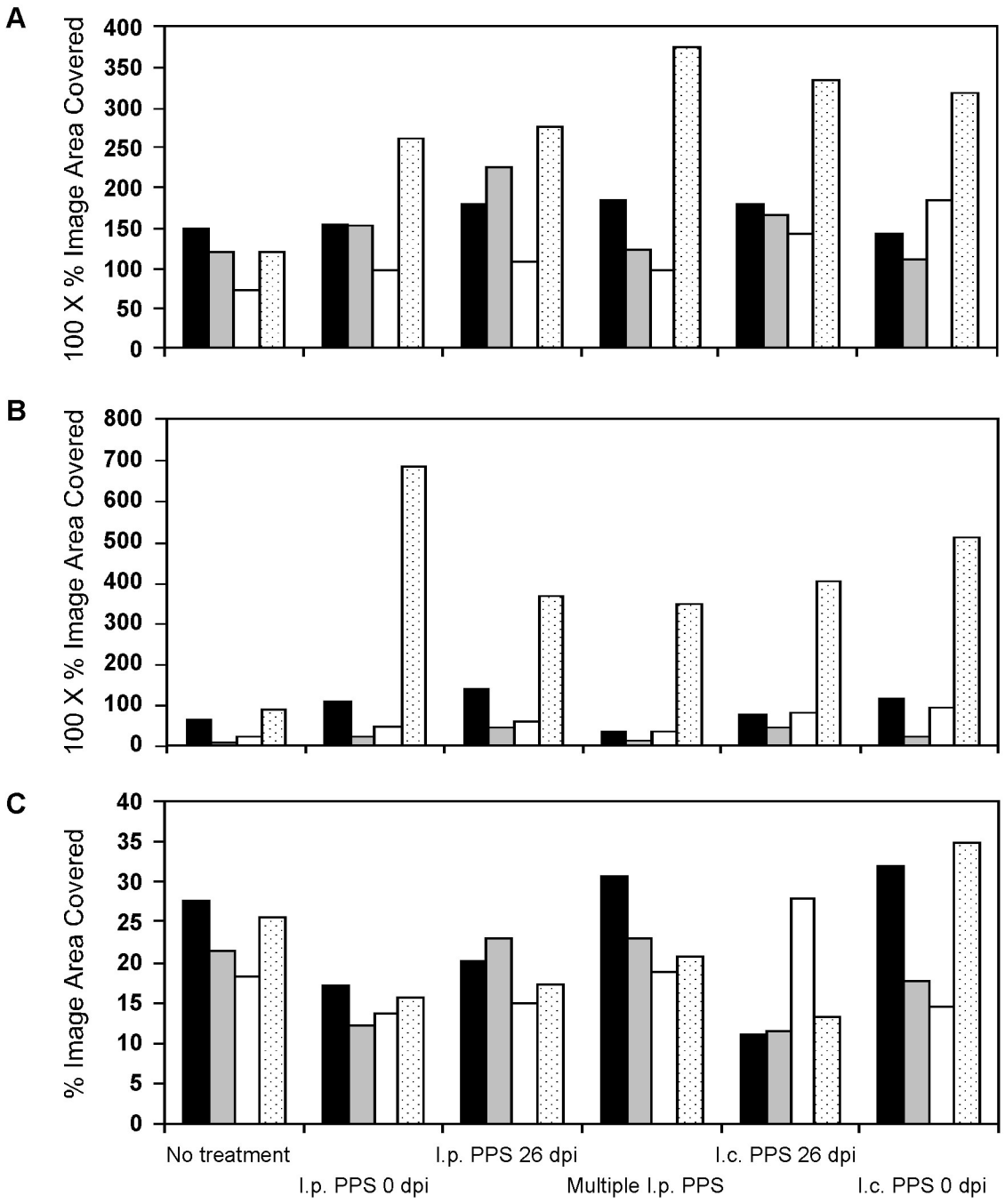

Total vacuole area (A), PrPSc deposition (B), and gliosis (C) were measured in the cortex (black bars), hippocampus (grey bars), hypothalamus (white bars), and thalamus (dotted white bars) of scrapie-infected hamsters that received one of six treatments. PPS: pentosan polysulphate; i.p.: intra-peritoneal; i.c.: intra-cerebral; dpi: days post injection. Multiple i.p.: at 26, 40, and 54 dpi.

intra-cerebral PPS treatment, indicating that the relatively successful PPS treatments slowed the appearance of vacuoles in all regions of the brain. When levels of PrP^{Sc} were compared in all treatment groups, a similar effect was observed (Figure 38 B). Briefly, two parallel increases were apparent with respect to PrP^{Sc} deposition: the first occurred in the first three treatment groups, and a second was observed in the last three (more successful) treatment groups. These observed patterns illustrate the two effects that act on the normal rate of accumulation of PrP^{Sc}: as time post infection increased, so did PrP^{Sc} accumulation; and, PPS treatments that were relatively successful (as determined by their effects on survival time) slowed the rate of accumulation of PrP^{Sc}. In contrast, when gliosis levels were compared between all treatment groups in all regions of the brain, no clear patterns relating to survival time or PPS treatment were observed (Figure 38 C).

In order to further evaluate the effects of PPS treatment on the appearance of histological hallmarks, a second exercise was undertaken. In each region of the brain, levels of each histological characteristic were plotted in individual animals as a function of time. Mean levels measured previously between 19 and 61 dpi were then added to these graphs. Finally, a trend line was added, representing the stage during which the histological characteristic of interest increased in the initial histological study. This trend line was then extended to cover the time frame relevant to the present study. This exercise made it possible to compare values attained in hamsters that had been treated

with PPS to the expected values if histological characteristics continued to increase at their usual rate.

When PrP^{Sc} values in the cortex were compared to the expected trend line, a number of individual animals conformed to the expected values (Figure 39 B). However, there were also a number of animals that produced values that were much lower than expected. As a general rule, animals that had longer survival times, and could therefore be categorized as having received more successful treatments, were less likely to reach expected values. When gliosis levels were evaluated, no individual animals reached the levels predicted by the trend line (Figure 39 C). In fact, no individual animals produced gliosis levels that were significantly greater than the mean value previously measured in pre-clinical hamsters at 61 dpi. In contrast, most individual hamsters conformed to expected vacuolation values (Figure 39 A). The exceptions to this rule were the two hamsters with the longest survival times, again indicating that when PPS treatment was most successful, it slowed the rate of accumulation of the histological characteristics of prion disease.

Results in the hippocampus were similar to those observed in the cortex (Figure 40). As before, few individual hamsters attained expected levels of PrP^{Sc} deposition, while measured levels of vacuolation were much closer to expected values. A common observation was that the individual animals with the longest survival times fell the furthest below expected values. In contrast to results in the cortex, gliosis levels in the hippocampus largely followed the expected trend line,

Figure 39. Effect of PPS treatment on histological change in the cortex.

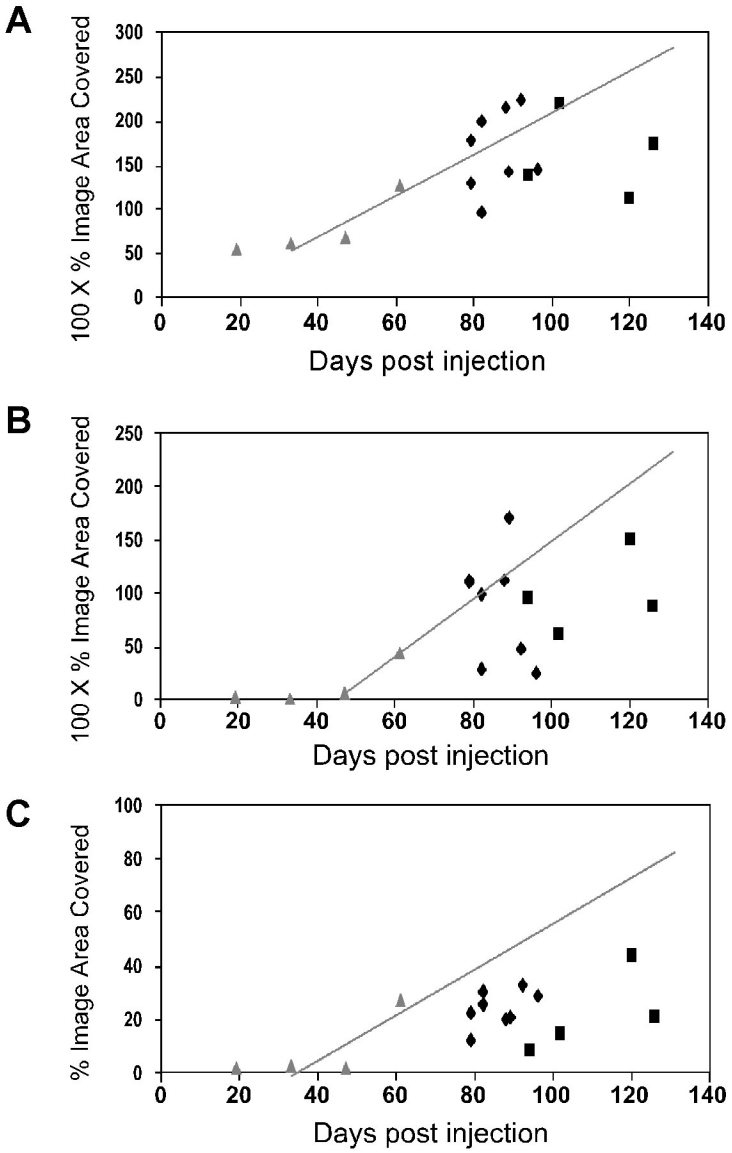

Measurements of total vacuole area (A), PrPSc deposition (B), and gliosis (C) in scrapie-infected hamsters treated with pentosan polysulphate (PPS) are compared to expected values. Black squares: individual hamsters treated intra-cerebrally with PPS; black diamonds: individual hamsters that were not treated with i.c. PPS; grey triangles: mean values calculated in untreated scrapie-infected hamsters at four time points in the initial histology study; grey line represents the expected values, based on the trend in the initial histology study.

Figure 40. Effect of PPS treatment on histological change in the hippocampus.

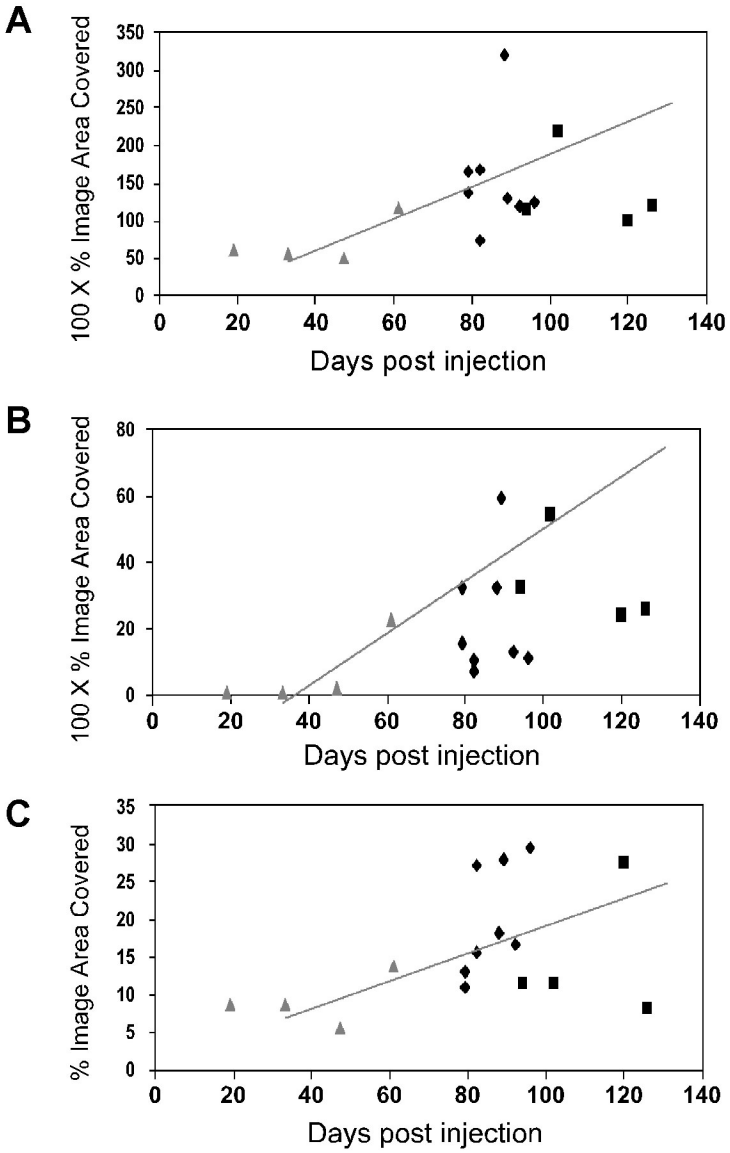

Measurements of total vacuole area (A), PrPSc deposition (B), and gliosis (C) in scrapie-infected hamsters treated with pentosan polysulphate (PPS) are compared to expected values. Black squares: individual hamsters treated intra-cerebrally with PPS; black diamonds: individual hamsters that were not treated with i.c. PPS; grey triangles: mean values calculated in untreated scrapie-infected hamsters at four time points in the initial histology study; grey line represents the expected values, based on the trend in the initial histology study.

although some individual animals had values either far above or far below the expected.

The hypothalamus was arguably the region of the brain that followed the expected trends most closely (Figure 41). Most individual hamsters came close to expected PrP^{Sc} deposition values, although none exceeded the expected levels. In fact, the individual animals in the present study seemed to share the same rate of increase in PrP^{Sc} levels, but with a delayed onset of this increase, i.e. levels increased in parallel with the trend line. Similarly to the hippocampus, gliosis levels in the hypothalamus broadly followed the trend line, although values in individual hamsters occasionally fell far from the line. Vacuolation levels measured in the present study followed the expected trend line very closely.

When the thalamus, the region most affected histologically both in the initial study and the present one, was evaluated, a varied picture was observed (Figure 42). While some individual hamsters reached expected PrP^{Sc} levels, most did not. Furthermore, as survival time increased, total PrP^{Sc} levels seemed to reach a plateau. With respect to gliosis, results were very similar to those observed in the cortex: no individual hamsters reached the expected values, and no values observed in the present study were significantly greater than the mean values previously measured in pre-clinical hamsters. Finally, vacuolation levels observed in the thalamus broadly followed the expected trend line, although the individual hamsters with the longest survival times fell short of expected values, in one case significantly.

Figure 41. Effect of PPS treatment on histological change in the hypothalamus.

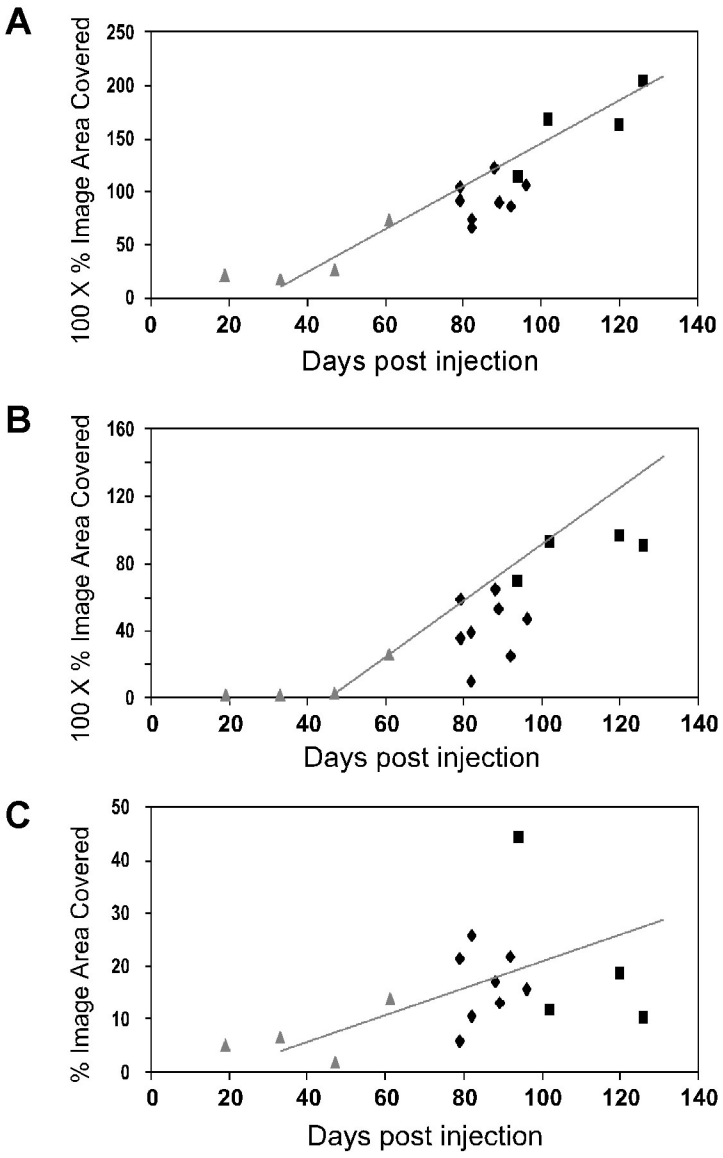

Measurements of total vacuole area (A), PrPSc deposition (B), and gliosis (C) in scrapie-infected hamsters treated with pentosan polysulphate (PPS) are compared to expected values. Black squares: individual hamsters treated intra-cerebrally with PPS; black diamonds: individual hamsters that were not treated with i.c. PPS; grey triangles: mean values calculated in untreated scrapie-infected hamsters at four time points in the initial histology study; grey line represents the expected values, based on the trend in the initial histology study.

Figure 42. Effect of PPS treatment on histological change in the thalamus.

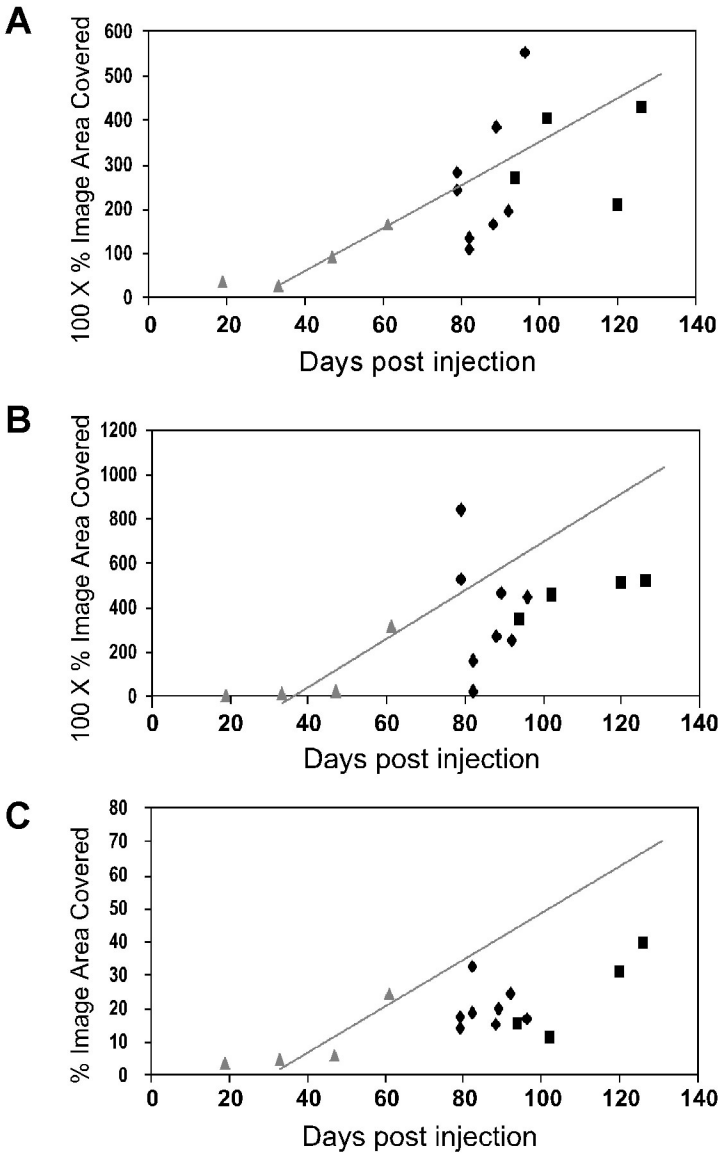

Measurements of total vacuole area (A), PrPSc deposition (B), and gliosis (C) in scrapie-infected hamsters treated with pentosan polysulphate (PPS) are compared to expected values. Black squares: individual hamsters treated intra-cerebrally with PPS; black diamonds: individual hamsters that were not treated with i.c. PPS; grey triangles: mean values calculated in untreated scrapie-infected hamsters at four time points in the initial histology study; grey line represents the expected values, based on the trend in the initial histology study.

4. Discussion

4.1 Pre-clinical Changes on Magnetic Resonance Images of Scrapie-infected Hamsters are Unrelated to Histological Changes

I have shown above that it is possible to distinguish infected hamsters from mock-infected and uninfected controls using MRI during the pre-clinical stage of disease, and to follow disease progression longitudinally in individual animals. Further to this, I have shown that the differences observed on pre-clinical MR images do not correlate with the typical histological hallmarks of prion disease, potentially identifying a new marker for damage in the brain. These histological hallmarks were measured using an image analysis system that was verified by comparing results that it produced to previously published data. Considering changes in T_2 relaxation time and apparent diffusion coefficient, it appears as though fluid accumulates in the hippocampus early in 263K scrapie disease progression in Syrian golden hamsters.

4.1.1 Scrapie-infected Hamsters can be Identified by Magnetic Resonance Image Abnormalities in the Hippocampus

By combining data from two consecutive T_2 MR image slices, hamsters infected intra-cerebrally with 263K scrapie were differentiated from mock-infected and uninfected controls by statistically significant hyper-intensities in the hippocampus at 33, 47, and 61 dpi, and from uninfected controls only at 19 dpi. In a similar manner, infected hamsters were differentiated from all uninfected hamsters (combined in a single group) at all four time points. Differences in relative T_2 values between mock-infected and uninfected control hamsters were

never statistically significant, although in one case, this may have been partly due to the use of less sensitive non-parametric statistical tests. The presence of lesions identified on T_2 maps was confirmed by their presence on ADC maps. Although statistically significant differences were more scarce in the comparison of ADC values, it was possible to distinguish between infected and all uninfected hamsters at all four time points in either one MRI slice or the other. When all scrapie-infected hamsters were compared to mock-infected and control hamsters, the only significant differences found were between scrapie-infected and mock-infected hamsters in Slice 5 at 33 and 47 dpi, and in Slice 6 at 61 dpi. Differences in relative ADC values between hamster groups were likely minimized by the fluctuation of raw ADC values in the thalamus, which may have resulted in overly high relative ADC values in the mock-infected and control groups. Both the fluctuation of raw ADC values and differences in these measurements between hamster groups in the thalamus were greater than the corresponding raw T_2 relaxation times, exacerbating this effect. When the relative T_2 and ADC values in the hippocampus of scrapie-infected hamsters in MRI slices 5 and 6 were compared, the respective curves were strikingly similar. This observation lends further support to the relationship between the increases in T_2 and ADC values; the nature of this relationship will be discussed further below.

The data presented here are significant, because all four of the time points studied were in the pre-clinical stage of disease; the documented incubation period of 263K scrapie in Syrian golden hamsters following i.c. infection is on the

order of 68-71 dpi [215,216]. Although the 263K strain of scrapie is very fast acting, it was remarkable to find significant differences as early as those reported here. Abnormalities on MR images have previously been reported in both humans [282,284,290–292] and rodents [288,289,293], with variable results; preliminary results from this study have also been published [294]. In the case of the human studies, all MRI scans were carried out during the symptomatic stage of disease. To my knowledge, only one other rodent study has identified pre-clinical differences between infected and control animals, at 120 dpi using the 139A scrapie strain in CD-1 mice [289]. While it is difficult to compare disease stages in two different TSE strains in two different hosts, it seems apparent that the differences presented in the current study represent an earlier stage of disease: here changes were observed at the one-quarter to one-third mark of the incubation period, compared to approximately the two-third mark in the previous study.

4.1.2 Histological Changes in Scrapie-infected Hamsters

4.1.2.1 Evaluation of ImagePro Software

In order to gain a clearer understanding of the reasons behind increased elative T_2 and apparent diffusion coefficient values in the hippocampus of infected hamsters, spongiform change, PrP^{Sc} deposition and gliosis were evaluated at all four time points at which MR images were collected. This was done using ImagePro image analysis software, once it was determined that the system could accurately measure histological characteristics. To make this determination, spongiform change in brain tissue removed from C57/Bl mice

infected with ME7 scrapie at the clinical stage of disease was measured using ImagePro, and the resulting lesion profile was compared to known values previously reported in the literature. More specifically, the ImagePro lesion profile was compared to a composite profile produced by taking the mean value in each region of the profiles reported by Fraser and Dickinson [191] and by Bruce *et. al.* [33]. Generally speaking, the ImagePro profile was satisfactorily similar to the composite literature profile in both individual values and shape of the profile. Differences were more prevalent and of a greater magnitude in the upper half of the scale. This is likely due at least in part to the differences that exist between the two scales used in the respective profiles. Taking a total vacuole area/image score for each mouse, which was used in turn to produce a mean score for each region, produced the ImagePro profile. Since these scores ranged to a maximum of 23000 pixels, they could easily be converted to a 0-5 scale by dividing each score by 5000, in order to match the scale used in the literature. This standard 0-5 scale is subjective, with each score corresponding to a verbal description. Fraser and Dickinson [191] define the scores as follows: 1, a few vacuoles, widely and evenly scattered; 2, a few vacuoles evenly scattered; 3, moderate numbers of vacuoles, evenly scattered; 4, many vacuoles with some confluence; and 5, dense vacuolation with most of field confluent. Since the vacuolation scores produced using this method are dependent upon the judgement of the pathologist evaluating the section, it is unlikely that linearity is maintained throughout the range of the scale. Figure 43 demonstrates a possible relationship between the total vacuole area/image and the 0-5 scale

Figure 43. Comparison of lesion profiles using subjective and linear scales.

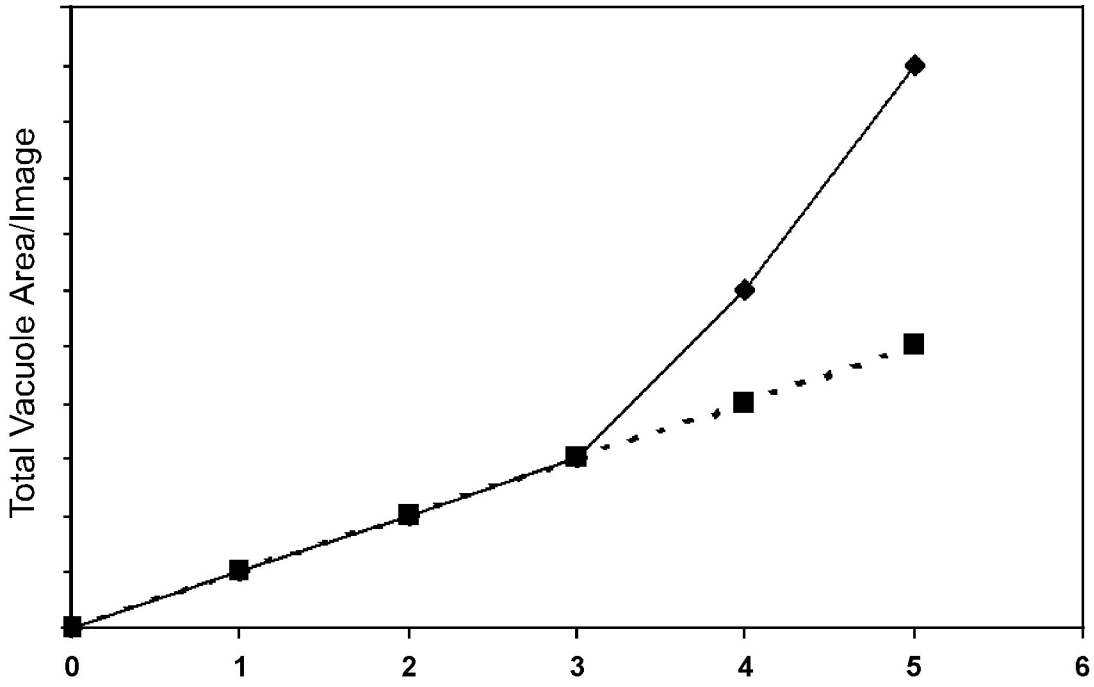

The relationship between total vacuole area per image and vacuole score is explored, with respect to the hypothetical differences between a subjective scale and a linear scale. Solid line: hypothetical subjective scale; broken line: linear scale.

based on the subjective descriptions above, compared to a purely linear scale. This relationship is most likely to remain close to linearity at values close to zero, while the relationship between total vacuole area/image and (subjective) vacuole score is likely to depart from linearity at higher values, as shown in Figure 43.

Without being able to determine the precise nature of this relationship, it is impossible to determine exactly how closely these two lesion profiles agree. However, by carrying out a brief exercise, it is possible to determine that differences observed between the ImagePro and literature lesion profiles were likely exaggerated. In comparing the lesion profile of C57Bl mice infected with ME7 scrapie produced by ImagePro to the composite lesion profile from the literature (Figure 17 A), the region with the most differences in both individual values and shape of the curve was the portion spanning areas 5-7 (thalamus, hippocampus, and septum). However, if those values greater than three in the ImagePro profile (thalamus=4.19; septum=4.54) are transformed using Figure 43, they become approximately 3.4 and 3.5, respectively. The effect of this transformation on the ImagePro lesion profile is two-fold: it decreases the magnitude of the differences in individual values in these two brain regions compared to the literature profile; and it flattens the area of the profile spanning regions 5-7, minimizing the major difference in shape between the two lesion profiles. If the relationship between total vacuole area/image and subjective vacuole score begins to depart from linearity earlier than at a score of 3, or if that departure is more drastic than illustrated in Figure 43, differences between the ImagePro and literature lesion profiles would be further minimized. In

conclusion, these two profiles were in close enough agreement to move forward using ImagePro as a method to quantify not only spongiform change, but also PrP^{Sc} deposition and gliosis in scrapie-infected hamsters.

4.1.2.2 The Thalamus is the Brain Region Most Affected by Histological Change in Scrapie-infected Hamsters

Since it was determined that ImagePro could be used to quantify the histological hallmarks of prion disease, it was used to evaluate spongiform change, PrP^{Sc} deposition, and gliosis in scrapie-infected hamsters, following some refinement (as described in Materials and Methods). When measurements of these histological characteristics were compared to MRI results, no correlations were found. In fact, the only significant differences observed between infected and uninfected hamsters in a given brain region were in spongiform change at 61 dpi and in PrP^{Sc} deposition at 47 and 61 dpi in the thalamus; and in gliosis at 19 dpi in the hippocampus and at 61 dpi in both the cortex and the thalamus. Of these statistical differences, the gliosis level at 19 dpi was the only one observed in the hippocampus, the region most affected according to MRI. However, examining the pattern of onset of gliosis in the hippocampus (Figure 19 C), it appears as though gliosis levels are effectively constant at a baseline level for the first three time points, before increasing at 61 dpi. The statistical difference observed was likely due not to a higher than normal measurement in infected animals, but rather to an abnormally low measurement in uninfected hamsters; in fact, gliosis levels in uninfected

hamsters showed more variability between time points in the hippocampus than in infected hamsters (data not shown).

There were other instances when large differences between infected and uninfected hamsters were found to be statistically insignificant due to large variances within groups, notably with respect to vacuolation at 47 dpi in the thalamus. This is an indication that although the incubation period of a given TSE is extremely consistent in a given host, variability remains in the degree of histological change, at least during the pre-clinical stage of disease. It was also possible to determine the order in which pathological characteristics appeared relative to one another, as well as the order in which each brain region studied was affected with respect to histology. The thalamus was clearly the region that first underwent the progression of pathological changes, as it was the only region which had significant differences between infected and uninfected hamsters in all categories at 61 dpi, and it was the only region in which significant and large non-significant differences were observed before 61 dpi. The hypothalamus was the only region where no significant differences were ever observed, indicating that it was the last of the four brains regions studied to undergo pathological changes. The cortex and hippocampus were intermediate with respect to the progression of pathological changes due to disease. Since there were significant differences in both PrP^{Sc} deposition and gliosis in the cortex, and in PrP^{Sc} deposition only in the hippocampus, it appears as though histological changes progress slightly more rapidly in the cortex than in the hippocampus. With respect to the order in which histological hallmarks appeared in scrapie-infected hamsters, PrP^{Sc}

deposition preceded both spongiform change and gliosis; from the available data, it is difficult to conclude that either of the latter two pathological changes occurred before the other.

When scrapie-infected hamsters were considered in isolation, differences in pathological characteristics were frequently observed between the four regions of interest. The only observed differences in gliosis levels involved higher than expected values in the hippocampus at 19 dpi. With respect to PrP^{Sc} deposition, levels in the thalamus were significantly greater than in most other brain regions studied from 33 to 61 dpi. In general, spongiform change, as reflected by total vacuole area and vacuole number, was significantly greater in the cortex and hippocampus at the early time points, and in the thalamus and cortex at 47 dpi, while there were no significant differences at 61 dpi. These data indicate that the background levels of vacuole scores are higher in the cortex and hippocampus than in the hypothalamus and thalamus, and that the thalamus is the first region to undergo a sizeable increase in spongiform change. The lack of significant differences at 61 dpi reflects the development of spongiform change in the other three regions of interest.

Since few statistical differences were observed between scrapie-infected and uninfected hamsters with respect to the histological hallmarks of prion disease, it was valuable to examine trends in measurements of histological markers. The appearance of spongiform change, PrP^{Sc}, and gliosis followed a common pattern in the hippocampus, cortex, and hypothalamus of 263K scrapie-infected hamsters: a baseline level was maintained until 47 dpi, followed by an

increase at 61 dpi. This same pattern held in the thalamus with respect to gliosis, whereas the increases in PrP^{Sc} levels and spongiform change occurred earlier. A linear increase in spongiform change was apparent through 47 and 61 dpi, while PrP^{Sc} levels increased at each time point, producing a curve that approached exponential characteristics. In broad terms, these results agree with previous studies involving the same scrapie and host strains and route of inoculation, although some differences exist in the details. Two studies sequentially evaluated spongiform change and gliosis following i.c. infection in regions of the brain including those examined here [219,221]. The earliest observation of both pathologies occurred between 49 and 57 dpi [221], although only minor changes were observed at 52 dpi in the other study [219]. Masters *et. al.* report that from 49-57 dpi onward, the degree of spongiform change in the cortex and the hippocampus is greater than in the thalamus and the hypothalamus, while gliosis is more prevalent in the thalamus and the cortex [221]. These results support the findings reported here regarding gliosis, but the highest degree of spongiform change observed here was in the thalamus from 47 dpi onward. At both 8-23 dpi and 32-35 dpi, GFAP staining was absent in all regions studied, while only very minor spongiform change was reported (scores < 0.5) in both the hippocampus and the thalamus [221], in agreement with data reported here. Two studies have reported the sequential, pre-clinical distribution of PrP^{Sc} in the brain following i.c. infection of Syrian golden hamsters with Sc237 scrapie, which is likely the same strain as 263K scrapie [222,223]. These studies evaluated PrP^{Sc} in the brains of infected hamsters between 7 and 65 dpi, either

by histoblot [222] or by determination of PrP^{Sc} concentration in different regions of the brain [223]. These data indicated that PrP^{Sc} accumulated earliest and most significantly in the thalamus, with significant deposition occurring at 28-35 dpi [222,223], in agreement with my data. Similarly, significant deposition in the cortex, hypothalamus, and hippocampus was observed only at 65 dpi [222,223].

4.1.2.3 Histological Changes Cannot Explain Magnetic Resonance Image Abnormalities Observed in Scrapie-infected Hamsters

Taken together, the histological observations reported here cannot explain the hyper-intensities found on T_2- and diffusion-weighted MR images, since those MR abnormalities precede histological changes, and since the regions most affected according to MRI and histology are not the same. These findings run in sharp contrast to previously published data regarding the relationship between abnormalities on T_2-weighted MR images and histological changes in rodents infected with prion disease. Sadowski *et. al.* carried out μMRI on mice infected with scrapie once clinical symptoms appeared (around 150 dpi), and up to 180 dpi, when severe neurological deficits were present [289]. They observed hyper-intensities in the septum, hippocampus, and cortex of infected mice, with corresponding increases in PrP^{Sc} deposition and gliosis, while spongiform change was not significant in these areas. Meanwhile, Chung *et. al.* carried out T_2-weighted MR imaging on 263K scrapie-infected hamsters during the clinical stage of disease (74 dpi) and compared the results to histological examination [288]. They concluded that spongiform change correlated with low signal intensity and gliosis correlated with high signal intensity, while PrP^{Sc} deposition

did not appear to affect T_2 relaxation time. In certain regions of the brain, where significant spongiform change and gliosis were evident, the MR signal appeared normal, due to contradictory effects. When the Chung model is applied, the Sadowski *et. al.* results can be explained satisfactorily, since significant gliosis was present in the hyper-intense regions, while vacuolation was not. However, the Chung model does not stand up to the results reported here. The cortex, hippocampus and hypothalamus all share the same pattern of onset of histological changes (Figure 21): vacuolation, PrP^{Sc} deposition, and gliosis all maintain approximately constant levels until 47 dpi, before increasing at 61 dpi. According to the model, no increases in MR image intensity would be expected in any of these regions before 61 dpi; even at this final time point, hyper-intensities would not necessarily be expected since spongiform change and gliosis both increase. While the MR results reported here agree with this prediction for both the cortex and the hypothalamus, the hippocampus is another case entirely: the hyper-intensity observed beginning as early as 19 dpi cannot be explained by the histological data, since any changes in histology in this region occur only at 61 dpi. The thalamus was the only region of the brain that did not follow the common pattern. In this case, both vacuolation and PrP^{Sc} deposition increased in advance of gliosis. Under the model, lower than normal signal intensity would be expected at 47 dpi in the thalamus, with a return to normal, or towards normality at 61 dpi, depending on the relative strength of the effects of vacuolation and gliosis. While Chung's model holds in the cortex and the

hypothalamus, it fails in both the region most affected histologically (the thalamus) and that most affected on MR images (the hippocampus).

4.1.2.4 Vasogenic Oedema May Explain Magnetic Resonance Image Abnormalities

T_2 relaxation time is determined by the relative mobility of water molecules. Bio-fluids are characterized by relatively long T_2 relaxation times, because of the high velocity of water molecules; dense, viscous fluids usually result in short T_2 relaxation times due to the reduced velocity of water molecules. Long T_2 relaxation times in tissues, therefore, are the result of the presence of relatively large amounts of bio-fluids. The observed increase in T_2 relaxation time in the hippocampus of infected hamsters is thus indicative of fluid build-up unrelated to the well-established pathological changes that occur during disease pathogenesis. The correlation of increased ADC values with high T_2 relaxation times supports this conclusion. The apparent diffusion coefficient is also a measure of the mobility of water molecules: high ADC values correspond to free movement of water, while low values indicate that water movement is restricted, for example by cell membranes. So, T_2 relaxation time can be thought of as a measure of the amount of fluid in a tissue, while apparent diffusion coefficient measures the ability of that fluid to move within the tissue. As such, long T_2 relaxation times and high ADC values observed in the hippocampus of infected hamsters would seem to indicate the accumulation of extracellular fluid, also known as vasogenic oedema. However, caution must be exercised in coming to this conclusion. Although high ADC values are associated with vasogenic

oedema, and low ADC values with cytotoxic oedema [295], the ability to make this distinction is dependent upon the parameters used during data collection. Due to the specific collection parameters used in the present study, it is impossible to exclude the presence of cytotoxic oedema in regions showing high ADC values. However, vasogenic oedema presents a much more attractive explanation due to the chronic nature of the abnormalities on both ADC and T_2 maps. Cytotoxic oedema is the result of accumulation of fluid inside cells, and is characterized by cellular swelling. Following initiation of swelling, individual oligodendrocytes [296] and neurons [297] mostly succumb to necrosis within 24 hours, while astrocytes begin to undergo necrosis after 24 hours [298]. As such, if cytotoxic oedema occurred, it would have only a transient effect on ADC values, but it would result in swelling followed by necrosis of neurons as well as glial cells. While hypertrophy of glial cells has been documented in this disease model [220], a high degree of gliosis only occurs at about 80 dpi [219]. Because of this, it is likely that the corresponding hyper-intensities on T_2- and diffusion-weighted MR images are the result of vasogenic oedema in the hippocampus of 263K scrapie-infected hamsters. In further support of this, breakdown of the blood-brain barrier, which is the cause of vasogenic oedema [295], has been reported in experimental prion disease [293,299], in both cases evaluated by MRI. Chung *et. al.* reported disruption of the blood-brain barrier during clinical scrapie in hamsters [293], while Brandner *et. al.* observed progressive break down specific to neural grafts over-expressing PrP^C in PrP null mice infected with scrapie [299]. In the latter paper, mice were imaged at two different time points,

either early or late in infection. Blood-brain-barrier disruption was already evident at the first time point studied, about twenty-five days prior to the appearance of histological changes in the neural grafts.

Interestingly, Sadowski *et. al.* found that hyper-intensities in pre-clinical mice were most evident in the hippocampus, accompanied by PrP^{Sc} and gliosis levels intermediate between clinical mice and controls [289]. While it may be that this hyper-intensity is a result of increased gliosis, it may also reflect a transition from the situation suggested here. It would be valuable to determine whether increased T_2 relaxation time and apparent diffusion coefficient in the hippocampus resulting from oedema is a common characteristic early in prion disease pathogenesis. It is possible that late in the disease course, as vacuolation and gliosis become more pronounced, their possible effects on T_2 relaxation time add to and potentially overshadow the effects of oedema. However, in 263K scrapie infection of Syrian hamsters at least, T_2 relaxation time and apparent diffusion coefficient are determined by the presence of oedema in the hippocampus early in disease progression.

4.1.2.5 Dysregulation of Aquaporin-4 Expression and Activity May Play a Role in Disease Progression

Increased expression of the water channels aquaporin-1 and –4 (AQP1 and AQP4) has been reported in cases of CJD, as well as in BSE-infected bovine-PrP transgenic mice [300]. In the case of the transgenic mice, AQP1 and AQP4 levels were elevated only at 270 dpi, when vacuoles and PrP^{Sc} deposits appeared. Expression of AQP4, the main water channel in the brain, is thought

to be regulated through protein kinase C (PKC) and/or mitogen-activated protein kinase (MAPK) signalling pathways. Specifically, AQP4 mRNA and protein levels are increased through a p38 MAPK-dependent pathway [301], and inhibited in a PKC-dependent manner [302]. In addition, PKC has been shown to inhibit the activity of AQP4 by phosphorylating it, causing a decrease in its permeability to water [303,304]. Although the function of PrP^C has not been fully elucidated, it has been implicated in cell signalling, including through both MAPK- [141,144] and PKC-dependent pathways [140]. Interestingly, the sequential activation of p38 MAPK has been demonstrated from 50 dpi onward in 263K scrapie-infected hamsters [305]. It is tempting to speculate that dysregulation of p38 MAPK and/or PKC signalling pathways due to a loss/modulation of normal PrP^C function may be responsible for the increased expression of AQP4 observed during the clinical stage of prion disease.

As a water channel, AQP4 is important in maintaining water homeostasis in the brain, and may therefore be implicated in cerebral oedema. AQP4 null mice have been evaluated in their response to both vasogenic and cytotoxic oedema. The absence of AQP4 was associated with improved neurological outcome and reduced brain swelling in models of cytotoxic oedema including water intoxication and ischemic stroke [306], and pneumococcal meningitis [307]. In contrast, AQP4 null mice faired worse than controls in models of vasogenic oedema including staphylococcal brain abscess [308], and intraparenchymal fluid infusion, freeze-injury, and brain tumour [309]. These observations indicate that AQP4 activity is helpful in combating vasogenic cerebral oedema, but detrimental

in cases of cytotoxic oedema. PrP^C expression is upregulated following focal cerebral ischemia [310], a model of cytotoxic oedema, and PrP^C deletion leads to worsened outcome following ischemic brain injury [311,312]. This supports the theory that loss of PrP^C function late in prion disease pathogenesis results in increased AQP4 expression, since increased AQP4 expression would be detrimental following ischemic brain injury. As stated above, the chronic oedema reported in this study is thought to be vasogenic in nature. If this is the case, normal AQP4 expression may be sufficient to prevent very severe vasogenic oedema during the early stages of disease pathogenesis. It is conceivable that increased expression of AQP4 late in prion disease, either as a result of loss of PrP^C function or potentially as upregulation in response to vasogenic oedema, leads to cytotoxic oedema. Cytotoxic oedema is a potential explanation for both hypertrophy of glial cells and neuronal death (through necrosis). Cerebral oedema itself can cause death as a result of elevated intra-cranial pressure due to increased total brain volume leading to brain ischemia or herniation [313]. As such, cerebral oedema may not only be an early marker of prion disease, but a potential contributor to cause of death as well.

In Figure 44, potential mechanisms for the effects of PrP^C/PrP^{Sc} on AQP4 expression, and the effects of AQP4 dysregulation on disease pathogenesis, respectively, are illustrated. These mechanisms postulate that scrapie infection results initially in oxidative stress, which causes progressive damage to the blood-brain-barrier, resulting in progressive vasogenic oedema. Oxidative stress in general, and nitric oxide (NO) in particular are inducers of

Figure 44. Model of interactions relating PrP and AQP4 expression.

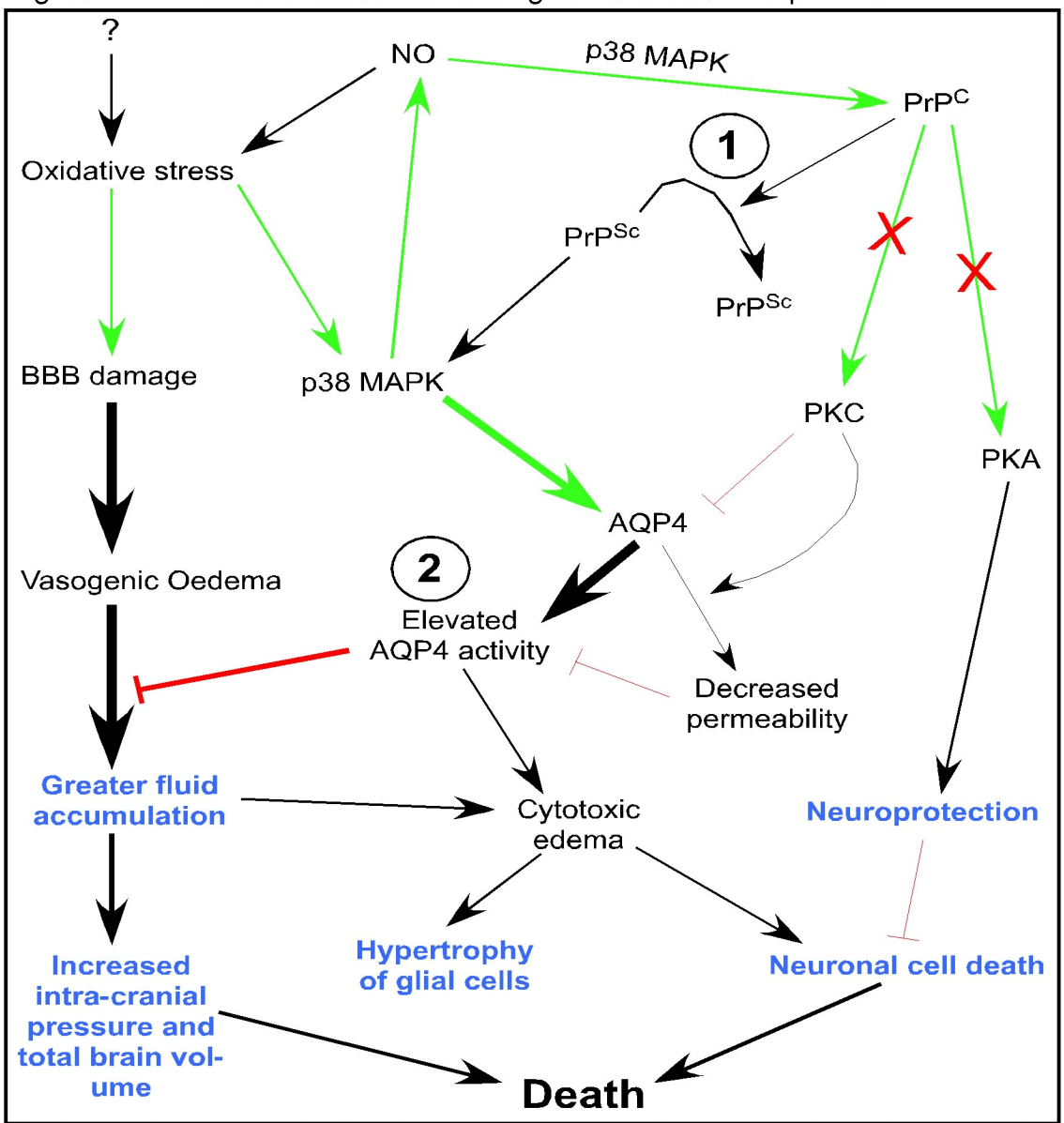

During early stages of prion disease pathogenesis, vasogenic oedema may be caused by leakiness of the blood brain barrier (BBB), which could be a result of oxidative stress caused by nitric oxide (NO) or other reactive oxygen species. This model attempts to explain how vasogenic oedema could be related to PrP and AQP4 (aquaporin-4) expression, and how it could ultimately lead to death. AQP4 expression is regulated positively by p38 MAPK (p38 Mitogen Activated Protein Kinase), and negatively by PKC (Protein Kinase C). Since PrP^{C} induces PKC, and PrP^{Sc} induces p38 MAPK, the PrP^{C}/PrP^{Sc} balance is the first important tipping point in this model (1). The second tipping point is the level of AQP4 activity (2). In the later stages of disease pathogenesis, increased AQP4 activity in the presence of large quantities of fluid would result in cytotoxic oedema causing hypertrophy of glial cells and neuronal cell death. PKA: Protein Kinase A; BBB: blood-brain-barrier.

p38 MAPK, which in turn induces expression of both PrP^C and AQP4, as well as being involved in further NO production. Normally functioning PrP^C is involved in cell signalling, including the induction of PKA and PKC. PKA has a role in neuroprotection, while PKC inhibits the expression and activity of AQP4. AQP4 functions to decrease vasogenic oedema by pumping excess fluid back into the blood. The two important tipping points in this model are the balance between PrP^C and PrP^{Sc}, and the activity of AQP4. As disease pathogenesis progresses, more and more PrP^C molecules are shunted into production of PrP^{Sc}, with less available for induction of PKC. PrP^{Sc} induces p38 MAPK, resulting in further induction of AQP4. In combination with reduced inhibition by PKC, this results in progressive increase of AQP4 activity. As pathogenesis progresses, two opposing forces would be at work in this model: progressive blood-brain-barrier disruption would lead to increased fluid accumulation, while progressively increasing AQP4 activity would work to prevent this. At some stage, there may be a tipping point when essentially all PrP^C being produced would be converted to PrP^{Sc}, resulting in greatly increased AQP4 expression due to the absence of PKC-dependent inhibition, as well as increased p38 MAPK-dependent induction. Despite the high AQP4 activity, fluid accumulation due to blood-brain-barrier breakdown would overcome the ability of AQP4 to inhibit it. In this environment, AQP4 expressed on glial cells and oligodendrocytes would begin to pump the excess fluid into the intracellular space, initiating not only cytotoxic oedema, but potentially the clinical stage of disease as well. At this stage, a three-pronged assault would be in place, potentially explaining death of the individual: neuronal

and glial cell death due to cytotoxic oedema; the absence or reduction of PKA-dependent neuroprotection; and increased intra-cerebral pressure and total brain volume.

For the first time, progressive increases in both T_2 relaxation time and apparent diffusion coefficient have been observed in the hippocampus of scrapie-infected hamsters beginning very early in disease progression. These MR image abnormalities are indicative of accumulation of fluid in the hippocampus, occurring earlier than any prion disease-associated histological changes. I speculate that alterations in AQP4 expression previously reported during clinical disease [300] may result in initiation of cytotoxic oedema, leading to glial cell swelling and neuronal death. To further explore the potential of the theories presented here, a number of issues must be clarified, including: the effects of PrP deletion on AQP4 expression in models of oedema; precise details of the regulation of AQP4 expression, and the potential role of PrP^C in those pathways; the presence or absence of oedema during the clinical stage of prion disease, and the type of oedema involved; the presence or absence of oedema early in the progression of other models of prion disease; the reason for the specific involvement of the hippocampus; and confirmation of blood-brain barrier leakiness early in disease progression, and its cause.

4.2 Evaluation of Pentosan Polysulphate as a Potential Treatment for Scrapie-infected Hamsters

After establishing a system by which prion disease progression could be followed in live animals, this system was used to test a potential drug treatment

for prion disease, pentosan polysulphate (PPS). Scrapie-infected and mock-infected hamsters were given one of five different treatment regimens that varied by route and timing of administration, or were not treated. Magnetic resonance imaging was carried out at two-week intervals until scrapie-infected hamsters showed severe signs of disease, or until 150 dpi in the case of mock-infected hamsters. Following sacrifice of the hamsters, they were examined for the histological hallmarks of prion disease.

Pentosan polysulphate is a semi-synthetic compound derived from beech wood that has anti-inflammatory and anti-coagulative properties [314]. It is a polymer of xylose, with two sulphate groups on each xylose molecule [314]. Because it is a hydrophilic molecule with a molecular weight of 4000 to 6000 Da [314], there is likely little, if any, penetration of the blood-brain-barrier (BBB) following peripheral administration, complicating its potential as a treatment for prion diseases. On the other hand, PPS has been FDA approved under the name Elmiron as a treatment for interstitial cystitis. Pharmacokinetic information on PPS deals almost exclusively with intravenous or oral administration. Under these conditions, low doses are cleared to the reticuloendothelial system [314,315], where excretion and breakdown of PPS is slow [314]. When high doses are given, the reticuloendothelial system is saturated, and the excess is secreted in the urine [315]. PPS is non-specifically desulfonated in a number of tissues and organs [316], and undergoes depolymerization in the kidneys [315].

PPS is one of a number of compounds that has been shown to slow the replication of PrP^{Sc} in cell culture [317,318] and in live animals [319]. It has also

shown promise in prolonging survival time [319–323] in rodents (including following i.c. infection [319,323]); and in human vCJD patients [275,276], although unsuccessful treatment in humans has also been reported [277]. PPS has even prevented disease completely under certain conditions following intra-peritoneal infection in some rodent models of scrapie [320,323]. Two potential mechanisms have been suggested for the anti-prion activity of PPS: it may prevent replication by removing PrP^{C} from the cell surface, and redistributing it into late endosomes or lysosomes [324], thus altering cellular trafficking of PrP^{C} that is necessary for conversion of PrP^{C} to PrP^{Sc} [325–328]; or it may competitively inhibit binding of PrP^{Sc} to a specific glycosaminoglycan that may be required for stabilization of PrP^{Sc} [317,329]. Because of its (relative) success in treating rodents infected intra-cerebrally with scrapie; its apparent status as the treatment of choice of humans afflicted with prion diseases; its FDA approval, albeit for a very different disease; and its ready availability, PPS was chosen to treat scrapie-infected hamsters.

4.2.1 Pentosan Polysulphate Treatment Regimens

According to the literature, two points may be made regarding the effectiveness of PPS treatment in prolonging survival time of rodents infected with prion disease: it is most effective when it is administered close to the time of infection (either before or after); and intra-cerebral treatment is more effective than intra-peritoneal treatment, especially following intra-cerebral infection. In fact, the most effective treatment appears to be a continuous, low dose of PPS administered through an intra-ventricular pump [319]; this is the method by which

human vCJD patients have been treated [275–277]. In choosing the treatment regimens for this study, there were three considerations: route of treatment administration; timing of treatment; and dose of treatment. With these considerations in mind, the objectives of the study were the following: to compare the effectiveness of intra-cerebral and intra-peritoneal PPS treatment following intra-cerebral scrapie-infection; and to compare the effectiveness of treatments administered at different time points. The first of these objectives was important to address because intra-cerebral treatment is highly invasive, so it would be desirable if prion disease could be successfully treated by a less invasive method. Treatments have previously been administered to prion-infected rodents at different time points; however, these time points have typically been chosen arbitrarily. Based on the initial MRI results presented here, it was possible to distinguish scrapie-infected from uninfected hamsters either at 19 or 33 dpi. This identified a possible treatment point that would have actual significance. By comparing the effectiveness of treatment at the time of infection to treatment initiated when scrapie-infected hamsters could be identified by MRI (26 dpi), it would be possible to determine whether treatments initiated following diagnosis could be effective, reflecting the ideal eventual clinical situation. Finally, since the most effective available treatment for prion disease appears to be a continuous low dose, it was attractive to determine whether multiple i.p. treatments would be more effective than a single treatment.

In deciding on the dose to use for both i.p. and i.c. PPS treatment, it was necessary to balance the desire to use the most effective dose (as high as

possible) with the desire to minimize potential side effects. In order to do this, the information available in the literature was used as a starting point. One study in particular was of use in determining the proper i.p. dose. Ladogana *et. al.* found that a dose of 100 mg/kg of PPS administered intra-peritoneally around the time of infection increased the incubation period of 263K scrapie in Syrian golden hamsters by 14 days following i.c. infection [323]. While it was relatively simple to determine a suitable dose for i.p. treatment, determining the intra-cerebral dose was another matter. Most studies concerned with the effectiveness of PPS treatment, and drug treatments in general, have been most interested in treating peripherally acquired prion disease, with treatments being administered intra-peritoneally while the infectious agent is still restricted to the peripheral nervous system. While administering treatments at this stage of disease pathogenesis results in a more successful outcome, the strategy remains somewhat puzzling for two reasons: as long as there is no way to diagnose disease at this stage, these results cannot be transferred from an experimental to a clinical setting; and it ignores altogether the forms of prion disease that are not acquired peripherally, including familial and sporadic forms which are the most common causes of prion disease in humans. Be that as it may, a side effect of this chosen strategy is that there is little data regarding safe and effective intra-cerebral treatments.

The best available example of intra-cerebral PPS treatment following intra-cerebral scrapie infection in rodents is the system established by Doh-Ura *et. al.*, using an intra-ventricular pump to administer a continuous low dose of PPS to transgenic mice expressing hamster PrP that had been infected with 263K

scrapie [319]. The maximum dose used in this study, with no adverse effects, was 460 μg/kg/day. However, doses of 345 and 460 μg/kg/day caused adverse effects in dogs, including partial or generalized seizures leading to death. Some of these dogs had large haematomas at the site of the intra-ventricular cannula. It has also been reported that intra-cerebral inoculation of PPS in mice does not result in serious side effects, although no specific doses are mentioned [314]. The authors go on to report on a personal communication, which indicated that i.c. injection of approximately 4 g/kg PPS resulted in a fatal intra-cerebral haemorrhage in all mice tested [314]. This left a very large gap in data with respect to different doses of PPS. Since it was impossible to use a low continuous dose in the study presented here, it was desirable to use as high a dose as possible in order to give the greatest chance of effectiveness before the drug was cleared. The initial dose chosen for i.c. injection was 20 mg/kg, but all hamsters receiving this dose exhibited adverse effects, including seizures interspersed with periods of inactivity. Five of the six hamsters were euthanized and haematomas at the site of injection were observed in all hamsters. This dose was much greater than that used in the Doh-Ura study, but was much lower than the 4 g/kg dose that was reported to be fatal in mice [314].

These results were reminiscent of those reported in dogs receiving a low continuous dose [319] and in mice receiving a much larger dose [314]. In order to correct this problem, a screening experiment was set up to determine a dose of i.c. PPS that would be tolerable for hamsters. Results and discussion of this experiment can be found in Appendix 1. Briefly, under a number of impossible-

to-verify assumptions, it was estimated that in both hamsters and dogs all PPS levels below 140 μg, to a maximum tested level of 120 μg were well tolerated, while all levels above 140 μg resulted in severe adverse effects in all animals tested. While equilibrium levels of PPS are unavailable, and the rate of clearing of PPS in the brain is unknown, it may be stated that the tolerable amount of PPS that can be injected intra-cerebrally in hamsters is no more than about 120 μg. The exercise in Appendix 1, estimating the PPS levels in the brain of dogs in the Doh-Ura study [319], at the very least is indicative that this level is a useful starting point in other species as well.

4.2.2 Effects of Pentosan Polysulphate on Disease Progression of Scrapie in Hamsters

4.2.2.1 Effects of Pentosan Polysulphate on Clinical Scrapie

In this study, the effects of PPS were examined with respect to four aspects of disease progression: progression of symptoms from their initial appearance until disease end point; survival time post infection; magnetic resonance images; and histological changes. The first of these presented no differences between scrapie-infected hamsters that received different PPS treatments and those that were not treated. In all cases, the duration of symptoms, from their first appearance until the time at which hamsters were euthanized, was on the order of ten to fourteen days. The first indication of disease was invariably slight bobbing of the head, which became progressively worse until near the end stage of disease it actually prevented the hamsters from feeding and drinking. The second obvious symptom of disease exhibited by

most hamsters was a tendency towards periods of hyperactivity of varying duration. These were sometimes interspersed cyclically with periods of no activity at later stages. Progressive ataxia of one or more limbs was another symptom. As it progressed, it resulted in problems with mobility, which varied according to the limbs that were affected. Less frequently, hamsters would spontaneously roll onto their back, typically during periods of hyperactivity. In the final stages of disease, hamsters would lose interest in food, or else would be unable to successfully feed themselves. As a result of failing to eat, sometimes in combination with continued hyperactivity, hamsters often lost significant body weight in the last few days before they were euthanized. Some hamsters did not remain hyperactive through the final stages of disease, rather becoming extremely lethargic, likely due to vastly decreased mobility due to severe ataxia.

While there were variations in many of the symptoms resulting from scrapie infection, PPS treatment did not obviously alter disease progression as measured from the first appearance of symptoms to the time at which hamsters were euthanized. This was not unexpected, since each treatment regimen was completed at least two weeks before the appearance of symptoms (most were completed more than forty days before symptoms appeared). PPS is thought to inhibit new formation of PrP^{Sc} from PrP^{C} either by competitively binding PrP [317,329], or by removing PrP^{C} from the normal sites of conversion [324]. Since PPS must be present to perform this action, its inhibitive effects are lost once it is cleared from its site of action (in this case the brain). In effect, PPS delays disease progression while it is present, but once it is cleared, disease progresses

as it normally would. In this study, since all PPS was expected to be cleared by the time symptoms appeared, it follows that disease would progress in the same manner in all hamster groups at this stage.

The symptoms described here are typical of prion disease in rodents. The central events in rodent disease progression are the loss of full control of movements, which was manifested in the progressive head bobbing, and ataxia. Ataxia of one or more limbs is the root of most of the observed abnormal movements in the latter stages of disease, with the individual manifestations dependent on which limb or limb combinations are ataxic. The periods of hyperactivity observed in most hamsters may have been due to nervousness at their loss of body control, although this could not be confirmed.

4.2.2.2 Effects of Pentosan Polysulphate Treatment on Survival Time of Scrapie-infected Hamsters

Although treatment with pentosan polysulphate did not alter scrapie disease progression during the symptomatic stage of disease, some of the treatment regimens tested did alter survival time following intra-cerebral scrapie infection. Hamsters received either no treatment, or one of the following five pentosan polysulphate (PPS) drug regimens: intra-cerebral (i.c.) injection at the time of infection or at twenty-six days post infection (dpi); intra-peritoneal (i.p.) injection at the time of infection or at twenty-six dpi; or multiple i.p. injections at twenty-six, forty, and fifty-four dpi. Statistically significant differences in survival time were observed between hamsters receiving intra-cerebral PPS at the time of infection and all other hamster groups. Some other general observations

regarding the efficacy of the different treatments in prolonging survival time could also be made: i.p. treatments initiated at 26 dpi, either as a single treatment or as multiple treatments, were entirely ineffective although multiple treatments resulted in marginally longer survival times; i.p. treatment at the time of infection was about as effective in prolonging survival time as i.c. treatment at 26 dpi; and i.c. treatment resulted in much greater variability in survival time than i.p. treatment. Most of these observations were not unexpected based on the literature. Studies have shown that intra-peritoneal treatment with PPS is unsuccessful unless it is administered early in infection [330], and the proposed mechanisms of action of PPS require that it co-localize with the site of replication of the infectious agent [317,324,329]. Taken together, these observations provide an explanation for the observations regarding i.p. PPS treatment initiated at 26 dpi.

Although it has not been explicitly shown that PPS cannot cross the blood brain barrier, it is believed that very little, if any, peripherally administered PPS can reach the brain because of its nature as a large hydrophilic molecule [314]. Despite this condition, PPS administered intra-peritoneally at a dose of 100 mg/kg has previously been shown to increase the incubation time of 263K scrapie in Syrian hamsters by 14 days following i.c. infection [323]. This result is supported by those reported here, as an increase in mean survival time of 11 days was observed compared to untreated hamsters. In fact, this increase in mean survival time was almost exactly the same as that produced by i.c. PPS treatment at 26 dpi. Since i.c. treatment delivers the PPS to the site of the

infectious agent, it would be expected to be more effective than i.p. treatment, given the difficulty that PPS has in crossing the blood brain barrier. On the other hand, treatment initiated at the earliest possible time point has been demonstrated to be more effective than treatment initiated at a later time point. These results indicate that the timing of treatment is of the utmost importance: even if PPS can be delivered directly to the site occupied by the infectious agent, if it is not administered in a timely manner, it will not be very effective. Explaining the effectiveness of i.p. PPS treatment following intra-cerebral scrapie infection in hamsters is not entirely straightforward. Murine models of prion disease have been shown to involve the periphery, in particular the lymphatic system [331,332], providing a potential explanation for the effect of intra-peritoneally administered PPS. However, in this particular model, splenectomy has been shown to have no effect on incubation period of intra-cerebrally infected, or intra-peritoneally infected hamsters [215,333]. While this observation sheds doubt on the involvement of the periphery in 263K scrapie disease progression following i.c. infection of Syrian golden hamsters, it does not eliminate it completely. An alternative explanation for the effectiveness of i.p. PPS treatment is that PPS is able to enter the brain at the site of injection of the infectious agent.

The fact that i.c. treatment at the time of infection was significantly more effective than any other treatment was not at all surprising, because it met the two requirements for successful treatment: it delivered PPS to the site of action; and it was administered as early as possible. On the other hand, the final observation, that intra-cerebral treatments resulted in much more variable effects

on survival time than intra-peritoneal treatments, was somewhat surprising. It had previously been observed that intra-peritoneal PPS treatment 24 hours after i.p. infection resulted in variable effects in 263K scrapie-infected hamsters, with some hamsters exhibiting very long incubation periods while others showed minimal effects [323]. In the same study, the effect of i.p. PPS treatment was much more consistent if treatment occurred within two hours of infection. This discrepancy was explained by the suggestion that the infectious agent is taken up by peripheral nerve endings within 24 hours of i.p. infection, at which point i.p. PPS is rendered ineffective [323]. The observations reported here with respect to i.p. PPS treatment do not have relevance to this potential mechanism, since treatment does not occur at the site of infection. It is possible that a similar effect could occur in the case of i.c. treatment: PPS may be more effective if it binds PrP^{Sc} before it associates with individual cells, and its ability to do this may indeed be variable between individual animals. It is possible that this variability is dependent merely on happenstance with respect to co-localization of PPS and PrP.

Although there appeared to be a clear order of effectiveness of the different PPS treatment regimens tested, a number of large differences in survival time between treatment groups were not found to be statistically significant. This was due largely to the small number of animals in each group (three). When the power of the comparison was tested under these conditions, it measured only 0.6149, providing a potential reason why apparent differences between treatment groups were not found to be significant. However, when the

standard error of the incubation period from the literature [215] was used in the power calculation, the resulting power was 1.0, indicating that the experimental design was not unreasonable given the available information.

Since the intra-cerebral treatment groups were grouped together for the purpose of MRI comparison, and because of the increased variability in survival time within these groups, all of the infected hamsters were divided into two groups: those that received intra-cerebral PPS injection, and those that did not. This exercise had the side effect of producing a more powerful comparison (power=0.761). Unsurprisingly, when these two new groups were compared, hamsters that received intra-cerebral PPS treatment had significantly longer survival times than those that did not.

4.2.2.3 Pentosan Polysulphate Causes Magnetic Resonance Image Abnormalities Similar to Those Resulting From Scrapie Infection

The most unexpected results observed in the study of the effects of PPS on scrapie infection in hamsters were observed on magnetic resonance images. In the initial MRI study presented here, progressive increases in both T_2 relaxation time and apparent diffusion coefficient were observed in the hippocampus of scrapie-infected hamsters beginning very early in disease progression. In the PPS study, T_2 maps only were evaluated, with a significant change in the manner in which measurements were corrected for differences in experimental conditions during data collection. Rather than expressing T_2 relaxation time in the hippocampus as a percentage of T_2 relaxation time in the thalamus, values were expressed as a percentage of T_2 relaxation time in a tube

of copper sulphate. This was an improvement in the system, because copper sulphate shortens the T_2 value of water, allowing for the observation of complete T_2 relaxation, resulting in a consistent high intensity signal. Since the copper sulphate solution was kept in a sealed tube, evaporation, which could result in changes in molarity, was not an issue. This reference sample facilitates the comparison of images obtained in different scanning sessions, since any observed differences in measurements of the reference sample can be attributed to differences in experimental conditions, and measurements of interest can be normalized using the reference. Upon analysis of the very first images collected, it was clear that PPS treatment had greatly complicated the MRI portion of the experiment. As seen in Figures 24, 32, and 35, intra-cerebral PPS treatment resulted in changes on T_2 maps that were similar to those produced by scrapie infection. Because i.c. PPS treatment not only affected T_2 relaxation time, but was also the most important influence on it, the evaluation was impossible to decipher as the experiment was originally designed. In order to attempt to simplify the situation by clearly identifying the two major influences on MR images, the number of hamster group/treatment combinations was reduced from twelve to four by combining groups as previously described, and as seen in Table 2.

In the initial MRI study, significant differences in relative T_2 values in the hippocampus in two consecutive MRI slices were observed between scrapie-infected and mock-infected and/or control hamsters as early as 19 dpi until 61 dpi. It was determined that these image abnormalities did not correlate with the

progression of histological changes, and that they likely resulted from the accumulation of bio-fluid (water) in the hippocampus (oedema). Because of these earlier results, the hippocampus was used as a starting point in determining whether or not regrouping the hamsters would allow a meaningful comparison. In each of the three slices of interest (5-7), the temporal pattern of relative T_2 values in the hippocampus of each hamster was compared to the mean value of the initial treatment group to which it belonged. The mean curves of each of these twelve group/treatment combinations were then compared to the mean curve of the new group to which it belonged. The conclusion drawn on the basis of this exercise was that each of the four newly formed groups gave a meaningful if not always ideal representation of all of the hamsters making up that group.

4.2.2.4 Scrapie-induced, and Intra-cerebral PPS-induced Changes on Magnetic Resonance Images are not Restricted to the Hippocampus

After establishing the validity of regrouping the hamsters into only four groups, these groups were compared with respect to relative T_2 values in the regions of interest in Slices 5-7. Initial examination of the patterns of relative T_2 values in the regions of interest allowed for a number of observations. Considering data from Slices 5 and 6, two statements may be made: in each hamster group, the relative T_2 value curves of the cortex, the thalamus, and the hypothalamus all closely followed that of the hippocampus; and the relative T_2 values in the hippocampus and the hypothalamus were consistently higher than those in the cortex and the thalamus in a given hamster group. Similarly, in Slice

7 the relative T_2 value curves of the cortex, and the septum closely followed that of the lateral ventricles and their surrounding region, and the relative T_2 values in the lateral ventricles were consistently higher than those in the cortex and the septum in a given hamster group. These data surprisingly indicate that scrapie-induced (and intra-cerebral PPS-induced) changes on T_2 maps are not restricted to the hippocampus as previously thought, but occurred in a number of other brain regions as well.

However, relative T_2 values in different brain regions were closest in the Mock-Infected No I.c. PPS group. In comparison, the groups that were influenced by scrapie-infection and/or intra-cerebral PPS treatment exhibited a larger difference in relative T_2 values between brain regions. This was particularly apparent in Slice 7, where measurements in the lateral ventricles and surrounding area were much greater than in the cortex and septum in these groups. Interestingly, in one case of vCJD treatment by continuous intra-ventricular PPS infusion, progressive enlargement of the lateral ventricles, as observed on repeated CT scans, was described [275]. The Slice 7 results presented here could also reflect enlargement of the lateral ventricles, which would result in greater representation of the lateral ventricles, as opposed to the surrounding areas, in these ROIs.

4.2.2.5 Effects of Different PPS Treatment Regimens on Magnetic Resonance Images of Scrapie- and Mock-infected Hamsters

In each of Slices 5-7, the following comparisons were carried out at each time point: data from all regions of interest were pooled to compare different hamster groups; data from all hamster groups were pooled to compare different regions of interest; and data from each region of interest in each hamster group were compared to all other group/region combinations. These data have been extensively described in the Results section, and only general trends will be summarized here. Considering first the comparison of different hamster groups, as a general rule in all three slices of interest, the Mock-Infected I.c. PPS group had the highest relative T_2 values. For most of the time course, the Mock-Infected No I.c. PPS group had the lowest relative T_2 values, with the two scrapie-infected groups maintaining intermediate values. Restricting the discussion to the most common situation that held the most significance, significant differences were often observed between all pairs of groups other than the two scrapie-infected groups during the period from 47 to 75 dpi. This can be taken as an indication that scrapie-infection altered relative T_2 values on its own; that intra-cerebral PPS altered relative T_2 values on its own; and that the respective effects of i.c. PPS and scrapie-infection were somehow antagonistic with respect to increasing relative T_2 values.

When data from all hamster groups were pooled to compare the different regions of interest in Slices 5 and 6, relative T_2 values in the hippocampus and/or

in the hypothalamus were frequently significantly greater than those in the cortex and/or in the thalamus, especially during the period between 47 and 89 dpi. In Slice 6, these observations extended both earlier and later than this time period. Similarly, in Slice 7, the lateral ventricles and surrounding regions had significantly greater relative T_2 values than both the cortex and the septum at nearly every time point studied. These data indicate a pre-disposition of the hippocampus, hypothalamus, and lateral ventricles and surrounding regions towards high relative T_2 values. However, the increased frequency of statistically significant differences between 47 and 89 dpi indicate that these regions are in fact more susceptible to scrapie- and i.c. PPS- induced changes.

When data from each region of interest in each hamster group were compared to all other group/region combinations, an extremely complex picture emerged in all three slices of interest. Some general statements may be made, however. Significant differences between brain regions in a given hamster group were rare; when they did occur, they generally involved differences between the cortex and either the hippocampus, the hypothalamus, or the lateral ventricles and surrounding regions. The most frequent instances of statistical significance occurred between Mock-Infected I.c. PPS hamsters and hamsters that did not receive intra-cerebral PPS, although differences between Scrapie-Infected No I.c. PPS and Mock-Infected No I.c. PPS hamsters were also observed. Based on these results, group effects can be considered to be dominant over region effects.

4.2.2.6 Effects of Pentosan Polysulphate Treatment on Histological Changes in Scrapie-infected Hamsters

Although it was determined in the first MRI experiment that abnormalities on MR images caused by scrapie infection could not be explained by histological changes, it was important to determine whether PPS treatment could influence the progression of histological changes in scrapie-infected hamsters, and whether it caused any changes in mock-infected hamsters. In order to accomplish this, hamsters were evaluated for these histological hallmarks after they were euthanized. The hippocampus, the cortex at the level of the thalamus, the thalamus, and the hypothalamus were evaluated in the four hamster groups used in the comparison of MRI results. When data from all regions were pooled and hamster groups were compared, the two scrapie-infected groups had significantly greater measurements than mock-infected groups with respect to all three histological hallmarks. Since this confirmed that mock-infection of hamsters did not result in the appearance of any histological changes typical of prion disease, mock-infected hamsters were excluded from further evaluation.

The two remaining hamster groups, namely Scrapie-Infected I.c. PPS and Scrapie-Infected No I.c. PPS, were compared with respect to hamster group, brain region, and Group x Region comparisons. When data from all regions of interest were pooled, no significant differences were found between Scrapie-Infected I.c. PPS and Scrapie-Infected No I.c. PPS hamsters with respect to any of the histological hallmarks of prion disease, although differences in PrP^{Sc} deposition approached statistical significance, with levels in hamsters that

received I.c. PPS greater than in those that did not. Given the difference in survival time between these two groups, significant differences in histological hallmarks would be expected if PPS did not affect their appearance. The fact that these were not observed supports the idea that histological change is slowed by I.c. PPS treatment.

When different regions of the brain were compared, levels of PrP^{Sc} deposition in the thalamus were significantly greater than in all other regions, while levels in the hippocampus were significantly lower than in all other regions. Total vacuole area in the thalamus was significantly greater than in the hippocampus and the hypothalamus, and approached statistical significance compared to the cortex. No significant differences were observed in gliosis levels between any regions of the brain. These results were very similar to those reported at 61 dpi in the previous study: differences in gliosis levels between brain regions remained non-existent; and the thalamus continued to be the most affected region with respect to both PrP^{Sc} deposition and vacuolation. Instances of significant differences in PrP^{Sc} levels increased, showing a natural progression from the previous results, as levels in these regions of interest retained their previous relative order. The biggest difference between these results and the results reported at 61 dpi relate to vacuolation. Even in this case, the regions of interest retained their previous relative order. However, spongiform change in the thalamus developed to a sufficient degree to allow for the observation of significant differences with respect to two of the other regions of interest.

The earlier histological data reported here has already been discussed in relation to two studies that sequentially evaluated spongiform change and gliosis following i.c. infection in regions of the brain including those examined here [219,221]. Masters *et. al*. report that from 49-57 dpi onward, the degree of spongiform change in the cortex and the hippocampus is greater than in the thalamus and the hypothalamus, while gliosis is more prevalent in the thalamus and the cortex [221]. These gliosis results were supported not only by the earlier findings reported here, but by the results of this latest study as well. In contrast, the latest results regarding spongiform change observed here continue to contrast sharply with those reported earlier with respect to the thalamus and the hippocampus in particular [221].

When hamster groups and all regions of interest were evaluated together, no significant differences were observed between any Group x Region combinations with respect to gliosis levels. Total vacuole levels in the hypothalamus of Scrapie-Infected No I.c. PPS hamsters were significantly lower than those in the thalamus and hypothalamus in Scrapie-Infected I.c. PPS hamsters and the thalamus of Scrapie-Infected No I.c. PPS hamsters. When PrP^{Sc} deposition was compared in Group x Region combinations, a large number of instances of statistical significance were observed, with the thalami in both hamster groups exhibiting the most significant differences. Without elaborating on these differences in detail, it is worth making three observations regarding this evaluation: measurements from the same brain region were invariably close between the two hamster groups, clearly indicating the importance of brain

region in the comparison; with respect to a given brain region, measurements in Scrapie-Infected I.c. PPS hamsters were invariably greater than those in Scrapie-Infected No I.c. PPS hamsters; and differences between hamster groups in a given brain region were never statistically significant. These data do much to support the conclusions drawn from the simple between groups and between regions comparisons: in general, histology in scrapie-infected hamsters did not differ according to the PPS treatment received; and brain region was the most important determinant of measurements of histological changes, with the thalamus again proving to be the region most affected histologically.

There were three effects that could have influenced the values of the histological hallmarks of prion disease measured at the end point of disease progression in hamsters: the normal rate at which these histological characteristics appear; the potential effects of PPS to slow this rate; and the difference in survival time between hamsters receiving different treatments. The expectation was that each of the histological characteristics would increase with time, and that PPS would act to slow the accumulation of PrP^{Sc} and vacuolation, if not gliosis. In order to evaluate the effects of PPS treatment on the appearance of histological hallmarks, each of the original six treatment groups were compared with respect to these hallmarks in each of the four regions of interest. Vacuolation levels in a given brain region increased loosely with incubation period in the four groups that did not receive intra-cerebral PPS treatment, but not in the two treatment groups that received intra-cerebral PPS treatment, indicating that the relatively successful PPS treatments slowed the

appearance of vacuoles in all regions of the brain. Results were similar with respect to PrP^{Sc} levels, with parallel increases over the three least successful treatments, and in the three more successful treatment groups. In contrast, when gliosis levels were compared between all treatment groups in all regions of the brain, no clear patterns relating to survival time or PPS treatment were observed.

In order to further evaluate the effects of PPS treatment on the appearance of histological hallmarks, levels in individual animals were compared to expected levels generated by extending a trend line representing the stage during which the histological characteristic of interest increased in the initial histological study. This made it possible to compare values measured in hamsters that had been treated with PPS to the expected values if histological characteristics continued to increase at their usual rate. This exercise revealed that: animals that had longer survival times, and could therefore be categorized as having received more successful treatments, were less likely to reach expected values; vacuolation levels were the most likely to reach expected levels; and the hypothalamus was the region that most closely followed the expected values with respect to all three histological characteristics of interest. It is also important to note that the trend lines used in this exercise were composed conservatively. That is, rather than simply extending the curve using a slope that was equivalent to the slope between the last two time points, the trend lines used typically took three time points into account. This had the effect of decreasing the slope of the trend line, and therefore decreasing expected values at

subsequent time points. The observations, then, that expected values usually were not met, and were less likely to be met in hamsters with longer survival times lend more weight to the conclusion that PPS treatment slowed the progressive development of histological changes typical of prion disease. These conclusions are supported by the observation that slow intra-ventricular PPS infusion greatly reduced PrP^{Sc} deposition, gliosis, and spongiform change, as well as infectivity following intra-cerebral infection [319].

4.2.3 Implications Raised by Results of the Pentosan Polysulphate Treatment Study

The results presented here raise four main questions: how or why does intra-cerebral PPS treatment cause hyper-intensity on T_2 maps, and can this observation be reconciled with the model suggested earlier? How can the apparently antagonistic effects of intra-cerebral PPS treatment and scrapie infection be reconciled with the model suggested earlier? Why do scrapie-infected hamsters receiving no treatment only exhibit increased relative T_2 values much later than in the initial MRI study? Why does it now appear as though a number of regions are affected (by hyper-intensity)?

4.2.3.1 Methodological Differences Between the Two MRI Experiments

In order to answer the latter two of these questions it is necessary to first discuss the differences between the two MRI experiments. In the first experiment, a copper sulphate standard was not used to produce relative T_2 values. Instead, the thalamus was chosen to fill this Role because it was the

region that showed the least variation in raw T_2 values between hamster groups at all four time points studied. This critical difference can at least partially explain why some brain regions not identified in the initial MRI study were found to be hyper-intense on T_2 maps when a copper sulphate standard was used. It may also partially explain why hyper-intensities in the hippocampus appeared later in scrapie-infected hamsters that were not treated with PPS than they did in the initial study. There are, however, a number of other elements that may have affected the results in the PPS study. First, the infectious agent used in the inoculum in the PPS study was made from brains of infected hamsters that were euthanized at 62 dpi, before the appearance of clinical symptoms, compared to clinically diseased hamster brains that were used in the first MRI study. It is possible that disease may have progressed at a slightly slower pace after infection with pre-clinical hamster brain homogenate, since the titre of the inoculum may have been reduced, resulting in a slight delay in the appearance of MRI abnormalities. Secondly, the number of hamsters in each of the original treatment groups was small (3), due to a premium on the available MRI time. It is possible that due to this small number of hamsters, the results may have been a slight misrepresentation of the true population values. This statement is perhaps supported by the data produced when all scrapie-infected hamsters that did not receive intra-cerebral PPS treatment were pooled together. These data showed increases in relative T_2 values that were initiated between 47 and 61 dpi. Since the survival times of hamsters that received these treatments were not significantly altered, it can be argued that disease progression was not

significantly altered either. Thus, the true results for this population were perhaps not as different from the earlier results as they initially seemed. Furthermore, the differences that were observed may be explained partially by the nature of the inoculum, and the method of correcting raw values for differences in experimental conditions during data collection, as discussed above.

4.2.3.2 Osmotic Oedema May Explain the Effects of Intra-cerebral Pentosan Polysulphate Treatment on Magnetic Resonance Images of Hamsters

In order to answer the first question outlined above, regarding the reason why intra-cerebral PPS treatment causes hyper-intensities on T_2 maps, it is beneficial to first revisit the model suggested earlier for the cause of hyper-intensities due to scrapie infection. Since abnormalities on MR images did not correlate with histological changes, and because increased T_2 relaxation time is indicative of increased levels of bio-fluids or water, it was suggested that these image abnormalities were the result of vasogenic oedema. It was further suggested that in the pre-clinical disease stages, oedema is counteracted by the action of AQP4 which pumps some water back across the blood brain barrier. In the later stages of disease, alteration to the function of PrP would result in dysregulation of AQP4 production and activity, resulting in increases in AQP4 activity. Under this model, a balance would be tipped, resulting in cytotoxic oedema due to two factors: continued fluid accumulation in the brain because of blood brain barrier leakiness; and high AQP4 activity, pumping water into the cells and eventually leading to cell death.

In order to determine whether this model can be reconciled with the observations presented here with respect to the effects of intra-cerebral PPS treatment, it is necessary to examine how PPS may produce oedema. The types of oedema discussed earlier are vasogenic oedema, the accumulation of water in the extracellular space caused by leakiness of the blood brain barrier, and cytotoxic oedema, the accumulation of water inside cells due to cellular injury [334]. However, oedema caused by PPS is likely due to the creation of an osmotic gradient between the plasma and the brain tissue; this is called osmotic oedema [334]. Osmotic oedema is most commonly associated with hyponatremia, when serum sodium concentrations are much lower than normal. This creates an osmotic gradient across the blood brain barrier, with osmolality in the brain higher than in the plasma. Water then moves into the brain to correct this imbalance, resulting in oedema. Additionally, this results in another osmotic gradient, between the extra- and intra-cellular spaces in the brain, causing cytotoxic oedema as water flows into cells to correct the gradient. Cerebral oedema caused by hyponatremia, or low serum sodium concentration, may be fatal in as many as 17.9% of cases [335–337]. The prognosis, with respect to the likelihood of seizures, coma, and death, is much improved if hyponatremia develops slowly [338]. This is due to the nature of the cellular response to hyponatremia. As cells initially fill with water in response to hyponatremia, they rapidly extrude electrolytes into the extra-cellular space, causing water to exit the cells as well [339]. If an osmotic gradient persists, cells extrude organic osmolytes, mostly consisting of amino acids, at a much slower rate to cause

further flow of water out of the cells [339]. In acute, rapidly developing hyponatremia, the delay in the cellular response between the extrusions of electrolytes and organic osmolytes prevents the cells from properly combating swelling; this results in seizures in as many as 29% of patients, and a mortality rate as high as 50% [340]. In comparison, if hyponatremia develops slowly, mortality is reduced to about 6%, and the incidence of seizures is reduced to 4% [340].

A parallel may be drawn between hyponatremic conditions and the potential effects of PPS injection in the brain. As in hyponatremia, the cerebral extra-cellular space following PPS injection is hyper-osmotic compared to the plasma. This can be corrected by an influx of water into the brain from the plasma, and it seems very likely that this is, in fact, the cause of oedema following intra-cerebral administration of PPS. If this is the case, it is reasonable to ask why some hamsters in this study did not experience adverse effects following i.c. PPS treatment. In considering this question, it is important to note a critical difference compared to hyponatremia: in this case, the relatively high osmolality in the brain is localized to the area around the injection site. This difference has a number of repercussions. First, since the osmotic gradient is localized (compared to systemic hypo-osmolality in the plasma), the amount of water necessary to balance it would be relatively small, potentially limiting the increase in intra-cerebral volume. Second, injection of PPS results in not only an osmotic gradient between the plasma and the cerebral extra-cellular space, but between the cerebral extra- and intra-cellular spaces as well. This means that

the increased osmolality in the extra-cellular space can be corrected by an influx of water from the plasma as well as extrusion of water from the cells. Although it is likely that the major contribution comes from the plasma, this influx of water is unlikely to be followed by cellular swelling. Third, since PPS was injected locally, it would diffuse slowly throughout the brain. This would have the effect of further limiting the amount of water needed to correct the osmotic imbalance between the cerebral extra-cellular space and both the plasma and the cerebral intra-cellular space.

The explanation for PPS-induced oedema outlined above is attractive in part because it may also explain the observation of seizures in dogs [319], and in hamsters receiving high doses of PPS. This concept is best illustrated by comparing two possible outcomes of intra-cerebral PPS administration: a low dose of i.c. PPS that is tolerated by the animal; and a high dose that causes seizures and death (even in the absence of haematomas [319]). In the first situation, a low dose of PPS would result in a local increase in osmolality in the cerebral extra-cellular space. As the PPS diffused on its own, the osmolality would gradually decrease. At the same time, there would be an influx of water from the plasma, perhaps with a contribution of water from cells around the injection site. It is possible that some cells would die because of a loss of water, but these effects would be relatively small, and would be restricted to the area immediately around the injection site. As water entered the cerebral extra-cellular space from the plasma, it would itself diffuse, and aid in the diffusion of PPS, resulting in a decrease in the local osmolality until osmotic equilibrium was

attained. In this way the influx of water would be limited, and cytotoxic oedema would be absent. In comparison, a high dose of PPS would create an osmotic gradient of greater magnitude, resulting in a larger influx of water from the plasma. While this in itself may be enough to cause injury, there would be secondary effects as well. The influx of water might be large enough that it overcompensates: as water diffuses throughout the brain, it may result in hypo-osmolality in the extra-cellular space away from the location of the injection. If this were to occur, water would begin to enter brain cells in order to restore osmotic equilibrium. In this manner, a situation of rapidly developing acute hyponatremia would be approximated. If the initial cellular response of extrusion of electrolytes was inadequate to restore osmotic equilibrium, the result may be unchecked cellular swelling, or cytotoxic oedema. It was previously noted that 29% of patients with acute hyponatremia experienced seizures, while the mortality rate in these patients was 50% [340]. The observation of seizures in dogs that received high doses of i.c. PPS, including in the absence of cerebral haematomas [319], as well as the seizures observed in hamsters receiving high doses of PPS in this study may be explained by a similar phenomenon.

The existence of the osmotic gradient is commonly put to therapeutic use to combat cerebral oedema. Mannitol is administered to produce hyper-osmolar plasma, so that water moves from the brain to the blood to restore osmotic equilibrium. It has been demonstrated that hyper-osmolar conditions induced by mannitol increase expression of aquaporins 4 (AQP4) and 9 (AQP9) through p38 Mitogen-activated Protein Kinase (p38 MAPK) [301]. It would be intriguing to

determine whether the induction of a hyper-osmolar state in hamsters would make higher doses of PPS tolerable by decreasing the osmotic gradient between the plasma and the brain, thereby decreasing cerebral oedema. In the model of disease progression presented earlier to explain abnormalities on MR images, it was suggested that vasogenic oedema occurs early in disease, as a result of progressive breakdown of the blood-brain-barrier. Since AQP4 has been shown to have beneficial effects in cases of vasogenic oedema [308,309], and since its expression can be induced by hyper-osmolar mannitol administration [301], it may be worth exploring whether mannitol can influence MR image abnormalities and/or prion disease progression.

4.2.3.3 Antagonistic Effects of Intra-cerebral PPS Treatment and Scrapie Infection on Magnetic Resonance Images may be Caused by Simultaneous Vasogenic and Osmotic Oedema

The proposed mechanisms described above may also be relevant to the second question raised by the results of the PPS treatment study, seeking an explanation for the apparently antagonistic effects of intra-cerebral PPS treatment and scrapie infection. According to the hypothesis that has been developed here, scrapie infection causes vasogenic oedema due to leakiness of the blood brain barrier, allowing water to enter the brain from the blood. In comparison, PPS has been proposed to cause osmotic oedema, due to the creation of an osmotic gradient between the blood and the brain, resulting from injection of a substance with high osmolality (PPS). Considering a scrapie-infected hamster, once vasogenic oedema has been initiated, the water content

in its brain will be higher than in an uninfected hamster. It follows then, that injection of PPS would result in an osmotic gradient of lesser magnitude, causing less infusion of water due to osmolality. Furthermore, if AQP4 expression is induced by hypo-osmolar plasma [301], it is not unreasonable to expect that it may similarly be induced by hyper-osmolar brain tissue. If this is the case, it may subsequently facilitate the removal of water from the brain tissue to the blood, since increased AQP4 activity has been shown to be beneficial in minimizing the effects of vasogenic oedema [308,309].

5. Conclusions and Future Directions

The studies presented here have addressed two unresolved aspects of prion research: diagnosis and treatment. As a consequence of some unexpected results, new avenues of research into prion disease pathogenesis have also been introduced. For the first time, progressive increases in both T_2 relaxation time and apparent diffusion coefficient have been observed in the hippocampus of scrapie-infected hamsters beginning very early in disease progression. Histological examination of four brain regions of interest at four time points corresponding to the collection of MR images revealed that the thalamus was the region that was affected earliest and most severely with respect to both spongiform change and PrP^{Sc} deposition, and that MR image abnormalities appeared before histological changes in any region. Since histological changes did not correlate with MR image abnormalities, either in timing or location, it was argued that MR image abnormalities were not caused by histological changes, at least at the pre-clinical stages studied initially. Vasogenic oedema resulting from leakiness of the blood brain barrier was proposed as an alternative explanation for MR image abnormalities, since increased T_2 relaxation time is indicative of increased bio-fluid content in the tissue. The observation of increased apparent diffusion coefficient in the same brain region supported this suggestion.

In order to explain the significance of oedema in the pre-clinical stage, and its potential role in disease pathogenesis, a speculative model was proposed, relating PrP^{Sc} replication, aquaporin-4 (AQP4) expression, and oedema (Figure 44). Briefly, it was suggested that conversion of PrP^{C} to PrP^{Sc} alters signalling

through PKC and p38 MAPK, resulting in dysregulation of AQP4 expression and activity. It was speculated further that this results in increased AQP4 expression and activity, which has previously been reported during clinical disease [300], and that in the presence of high levels of extra-cellular fluid due to vasogenic oedema, initiation of cytotoxic oedema results during the clinical stage of disease, leading to glial cell swelling and neuronal death.

A subsequent MRI study, during which various pentosan polysulphate treatment regimens were tested, produced a number of surprising results: intra-cerebral treatment with PPS resulted in image abnormalities on T_2 maps that were similar to those observed following scrapie infection; paradoxically, although i.c. PPS treatment and scrapie infection both produced increased relative T_2 values, these effects appeared to be antagonistic rather than additive; and increases in T_2 relaxation time in scrapie-infected hamsters (and in i.c. PPS treated hamsters) were not restricted to the hippocampus, as previously thought, but rather affected all regions studied. As previously concluded, histological changes characteristic of prion disease, this time measured at the end stage of disease, did not correlate with MR image abnormalities, and the thalamus was again the region that was most affected by spongiform change and PrP^{Sc} accumulation in scrapie-infected hamsters. The observed effects of PPS treatment on survival time and histological hallmarks of prion disease did not deviate much from the expected. Intra-cerebral PPS treatment at the time of scrapie-infection was by far the most effective treatment in prolonging survival time, while i.c. treatment at 26 dpi, and i.p. treatment at the time of infection were

moderately effective. These results confirm that peripheral treatment with PPS is not viable, and that while PPS may be the best treatment option currently available, its effectiveness as anything more than a post-exposure prophylactic is lacking. Measurements of histological changes were compared to expected values that were based on the rate of appearance of histological changes in the initial study. Pentosan polysulphate treatment appears to slow the development of histological changes, particularly if it is administered intra-cerebrally, since hamsters that received the most successful treatments were the least likely to reach expected values of spongiform change, PrP^{Sc} deposition, and gliosis.

As mentioned earlier, the second MRI study produced a number of surprising results. It is likely that MR image abnormalities in regions other than the hippocampus that were missed in the initial MRI study were observed in the latter study because of a difference in the method for producing relative values. In the second study, a copper sulphate standard was used to produce relative values, an improvement over the similar use of the thalamus in the initial study. In order to explain the other two unexpected results, concerning the effects of i.c. PPS treatment on MR images, and the paradoxically antagonistic effects of scrapie infection and i.c. PPS treatment, the previous model for disease pathogenesis in relation to oedema, AQP4 expression and activity, and PrP^{Sc} replication was revisited. In the context of this model, it was proposed that i.c. PPS treatment induced oedema through the creation of an osmotic gradient, as opposed to breakdown of the blood brain barrier. This provided a potentially suitable explanation for the antagonistic effects of i.c. PPS treatment and scrapie

infection on T_2 maps, since fluid influx across a leaky blood brain barrier would reduce the effects of increased osmolality due to PPS injection by lessening the magnitude of the osmotic gradient. Furthermore, osmotic oedema also provided a potential explanation for death in both hamsters and dogs [319] receiving high doses of i.c. PPS, while animals receiving lower doses did not experience adverse effects: higher doses would produce an osmotic gradient of greater magnitude, resulting in a greater influx of water.

To further explore the potential of the theories presented here, a number of issues must be clarified. The first of these is whether MR image abnormalities are in fact due to oedema, and if so, the nature of the oedema throughout the disease course. I have proposed that vasogenic oedema occurs in scrapie-infected hamsters well before the appearance of clinical symptoms. Since vasogenic oedema occurs as a result of breakdown of the blood brain barrier, confirmation of this breakdown would provide evidence of vasogenic oedema. A study consisting of MR imaging using the contrast agent gadolinium between 19 dpi and the appearance of clinical symptoms would be sufficient to evaluate the competence of the blood brain barrier, since gadolinium normally cannot cross the BBB [341], but would be able to cross it if it were compromised. I have speculated that at the clinical stage of disease progression, cytotoxic oedema is initiated. In order to prove or disprove this hypothesis, another MRI experiment could be carried out, collecting both T_2 and ADC data until the clinical stage of disease. As long as oedema is strictly vasogenic in nature, both T_2 and ADC would be expected to increase; if cytotoxic oedema appears at the clinical stage,

ADC would be expected to decrease at this stage, since the fluid accumulation inside cells would decrease the overall ability of fluid to diffuse within the tissue.

The most critical unknown element of the theories proposed here is the involvement of AQP4. Although upregulation of AQP4 protein levels has been demonstrated in cases of CJD and in BSE-infected transgenic mice [300], and AQP4 expression and activity appears to be regulated by p38 MAPK [301] and PKC [302–304,342] – two enzymes that are involved in PrP signalling [140,343], no direct links between PrP and AQP4 expression or activity have been established. The first requirement to confirm the proposed involvement of AQP4 in disease pathogenesis is to clearly establish the details of its regulation, in particular with respect to the prion protein. In order to do this, two hypotheses must be tested: PrP^{Sc} induces AQP4 expression in a p38 MAPK-dependent manner; and PrP^{C} inhibits AQP4 expression and activity in a PKC-dependent manner. Recombinant PrP^{C} has previously been shown to induce axon growth and neuronal polarity in a PKC-dependent manner in cell culture [140]. In a similar experiment, it would be possible to determine the effects of recombinant PrP^{C} on AQP4 expression and phosphorylation levels (and therefore its activity), as well as the involvement of PKC, in astrocyte cell cultures. If the proposed model is correct, recombinant PrP^{C} would result in a decrease in AQP4 expression and activity, and these effects would be abolished by PKC inhibitors. It has also been shown that the neurotoxic recombinant prion protein fragment PrP-(106-126) induces nitric oxide (NO) production through a pathway that involves p38 MAPK activation in human microglial cell cultures [343]. In another

experiment, the effects of PrP-(106-126) on AQP4 expression and activity, and the potential role of p38 MAPK in this pathway, could be determined in cell culture. If PrP-(106-126) induces AQP4 expression, and if p38 MAPK inhibitors abolish this effect, it would provide significant support for the model I have proposed.

If PrP^{C} and PrP^{Sc} prove to be involved in the regulation of AQP4, supporting the model proposed in this volume, a number of other avenues of research could be explored. AQP4-null and PrP-null mice are both available, and may be informative in the elaboration of different aspects of these potential interactions. For example, it would be interesting to infect AQP4-null mice with scrapie, and follow disease progression by MRI. Since AQP4 combats vasogenic oedema [308,309], AQP4 null mice would be expected to fare worse than controls during the early stages of scrapie infection, perhaps decreasing incubation period and survival time, while MR images would be expected to show evidence of more severe vasogenic oedema. It is possible that an influx of water across a disrupted blood brain barrier, in the absence of the effects of AQP4, may result in death as a result of increased intra-cranial pressure and total brain volume, or it may induce the initiation of cytotoxic oedema at an earlier time point. If these results are not observed, it is possible that one of the other aquaporins may compensate for AQP4 in its absence. Increased expression of PrP^{C} has been observed in focal cerebral ischemia (a model of cytotoxic oedema) [310]. If the model that I have proposed is correct, then increased PrP^{C} expression may prevent excessive expression and activity of AQP4 under

conditions in which it would be detrimental (cytotoxic oedema). Inducing oedema in PrP-null and control mice, and comparing the outcomes could test this theory. Deletion of PrP was found to be detrimental following induction of ischemia [311], although AQP4 expression levels were not evaluated. Both AQP4-null and PrP-null mice could be used in an almost limitless number of ways to evaluate other aspects of the mechanisms suggested here.

I have postulated that intra-cerebral injection of PPS results in osmotic oedema by creating an osmotic gradient, resulting in an influx of water from the blood to the brain tissue. In order to test this hypothesis, hyper-osmolar conditions in the brain tissue could be created by injection of mannitol. This would be expected to have a similar effect on T_2 maps to that observed following intra-cerebral treatment with PPS. When an osmotic gradient exists across the blood brain barrier, water moves down the gradient through AQP4. If PPS was injected intra-cerebrally in AQP4-null mice, this gradient could not be corrected by an influx of water from the blood. Instead, cells would be expected to lose water content, and likely become necrotic as a result. Results such as these would provide further support to the model I have proposed.

The results presented are indicative of the accumulation of water in the brain before the appearance of clinical symptoms of scrapie infection, likely as a result of breakdown of the blood brain barrier. Furthermore, it is apparent that this vasogenic oedema materializes before the appearance of significant levels of the typical histological hallmarks of prion disease (spongiform change, PrP^{Sc} deposition, and gliosis). These results spurred the proposition of a model to

explain the appearance of oedema, as well as its potential role in disease pathogenesis. This model is attractive not only for its potential to explain scrapie-induced MR image abnormalities and possibly even the direct cause of death, but the effects of intra-cerebral PPS treatment as well. Because this model is critically dependent on the suggested effects of PrP^{C} and PrP^{Sc} on the regulation of AQP4, some possible studies have been suggested in order to prove or disprove this connection. Further to these, a number of other directions in research have been suggested to explore the proposed model, although the list I have provided is by no means exhaustive, and is highly dependent on initial results in the studies I have suggested. The field of prion research has always been rife with controversy, and characterized by surprising results. It should therefore perhaps not be unexpected that something so seemingly unrelated to prions as water imbalance may prove to be critical to disease pathogenesis.

Reference List

1. Collinge J (1997) Human prion diseases and bovine spongiform encephalopathy (BSE). Hum Mol Genet JID - 9208958 6: 1699-1705.
2. Pan KM, Baldwin M, Nguyen J, Gasset M, Serban A, Groth D, Mehlhorn I, Huang Z, Fletterick RJ, Cohen FE (1993) Conversion of alpha-helices into beta-sheets features in the formation of the scrapie prion proteins. Proc Natl Acad Sci U S A JID - 7505876 90: 10962-10966.
3. Pergami P, Jaffe H, Safar J (1996) Semipreparative chromatographic method to purify the normal cellular isoform of the prion protein in nondenatured form. Anal Biochem JID - 0370535 236: 63-73.
4. Oesch B, Westaway D, Walchli M, McKinley MP, Kent SB, Aebersold R, Barry RA, Tempst P, Teplow DB, Hood LE (1985) A cellular gene encodes scrapie PrP 27-30 protein. Cell JID - 0413066 40: 735-746.
5. Prusiner SB (1998) Prions. Proc Natl Acad Sci U S A JID - 7505876 95: 13363-13383.
6. Bruce ME, Will RG, Ironside JW, McConnell I, Drummond D, Suttie A, McCardle L, Chree A, Hope J, Birkett C, Cousens S, Fraser H, Bostock CJ (1997) Transmissions to mice indicate that 'new variant' CJD is caused by the BSE agent. Nature JID - 0410462 389: 498-501.
7. Collinge J, Sidle KC, Meads J, Ironside J, Hill AF (1996) Molecular analysis of prion strain variation and the aetiology of 'new variant' CJD. Nature JID - 0410462 383: 685-690.
8. Hill AF, Butterworth RJ, Joiner S, Jackson G, Rossor MN, Thomas DJ, Frosh A, Tolley N, Bell JE, Spencer M, King A, al-Sarraj S, Ironside JW, Lantos PL, Collinge J (1999) Investigation of variant Creutzfeldt-Jakob disease and other human prion diseases with tonsil biopsy samples. Lancet JID - 2985213R 353: 183-189.
9. Sigurdsson B (1954) Rida, a chronic encephalitis of sheep: With general remarks on infections which develop slowly and some of their special characteristics. British Veterinary Journal 110: 341-354.
10. Stamp JT (1958) Scrapie disease of sheep. The Veterinary Record 70: 50-55.
11. Gordon WS (1957) The Speaker's Introduction. The Veterinary Record 69: 1324-1328.
12. Gordon WS, Pattison IH (1957) The experimental production of scrapie in goats. The Veterinary Record 69: 1444.
13. Zigas V, Gajdusek DC (1957) Kuru: clinical study of a new syndrome resembling paralysis agitans in natives of the Eastern Highlands of Australian New Guinea. The Medical Journal of Australia 2: 745-754.
14. Gajdusek DC, Zigas V (1957) Degenerative disease of the central nervous system in New Guinea: The endemic occurrence of "Kuru" in the native population. The New England Journal of Medicine 257: 974-978.
15. Hadlow WJ (1959) Scrapie and Kuru. Lancet 11: 289-290.
16. Klatzo I, Gajdusek DC, Zigas V (1959) Pathology of Kuru. Laboratory Investigation 8: 799-847.
17. Gajdusek DC, Gibbs CJ, Alpers M (1966) Experimental transmission of a Kuru-like syndrome to chimpanzees. Nature 209: 794-796.
18. Alper T, Haig DA, Clarke MC (1966) The exceptionally small size of the scrapie agent. Biochem Biophys Res Commun JID - 0372516 22: 278-284.
19. Alper T, Cramp WA, Haig DA, Clarke MC (1967) Does the agent of scrapie replicate without nucleic acid? Nature 214: 764-766.
20. Latarjet R, Muel B, Haig DA, Clarke MC, Alper T (1970) Inactivation of the scrapie agent by near monochromatic ultraviolet light. Nature 227: 1341-1343.
21. Gibbs CJ, Jr., Gajdusek DC, Latarjet R (1978) Unusual resistance to ionizing radiation of the viruses of kuru, Creutzfeldt-Jakob disease, and scrapie. Proc Natl Acad Sci U S A 75: 6268-6270.
22. Griffith JS (1967) Self-replication and scrapie. Nature JID - 0410462 215: 1043-1044.

23. Pattison IH, Jones KM (1967) The possible nature of the transmissible agent of scrapie. Vet Rec JID - 0031164 80: 2-9.
24. Prusiner SB (1982) Novel proteinaceous infectious particles cause scrapie. Science JID - 0404511 216: 136-144.
25. Bolton DC, McKinley MP, Prusiner SB (1982) Identification of a protein that purifies with the scrapie prion. Science JID - 0404511 218: 1309-1311.
26. Prusiner SB, Bolton DC, Groth DF, Bowman KA, Cochran SP, McKinley MP (1982) Further purification and characterization of scrapie prions. Biochemistry JID - 0370623 21: 6942-6950.
27. Prusiner SB, Groth DF, Bolton DC, Kent SB, Hood LE (1984) Purification and structural studies of a major scrapie prion protein. Cell 38: 127-134.
28. Basler K, Oesch B, Scott M, Westaway D, Walchli M, Groth DF, McKinley MP, Prusiner SB, Weissmann C (1986) Scrapie and cellular PrP isoforms are encoded by the same chromosomal gene. Cell 46: 417-428.
29. Meyer RK, McKinley MP, Bowman KA, Braunfeld MB, Barry RA, Prusiner SB (1986) Separation and properties of cellular and scrapie prion proteins. Proc Natl Acad Sci U S A 83: 2310-2314.
30. Locht C, Chesebro B, Race R, Keith JM (1986) Molecular cloning and complete sequence of prion protein cDNA from mouse brain infected with the scrapie agent. Proc Natl Acad Sci U S A 83: 6372-6376.
31. Chesebro B (1998) BSE and prions: uncertainties about the agent. Science 279: 42-43.
32. Soto C, Castilla J (2004) The controversial protein-only hypothesis of prion propagation. Nat Med 10 Suppl: S63-S67.
33. Bruce ME, McConnell I, Fraser H, Dickinson AG (1991) The disease characteristics of different strains of scrapie in Sinc congenic mouse lines: implications for the nature of the agent and host control of pathogenesis. J Gen Virol JID - 0077340 72 (Pt 3): 595-603.
34. Bessen RA, Marsh RF (1992) Identification of two biologically distinct strains of transmissible mink encephalopathy in hamsters. J Gen Virol 73 (Pt 2): 329-334.
35. Bruce ME (1993) Scrapie strain variation and mutation. Br Med Bull 49: 822-838.
36. Fraser H (1993) Diversity in the neuropathology of scrapie-like diseases in animals. Br Med Bull 49: 792-809.
37. Bessen RA, Marsh RF (1992) Biochemical and physical properties of the prion protein from two strains of the transmissible mink encephalopathy agent. J Virol JID - 0113724 66: 2096-2101.
38. Parchi P, Castellani R, Capellari S, Ghetti B, Young K, Chen SG, Farlow M, Dickson DW, Sima AA, Trojanowski JQ, Petersen RB, Gambetti P (1996) Molecular basis of phenotypic variability in sporadic Creutzfeldt-Jakob disease. Ann Neurol 39: 767-778.
39. Khalili-Shirazi A, Summers L, Linehan J, Mallinson G, Anstee D, Hawke S, Jackson GS, Collinge J (2005) PrP glycoforms are associated in a strain-specific ratio in native PrPSc. J Gen Virol 86: 2635-2644.
40. Bruce ME, McBride PA, Farquhar CF (1989) Precise targeting of the pathology of the sialoglycoprotein, PrP, and vacuolar degeneration in mouse scrapie. Neurosci Lett 102: 1-6.
41. Bruce ME, Boyle A, Cousens S, McConnell I, Foster J, Goldmann W, Fraser H (2002) Strain characterization of natural sheep scrapie and comparison with BSE. J Gen Virol 83: 695-704.
42. Lasmezas CI, Deslys JP, Demaimay R, Adjou KT, Hauw JJ, Dormont D (1996) Strain specific and common pathogenic events in murine models of scrapie and bovine spongiform encephalopathy. J Gen Virol 77 (Pt 7): 1601-1609.
43. Fraser H, Dickinson AG (1973) Scrapie in mice. Agent-strain differences in the distribution and intensity of grey matter vacuolation. J Comp Pathol 83: 29-40.
44. Wadsworth JD, Hill AF, Joiner S, Jackson GS, Clarke AR, Collinge J (1999) Strain-specific prion-protein conformation determined by metal ions. Nat Cell Biol JID - 100890575 1: 55-59.

45. Safar J, Wille H, Itri V, Groth D, Serban H, Torchia M, Cohen FE, Prusiner SB (1998) Eight prion strains have PrP(Sc) molecules with different conformations. Nat Med JID - 9502015 4: 1157-1165.
46. Weissmann C (1991) A 'unified theory' of prion propagation. Nature JID - 0410462 352: 679-683.
47. Aguzzi A, Heikenwalder M, Polymenidou M (2007) Insights into prion strains and neurotoxicity. Nat Rev Mol Cell Biol 8: 552-561.
48. Bartz JC, Bessen RA, McKenzie D, Marsh RF, Aiken JM (2000) Adaptation and selection of prion protein strain conformations following interspecies transmission of transmissible mink encephalopathy. J Virol 74: 5542-5547.
49. Peretz D, Scott MR, Groth D, Williamson RA, Burton DR, Cohen FE, Prusiner SB (2001) Strain-specified relative conformational stability of the scrapie prion protein. Protein Sci 10: 854-863.
50. Bessen RA, Marsh RF (1994) Distinct PrP properties suggest the molecular basis of strain variation in transmissible mink encephalopathy. J Virol 68: 7859-7868.
51. Telling GC, Parchi P, DeArmond SJ, Cortelli P, Montagna P, Gabizon R, Mastrianni J, Lugaresi E, Gambetti P, Prusiner SB (1996) Evidence for the conformation of the pathologic isoform of the prion protein enciphering and propagating prion diversity. Science JID - 0404511 274: 2079-2082.
52. Prusiner SB (1997) Prion diseases and the BSE crisis. Science 278: 245-251.
53. Caughey B, Raymond GJ, Bessen RA (1998) Strain-dependent differences in beta-sheet conformations of abnormal prion protein. J Biol Chem JID - 2985121R 273: 32230-32235.
54. Aucouturier P, Kascsak RJ, Frangione B, Wisniewski T (1999) Biochemical and conformational variability of human prion strains in sporadic Creutzfeldt-Jakob disease. Neurosci Lett 274: 33-36.
55. Safar J, Cohen FE, Prusiner SB (2000) Quantitative traits of prion strains are enciphered in the conformation of the prion protein. Arch Virol Suppl JID - 9214275 227-235.
56. Bellon A, Seyfert-Brandt W, Lang W, Baron H, Groner A, Vey M (2003) Improved conformation-dependent immunoassay: suitability for human prion detection with enhanced sensitivity. J Gen Virol 84: 1921-1925.
57. Jones EM, Surewicz WK (2005) Fibril conformation as the basis of species- and strain-dependent seeding specificity of mammalian prion amyloids. Cell 121: 63-72.
58. Morales R, Abid K, Soto C (2007) The prion strain phenomenon: molecular basis and unprecedented features. Biochim Biophys Acta 1772: 681-691.
59. Nonno R, Di Bari MA, Cardone F, Vaccari G, Fazzi P, Dell'Omo G, Cartoni C, Ingrosso L, Boyle A, Galeno R, Sbriccoli M, Lipp HP, Bruce M, Pocchiari M, Agrimi U (2006) Efficient transmission and characterization of Creutzfeldt-Jakob disease strains in bank voles. PLoS Pathog 2: e12.
60. Silveira JR, Raymond GJ, Hughson AG, Race RE, Sim VL, Hayes SF, Caughey B (2005) The most infectious prion protein particles. Nature 437: 257-261.
61. Collinge J (2005) Molecular neurology of prion disease. J Neurol Neurosurg Psychiatry 76: 906-919.
62. Manuelidis L, Yu ZX, Barquero N, Mullins B (2007) Cells infected with scrapie and Creutzfeldt-Jakob disease agents produce intracellular 25-nm virus-like particles. Proc Natl Acad Sci U S A 104: 1965-1970.
63. Prusiner SB, Groth D, Serban A, Stahl N, Gabizon R (1993) Attempts to restore scrapie prion infectivity after exposure to protein denaturants. Proc Natl Acad Sci U S A 90: 2793-2797.
64. McKinley MP, Bolton DC, Prusiner SB (1983) A protease-resistant protein is a structural component of the scrapie prion. Cell JID - 0413066 35: 57-62.
65. Prusiner SB, McKinley MP, Bowman KA, Bolton DC, Bendheim PE, Groth DF, Glenner GG (1983) Scrapie prions aggregate to form amyloid-like birefringent rods. Cell JID - 0413066 35: 349-358.
66. Bolton DC, McKinley MP, Prusiner SB (1984) Molecular characteristics of the major scrapie prion protein. Biochemistry JID - 0370623 23: 5898-5906.

67. Riesner D, Kellings K, Post K, Wille H, Serban H, Groth D, Baldwin MA, Prusiner SB (1996) Disruption of prion rods generates 10-nm spherical particles having high alpha-helical content and lacking scrapie infectivity. J Virol 70: 1714-1722.
68. Prusiner SB, Scott M, Foster D, Pan KM, Groth D, Mirenda C, Torchia M, Yang SL, Serban D, Carlson GA, . (1990) Transgenetic studies implicate interactions between homologous PrP isoforms in scrapie prion replication. Cell 63: 673-686.
69. Bueler H, Aguzzi A, Sailer A, Greiner RA, Autenried P, Aguet M, Weissmann C (1993) Mice devoid of PrP are resistant to scrapie. Cell 73: 1339-1347.
70. Prusiner SB, Groth D, Serban A, Koehler R, Foster D, Torchia M, Burton D, Yang SL, DeArmond SJ (1993) Ablation of the prion protein (PrP) gene in mice prevents scrapie and facilitates production of anti-PrP antibodies. Proc Natl Acad Sci U S A 90: 10608-10612.
71. Sailer A, Bueler H, Fischer M, Aguzzi A, Weissmann C (1994) No propagation of prions in mice devoid of PrP. Cell 77: 967-968.
72. Manson JC, Clarke AR, McBride PA, McConnell I, Hope J (1994) PrP gene dosage determines the timing but not the final intensity or distribution of lesions in scrapie pathology. Neurodegeneration 3: 331-340.
73. Sakaguchi S, Katamine S, Shigematsu K, Nakatani A, Moriuchi R, Nishida N, Kurokawa K, Nakaoke R, Sato H, Jishage K, . (1995) Accumulation of proteinase K-resistant prion protein (PrP) is restricted by the expression level of normal PrP in mice inoculated with a mouse-adapted strain of the Creutzfeldt-Jakob disease agent. J Virol 69: 7586-7592.
74. Castilla J, Saa P, Hetz C, Soto C (2005) In vitro generation of infectious scrapie prions. Cell 121: 195-206.
75. Aguzzi A, Heikenwalder M (2006) Pathogenesis of prion diseases: current status and future outlook. Nat Rev Microbiol 4: 765-775.
76. Abid K, Soto C (2006) The intriguing prion disorders. Cell Mol Life Sci 63: 2342-2351.
77. Gossert AD, Bonjour S, Lysek DA, Fiorito F, Wuthrich K (2005) Prion protein NMR structures of elk and of mouse/elk hybrids. Proc Natl Acad Sci U S A 102: 646-650.
78. Riek R, Hornemann S, Wider G, Glockshuber R, Wuthrich K (1997) NMR characterization of the full-length recombinant murine prion protein, mPrP(23-231). FEBS Lett 413: 282-288.
79. Brockes JP (1999) Topics in prion cell biology. Curr Opin Neurobiol 9: 571-577.
80. Zahn R, Liu A, Luhrs T, Riek R, von SC, Lopez GF, Billeter M, Calzolai L, Wider G, Wuthrich K (2000) NMR solution structure of the human prion protein. Proc Natl Acad Sci U S A 97: 145-150.
81. Harris DA (2003) Trafficking, turnover and membrane topology of PrP. Br Med Bull 66: 71-85.
82. Stahl N, Borchelt DR, Hsiao K, Prusiner SB (1987) Scrapie prion protein contains a phosphatidylinositol glycolipid. Cell 51: 229-240.
83. Wiseman F, Cancellotti E, Manson J (2005) Glycosylation and misfolding of PrP. Biochem Soc Trans 33: 1094-1095.
84. Rogers M, Taraboulos A, Scott M, Groth D, Prusiner SB (1990) Intracellular accumulation of the cellular prion protein after mutagenesis of its Asn-linked glycosylation sites. Glycobiology 1: 101-109.
85. Taraboulos A, Rogers M, Borchelt DR, McKinley MP, Scott M, Serban D, Prusiner SB (1990) Acquisition of protease resistance by prion proteins in scrapie-infected cells does not require asparagine-linked glycosylation. Proc Natl Acad Sci U S A 87: 8262-8266.
86. Cancellotti E, Wiseman F, Tuzi NL, Baybutt H, Monaghan P, Aitchison L, Simpson J, Manson JC (2005) Altered glycosylated PrP proteins can have different neuronal trafficking in brain but do not acquire scrapie-like properties. J Biol Chem 280: 42909-42918.
87. Tuzi NL, Cancellotti E, Baybutt H, Blackford L, Bradford B, Plinston C, Coghill A, Hart P, Piccardo P, Barron RM, Manson JC (2008) Host PrP glycosylation: a major factor determining the outcome of prion infection. PLoS Biol 6: e100.

88. DeArmond SJ, Sanchez H, Yehiely F, Qiu Y, Ninchak-Casey A, Daggett V, Camerino AP, Cayetano J, Rogers M, Groth D, Torchia M, Tremblay P, Scott MR, Cohen FE, Prusiner SB (1997) Selective neuronal targeting in prion disease. Neuron 19: 1337-1348.
89. Neuendorf E, Weber A, Saalmueller A, Schatzl H, Reifenberg K, Pfaff E, Groschup MH (2004) Glycosylation deficiency at either one of the two glycan attachment sites of cellular prion protein preserves susceptibility to bovine spongiform encephalopathy and scrapie infections. J Biol Chem 279: 53306-53316.
90. Madore N, Smith KL, Graham CH, Jen A, Brady K, Hall S, Morris R (1999) Functionally different GPI proteins are organized in different domains on the neuronal surface. EMBO J 18: 6917-6926.
91. Vey M, Pilkuhn S, Wille H, Nixon R, DeArmond SJ, Smart EJ, Anderson RG, Taraboulos A, Prusiner SB (1996) Subcellular colocalization of the cellular and scrapie prion proteins in caveolae-like membranous domains. Proc Natl Acad Sci U S A 93: 14945-14949.
92. Taraboulos A, Scott M, Semenov A, Avrahami D, Laszlo L, Prusiner SB (1995) Cholesterol depletion and modification of COOH-terminal targeting sequence of the prion protein inhibit formation of the scrapie isoform. J Cell Biol 129: 121-132.
93. Baron GS, Caughey B (2003) Effect of glycosylphosphatidylinositol anchor-dependent and -independent prion protein association with model raft membranes on conversion to the protease-resistant isoform. J Biol Chem 278: 14883-14892.
94. Walmsley AR, Zeng F, Hooper NM (2003) The N-terminal region of the prion protein ectodomain contains a lipid raft targeting determinant. J Biol Chem 278: 37241-37248.
95. Morris RJ, Parkyn CJ, Jen A (2006) Traffic of prion protein between different compartments on the neuronal surface, and the propagation of prion disease. FEBS Lett 580: 5565-5571.
96. Sunyach C, Jen A, Deng J, Fitzgerald KT, Frobert Y, Grassi J, McCaffrey MW, Morris R (2003) The mechanism of internalization of glycosylphosphatidylinositol-anchored prion protein. EMBO J 22: 3591-3601.
97. Taylor DR, Hooper NM (2006) The prion protein and lipid rafts. Mol Membr Biol 23: 89-99.
98. Shyng SL, Moulder KL, Lesko A, Harris DA (1995) The N-terminal domain of a glycolipid-anchored prion protein is essential for its endocytosis via clathrin-coated pits. J Biol Chem 270: 14793-14800.
99. Pan T, Wong BS, Liu T, Li R, Petersen RB, Sy MS (2002) Cell-surface prion protein interacts with glycosaminoglycans. Biochem J 368: 81-90.
100. Warner RG, Hundt C, Weiss S, Turnbull JE (2002) Identification of the heparan sulfate binding sites in the cellular prion protein. J Biol Chem 277: 18421-18430.
101. Parkyn CJ, Vermeulen EG, Mootoosamy RC, Sunyach C, Jacobsen C, Oxvig C, Moestrup S, Liu Q, Bu G, Jen A, Morris RJ (2008) LRP1 controls biosynthetic and endocytic trafficking of neuronal prion protein. J Cell Sci 121: 773-783.
102. Taylor DR, Hooper NM (2007) The low-density lipoprotein receptor-related protein 1 (LRP1) mediates the endocytosis of the cellular prion protein. Biochem J 402: 17-23.
103. Prusiner SB (1991) Molecular biology of prion diseases. Science 252: 1515-1522.
104. Cohen FE, Prusiner SB (1998) Pathologic conformations of prion proteins. Annu Rev Biochem 67: 793-819.
105. Jarrett JT, Lansbury PT, Jr. (1993) Seeding "one-dimensional crystallization" of amyloid: a pathogenic mechanism in Alzheimer's disease and scrapie? Cell 73: 1055-1058.
106. Kocisko DA, Come JH, Priola SA, Chesebro B, Raymond GJ, Lansbury PT, Caughey B (1994) Cell-free formation of protease-resistant prion protein. Nature JID - 0410462 370: 471-474.
107. Telling GC, Scott M, Mastrianni J, Gabizon R, Torchia M, Cohen FE, DeArmond SJ, Prusiner SB (1995) Prion propagation in mice expressing human and chimeric PrP transgenes implicates the interaction of cellular PrP with another protein. Cell JID - 0413066 83: 79-90.
108. Ryou C (2007) Prions and prion diseases: fundamentals and mechanistic details. J Microbiol Biotechnol 17: 1059-1070.

109. Lucassen R, Nishina K, Supattapone S (2003) In vitro amplification of protease-resistant prion protein requires free sulfhydryl groups. Biochemistry 42: 4127-4135.
110. Saborio GP, Permanne B, Soto C (2001) Sensitive detection of pathological prion protein by cyclic amplification of protein misfolding. Nature JID - 0410462 411: 810-813.
111. Cohen FE, Pan KM, Huang Z, Baldwin M, Fletterick RJ, Prusiner SB (1994) Structural clues to prion replication. Science JID - 0404511 264: 530-531.
112. Legname G, Baskakov IV, Nguyen HO, Riesner D, Cohen FE, DeArmond SJ, Prusiner SB (2004) Synthetic mammalian prions. Science 305: 673-676.
113. Baron GS, Wehrly K, Dorward DW, Chesebro B, Caughey B (2002) Conversion of raft associated prion protein to the protease-resistant state requires insertion of PrP-res (PrP(Sc)) into contiguous membranes. EMBO J 21: 1031-1040.
114. Eberl H, Tittmann P, Glockshuber R (2004) Characterization of recombinant, membrane-attached full-length prion protein. J Biol Chem 279: 25058-25065.
115. Hicks MR, Gill AC, Bath IK, Rullay AK, Sylvester ID, Crout DH, Pinheiro TJ (2006) Synthesis and structural characterization of a mimetic membrane-anchored prion protein. FEBS J 273: 1285-1299.
116. Naslavsky N, Shmeeda H, Friedlander G, Yanai A, Futerman AH, Barenholz Y, Taraboulos A (1999) Sphingolipid depletion increases formation of the scrapie prion protein in neuroblastoma cells infected with prions. J Biol Chem 274: 20763-20771.
117. Campana V, Sarnataro D, Fasano C, Casanova P, Paladino S, Zurzolo C (2006) Detergent-resistant membrane domains but not the proteasome are involved in the misfolding of a PrP mutant retained in the endoplasmic reticulum. J Cell Sci 119: 433-442.
118. Sarnataro D, Campana V, Paladino S, Stornaiuolo M, Nitsch L, Zurzolo C (2004) PrP(C) association with lipid rafts in the early secretory pathway stabilizes its cellular conformation. Mol Biol Cell 15: 4031-4042.
119. Naslavsky N, Stein R, Yanai A, Friedlander G, Taraboulos A (1997) Characterization of detergent-insoluble complexes containing the cellular prion protein and its scrapie isoform. J Biol Chem 272: 6324-6331.
120. Rivera-Milla E, Oidtmann B, Panagiotidis CH, Baier M, Sklaviadis T, Hoffmann R, Zhou Y, Solis GP, Stuermer CA, Malaga-Trillo E (2006) Disparate evolution of prion protein domains and the distinct origin of Doppel- and prion-related loci revealed by fish-to-mammal comparisons. FASEB J 20: 317-319.
121. Bueler H, Fischer M, Lang Y, Bluethmann H, Lipp HP, DeArmond SJ, Prusiner SB, Aguet M, Weissmann C (1992) Normal development and behaviour of mice lacking the neuronal cell-surface PrP protein. Nature JID - 0410462 356: 577-582.
122. Manson JC, Clarke AR, Hooper ML, Aitchison L, McConnell I, Hope J (1994) 129/Ola mice carrying a null mutation in PrP that abolishes mRNA production are developmentally normal. Mol Neurobiol 8: 121-127.
123. Mallucci GR, Ratte S, Asante EA, Linehan J, Gowland I, Jefferys JG, Collinge J (2002) Post-natal knockout of prion protein alters hippocampal CA1 properties, but does not result in neurodegeneration. EMBO J JID - 8208664 21: 202-210.
124. Bounhar Y, Zhang Y, Goodyer CG, LeBlanc A (2001) Prion protein protects human neurons against Bax-mediated apoptosis. J Biol Chem 276: 39145-39149.
125. Roucou X, Guo Q, Zhang Y, Goodyer CG, LeBlanc AC (2003) Cytosolic prion protein is not toxic and protects against Bax-mediated cell death in human primary neurons. J Biol Chem 278: 40877-40881.
126. Kuwahara C, Takeuchi AM, Nishimura T, Haraguchi K, Kubosaki A, Matsumoto Y, Saeki K, Matsumoto Y, Yokoyama T, Itohara S, Onodera T (1999) Prions prevent neuronal cell-line death. Nature 400: 225-226.
127. Sakudo A, Lee DC, Saeki K, Nakamura Y, Inoue K, Matsumoto Y, Itohara S, Onodera T (2003) Impairment of superoxide dismutase activation by N-terminally truncated prion protein (PrP) in PrP-deficient neuronal cell line. Biochem Biophys Res Commun 308: 660-667.
128. Drisaldi B, Coomaraswamy J, Mastrangelo P, Strome B, Yang J, Watts JC, Chishti MA, Marvi M, Windl O, Ahrens R, Major F, Sy MS, Kretzschmar H, Fraser PE, Mount HT,

Westaway D (2004) Genetic mapping of activity determinants within cellular prion proteins: N-terminal modules in PrPC offset pro-apoptotic activity of the Doppel helix B/B' region. J Biol Chem 279: 55443-55454.
129. Qin K, Zhao L, Tang Y, Bhatta S, Simard JM, Zhao RY (2006) Doppel-induced apoptosis and counteraction by cellular prion protein in neuroblastoma and astrocytes. Neuroscience 141: 1375-1388.
130. Brown DR, Schulz-Schaeffer WJ, Schmidt B, Kretzschmar HA (1997) Prion protein-deficient cells show altered response to oxidative stress due to decreased SOD-1 activity. Exp Neurol 146: 104-112.
131. Brown DR, Nicholas RS, Canevari L (2002) Lack of prion protein expression results in a neuronal phenotype sensitive to stress. J Neurosci Res 67: 211-224.
132. Wong BS, Liu T, Li R, Pan T, Petersen RB, Smith MA, Gambetti P, Perry G, Manson JC, Brown DR, Sy MS (2001) Increased levels of oxidative stress markers detected in the brains of mice devoid of prion protein. J Neurochem JID - 2985190R 76: 565-572.
133. de Almeida CJ, Chiarini LB, da Silva JP, PM ES, Martins MA, Linden R (2005) The cellular prion protein modulates phagocytosis and inflammatory response. J Leukoc Biol 77: 238-246.
134. Brown DR, Qin K, Herms JW, Madlung A, Manson J, Strome R, Fraser PE, Kruck T, von Bohlen A, Schulz-Schaeffer W, Giese A, Westaway D, Kretzschmar H (1997) The cellular prion protein binds copper in vivo. Nature JID - 0410462 390: 684-687.
135. Jackson GS, Murray I, Hosszu LL, Gibbs N, Waltho JP, Clarke AR, Collinge J (2001) Location and properties of metal-binding sites on the human prion protein. Proc Natl Acad Sci U S A 98: 8531-8535.
136. Kramer ML, Kratzin HD, Schmidt B, Romer A, Windl O, Liemann S, Hornemann S, Kretzschmar H (2001) Prion protein binds copper within the physiological concentration range. J Biol Chem 276: 16711-16719.
137. Stockel J, Safar J, Wallace AC, Cohen FE, Prusiner SB (1998) Prion protein selectively binds copper(II) ions. Biochemistry 37: 7185-7193.
138. Andrews NJ (8 A.D.) Incidence of variant Creutzfeld-Jakob disease diagnoses and deaths in the UK January 1994 - December 2007. 1-6.
139. Mouillet-Richard S, Ermonval M, Chebassier C, Laplanche JL, Lehmann S, Launay JM, Kellermann O (2000) Signal transduction through prion protein. Science JID - 0404511 289: 1925-1928.
140. Kanaani J, Prusiner SB, Diacovo J, Baekkeskov S, Legname G (2005) Recombinant prion protein induces rapid polarization and development of synapses in embryonic rat hippocampal neurons in vitro. J Neurochem 95: 1373-1386.
141. Chen S, Mange A, Dong L, Lehmann S, Schachner M (2003) Prion protein as trans-interacting partner for neurons is involved in neurite outgrowth and neuronal survival. Mol Cell Neurosci 22: 227-233.
142. Zanata SM, Lopes MH, Mercadante AF, Hajj GN, Chiarini LB, Nomizo R, Freitas AR, Cabral AL, Lee KS, Juliano MA, de OE, Jachieri SG, Burlingame A, Huang L, Linden R, Brentani RR, Martins VR (2002) Stress-inducible protein 1 is a cell surface ligand for cellular prion that triggers neuroprotection. EMBO J 21: 3307-3316.
143. Chiarini LB, Freitas AR, Zanata SM, Brentani RR, Martins VR, Linden R (2002) Cellular prion protein transduces neuroprotective signals. EMBO J 21: 3317-3326.
144. Lopes MH, Hajj GN, Muras AG, Mancini GL, Castro RM, Ribeiro KC, Brentani RR, Linden R, Martins VR (2005) Interaction of cellular prion and stress-inducible protein 1 promotes neuritogenesis and neuroprotection by distinct signaling pathways. J Neurosci 25: 11330-11339.
145. Wang V, Chuang TC, Hsu YD, Chou WY, Kao MC (2005) Nitric oxide induces prion protein via MEK and p38 MAPK signaling. Biochem Biophys Res Commun 333: 95-100.
146. Schmitt-Ulms G, Legname G, Baldwin MA, Ball HL, Bradon N, Bosque PJ, Crossin KL, Edelman GM, DeArmond SJ, Cohen FE, Prusiner SB (2001) Binding of neural cell adhesion molecules (N-CAMs) to the cellular prion protein. J Mol Biol 314: 1209-1225.

147. Graner E, Mercadante AF, Zanata SM, Forlenza OV, Cabral AL, Veiga SS, Juliano MA, Roesler R, Walz R, Minetti A, Izquierdo I, Martins VR, Brentani RR (2000) Cellular prion protein binds laminin and mediates neuritogenesis. Brain Res Mol Brain Res 76: 85-92.
148. Mabbott NA, MacPherson GG (2006) Prions and their lethal journey to the brain. Nat Rev Microbiol 4: 201-211.
149. Kitamoto T, Muramoto T, Mohri S, Doh-Ura K, Tateishi J (1991) Abnormal isoform of prion protein accumulates in follicular dendritic cells in mice with Creutzfeldt-Jakob disease. J Virol 65: 6292-6295.
150. Mabbott NA, Young J, McConnell I, Bruce ME (2003) Follicular dendritic cell dedifferentiation by treatment with an inhibitor of the lymphotoxin pathway dramatically reduces scrapie susceptibility. J Virol 77: 6845-6854.
151. Montrasio F, Frigg R, Glatzel M, Klein MA, Mackay F, Aguzzi A, Weissmann C (2000) Impaired prion replication in spleens of mice lacking functional follicular dendritic cells. Science 288: 1257-1259.
152. Mohan J, Bruce ME, Mabbott NA (2005) Neuroinvasion by scrapie following inoculation via the skin is independent of migratory Langerhans cells. J Virol 79: 1888-1897.
153. Mabbott NA, Mackay F, Minns F, Bruce ME (2000) Temporary inactivation of follicular dendritic cells delays neuroinvasion of scrapie. Nat Med 6: 719-720.
154. Klein MA, Frigg R, Raeber AJ, Flechsig E, Hegyi I, Zinkernagel RM, Weissmann C, Aguzzi A (1998) PrP expression in B lymphocytes is not required for prion neuroinvasion. Nat Med JID - 9502015 4: 1429-1433.
155. Klein MA, Frigg R, Flechsig E, Raeber AJ, Kalinke U, Bluethmann H, Bootz F, Suter M, Zinkernagel RM, Aguzzi A (1997) A crucial role for B cells in neuroinvasive scrapie. Nature JID - 0410462 390: 687-690.
156. Blattler T, Brandner S, Raeber AJ, Klein MA, Voigtlander T, Weissmann C, Aguzzi A (1997) PrP-expressing tissue required for transfer of scrapie infectivity from spleen to brain. Nature JID - 0410462 389: 69-73.
157. Montrasio F, Cozzio A, Flechsig E, Rossi D, Klein MA, Rulicke T, Raeber AJ, Vosshenrich CA, Proft J, Aguzzi A, Weissmann C (2001) B lymphocyte-restricted expression of prion protein does not enable prion replication in prion protein knockout mice. Proc Natl Acad Sci U S A 98: 4034-4037.
158. Mabbott NA, Bruce ME, Botto M, Walport MJ, Pepys MB (2001) Temporary depletion of complement component C3 or genetic deficiency of C1q significantly delays onset of scrapie. Nat Med 7: 485-487.
159. Klein MA, Kaeser PS, Schwarz P, Weyd H, Xenarios I, Zinkernagel RM, Carroll MC, Verbeek JS, Botto M, Walport MJ, Molina H, Kalinke U, cha-Orbea H, Aguzzi A (2001) Complement facilitates early prion pathogenesis. Nat Med 7: 488-492.
160. Van den Berg TK, Yoshida K, Dijkstra CD (1995) Mechanism of immune complex trapping by follicular dendritic cells. Curr Top Microbiol Immunol 201: 49-67.
161. Kaeser PS, Klein MA, Schwarz P, Aguzzi A (2001) Efficient lymphoreticular prion propagation requires PrP(c) in stromal and hematopoietic cells. J Virol 75: 7097-7106.
162. Aguzzi A (2006) Prion diseases of humans and farm animals: epidemiology, genetics, and pathogenesis. J Neurochem 97: 1726-1739.
163. Carp RI, Callahan SM (1981) In vitro interaction of scrapie agent and mouse peritoneal macrophages. Intervirology 16: 8-13.
164. Carp RI, Callahan SM (1982) Effect of mouse peritoneal macrophages on scrapie infectivity during extended in vitro incubation. Intervirology 17: 201-207.
165. Shortman K, Liu YJ (2002) Mouse and human dendritic cell subtypes. Nat Rev Immunol 2: 151-161.
166. Huang FP, Farquhar CF, Mabbott NA, Bruce ME, MacPherson GG (2002) Migrating intestinal dendritic cells transport PrP(Sc) from the gut. J Gen Virol 83: 267-271.
167. Mohan J, Hopkins J, Mabbott NA (2005) Skin-derived dendritic cells acquire and degrade the scrapie agent following in vitro exposure. Immunology 116: 122-133.
168. Aguzzi A, Sigurdson CJ (2004) Antiprion immunotherapy: to suppress or to stimulate? Nat Rev Immunol 4: 725-736.

169. Prinz M, Huber G, Macpherson AJ, Heppner FL, Glatzel M, Eugster HP, Wagner N, Aguzzi A (2003) Oral prion infection requires normal numbers of Peyer's patches but not of enteric lymphocytes. Am J Pathol 162: 1103-1111.
170. Sigurdson CJ, Barillas-Mury C, Miller MW, Oesch B, van Keulen LJ, Langeveld JP, Hoover EA (2002) PrP(CWD) lymphoid cell targets in early and advanced chronic wasting disease of mule deer. J Gen Virol 83: 2617-2628.
171. Heggebo R, Press CM, Gunnes G, Ulvund MJ, Tranulis MA, Lsverk T (2003) Detection of PrPSc in lymphoid tissues of lambs experimentally exposed to the scrapie agent. J Comp Pathol 128: 172-181.
172. Beekes M, McBride PA (2000) Early accumulation of pathological PrP in the enteric nervous system and gut-associated lymphoid tissue of hamsters orally infected with scrapie. Neurosci Lett JID - 7600130 278: 181-184.
173. Heppner FL, Christ AD, Klein MA, Prinz M, Fried M, Kraehenbuhl JP, Aguzzi A (2001) Transepithelial prion transport by M cells. Nat Med 7: 976-977.
174. Kreitman M, Di RA (2004) Balancing claims for balancing selection. Trends Genet 20: 300-304.
175. Peden AH, Head MW, Ritchie DL, Bell JE, Ironside JW (2004) Preclinical vCJD after blood transfusion in a PRNP codon 129 heterozygous patient. Lancet 364: 527-529.
176. Aguzzi A, Glatzel M (2004) vCJD tissue distribution and transmission by transfusion--a worst-case scenario coming true? Lancet 363: 411-412.
177. Prinz M, Heikenwalder M, Junt T, Schwarz P, Glatzel M, Heppner FL, Fu YX, Lipp M, Aguzzi A (2003) Positioning of follicular dendritic cells within the spleen controls prion neuroinvasion. Nature 425: 957-962.
178. Clarke MC, Kimberlin RH (1984) Pathogenesis of mouse scrapie: distribution of agent in the pulp and stroma of infected spleens. Vet Microbiol 9: 215-225.
179. Cole S, Kimberlin RH (1985) Pathogenesis of mouse scrapie: dynamics of vacuolation in brain and spinal cord after intraperitoneal infection. Neuropathol Appl Neurobiol 11: 213-227.
180. McBride PA, Beekes M (1999) Pathological PrP is abundant in sympathetic and sensory ganglia of hamsters fed with scrapie. Neurosci Lett 265: 135-138.
181. Glatzel M, Heppner FL, Albers KM, Aguzzi A (2001) Sympathetic innervation of lymphoreticular organs is rate limiting for prion neuroinvasion. Neuron 31: 25-34.
182. Beekes M, Baldauf E, Diringer H (1996) Sequential appearance and accumulation of pathognomonic markers in the central nervous system of hamsters orally infected with scrapie. J Gen Virol JID - 0077340 77 (Pt 8): 1925-1934.
183. Baldauf E, Beekes M, Diringer H (1997) Evidence for an alternative direct route of access for the scrapie agent to the brain bypassing the spinal cord. J Gen Virol JID - 0077340 78 (Pt 5): 1187-1197.
184. McBride PA, Schulz-Schaeffer WJ, Donaldson M, Bruce M, Diringer H, Kretzschmar HA, Beekes M (2001) Early spread of scrapie from the gastrointestinal tract to the central nervous system involves autonomic fibers of the splanchnic and vagus nerves. J Virol JID - 0113724 75: 9320-9327.
185. Beekes M, McBride PA, Baldauf E (1998) Cerebral targeting indicates vagal spread of infection in hamsters fed with scrapie. J Gen Virol JID - 0077340 79 (Pt 3): 601-607.
186. Westergard L, Christensen HM, Harris DA (2007) The cellular prion protein (PrP(C)): its physiological function and role in disease. Biochim Biophys Acta 1772: 629-644.
187. Brandner S, Isenmann S, Raeber A, Fischer M, Sailer A, Kobayashi Y, Marino S, Weissmann C, Aguzzi A (1996) Normal host prion protein necessary for scrapie-induced neurotoxicity. Nature JID - 0410462 379: 339-343.
188. Mallucci G, Dickinson A, Linehan J, Klohn PC, Brandner S, Collinge J (2003) Depleting neuronal PrP in prion infection prevents disease and reverses spongiosis. Science 302: 871-874.
189. Brandner S, Raeber A, Sailer A, Blattler T, Fischer M, Weissmann C, Aguzzi A (1996) Normal host prion protein (PrPC) is required for scrapie spread within the central nervous system. Proc Natl Acad Sci U S A JID - 7505876 93: 13148-13151.

190. Chesebro B, Trifilo M, Race R, Meade-White K, Teng C, LaCasse R, Raymond L, Favara C, Baron G, Priola S, Caughey B, Masliah E, Oldstone M (2005) Anchorless prion protein results in infectious amyloid disease without clinical scrapie. Science 308: 1435-1439.
191. Fraser H, Dickinson AG (1968) The sequential development of the brain lesion of scrapie in three strains of mice. J Comp Pathol JID - 0102444 78: 301-311.
192. Sutherland K, Rutovitz D, Bell JE, Ironside JW (1994) Evaluation of a novel application of image analysis. 378-381.
193. Sutherland K, Ironside JW (1994) Novel application of image analysis to the detection of spongiform change. Anal Quant Cytol Histol 16: 430-434.
194. Sutherland K, MacDonald ST, Ironside JW (1996) Quantificatio nand analysis of the neuropathological features of Creutzfeld-Jakob disease. Journal of Neuroscience Methods 64: 121-132.
195. Taraboulos A, Jendroska K, Serban D, Yang SL, DeArmond SJ, Prusiner SB (1992) Regional mapping of prion proteins in brain. Proc Natl Acad Sci U S A JID - 7505876 89: 7620-7624.
196. Schulz-Schaeffer WJ, Tschoke S, Kranefuss N, Drose W, Hause-Reitner D, Giese A, Groschup MH, Kretzschmar HA (2000) The paraffin-embedded tissue blot detects PrP(Sc) early in the incubation time in prion diseases. Am J Pathol JID - 0370502 156: 51-56.
197. Ritchie DL, Head MW, Ironside JW (2004) Advances in the detection of prion protein in peripheral tissues of variant Creutzfeldt-Jakob disease patients using paraffin-embedded tissue blotting. Neuropathol Appl Neurobiol 30: 360-368.
198. Lezmi S, Bencsik A, Baron T (2006) PET-blot analysis contributes to BSE strain recognition in C57Bl/6 mice. J Histochem Cytochem 54: 1087-1094.
199. Bellon A, Seyfert-Brandt W, Lang W, Baron H, Groner A, Vey M (2003) Improved conformation-dependent immunoassay: suitability for human prion detection with enhanced sensitivity. J Gen Virol 84: 1921-1925.
200. Safar JG, Scott M, Monaghan J, Deering C, Didorenko S, Vergara J, Ball H, Legname G, Leclerc E, Solforosi L, Serban H, Groth D, Burton DR, Prusiner SB, Williamson RA (2002) Measuring prions causing bovine spongiform encephalopathy or chronic wasting disease by immunoassays and transgenic mice. Nat Biotechnol JID - 9604648 20: 1147-1150.
201. Thackray AM, Hopkins L, Klein MA, Bujdoso R (2007) Mouse-adapted ovine scrapie prion strains are characterized by different conformers of PrPSc. J Virol 81: 12119-12127.
202. Wadsworth JD, Joiner S, Hill AF, Campbell TA, Desbruslais M, Luthert PJ, Collinge J (2001) Tissue distribution of protease resistant prion protein in variant Creutzfeldt-Jakob disease using a highly sensitive immunoblotting assay. Lancet JID - 2985213R 358: 171-180.
203. Biasini E, Massignan T, Fioriti L, Rossi V, Dossena S, Salmona M, Forloni G, Bonetto V, Chiesa R (2006) Analysis of the cerebellar proteome in a transgenic mouse model of inherited prion disease reveals preclinical alteration of calcineurin activity. Proteomics 6: 2823-2834.
204. Chich JF, Schaeffer B, Bouin AP, Mouthon F, Labas V, Larramendy C, Deslys JP, Grosclaude J (2007) Prion infection-impaired functional blocks identified by proteomics enlighten the targets and the curing pathways of an anti-prion drug. Biochim Biophys Acta 1774: 154-167.
205. Piubelli C, Fiorini M, Zanusso G, Milli A, Fasoli E, Monaco S, Righetti PG (2006) Searching for markers of Creutzfeldt-Jakob disease in cerebrospinal fluid by two-dimensional mapping. Proteomics 6 Suppl 1: S256-S261.
206. Xiang W, Windl O, Westner IM, Neumann M, Zerr I, Lederer RM, Kretzschmar HA (2005) Cerebral gene expression profiles in sporadic Creutzfeldt-Jakob disease. Ann Neurol 58: 242-257.
207. Xiang W, Windl O, Wunsch G, Dugas M, Kohlmann A, Dierkes N, Westner IM, Kretzschmar HA (2004) Identification of differentially expressed genes in scrapie-infected mouse brains by using global gene expression technology. J Virol 78: 11051-11060.

208. Booth S, Bowman C, Baumgartner R, Dolenko B, Sorensen G, Robertson C, Coulthart M, Phillipson C, Somorjai R (2004) Molecular classification of scrapie strains in mice using gene expression profiling. Biochem Biophys Res Commun 325: 1339-1345.
209. Booth S, Bowman C, Baumgartner R, Sorensen G, Robertson C, Coulthart M, Phillipson C, Somorjai RL (2004) Identification of central nervous system genes involved in the host response to the scrapie agent during preclinical and clinical infection. J Gen Virol 85: 3459-3471.
210. Brown P, Bradley R (1998) 1755 and all that: a historical primer of transmissible spongiform encephalopathy. BMJ 317: 1688-1692.
211. Johnson CJ, Phillips KE, Schramm PT, McKenzie D, Aiken JM, Pedersen JA (2006) Prions adhere to soil minerals and remain infectious. PLoS Pathog 2: e32.
212. Genovesi S, Leita L, Sequi P, Andrighetto I, Sorgato MC, Bertoli A (2007) Direct detection of soil-bound prions. PLoS ONE 2: e1069.
213. Johnson CJ, Pedersen JA, Chappell RJ, McKenzie D, Aiken JM (2007) Oral Transmissibility of Prion Disease Is Enhanced by Binding to Soil Particles. PLoS Pathog 3: e93.
214. Lasmezas CI, Fournier JG, Nouvel V, Boe H, Marce D, Lamoury F, Kopp N, Hauw JJ, Ironside J, Bruce M, Dormont D, Deslys JP (2001) Adaptation of the bovine spongiform encephalopathy agent to primates and comparison with Creutzfeldt-- Jakob disease: implications for human health. Proc Natl Acad Sci U S A JID - 7505876 98: 4142-4147.
215. Kimberlin RH, Walker C (1977) Characteristics of a short incubation model of scrapie in the golden hamster. J Gen Virol JID - 0077340 34: 295-304.
216. Kimberlin RH, Cole S, Walker CA (1987) Pathogenesis of scrapie is faster when infection is intraspinal instead of intracerebral. Microb Pathog JID - 8606191 2: 405-415.
217. Kimberlin RH, Walker CA (1978) Evidence that the transmission of one source of scrapie agent to hamsters involves separation of agent strains from a mixture. J Gen Virol JID - 0077340 39: 487-496.
218. Liberski PP, Asher DM, Yanagihara R, Gibbs CJJ, Gajdusek DC (1989) Serial ultrastructural studies of scrapie in hamsters. J Comp Pathol JID - 0102444 101: 429-442.
219. Liberski PP, Alwasiak J (1983) Neuropathology of experimental transmissible spongiform encephalopathy (263 K strain of scrapie in golden Syrian hamsters). I. Standard pathology and development of lesions. Neuropatol Pol JID - 0020712 21: 377-392.
220. Liberski PP (1987) Astrocytic reaction in experimental scrapie in hamsters. J Comp Pathol JID - 0102444 97: 73-78.
221. Masters CL, Rohwer RG, Franko MC, Brown P, Gajdusek DC (1984) The sequential development of spongiform change and gliosis of scrapie in the golden Syrian hamster. J Neuropathol Exp Neurol JID - 2985192R 43: 242-252.
222. Hecker R, Taraboulos A, Scott M, Pan KM, Yang SL, Torchia M, Jendroska K, DeArmond SJ, Prusiner SB (1992) Replication of distinct scrapie prion isolates is region specific in brains of transgenic mice and hamsters. Genes Dev 6: 1213-1228.
223. Jendroska K, Heinzel FP, Torchia M, Stowring L, Kretzschmar HA, Kon A, Stern A, Prusiner SB, DeArmond SJ (1991) Proteinase-resistant prion protein accumulation in Syrian hamster brain correlates with regional pathology and scrapie infectivity. Neurology 41: 1482-1490.
224. Wilesmith JW, Ryan JB, Atkinson MJ (1991) Bovine spongiform encephalopathy: epidemiological studies on the origin. Vet Rec 128: 199-203.
225. Beringue V, Bencsik A, Le DA, Reine F, Lai TL, Chenais N, Tilly G, Biacabe AG, Baron T, Vilotte JL, Laude H (2006) Isolation from cattle of a prion strain distinct from that causing bovine spongiform encephalopathy. PLoS Pathog 2: e112.
226. Biacabe AG, Laplanche JL, Ryder S, Baron T (2004) Distinct molecular phenotypes in bovine prion diseases. EMBO Rep 5: 110-115.
227. Yamakawa Y, Hagiwara K, Nohtomi K, Nakamura Y, Nishijima M, Higuchi Y, Sato Y, Sata T (2003) Atypical proteinase K-resistant prion protein (PrPres) observed in an apparently healthy 23-month-old Holstein steer. Jpn J Infect Dis 56: 221-222.

228. Casalone C, Zanusso G, Acutis P, Ferrari S, Capucci L, Tagliavini F, Monaco S, Caramelli M (2004) Identification of a second bovine amyloidotic spongiform encephalopathy: molecular similarities with sporadic Creutzfeldt-Jakob disease. Proc Natl Acad Sci U S A 101: 3065-3070.
229. Capobianco R, Casalone C, Suardi S, Mangieri M, Miccolo C, Limido L, Catania M, Rossi G, Di FG, Giaccone G, Bruzzone MG, Minati L, Corona C, Acutis P, Gelmetti D, Lombardi G, Groschup MH, Buschmann A, Zanusso G, Monaco S, Caramelli M, Tagliavini F (2007) Conversion of the BASE prion strain into the BSE strain: the origin of BSE? PLoS Pathog 3: e31.
230. Baron TG, Biacabe AG, Bencsik A, Langeveld JP (2006) Transmission of new bovine prion to mice. Emerg Infect Dis 12: 1125-1128.
231. Buschmann A, Gretzschel A, Biacabe AG, Schiebel K, Corona C, Hoffmann C, Eiden M, Baron T, Casalone C, Groschup MH (2006) Atypical BSE in Germany--proof of transmissibility and biochemical characterization. Vet Microbiol 117: 103-116.
232. Clawson ML, Richt JA, Baron T, Biacabe AG, Czub S, Heaton MP, Smith TP, Laegreid WW (2008) Association of a bovine prion gene haplotype with atypical BSE. PLoS ONE 3: e1830.
233. Will RG, Alperovitch A, Poser S, Pocchiari M, Hofman A, Mitrova E, de SR, D'Alessandro M, asnerie-Laupretre N, Zerr I, van DC (1998) Descriptive epidemiology of Creutzfeldt-Jakob disease in six European countries, 1993-1995. EU Collaborative Study Group for CJD. Ann Neurol 43: 763-767.
234. Ironside JW (1998) Prion diseases in man. J Pathol JID - 0204634 186: 227-234.
235. Prusiner SB (1998) The prion diseases. Brain Pathol JID - 9216781 8: 499-513.
236. Dlouhy SR, Hsiao K, Farlow MR, Foroud T, Conneally PM, Johnson P, Prusiner SB, Hodes ME, Ghetti B (1992) Linkage of the Indiana kindred of Gerstmann-Straussler-Scheinker disease to the prion protein gene. Nat Genet 1: 64-67.
237. Gabizon R, Rosenmann H, Meiner Z, Kahana I, Kahana E, Shugart Y, Ott J, Prusiner SB (1993) Mutation and polymorphism of the prion protein gene in Libyan Jews with Creutzfeldt-Jakob disease (CJD). Am J Hum Genet 53: 828-835.
238. Hsiao K, Baker HF, Crow TJ, Poulter M, Owen F, Terwilliger JD, Westaway D, Ott J, Prusiner SB (1989) Linkage of a prion protein missense variant to Gerstmann-Straussler syndrome. Nature JID - 0410462 338: 342-345.
239. Petersen RB, Tabaton M, Berg L, Schrank B, Torack RM, Leal S, Julien J, Vital C, Deleplanque B, Pendlebury WW, . (1992) Analysis of the prion protein gene in thalamic dementia. Neurology 42: 1859-1863.
240. Poulter M, Baker HF, Frith CD, Leach M, Lofthouse R, Ridley RM, Shah T, Owen F, Collinge J, Brown J, . (1992) Inherited prion disease with 144 base pair gene insertion. 1. Genealogical and molecular studies. Brain 115 (Pt 3): 675-685.
241. Belay ED (1999) Transmissible spongiform encephalopathies in humans. Annu Rev Microbiol JID - 0372370 53: 283-314.
242. Duffy P, Wolf J, Collins G, DeVoe AG, Streeten B, Cowen D (1974) Letter: Possible person-to-person transmission of Creutzfeldt-Jakob disease. N Engl J Med 290: 692-693.
243. Will RG, Matthews WB (1982) Evidence for case-to-case transmission of Creutzfeldt-Jakob disease. J Neurol Neurosurg Psychiatry 45: 235-238.
244. Bernoulli C, Siegfried J, Baumgartner G, Regli F, Rabinowicz T, Gajdusek DC, Gibbs CJ, Jr. (1977) Danger of accidental person-to-person transmission of Creutzfeldt-Jakob disease by surgery. Lancet 1: 478-479.
245. Cochius JI, Burns RJ, Blumbergs PC, Mack K, Alderman CP (1990) Creutzfeldt-Jakob disease in a recipient of human pituitary-derived gonadotrophin. Aust N Z J Med 20: 592-593.
246. Cochius JI, Hyman N, Esiri MM (1992) Creutzfeldt-Jakob disease in a recipient of human pituitary-derived gonadotrophin: a second case. J Neurol Neurosurg Psychiatry 55: 1094-1095.
247. Prusiner SB (1989) Scrapie prions. Annu Rev Microbiol 43: 345-374.
248. Gajdusek DC (1977) Unconventional viruses and the origin and disappearance of kuru. Science 197: 943-960.

249. Wells GA, Scott AC, Johnson CT, Gunning RF, Hancock RD, Jeffrey M, Dawson M, Bradley R (1987) A novel progressive spongiform encephalopathy in cattle. Vet Rec 121: 419-420.
250. Britton TC, al-Sarraj S, Shaw C, Campbell T, Collinge J (1995) Sporadic Creutzfeldt-Jakob disease in a 16-year-old in the UK. Lancet JID - 2985213R 346: 1155-Britton, T.
251. Bateman D, Hilton D, Love S, Zeidler M, Beck J, Collinge J (1995) Sporadic Creutzfeldt-Jakob disease in a 18-year-old in the UK. Lancet JID - 2985213R 346: 1155-1156.
252. Hill AF, Desbruslais M, Joiner S, Sidle KC, Gowland I, Collinge J, Doey LJ, Lantos P (1997) The same prion strain causes vCJD and BSE. Nature JID - 0410462 389: 448-50, 526.
253. Scott MR, Will R, Ironside J, Nguyen HO, Tremblay P, DeArmond SJ, Prusiner SB (1999) Compelling transgenetic evidence for transmission of bovine spongiform encephalopathy prions to humans. Proc Natl Acad Sci U S A JID - 7505876 96: 15137-15142.
254. Lasmezas CI, Deslys JP, Demaimay R, Adjou KT, Lamoury F, Dormont D, Robain O, Ironside J, Hauw JJ (1996) BSE transmission to macaques. Nature JID - 0410462 381: 743-744.
255. Will RG, Ironside JW, Zeidler M, Cousens SN, Estibeiro K, Alperovitch A, Poser S, Pocchiari M, Hofman A, Smith PG (1996) A new variant of Creutzfeldt-Jakob disease in the UK. Lancet 347: 921-925.
256. Chazot G, Broussolle E, Lapras C, Blattler T, Aguzzi A, Kopp N (1996) New variant of Creutzfeldt-Jakob disease in a 26-year-old French man. Lancet 347: 1181.
257. National Creutzfeld-Jakob Disease Surveillance Unit (8 A.D. May) www.cjd.ed.ac.uk/vcjdworld.htm.
258. Will RG, Zeidler M, Stewart GE, Macleod MA, Ironside JW, Cousens SN, Mackenzie J, Estibeiro K, Green AJ, Knight RS (2000) Diagnosis of new variant Creutzfeldt-Jakob disease. Ann Neurol JID - 7707449 47: 575-582.
259. Will RG, Zeidler M, Brown P, Harrington M, Lee KH, Kenney KL (1996) Cerebrospinal-fluid test for new-variant Creutzfeldt-Jakob disease. Lancet 348: 955.
260. Will R (1999) New variant Creutzfeldt-Jakob disease. Biomed Pharmacother JID - 8213295 53: 9-13.
261. 2007) Fourth case of transfusion-associated vCJD infection in the United Kingdom. Euro Surveill 12: E070118.
262. Hewitt PE, Llewelyn CA, Mackenzie J, Will RG (2006) Three reported cases of variant Creutzfeldt-Jakob disease transmission following transfusion of labile blood components. Vox Sang 91: 348.
263. Llewelyn CA, Hewitt PE, Knight RS, Amar K, Cousens S, Mackenzie J, Will RG (2004) Possible transmission of variant Creutzfeldt-Jakob disease by blood transfusion. Lancet 363: 417-421.
264. Wroe SJ, Pal S, Siddique D, Hyare H, Macfarlane R, Joiner S, Linehan JM, Brandner S, Wadsworth JD, Hewitt P, Collinge J (2006) Clinical presentation and pre-mortem diagnosis of variant Creutzfeldt-Jakob disease associated with blood transfusion: a case report. Lancet 368: 2061-2067.
265. Collinge J (1999) Variant Creutzfeldt-Jakob disease. Lancet JID - 2985213R 354: 317-323.
266. Collee JG, Bradley R, Liberski PP (2006) Variant CJD (vCJD) and bovine spongiform encephalopathy (BSE): 10 and 20 years on: part 2. Folia Neuropathol 44: 102-110.
267. Brown P, Preece MA, Will RG (1992) "Friendly fire" in medicine: hormones, homografts, and Creutzfeldt-Jakob disease. Lancet 340: 24-27.
268. Owen F, Poulter M, Collinge J, Crow TJ (1990) A codon 129 polymorphism in the PRIP gene. Nucleic Acids Res 18: 3103.
269. Collinge J, Whitfield J, McKintosh E, Beck J, Mead S, Thomas DJ, Alpers MP (2006) Kuru in the 21st century--an acquired human prion disease with very long incubation periods. Lancet 367: 2068-2074.
270. Lee HS, Brown P, Cervenakova L, Garruto RM, Alpers MP, Gajdusek DC, Goldfarb LG (2001) Increased susceptibility to Kuru of carriers of the PRNP 129 methionine/methionine genotype. J Infect Dis 183: 192-196.

271. Cervenakova L, Goldfarb LG, Garruto R, Lee HS, Gajdusek DC, Brown P (1998) Phenotype-genotype studies in kuru: implications for new variant Creutzfeldt-Jakob disease. Proc Natl Acad Sci U S A 95: 13239-13241.
272. Poser S, Zerr I, Schroeter A, Otto M, Giese A, Steinhoff BJ, Kretzschmar HA (2000) Clinical and differential diagnosis of Creutzfeldt-Jakob disease. Arch Virol Suppl JID - 9214275 153-159.
273. Sakaguchi S (2008) Recent Developments in Therapeutics for Prion Diseases. Expert Opinion on Therapeutic Patents 18: 35-59.
274. Rainov NG, Tsuboi Y, Krolak-Salmon P, Vighetto A, Doh-Ura K (2007) Experimental treatments for human transmissible spongiform encephalopathies: is there a role for pentosan polysulfate? Expert Opin Biol Ther 7: 713-726.
275. Todd NV, Morrow J, Doh-Ura K, Dealler S, O'Hare S, Farling P, Duddy M, Rainov NG (2005) Cerebroventricular infusion of pentosan polysulphate in human variant Creutzfeldt-Jakob disease. J Infect 50: 394-396.
276. Parry A, Baker I, Stacey R, Wimalaratna S (2007) Long term survival in a patient with variant Creutzfeldt-Jakob disease treated with intraventricular pentosan polysulphate. J Neurol Neurosurg Psychiatry 78: 733-734.
277. Whittle IR, Knight RS, Will RG (2006) Unsuccessful intraventricular pentosan polysulphate treatment of variant Creutzfeldt-Jakob disease. Acta Neurochir (Wien) 148: 677-679.
278. Nakajima M, Yamada T, Kusuhara T, Furukawa H, Takahashi M, Yamauchi A, Kataoka Y (2004) Results of quinacrine administration to patients with Creutzfeldt-Jakob disease. Dement Geriatr Cogn Disord 17: 158-163.
279. Otto M, Cepek L, Ratzka P, Doehlinger S, Boekhoff I, Wiltfang J, Irle E, Pergande G, Ellers-Lenz B, Windl O, Kretzschmar HA, Poser S, Prange H (2004) Efficacy of flupirtine on cognitive function in patients with CJD: A double-blind study. Neurology 62: 714-718.
280. Schild HH (1990) MRI Made Easy (...Well Almost). Berlin/Bergkamen: Schering AG.
281. Samman I, Schulz-Schaeffer WJ, Wohrle JC, Sommer A, Kretzschmar HA, Hennerici M (1999) Clinical range and MRI in Creutzfeldt-Jakob disease with heterozygosity at codon 129 and prion protein type 2. J Neurol Neurosurg Psychiatry JID - 2985191R 67: 678-681.
282. Di RA, Molinari S, Stollman AL, Decker A, Yahr MD (1993) MRI abnormalities in Creutzfeldt-Jakob disease. Neuroradiology 35: 584-585.
283. Hutzelmann A, Biederer J (1998) MRI follow-up in a case of clinically diagnosed Creutzfeld-Jakob disease. Eur Radiol 8: 421-423.
284. de Priester JA, Jansen GH, de KJ, Wilmink JT (1999) New MRI findings in Creutzfeldt-Jakob disease: high signal in the globus pallidus on T1-weighted images. Neuroradiology JID - 1302751 41: 265-268.
285. Murata T, Shiga Y, Higano S, Takahashi S, Mugikura S (2002) Conspicuity and evolution of lesions in Creutzfeldt-Jakob disease at diffusion-weighted imaging. AJNR Am J Neuroradiol JID - 8003708 23: 1164-1172.
286. Nitrini R, Mendonca RA, Huang N, LeBlanc A, Livramento JA, Marie SK (2001) Diffusion-weighted MRI in two cases of familial Creutzfeldt--Jakob disease. J Neurol Sci JID - 0375403 184: 163-167.
287. Mittal S, Farmer P, Kalina P, Kingsley PB, Halperin J (2002) Correlation of diffusion-weighted magnetic resonance imaging with neuropathology in Creutzfeldt-Jakob disease. Arch Neurol JID - 0372436 59: 128-134.
288. Chung YL, Williams A, Ritchie D, Williams SC, Changani KK, Hope J, Bell JD (1999) Conflicting MRI signals from gliosis and neuronal vacuolation in prion diseases. Neuroreport 10: 3471-3477.
289. Sadowski M, Tang CY, Aguinaldo JG, Carp R, Meeker HC, Wisniewski T (2003) In vivo micro magnetic resonance imaging signal changes in scrapie infected mice. Neurosci Lett 345: 1-4.
290. Coulthard A, Hall K, English PT, Ince PG, Burn DJ, Bates D (1999) Quantitative analysis of MRI signal intensity in new variant Creutzfeldt-Jakob disease. Br J Radiol JID - 0373125 72: 742-748.

291. Gertz HJ, Henkes H, Cervos-Navarro J (1988) Creutzfeldt-Jakob disease: correlation of MRI and neuropathologic findings. Neurology JID - 0401060 38: 1481-1482.
292. Zeidler M, Sellar RJ, Collie DA, Knight R, Stewart G, Macleod MA, Ironside JW, Cousens S, Colchester AC, Hadley DM, Will RG, Colchester AF (2000) The pulvinar sign on magnetic resonance imaging in variant Creutzfeldt-Jakob disease. Lancet JID - 2985213R 355: 1412-1418.
293. Chung YL, Williams A, Beech JS, Williams SC, Bell JD, Cox IJ, Hope J (1995) MRI assessment of the blood-brain barrier in a hamster model of scrapie. Neurodegeneration 4: 203-207.
294. Dubois J, Baydack R, McKenzie E, Booth T, Jackson M (2003) Scrapie infection investigated by magnetic resonance imaging and Fourier transform infrared microscopy. Vibrational Spectroscopy 32: 95-105.
295. Heo JH, Han SW, Lee SK (2005) Free radicals as triggers of brain edema formation after stroke. Free Radic Biol Med 39: 51-70.
296. Pantoni L, Garcia JH, Gutierrez JA (1996) Cerebral white matter is highly vulnerable to ischemia. Stroke 27: 1641-1646.
297. Garcia JH, Liu KF, Ho KL (1995) Neuronal necrosis after middle cerebral artery occlusion in Wistar rats progresses at different time intervals in the caudoputamen and the cortex. Stroke 26: 636-642.
298. Garcia JH, Liu KF, Yoshida Y, Chen S, Lian J (1994) Brain microvessels: factors altering their patency after the occlusion of a middle cerebral artery (Wistar rat). Am J Pathol 145: 728-740.
299. Brandner S, Isenmann S, Kuhne G, Aguzzi A (1998) Identification of the end stage of scrapie using infected neural grafts. Brain Pathol JID - 9216781 8: 19-27.
300. Rodriguez A, Perez-Gracia E, Espinosa JC, Pumarola M, Torres JM, Ferrer I (2006) Increased expression of water channel aquaporin 1 and aquaporin 4 in Creutzfeldt-Jakob disease and in bovine spongiform encephalopathy-infected bovine-PrP transgenic mice. Acta Neuropathol (Berl) 112: 573-585.
301. Arima H, Yamamoto N, Sobue K, Umenishi F, Tada T, Katsuya H, Asai K (2003) Hyperosmolar mannitol simulates expression of aquaporins 4 and 9 through a p38 mitogen-activated protein kinase-dependent pathway in rat astrocytes. J Biol Chem 278: 44525-44534.
302. Yamamoto N, Sobue K, Miyachi T, Inagaki M, Miura Y, Katsuya H, Asai K (2001) Differential regulation of aquaporin expression in astrocytes by protein kinase C. Brain Res Mol Brain Res 95: 110-116.
303. Zelenina M, Zelenin S, Bondar AA, Brismar H, Aperia A (2002) Water permeability of aquaporin-4 is decreased by protein kinase C and dopamine. Am J Physiol Renal Physiol 283: F309-F318.
304. Han Z, Wax MB, Patil RV (1998) Regulation of aquaporin-4 water channels by phorbol ester-dependent protein phosphorylation. J Biol Chem 273: 6001-6004.
305. Lee HP, Jun YC, Choi JK, Kim JI, Carp RI, Kim YS (2005) Activation of mitogen-activated protein kinases in hamster brains infected with 263K scrapie agent. J Neurochem 95: 584-593.
306. Manley GT, Fujimura M, Ma T, Noshita N, Filiz F, Bollen AW, Chan P, Verkman AS (2000) Aquaporin-4 deletion in mice reduces brain edema after acute water intoxication and ischemic stroke. Nat Med 6: 159-163.
307. Papadopoulos MC, Verkman AS (2005) Aquaporin-4 gene disruption in mice reduces brain swelling and mortality in pneumococcal meningitis. J Biol Chem 280: 13906-13912.
308. Bloch O, Papadopoulos MC, Manley GT, Verkman AS (2005) Aquaporin-4 gene deletion in mice increases focal edema associated with staphylococcal brain abscess. J Neurochem 95: 254-262.
309. Papadopoulos MC, Manley GT, Krishna S, Verkman AS (2004) Aquaporin-4 facilitates reabsorption of excess fluid in vasogenic brain edema. FASEB J 18: 1291-1293.
310. Weise J, Crome O, Sandau R, Schulz-Schaeffer W, Bahr M, Zerr I (2004) Upregulation of cellular prion protein (PrPc) after focal cerebral ischemia and influence of lesion severity. Neurosci Lett 372: 146-150.

311. Weise J, Sandau R, Schwarting S, Crome O, Wrede A, Schulz-Schaeffer W, Zerr I, Bahr M (2006) Deletion of cellular prion protein results in reduced Akt activation, enhanced postischemic caspase-3 activation, and exacerbation of ischemic brain injury. Stroke 37: 1296-1300.
312. Spudich A, Frigg R, Kilic E, Kilic U, Oesch B, Raeber A, Bassetti CL, Hermann DM (2005) Aggravation of ischemic brain injury by prion protein deficiency: role of ERK-1/-2 and STAT-1. Neurobiol Dis 20: 442-449.
313. Verkman AS, Binder DK, Bloch O, Auguste K, Papadopoulos MC (2006) Three distinct roles of aquaporin-4 in brain function revealed by knockout mice. Biochim Biophys Acta 1758: 1085-1093.
314. Dealler S, Rainov NG (2003) Pentosan polysulfate as a prophylactic and therapeutic agent against prion disease. IDrugs 2003 May ;6 (5):470 -8 6: 470-478.
315. MacGregor IR, Dawes J, Paton L, Pepper DS, Prowse CV, Smith M (1984) Metabolism of sodium pentosan polysulphate in man--catabolism of iodinated derivatives. Thromb Haemost 51: 321-325.
316. Dawes J, Pepper DS (1992) Human vascular endothelial cells catabolise exogenous glycosaminoglycans by a novel route. Thromb Haemost 67: 468-472.
317. Caughey B, Raymond GJ (1993) Sulfated polyanion inhibition of scrapie-associated PrP accumulation in cultured cells. J Virol 67: 643-650.
318. Kocisko DA, Engel AL, Harbuck K, Arnold KM, Olsen EA, Raymond LD, Vilette D, Caughey B (2005) Comparison of protease-resistant prion protein inhibitors in cell cultures infected with two strains of mouse and sheep scrapie. Neurosci Lett 388: 106-111.
319. Doh-Ura K, Ishikawa K, Murakami-Kubo I, Sasaki K, Mohri S, Race R, Iwaki T (2004) Treatment of transmissible spongiform encephalopathy by intraventricular drug infusion in animal models. J Virol 2004 May ;78 (10):4999 -5006 78: 4999-5006.
320. Farquhar C, Dickinson A, Bruce M (1999) Prophylactic potential of pentosan polysulphate in transmissible spongiform encephalopathies. Lancet 353: 117.
321. Farquhar C, McConnell I, Graham J, Cumming S, Prescott RJ (2002) Pentosan polysulphate has prophylactic potential for Transmissible Spongiform Encephalopathies. ABS 0-ABS 06.
322. Diringer H, Ehlers B (1991) Chemoprophylaxis of scrapie in mice. J Gen Virol 72 (Pt 2): 457-460.
323. Ladogana A, Casaccia P, Ingrosso L, Cibati M, Salvatore M, Xi YG, Masullo C, Pocchiari M (1992) Sulphate polyanions prolong the incubation period of scrapie-infected hamsters. J Gen Virol 73 (Pt 3): 661-665.
324. Shyng SL, Lehmann S, Moulder KL, Harris DA (1995) Sulfated glycans stimulate endocytosis of the cellular isoform of the prion protein, PrPC, in cultured cells. J Biol Chem 270: 30221-30229.
325. Borchelt DR, Taraboulos A, Prusiner SB (1992) Evidence for synthesis of scrapie prion proteins in the endocytic pathway. J Biol Chem 267: 16188-16199.
326. Caughey B, Raymond GJ, Ernst D, Race RE (1991) N-terminal truncation of the scrapie-associated form of PrP by lysosomal protease(s): implications regarding the site of conversion of PrP to the protease-resistant state. J Virol 65: 6597-6603.
327. Taraboulos A, Raeber AJ, Borchelt DR, Serban D, Prusiner SB (1992) Synthesis and trafficking of prion proteins in cultured cells. Mol Biol Cell 3: 851-863.
328. Caughey B, Raymond GJ (1991) The scrapie-associated form of PrP is made from a cell surface precursor that is both protease- and phospholipase-sensitive. J Biol Chem JID - 2985121R 266: 18217-18223.
329. Priola SA, Caughey B (1994) Inhibition of scrapie-associated PrP accumulation. Probing the role of glycosaminoglycans in amyloidogenesis. Mol Neurobiol 8: 113-120.
330. Rossi G, Salmona M, Forloni G, Bugiani O, Tagliavini F (2003) Therapeutic approaches to prion diseases. Clin Lab Med 23: 187-208.
331. Fraser H, Dickinson AG (1978) Studies of the lymphoreticular system in the pathogenesis of scrapie: the role of spleen and thymus. J Comp Pathol 88: 563-573.

332. Dickinson AG, Fraser H (1972) Scrapie: effect of Dh gene on incubation period of extraneurally injected agent. Heredity 29: 91-93.
333. Kimberlin RH, Walker CA (1986) Pathogenesis of scrapie (strain 263K) in hamsters infected intracerebrally, intraperitoneally or intraocularly. J Gen Virol JID - 0077340 67 (Pt 2): 255-263.
334. Unterberg AW, Stover J, Kress B, Kiening KL (2004) Edema and brain trauma. Neuroscience 129: 1021-1029.
335. Anderson RJ, Chung HM, Kluge R, Schrier RW (1985) Hyponatremia: a prospective analysis of its epidemiology and the pathogenetic role of vasopressin. Ann Intern Med 102: 164-168.
336. Tierney WM, Martin DK, Greenlee MC, Zerbe RL, McDonald CJ (1986) The prognosis of hyponatremia at hospital admission. J Gen Intern Med 1: 380-385.
337. Lee CT, Guo HR, Chen JB (2000) Hyponatremia in the emergency department. Am J Emerg Med 18: 264-268.
338. Sterns RH, Silver SM (2006) Brain volume regulation in response to hypo-osmolality and its correction. Am J Med 119: S12-S16.
339. Lin M, Liu SJ, Lim IT (2005) Disorders of water imbalance. Emerg Med Clin North Am 23: 749-70, ix.
340. Arieff AI, Llach F, Massry SG (1976) Neurological manifestations and morbidity of hyponatremia: correlation with brain water and electrolytes. Medicine (Baltimore) 55: 121-129.
341. Ogami R, Nakahara T, Hamasaki O (2008) Probable blood-brain barrier disruption after carotid artery stenting. Neurol Med Chir (Tokyo) 48: 121-125.
342. Tang Y, Cai D, Chen Y (2007) Thrombin inhibits aquaporin 4 expression through protein kinase C-dependent pathway in cultured astrocytes. J Mol Neurosci 31: 83-93.
343. Fabrizi C, Silei V, Menegazzi M, Salmona M, Bugiani O, Tagliavini F, Suzuki H, Lauro GM (2001) The stimulation of inducible nitric-oxide synthase by the prion protein fragment 106--126 in human microglia is tumor necrosis factor-alpha-dependent and involves p38 mitogen-activated protein kinase. J Biol Chem 276: 25692-25696.

Appendix 1 – Results of Pentosan Polysulphate Toxicity Study.

As noted in the Materials and Methods section, the original dose of PPS used for i.c. treatments was 20 mg/kg. When the first six mock-infected hamsters were given this dose of PPS, they experienced adverse effects. The typical picture consisted of recovery from isoflurane anaesthetic that seemed normal, if slightly slower than usual. Behaviour remained normal for five to twenty minutes, including exploring the recovery cage, with or without eating/drinking. At some point, during this time, the hamsters began to have seizures, normally consisting of full body convulsions lasting up to fifteen seconds at a time. In between seizures, the hamsters were typically immobile. At the beginning, seizures occurred as often as every minute, becoming progressively less frequent, and in some cases stopping all together after about one hour. All but one of these hamsters was euthanized, in each case whenever it became apparent that the hamster would not survive, or was experiencing severe discomfort. The skulls of all of the euthanized hamsters were opened, and in each case, an haematoma, typically large, was evident at the site of injection.

The one surviving hamster belonged to the group receiving treatment at 26 dpi. Following injection, the hamster recovered slowly although seemingly well. Once it was transferred back to its cage from the recovery cage, at 45 minutes post injection, it stopped moving. It was monitored for the next hour and a half during which time it began to move around again; it was then returned to the animal facility, where the staff continued to monitor it for a further four hours.

For about one hour of this time, the hamster experienced small absent seizures about every ten minutes before falling asleep. The hamster was monitored again the following morning, at which time it exhibited normal behaviour over the four hours of observation, including such activity as climbing on the cage bars. It was determined that the hamster could be kept, and in fact it continued to be MR imaged until 150 dpi, when it was euthanized. However, it should be noted that from the time of PPS injection at 26 dpi, until 150 dpi, this hamster gained only a few grams in body weight.

In order to determine a tolerable dose of PPS, hamsters were injected intra-cerebrally with a mixture of control brain homogenate and PPS, corresponding to doses of 0.5 mg/kg; 1 mg/kg; 2 mg/kg; and 5 mg/kg. The hamsters that received the 5 mg/kg dose demonstrated adverse effects similar to those described above, including seizures. They were euthanized and dissected, and haematomas were again observed at the site of injection. None of the hamsters receiving any of the three lower doses of PPS showed any ill effects. Because of this, the largest dose (2 mg/kg) of PPS that did not result in adverse effects was chosen as the dose to be used in the main drug treatment study. However, when the scrapie-infected hamsters received their i.c. PPS treatment at 0 dpi, two out of three hamsters experienced similar symptoms consisting of six or seven petit mal seizures, decreasing in severity and frequency. These were followed by upwards of one hour of sleep followed by sluggish movements, and walking around the cage low to the ground, before their actions returned to normal. The following day, the activities of all hamsters remained normal and

they remained in the study. However, as a consequence of these results, the i.c. dose of PPS for the groups receiving treatment at 26 dpi was adjusted to 1 mg/kg.

Hamsters receiving this dose (at 26 dpi) tolerated it well. In the case of one mock-infected hamster, it occasionally arched its head backwards and blinked rapidly in the 45 minutes following the procedure. It is important to consider that the procedure for treatment at 26 dpi was much more invasive, involving drilling of the skull with a dental drill, and that the response of hamsters undergoing this procedure was also influenced by this high degree of invasiveness.

In order to determine the reasons why largely variable doses result in similar adverse effects in different species, it is useful to consider the size of the animal being treated. A better understanding of the situation can be established by examining how a dose expressed in mg/kg body weight of the animal being treated translates to a raw quantity of PPS injected. Beginning with the hamsters in this study that exhibited adverse effects: a dose of 20 mg/kg translated to 1.5 mg and 2.5 mg of PPS at 0 dpi, and 26 dpi, respectively; the 5 mg/kg dose converted to 350 μg PPS; and the 2 mg/kg dose corresponded to 140 μg PPS (this dose was well tolerated by mock-infected hamsters, but caused some adverse effects in scrapie-infected hamsters). The hamsters that tolerated intra-cerebral PPS received doses of either 1 mg/kg translating to 70μg of PPS at 0 dpi, or 115-120μg PPS at 26 dpi; or 0.5 mg/kg, translating to 35μg PPS. In comparison, dogs in the Doh-Ura study received slow continuous infusions of

PPS at doses of 230 μg/kg/day; 345 μg/kg/day; and 460 μg/kg/day [300]. If the weight of the dogs may be conservatively estimated as 10 kg, these doses translate to 2.3 g/day; 3.45 g/day; and 4.6 g/day. A low continuous infusion of a drug will eventually result in a constant level of the drug in the brain, as an equilibrium is reached between newly infused drug and drug being cleared. It is reasonable to assume that this stable level will be reached within 24 hours of the initiation of treatment; Doh-Ura *et. al.* report that when dogs exhibited adverse effects of PPS treatment, it occurred within 24 hours [300]. Without any means of definitively determining what this level is, the amount of drug infused per hour may be used as a reasonable approximation. If this assumption is applied to the dogs in the Doh-Ura study, the resulting PPS levels that were either completely tolerated, or caused seizures in either some, or all, dogs are: 95.83 μg; 143.75 μg; and 191.67 μg, respectively.

When data collected in dogs is compared to the hamster data presented here, there appears to be a clear level at which PPS causes adverse effects: in both hamsters and dogs, PPS levels around 140 μg caused seizures in some, but not all animals tested. In comparison, all PPS levels below 140 μg, to a maximum tested level of 120 μg were well tolerated, while all levels above 140 μg resulted in severe adverse effects in all animals tested. While this exercise produced attractive similarities in data collected in hamsters and dogs, it is important to realize that the numbers representing stable PPS levels in dogs are merely a very rough estimate produced under a number of unverified assumptions. The equilibrium levels of PPS in the brain of dogs were not

measured, and the rate of clearing of PPS in the brain is unknown in any of these animals, so the accuracy of these estimates is very much in question. However, the tolerable amount of PPS injected intra-cerebrally in hamsters can be said to be no more than about 120 μg. The above exercise estimating the PPS levels in the brain of dogs in the Doh-Ura study [300] at the very least is indicative that this level is a useful starting point in other species as well.

The other available data regarding PPS toxicity following intra-cerebral injection also bears further examination. In a review article, a personal communication is presented, indicating that a dose of approximately 4 g/kg PPS injected intra-cerebrally in mice caused fatal cerebral haemorrhages in all cases [297]. It also indicates that the amount of PPS injected was 5 mg, and that this is 50-fold the anticoagulant dose [297]. These statements hold an inherent contradiction. If the weight of a mouse at the time of injection can reasonably be assumed to be 20 g, then a dose of 4 g/kg would equate to a total of 80 mg PPS injected, not 5 mg. It is unclear whether the actual PPS dose given to these mice, which resulted in fatal cerebral haemorrhage, was 4 g/kg or a total of 5 mg. This is unfortunate, because the initial dose for the study presented here (20 mg/kg) was chosen using the 4 g/kg dose as a guideline. As it happens, the highest amount of PPS injected in hamsters was 2.5 mg (at 26 dpi), causing seizures in all animals. If the dose given to the mice discussed above was a total of 5 mg, then this result is not unexpected. It is also interesting that when 5 mg is divided by 50, it gives 100 μg, which according to this article is the anticoagulant dose of PPS [297]. The highest tolerable dose in hamsters was

120 μg, so if 100 μg is in fact the anticoagulant dose, then it makes sense that doses much greater than this result in cerebral haemorrhage and death.

Appendix 2 – Tables of Statistical Differences Observed on MRI During PPS Study.

Table 20. MRI Slice 6 Group x Region Comparison at 19 dpi.							
		p values					
		Mock-Infected I.c. PPS			Mock-Infected No I.c. PPS		
		Hippo	Cortex	Hypothal	Hippo	Cortex	Hypothal
Infected No I.c. PPS	Hippo	<0.002	0.117	0.120	<0.004	0.122	0.158
Infected No I.c. PPS	Cortex	<0.001	<0.005	<0.015	<0.001	<0.001	<0.002
Infected No I.c. PPS	Thalamus	<0.001	<0.03	<0.04	<0.001	<0.025	<0.04
Infected No I.c. PPS	Hypothal	<0.03	0.438	0.316	0.246	0.814	0.721

Statistically significant results indicated in black. Hippo: Hippocampus; Hypo: Hypothalamus. Dpi: days post injection; I.c.: intra-cerebral; PPS: pentosan polysulphate.

Table 21. MRI Slice 6 Group x Region Comparison at 33 days post injection.										
Group/Region ID			p values							
	Group	Region	1	2	3	4	5	6	7	8
1	A	Hippo		0.904	0.964	0.999	<0.001	<0.001	<0.001	<0.001
2		Cortex	0.904		1	1	<0.001	<0.001	<0.001	0.06
3		Thal	0.964	1		1	0.051	<0.001	<0.005	0.381
4		Hypo	0.999	1	1		<0.01	<0.001	<0.001	0.144
5	B	Hippo	<0.001	<0.001	0.051	<0.01		0.706	0.995	1
6		Cortex	<0.001	<0.001	<0.001	<0.001	0.706		1	0.479
7		Thal	<0.001	<0.001	<0.005	<0.001	0.995	1		0.93
8		Hypo	<0.001	0.06	0.381	0.144	1	0.479	0.93	
9	C	Hippo	0.999	1	1	1	<0.001	<0.001	<0.001	<0.006
10		Cortex	0.879	1	1	1	<0.001	<0.001	<0.001	0.072
11		Thal	0.943	1	1	1	0.07	<0.001	<0.01	0.449
12		Hypo	1	1	1	1	<0.005	<0.001	<0.001	0.09
13	D	Hippo	<0.001	0.11	0.615	0.275	0.932	,0.01	0.292	1
14		Cortex	<0.001	<0.001	<0.015	<0.002	1	0.987	1	0.996
15		Thal	<0.001	<0.015	0.159	<0.05	1	0.864	0.997	1
16		Hypo	<0.01	0.693	0.953	0.758	0.799	0.012	0.203	0.999
	Group	Region	9	10	11	12	13	14	15	16
1	A	Hippo	0.999	0.879	0.943	1	<0.001	<0.001	<0.001	<0.01
2		Cortex	1	1	1	1	0.11	<0.001	<0.015	0.693
3		Thal	1	1	1	1	0.615	<0.015	0.159	0.953
4		Hypo	1	1	1	1	0.275	<0.002	<0.05	0.758
5	B	Hippo	<0.001	<0.001	0.07	<0.005	0.932	1	1	0.799
6		Cortex	<0.001	<0.001	<0.001	<0.001	<0.01	0.987	0.864	<0.015
7		Thal	<0.001	<0.001	<0.01	<0.001	0.292	1	0.997	0.203
8		Hypo	<0.01	0.072	0.449	0.09	1	0.996	1	0.999
9	C	Hippo		1	1	1	<0.01	<0.001	<0.001	0.237
10		Cortex	1		1	1	0.133	<0.001	<0.015	0.736
11		Thal	1	1		1	0.691	<0.015	0.2	0.972
12		Hypo	1	1	1		0.179	<0.001	<0.03	0.637
13	D	Hippo	<0.01	0.133	0.691	0.179		0.482	0.996	1
14		Cortex	<0.001	<0.001	<0.015	<0.001	0.482		1	0.367
15		Thal	<0.001	<0.015	0.201	<0.03	0.996	1		0.959
16		Hypo	0.237	0.736	0.972	0.637	1	0.367	0.959	

Statistically significant results indicated in black. A: Mock-infected i.c. PPS; B: Mock-infected No i.c. PPS; C: Scrapie-Infected i.c. PPS; D: Scrapie-Infected No i.c. PPS. Hippo: Hippocampus; Thal: Thalamus; Hypo: Hypothalamus.

Table 22. MRI Slice 6 Group x Region Comparison at 47 dpi.										
Group/Region ID			p values							
	Group	Region	1	2	3	4	5	6	7	8
1	A	Hippo		0.76	0.786	1	<0.001	<0.001	<0.001	<0.001
2		Cortex	0.76		1	0.998	<0.001	<0.001	<0.001	<0.001
3		Thal	0.786	1		0.994	<0.01	<0.001	<0.001	<0.03
4		Hypo	1	0.998	0.994		<0.001	<0.001	<0.001	<0.001
5	B	Hippo	<0.001	<0.001	<0.01	<0.001		<0.025	0.808	1
6		Cortex	<0.001	<0.001	<0.001	<0.001	<0.025		1	0.134
7		Thal	<0.001	<0.001	<0.001	<0.001	0.808	1		0.905
8		Hypo	<0.001	<0.001	<0.03	<0.001	1	0.134	0.905	
9	C	Hippo	0.18	1	1	0.866	<0.001	<0.001	<0.001	<0.01
10		Cortex	<0.001	0.594	0.974	0.121	0.167	<0.001	<0.002	0.45
11		Thal	<0.03	0.877	0.994	0.331	0.595	<0.001	<0.05	0.781
12		Hypo	0.678	1	1	0.984	<0.015	<0.001	<0.001	<0.05
13	D	Hippo	<0.001	<0.001	<0.02	<0.001	1	<0.005	0.538	1
14		Cortex	<0.001	<0.001	<0.001	<0.001	0.916	0.887	1	0.976
15		Thal	<0.001	<0.001	<0.005	<0.001	1	0.508	0.997	1
16		Hypo	<0.001	0.363	0.91	0.057	0.368	<0.001	<0.01	0.686
	Group	Region	9	10	11	12	13	14	15	16
1	A	Hippo	0.18	<0.001	<0.03	0.678	<0.001	<0.001	<0.001	<0.001
2		Cortex	1	0.594	0.877	1	<0.001	<0.001	<0.001	0.363
3		Thal	1	0.974	0.994	1	<0.02	<0.001	<0.005	0.91
4		Hypo	0.866	0.121	0.331	0.984	<0.001	<0.001	<0.001	0.057
5	B	Hippo	<0.001	0.167	0.595	<0.015	1	0.916	1	0.368
6		Cortex	<0.001	<0.001	<0.001	<0.001	<0.005	0.887	0.508	<0.001
7		Thal	<0.001	<0.002	<0.05	<0.001	0.538	1	0.997	<0.01
8		Hypo	<0.01	0.45	0.781	<0.05	1	0.976	1	0.686
9	C	Hippo		0.985	0.998	1	<0.002	<0.001	<0.001	0.921
10		Cortex	0.985		1	0.991	0.383	<0.001	0.138	1
11		Thal	0.998	1		0.998	0.801	<0.05	0.453	1
12		Hypo	1	0.991	0.998		<0.05	<0.001	<0.01	0.957
13	D	Hippo	<0.002	0.383	0.801	<0.05		0.647	1	0.652
14		Cortex	<0.001	<0.001	<0.05	<0.001	0.647		1	<0.005
15		Thal	<0.001	0.138	0.453	<0.01	1	1		0.288
16		Hypo	0.921	1	1	0.957	0.652	<0.005	0.288	

Statistically significant results indicated in black. A: Mock-infected i.c. PPS; B: Mock-infected No i.c. PPS; C: Scrapie-Infected i.c. PPS; D: Scrapie-Infected No i.c. PPS. Hippo: Hippocampus; Thal: Thalamus; Hypo: Hypothalamus.

Table 23. MRI Slice 6 Group x Region Comparison at 61 dpi.

Group/Region ID			p values							
	Group	Region	1	2	3	4	5	6	7	8
1	A	Hippo		1	1	1	<0.001	<0.001	<0.001	<0.05
2		Cortex	1		1	1	0.17	<0.002	0.057	1
3		Thal	1	1		1	1	0.249	1	1
4		Hypo	1	1	1		0.13	<0.005	<0.05	0.593
5	B	Hippo	<0.001	0.17	1	0.13		1	1	1
6		Cortex	<0.001	<0.002	0.249	<0.005	1		1	1
7		Thal	<0.001	0.057	1	<0.05	1	1		1
8		Hypo	<0.05	1	1	0.593	1	1	1	
9	C	Hippo	1	1	1	1	0.121	<0.001	<0.05	1
10		Cortex	1	1	1	1	1	0.124	1	1
11		Thal	1	1	1	1	1	1	1	1
12		Hypo	1	1	1	1	1	0.167	1	1
13	D	Hippo	0.717	1	1	1	1	<0.05	1	1
14		Cortex	<0.01	0.831	1	0.464	1	1	1	1
15		Thal	0.254	1	1	1	1	1	1	1
16		Hypo	1	1	1	1	1	<0.05	0.782	1

	Group	Region	9	10	11	12	13	14	15	16
1	A	Hippo	1	1	1	1	0.717	<0.01	0.254	1
2		Cortex	1	1	1	1	1	0.831	1	1
3		Thal	1	1	1	1	1	1	1	1
4		Hypo	1	1	1	1	1	0.464	1	1
5	B	Hippo	0.121	1	1	1	1	1	1	1
6		Cortex	<0.001	0.124	1	0.167	<0.05	1	1	<0.05
7		Thal	<0.05	1	1	1	1	1	1	0.782
8		Hypo	1	1	1	1	1	1	1	1
9	C	Hippo		1	1	1	1	0.616	1	1
10		Cortex	1		1	1	1	1	1	1
11		Thal	1	1		1	1	1	1	1
12		Hypo	1	1	1		1	1	1	1
13	D	Hippo	1	1	1	1		1	1	1
14		Cortex	0.616	1	1	1	1		1	1
15		Thal	1	1	1	1	1	1		1
16		Hypo	1	1	1	1	1	1	1	

Statistically significant results indicated in black. A: Mock-infected i.c. PPS; B: Mock-infected No i.c. PPS; C: Scrapie-Infected i.c. PPS; D: Scrapie-Infected No i.c. PPS. Hippo: Hippocampus; Thal: Thalamus; Hypo: Hypothalamus.

Table 24. MRI Slice 6 Group x Region Comparison at 75 dpi.										
Group/Region ID			p values							
	Group	Region	1	2	3	4	5	6	7	8
1	A	Hippo		1	1	1	<0.001	<0.001	<0.001	<0.001
2		Cortex	1		1	1	<0.001	<0.001	<0.001	<0.025
3		Thal	1	1		1	<0.02	<0.001	<0.015	0.435
4		Hypo	1	1	1		<0.001	<0.001	<0.001	<0.03
5	B	Hippo	<0.001	<0.001	<0.02	<0.001		1	1	1
6		Cortex	<0.001	<0.001	<0.001	<0.001	1		1	1
7		Thal	<0.001	<0.001	<0.015	<0.001	1	1		1
8		Hypo	<0.001	<0.025	0.435	<0.03	1	1	1	
9	C	Hippo	0.829	1	1	1	0.198	<0.005	0.166	1
10		Cortex	<0.001	<0.05	0.671	<0.05	1	1	1	1
11		Thal	0.117	1	1	0.815	1	1	1	1
12		Hypo	1	1	1	1	1	0.341	1	1
13	D	Hippo	1	1	1	1	<0.001	<0.001	<0.002	0.351
14		Cortex	<0.01	0.475	1	0.411	0.724	<0.015	0.638	1
15		Thal	0.254	1	1	1	0.79	<0.03	0.567	1
16		Hypo	1	1	1	1	0.135	<0.005	0.119	1
	Group	Region	9	10	11	12	13	14	15	16
1	A	Hippo	0.829	<0.001	0.117	1	1	<0.01	0.254	1
2		Cortex	1	<0.05	1	1	1	0.475	1	1
3		Thal	1	0.671	1	1	1	1	1	1
4		Hypo	1	<0.05	0.815	1	1	0.411	1	1
5	B	Hippo	0.198	1	1	1	<0.001	0.724	0.79	0.135
6		Cortex	<0.005	1	1	0.341	<0.001	<0.015	<0.03	<0.005
7		Thal	0.166	1	1	1	<0.002	0.638	0.567	0.119
8		Hypo	1	1	1	1	0.351	1	1	1
9	C	Hippo		1	1	1	1	1	1	1
10		Cortex	1		1	1	0.653	1	1	1
11		Thal	1	1		1	1	1	1	1
12		Hypo	1	1	1		1	1	1	1
13	D	Hippo	1	0.653	1	1		1	1	1
14		Cortex	1	1	1	1	1		1	1
15		Thal	1	1	1	1	1	1		1
16		Hypo	1	1	1	1	1	1	1	

Statistically significant results indicated in black. A: Mock-infected i.c. PPS; B: Mock-infected No i.c. PPS; C: Scrapie-Infected i.c. PPS; D: Scrapie-Infected No i.c. PPS. Hippo: Hippocampus; Thal: Thalamus; Hypo: Hypothalamus.

Table 25. MRI Slice 6 Group x Region Comparison at 89 dpi.

Group/Region ID			p values							
	Group	Region	1	2	3	4	5	6	7	8
1	A	Hippo		1	1	1	<0.001	<0.001	<0.001	<0.01
2		Cortex	1		1	1	<0.03	<0.001	<0.005	0.392
3		Thal	1	1		1	0.916	<0.02	0.101	1
4		Hypo	1	1	1		0.107	<0.002	<0.01	0.537
5	B	Hippo	<0.001	<0.03	0.916	0.107		1	1	1
6		Cortex	<0.001	<0.001	<0.02	<0.002	1		1	1
7		Thal	<0.001	<0.005	0.101	<0.01	1	1		1
8		Hypo	<0.01	0.392	1	0.537	1	1	1	
9	C	Hippo	1	1	1	1	1	0.059	0.417	1
10		Cortex	<0.01	0.36	1	0.467	1	1	1	1
11		Thal	0.621	1	1	1	1	1	1	1
12		Hypo	1	1	1	1	1	1	1	1
13	D	Hippo	<0.03	0.884	1	0.903	1	1	1	1
14		Cortex	<0.001	<0.005	0.08	<0.01	1	1	1	1
15		Thal	0.053	0.821	1	0.693	1	1	1	1
16		Hypo	0.233	1	1	1	1	1	1	1

	Group	Region	9	10	11	12	13	14	15	16
1	A	Hippo	1	<0.01	0.621	1	<0.03	<0.001	0.053	0.233
2		Cortex	1	0.36	1	1	0.884	<0.005	0.821	1
3		Thal	1	1	1	1	1	0.08	1	1
4		Hypo	1	0.467	1	1	0.903	<0.01	0.693	1
5	B	Hippo	1	1	1	1	1	1	1	1
6		Cortex	0.059	1	1	1	1	1	1	1
7		Thal	0.417	1	1	1	1	1	1	1
8		Hypo	1	1	1	1	1	1	1	1
9	C	Hippo		1	1	1	1	0.333	1	1
10		Cortex	1		1	1	1	1	1	1
11		Thal	1	1		1	1	1	1	1
12		Hypo	1	1	1		1	1	1	1
13	D	Hippo	1	1	1	1		1	1	1
14		Cortex	0.333	1	1	1	1		1	1
15		Thal	1	1	1	1	1	1		1
16		Hypo	1	1	1	1	1	1	1	

Statistically significant results indicated in black. A: Mock-infected i.c. PPS; B: Mock-infected No i.c. PPS; C: Scrapie-Infected i.c. PPS; D: Scrapie-Infected No i.c. PPS. Hippo: Hippocampus; Thal: Thalamus; Hypo: Hypothalamus.

Table 26. MRI Slice 6 Group x Region Comparison at 103 dpi.								
Group/Region ID			p values					
	Group	Region	1	2	3	4	5	6
1	A	Hippo		0.327	0.557	0.995	<0.001	<0.001
2		Cortex	0.327		1	0.998	<0.015	<0.001
3		Thal	0.557	1		0.998	0.18	<0.025
4		Hypo	0.995	0.998	0.998		<0.01	<0.001
5	B	Hippo	<0.001	<0.015	0.18	<0.01		0.983
6		Cortex	<0.001	<0.001	<0.025	<0.001	0.983	
7		Thal	<0.001	<0.01	0.082	<0.005	1	1
8		Hypo	<0.001	0.246	0.641	0.078	1	0.839
9	C	Hippo	<0.001	<0.01	<0.05	<0.005	0.852	0.996
10		Cortex	<0.001	<0.001	<0.002	<0.001	0.175	0.569
11		Thal	<0.001	<0.05	0.08	<0.015	0.839	0.982
12		Hypo	<0.002	0.114	0.212	<0.05	0.977	1
	Group	Region	9	10	11	12	13	14
1	A	Hippo	<0.001	<0.001	<0.001	<0.001	<0.001	<0.002
2		Cortex	<0.01	0.246	<0.01	<0.001	<0.05	0.114
3		Thal	0.082	0.641	<0.05	<0.002	0.081	0.212
4		Hypo	<0.005	0.078	<0.005	<0.001	<0.015	<0.05
5	B	Hippo	1	1	0.852	0.175	0.839	0.977
6		Cortex	1	0.839	0.996	0.569	0.982	1
7		Thal		0.973	0.993	0.573	0.975	0.999
8		Hypo	0.973		0.65	0.093	0.675	0.908
9	C	Hippo	0.993	0.65		0.999	1	1
10		Cortex	0.573	0.093	0.999		1	1
11		Thal	0.975	0.675	1	1		1
12		Hypo	0.999	0.908	1	1	1	

Statistically significant results indicated in black. A: Mock-infected i.c. PPS; B: Mock-infected No i.c. PPS; C: Scrapie-Infected i.c. PPS. Hippo: Hippocampus; Thal: Thalamus; Hypo: Hypothalamus.

Table 27. MRI Slice 6 Group x Region Comparison at 117 dpi.								
Group/Region ID			p values					
	Group	Region	1	2	3	4	5	6
1	A	Hippo		1	1	1	<0.005	<0.001
2		Cortex	1		1	1	0.076	<0.001
3		Thal	1	1		1	1	<0.02
4		Hypo	1	1	1		0.242	<0.002
5	B	Hippo	<0.005	0.076	1	0.242		1
6		Cortex	<0.001	<0.001	<0.02	<0.002	1	
7		Thal	<0.001	<0.005	0.165	<0.02	1	1
8		Hypo	0.282	1	1	1	1	0.859
9	C	Hippo	0.445	1	1	1	1	1
10		Cortex	<0.01	0.055	0.351	0.073	1	1
11		Thal	0.777	1	1	1	1	1
12		Hypo	1	1	1	1	1	1
	Group	Region	9	10	11	12	13	14
1	A	Hippo	<0.001	0.282	0.445	<0.01	0.777	1
2		Cortex	<0.005	1	1	0.055	1	1
3		Thal	0.165	1	1	0.351	1	1
4		Hypo	<0.02	1	1	0.073	1	1
5	B	Hippo	1	1	1	1	1	1
6		Cortex	1	0.859	1	1	1	1
7		Thal		1	1	1	1	1
8		Hypo	1		1	1	1	1
9	C	Hippo	1	1		1	1	1
10		Cortex	1	1	1		1	1
11		Thal	1	1	1	1		1
12		Hypo	1	1	1	1	1	

Statistically significant results indicated in black. A: Mock-infected i.c. PPS; B: Mock-infected No i.c. PPS; C: Scrapie-Infected i.c. PPS. Hippo: Hippocampus; Thal: Thalamus; Hypo: Hypothalamus.

Table 28. MRI Slice 5 Group x Region Comparison at 19 dpi.									
		p values							
		Mock-Infected I.c. PPS				Mock-Infected No I.c. PPS			
		Hippo	Cortex	Thal	Hypo	Hippo	Cortex	Thal	Hypo
D	Hippo	<0.001	<0.03	0.513	0.171	<0.001	<0.002	0.175	<0.02
	Cortex	<0.001	<0.001	0.146	<0.03	<0.001	<0.001	<0.005	<0.001
	Thal	<0.001	<0.01	0.267	0.068	<0.001	<0.001	0.057	<0.01
	Hypo	<0.01	0.199	0.817	0.441	0.09	0.198	0.783	0.319
		Scrapie-Infected I.c. PPS				Scrapie-Infected No I.c. PPS			
		Hippo	Cortex	Thal	Hypo	Hippo	Cortex	Thal	Hypo
D	Hippo	0.235	0.855	0.998	0.911		0.989	1	1
	Cortex	<0.025	0.285	0.904	0.526	0.989		1	0.909
	Thal	0.085	0.544	0.962	0.697	1	1		0.993
	Hypo	0.682	0.993	1	0.99	1	0.909	0.993	

Statistically significant results indicated in black. D: Scrapie-Infected No i.c. PPS. Hippo: Hippocampus; Thal: Thalamus; Hypo: Hypothalamus.

Table 29. MRI Slice 5 Group x Region Comparison at 33 dpi.

Group/Region ID			p values							
	Group	Region	1	2	3	4	5	6	7	8
1	A	Hippo		1	1	1	<0.002	<0.001	<0.001	0.135
2		Cortex	1		1	1	<0.01	<0.001	<0.005	0.386
3		Thal	1	1		1	0.264	<0.015	0.097	1
4		Hypo	1	1	1		<0.05	<0.002	<0.02	0.519
5	B	Hippo	<0.002	<0.01	0.264	<0.05		1	1	1
6		Cortex	<0.001	<0.001	<0.015	<0.002	1		1	1
7		Thal	<0.001	<0.005	0.097	<0.02	1	1		1
8		Hypo	0.135	0.386	1	0.519	1	1	1	
9	C	Hippo	1	1	1	1	<0.002	<0.001	<0.001	0.11
10		Cortex	1	1	1	1	<0.001	<0.001	<0.001	0.072
11		Thal	1	1	1	1	0.254	<0.015	0.093	1
12		Hypo	1	1	1	1	<0.05	<0.001	<0.015	0.453
13	D	Hippo	0.247	0.776	1	1	1	0.484	1	1
14		Cortex	<0.005	<0.015	0.325	<0.05	1	1	1	1
15		Thal	<0.05	0.122	0.979	0.209	1	1	1	1
16		Hypo	1	1	1	1	1	1	1	1

	Group	Region	9	10	11	12	13	14	15	16
1	A	Hippo	1	1	1	1	0.247	<0.005	<0.05	1
2		Cortex	1	1	1	1	0.776	<0.015	0.122	1
3		Thal	1	1	1	1	1	0.325	0.979	1
4		Hypo	1	1	1	1	1	<0.05	0.209	1
5	B	Hippo	<0.002	<0.001	0.254	<0.05	1	1	1	1
6		Cortex	<0.001	<0.001	<0.015	<0.001	0.484	1	1	1
7		Thal	<0.001	<0.001	0.093	<0.015	1	1	1	1
8		Hypo	0.11	0.072	1	0.453	1	1	1	1
9	C	Hippo		1	1	1	0.197	<0.002	<0.05	1
10		Cortex	1		1	1	0.122	<0.001	<0.02	0.906
11		Thal	1	1		1	1	0.313	0.949	1
12		Hypo	1	1	1		0.975	<0.05	0.181	1
13	D	Hippo	0.197	0.122	1	0.975		1	1	1
14		Cortex	<0.002	<0.001	0.313	<0.05	1		1	1
15		Thal	<0.05	<0.02	0.949	0.181	1	1		1
16		Hypo	1	0.906	1	1	1	1	1	

Statistically significant results indicated in black. A: Mock-infected i.c. PPS; B: Mock-infected No i.c. PPS; C: Scrapie-Infected i.c. PPS; D: Scrapie-Infected No i.c. PPS. Hippo: Hippocampus; Thal: Thalamus; Hypo: Hypothalamus.

Table 30. MRI Slice 5 Group x Region Comparison at 47 dpi.										
Group/Region ID			p values							
	Group	Region	1	2	3	4	5	6	7	8
1	A	Hippo		0.998	0.984	1	<0.001	<0.001	<0.001	<0.001
2		Cortex	0.998		1	1	<0.001	<0.001	<0.001	<0.001
3		Thal	0.984	1		1	<0.001	<0.001	<0.001	<0.03
4		Hypo	1	1	1		<0.001	<0.001	<0.001	<0.001
5	B	Hippo	<0.001	<0.001	<0.001	<0.001		0.61	1	0.997
6		Cortex	<0.001	<0.001	<0.001	<0.001	0.61		1	0.111
7		Thal	<0.001	<0.001	<0.001	<0.001	1	1		0.86
8		Hypo	<0.001	<0.001	<0.03	<0.001	0.997	0.111	0.86	
9	C	Hippo	0.144	0.899	1	0.807	<0.001	<0.001	<0.001	0.112
10		Cortex	<0.02	0.447	0.974	0.403	<0.005	<0.001	<0.002	0.495
11		Thal	0.051	0.523	0.954	0.427	0.274	<0.005	0.09	0.959
12		Hypo	0.792	1	1	0.993	<0.002	<0.001	<0.001	0.161
13	D	Hippo	<0.001	<0.001	0.13	<0.005	0.239	<0.001	0.074	1
14		Cortex	<0.001	<0.001	<0.001	<0.001	1	0.234	0.99	1
15		Thal	<0.001	<0.001	<0.015	<0.001	1	0.251	0.959	1
16		Hypo	<0.001	<0.015	0.399	<0.03	0.359	<0.001	0.117	0.998
	Group	Region	9	10	11	12	13	14	15	16
1	A	Hippo	0.144	<0.02	0.051	0.792	<0.001	<0.001	<0.001	<0.001
2		Cortex	0.899	0.447	0.523	1	<0.001	<0.001	<0.001	<0.015
3		Thal	1	0.974	0.954	1	0.13	<0.001	<0.015	0.399
4		Hypo	0.807	0.403	0.427	0.993	<0.005	<0.001	<0.001	<0.03
5	B	Hippo	<0.001	<0.005	0.274	<0.002	0.239	1	1	0.359
6		Cortex	<0.001	<0.001	<0.005	<0.001	<0.001	0.234	0.251	<0.001
7		Thal	<0.001	<0.002	0.09	<0.001	0.074	0.99	0.959	0.117
8		Hypo	0.112	0.495	0.959	0.161	1	1	1	0.998
9	C	Hippo		1	1	1	0.414	<0.001	<0.05	0.853
10		Cortex	1		1	1	0.922	<0.025	0.297	0.997
11		Thal	1	1		0.999	1	0.512	0.884	1
12		Hypo	1	1	0.999		0.486	<0.01	0.086	0.807
13	D	Hippo	0.414	0.922	1	0.486		0.617	0.992	1
14		Cortex	<0.001	<0.025	0.512	<0.01	0.617		1	0.688
15		Thal	<0.05	0.297	0.884	0.086	0.992	1		0.984
16		Hypo	0.853	0.997	1	0.807	1	0.688	0.984	

Statistically significant results indicated in black. A: Mock-infected i.c. PPS; B: Mock-infected No i.c. PPS; C: Scrapie-Infected i.c. PPS; D: Scrapie-Infected No i.c. PPS. Hippo: Hippocampus; Thal: Thalamus; Hypo: Hypothalamus.

Table 31. MRI Slice 5 Group x Region Comparison at 61 dpi.										
Group/Region ID			p values							
	Group	Region	1	2	3	4	5	6	7	8
1	A	Hippo		0.997	0.998	1	<0.001	<0.001	<0.001	<0.03
2		Cortex	0.997		1	1	<0.05	<0.001	<0.05	0.57
3		Thal	0.998	1		1	0.471	0.056	0.379	0.942
4		Hypo	1	1	1		<0.05	<0.001	<0.03	0.329
5	B	Hippo	<0.001	<0.05	0.471	<0.05		0.991	1	1
6		Cortex	<0.001	<0.001	0.056	<0.001	0.991		1	0.854
7		Thal	<0.001	<0.05	0.379	<0.03	1	1		0.999
8		Hypo	<0.03	0.57	0.942	0.329	1	0.854	0.999	
9	C	Hippo	0.995	1	1	1	<0.05	<0.001	0.053	0.627
10		Cortex	0.619	1	1	0.964	0.61	<0.05	0.525	0.995
11		Thal	0.941	1	1	0.997	0.842	0.235	0.737	0.998
12		Hypo	1	1	1	1	0.136	<0.01	0.111	0.66
13	D	Hippo	0.444	0.999	1	0.951	0.171	<0.002	0.199	0.96
14		Cortex	<0.015	0.58	0.971	0.353	0.988	0.241	0.956	1
15		Thal	0.064	0.77	0.984	0.49	0.999	0.647	0.992	1
16		Hypo	0.675	1	1	0.974	0.544	<0.05	0.468	0.992
	Group	Region	9	10	11	12	13	14	15	16
1	A	Hippo	0.995	0.619	0.941	1	0.444	<0.015	0.064	0.675
2		Cortex	1	1	1	1	0.999	0.58	0.77	1
3		Thal	1	1	1	1	1	0.971	0.984	1
4		Hypo	1	0.964	0.997	1	0.951	0.353	0.49	0.974
5	B	Hippo	<0.05	0.61	0.842	0.136	0.171	0.988	0.999	0.544
6		Cortex	<0.001	<0.05	0.235	<0.01	<0.002	0.241	0.647	<0.05
7		Thal	0.053	0.525	0.737	0.111	0.199	0.956	0.992	0.468
8		Hypo	0.627	0.995	0.998	0.66	0.96	1	1	0.992
9	C	Hippo		1	1	1	1	0.645	0.816	1
10		Cortex	1		1	0.999	1	0.999	1	1
11		Thal	1	1		1	1	1	1	1
12		Hypo	1	0.999	1		0.998	0.717	0.812	0.999
13	D	Hippo	1	1	1	0.998		0.976	0.995	1
14		Cortex	0.645	0.999	1	0.717	0.976		1	0.998
15		Thal	0.816	1	1	0.812	0.995	1		0.999
16		Hypo	1	1	1	0.999	1	0.998	0.999	

Statistically significant results indicated in black. A: Mock-infected i.c. PPS; B: Mock-infected No i.c. PPS; C: Scrapie-Infected i.c. PPS; D: Scrapie-Infected No i.c. PPS. Hippo: Hippocampus; Thal: Thalamus; Hypo: Hypothalamus.

Table 32. MRI Slice 5 Group x Region Comparison at 75 dpi.										
Group/Region ID			p values							
	Group	Region	1	2	3	4	5	6	7	8
1	A	Hippo		1	1	1	<0.001	<0.001	<0.001	<0.005
2		Cortex	1		1	1	<0.001	<0.001	<0.001	<0.05
3		Thal	1	1		1	<0.05	<0.001	<0.03	0.644
4		Hypo	1	1	1		<0.005	<0.001	<0.002	0.074
5	B	Hippo	<0.001	<0.001	<0.05	<0.005		1	1	1
6		Cortex	<0.001	<0.001	<0.001	<0.001	1		1	1
7		Thal	<0.001	<0.001	<0.03	<0.002	1	1		1
8		Hypo	<0.005	<0.05	0.644	0.074	1	1	1	
9	C	Hippo	1	1	1	1	1	<0.03	0.759	1
10		Cortex	<0.01	<0.05	0.802	0.096	1	1	1	1
11		Thal	0.537	1	1	1	1	1	1	1
12		Hypo	1	1	1	1	1	0.363	1	1
13	D	Hippo	1	1	1	1	<0.03	<0.001	<0.03	1
14		Cortex	0.156	0.968	1	1	0.936	<0.005	0.538	1
15		Thal	1	1	1	1	0.968	<0.015	0.486	1
16		Hypo	1	1	1	1	0.057	<0.001	<0.05	1
	Group	Region	9	10	11	12	13	14	15	16
1	A	Hippo	1	.01	0.537	1	1	0.156	1	1
2		Cortex	1	<0.05	1	1	1	0.968	1	1
3		Thal	1	0.802	1	1	1	1	1	1
4		Hypo	1	0.096	1	1	1	1	1	1
5	B	Hippo	1	1	1	1	<0.03	0.936	0.968	0.057
6		Cortex	<0.03	1	1	0.363	<0.001	<0.005	<0.015	<0.001
7		Thal	0.759	1	1	1	<0.03	0.538	0.486	<0.05
8		Hypo	1	1	1	1	1	1	1	1
9	C	Hippo		1	1	1	1	1	1	1
10		Cortex	1		1	1	1	1	1	1
11		Thal	1	1		1	1	1	1	1
12		Hypo	1	1	1		1	1	1	1
13	D	Hippo	1	1	1	1		1	1	1
14		Cortex	1	1	1	1	1		1	1
15		Thal	1	1	1	1	1	1		1
16		Hypo	1	1	1	1	1	1	1	

Statistically significant results indicated in black. A: Mock-infected i.c. PPS; B: Mock-infected No i.c. PPS; C: Scrapie-Infected i.c. PPS; D: Scrapie-Infected No i.c. PPS. Hippo: Hippocampus; Thal: Thalamus; Hypo: Hypothalamus.

Table 33. MRI Slice 5 Group x Region Comparison at 89 dpi.										
Group/Region ID			p values							
	Group	Region	1	2	3	4	5	6	7	8
1	A	Hippo		1	1	1	<0.001	<0.001	<0.001	<0.05
2		Cortex	1		1	1	<0.005	<0.001	<0.002	0.295
3		Thal	1	1		1	0.401	<0.015	0.122	1
4		Hypo	1	1	1		<0.03	<0.001	<0.01	0.52
5	B	Hippo	<0.001	<0.005	0.401	<0.03		1	1	1
6		Cortex	<0.001	<0.001	<0.015	<0.001	1		1	1
7		Thal	<0.001	<0.002	0.122	<0.01	1	1		1
8		Hypo	<0.05	0.295	1	0.52	1	1	1	
9	C	Hippo	0.171	0.967	1	1	1	1	1	1
10		Cortex	<0.01	<0.05	1	0.118	1	1	1	1
11		Thal	0.968	1	1	1	1	1	1	1
12		Hypo	1	1	1	1	1	1	1	1
13	D	Hippo	0.055	0.327	1	0.47	1	1	1	1
14		Cortex	<0.001	<0.001	<0.05	<0.002	1	1	1	1
15		Thal	0.107	0.416	1	0.435	1	1	1	1
16		Hypo	1	1	1	1	1	1	1	1
	Group	Region	9	10	11	12	13	14	15	16
1	A	Hippo	0.171	<0.01	0.968	1	0.055	<0.001	0.107	1
2		Cortex	0.967	<0.05	1	1	0.327	<0.001	0.416	1
3		Thal	1	1	1	1	1	<0.05	1	1
4		Hypo	1	0.118	1	1	0.47	<0.002	0.435	1
5	B	Hippo	1	1	1	1	1	1	1	1
6		Cortex	1	1	1	1	1	1	1	1
7		Thal	1	1	1	1	1	1	1	1
8		Hypo	1	1	1	1	1	1	1	1
9	C	Hippo		1	1	1	1	1	1	1
10		Cortex	1		1	1	1	1	1	1
11		Thal	1	1		1	1	1	1	1
12		Hypo	1	1	1		1	1	1	1
13	D	Hippo	1	1	1	1		1	1	1
14		Cortex	1	1	1	1	1		1	1
15		Thal	1	1	1	1	1	1		1
16		Hypo	1	1	1	1	1	1	1	

Statistically significant results indicated in black. A: Mock-infected i.c. PPS; B: Mock-infected No i.c. PPS; C: Scrapie-Infected i.c. PPS; D: Scrapie-Infected No i.c. PPS. Hippo: Hippocampus; Thal: Thalamus; Hypo: Hypothalamus.

Table 34. MRI Slice 5 Group x Region Comparison at 103 dpi.								
Group/Region ID			p values					
	Group	Region	1	2	3	4	5	6
1	A	Hippo		0.995	0.975	1	<0.001	<0.001
2		Cortex	0.995		1	0.999	<0.005	<0.001
3		Thal	0.975	1		0.994	0.242	<0.025
4		Hypo	1	0.999	0.994		<0.005	<0.001
5	B	Hippo	<0.001	<0.005	0.242	<0.005		0.952
6		Cortex	<0.001	<0.001	<0.025	<0.001	0.952	
7		Thal	<0.001	<0.001	0.054	<0.001	0.987	1
8		Hypo	<0.001	<0.03	0.365	<0.015	1	0.991
9	C	Hippo	<0.001	<0.001	<0.005	<0.001	0.209	0.694
10		Cortex	<0.001	<0.001	<0.001	<0.001	<0.05	0.255
11		Thal	<0.002	<0.015	0.053	<0.005	0.685	0.951
12		Hypo	<0.01	0.051	0.174	<0.025	0.94	0.999
	Group	Region	7	8	9	10	11	12
1	A	Hippo	<0.001	<0.001	<0.001	<0.001	<0.002	<0.01
2		Cortex	<0.001	<0.03	<0.001	<0.001	<0.015	0.051
3		Thal	0.053	0.365	<0.005	<0.001	0.053	0.174
4		Hypo	<0.001	<0.015	<0.001	<0.001	<0.005	<0.025
5	B	Hippo	0.987	1	0.209	<0.05	0.685	0.94
6		Cortex	1	0.991	0.694	0.255	0.951	0.999
7		Thal		0.997	0.787	0.364	0.965	0.999
8		Hypo	0.997		0.306	0.073	0.739	0.956
9	C	Hippo	0.787	0.306		1	1	1
10		Cortex	0.364	0.073	1		1	0.999
11		Thal	0.965	0.739	1	1		1
12		Hypo	0.999	0.956	1	0.999	1	

Statistically significant results indicated in black. A: Mock-infected i.c. PPS; B: Mock-infected No i.c. PPS; C: Scrapie-Infected i.c. PPS. Hippo: Hippocampus; Thal: Thalamus; Hypo: Hypothalamus.

Table 35. MRI Slice 5 Group x Region Comparison at 117 dpi.								
Group/Region ID			p values					
	Group	Region	1	2	3	4	5	6
1	A	Hippo		1	0.882	1	<0.001	<0.001
2		Cortex	1		0.997	1	<0.001	<0.001
3		Thal	0.882	0.997		0.945	<0.05	<0.002
4		Hypo	1	1	0.94		<0.001	<0.001
5	B	Hippo	<0.001	<0.001	<0.05	<0.001		0.887
6		Cortex	<0.001	<0.001	<0.002	<0.001	0.887	
7		Thal	<0.001	<0.001	<0.002	<0.001	0.714	1
8		Hypo	<0.001	<0.001	0.075	<0.001	1	0.985
9	C	Hippo	<0.001	<0.001	<0.001	<0.001	0.188	0.735
10		Cortex	<0.001	<0.001	<0.001	<0.001	<0.01	0.082
11		Thal	<0.001	<0.001	<0.015	<0.001	0.659	0.961
12		Hypo	<0.001	<0.002	<0.03	<0.001	0.815	0.991
	Group	Region	7	8	9	10	11	12
1	A	Hippo	<0.001	<0.001	<0.001	<0.001	<0.001	<0.001
2		Cortex	<0.001	<0.001	<0.001	<0.001	<0.001	<0.002
3		Thal	<0.002	0.075	<0.001	<0.001	<0.015	<0.03
4		Hypo	<0.001	<0.001	<0.001	<0.001	<0.001	<0.001
5	B	Hippo	0.714	1	0.188	<0.01	0.659	0.815
6		Cortex	1	0.985	0.735	0.082	0.961	0.991
7		Thal		0.903	0.955	0.307	0.996	1
8		Hypo	0.903		0.313	<0.02	0.743	0.873
9	C	Hippo	0.955	0.313		0.999	1	1
10		Cortex	0.307	<0.02	0.999		1	1
11		Thal	0.996	0.743	1	1		1
12		Hypo	1	0.873	1	0.998	1	

Statistically significant results indicated in black. A: Mock-infected i.c. PPS; B: Mock-infected No i.c. PPS; C: Scrapie-Infected i.c. PPS. Hippo: Hippocampus; Thal: Thalamus; Hypo: Hypothalamus.

Table 36. MRI Slice 7 Group x Region Comparison at 19 dpi.								
Group/Region ID			p values					
	Group	Region	1	2	3	4	5	6
1	A	Ventricles		0.921	0.973	0.234	<0.05	0.068
2		Cortex	0.921		1	1	0.983	0.978
3		Septum	0.973	1		1	0.999	0.999
4	B	Ventricles	0.234	1	1		0.998	0.997
5		Cortex	<0.05	0.983	0.999	0.998		1
6		Septum	0.068	0.978	0.999	0.997	1	
7	C	Ventricles	0.998	1	1	0.956	0.67	0.683
8		Cortex	0.167	0.984	0.998	0.999	1	1
9		Septum	0.56	0.999	1	1	1	1
10	D	Ventricles	<0.005	0.635	0.951	0.411	0.969	0.999
11		Cortex	<0.001	<0.05	0.408	<0.001	<0.025	0.249
12		Septum	<0.001	0.127	0.571	<0.025	0.25	0.622
			7	8	9	10	11	12
1	A	Ventricles	0.998	0.167	0.56	<0.005	<0.001	<0.001
2		Cortex	1	0.984	0.999	0.635	<0.05	0.127
3		Septum	1	0.998	1	0.951	0.408	0.571
4	B	Ventricles	0.956	0.999	1	0.411	<0.001	<0.025
5		Cortex	0.67	1	1	0.969	<0.025	0.25
6		Septum	0.683	1	1	0.999	0.2	0.622
7	C	Ventricles		0.786	0.965	0.159	<0.005	<0.015
8		Cortex	0.786		1	1	0.858	0.957
9		Septum	0.965	1		1	0.96	0.986
10	D	Ventricles	0.159	1	1		0.551	0.927
11		Cortex	<0.005	0.858	0.96	0.551		1
12		Septum	<0.015	0.957	0.986	0.927	1	

Statistically significant results indicated in black. A: Mock-infected i.c. PPS; B: Mock-infected No i.c. PPS; C: Scrapie-Infected i.c. PPS; D: Scrapie-Infected No i.c. PPS.

Table 37. MRI Slice 7 Group x Region Comparison at 33 dpi.								
Group/Region ID			p values					
	Group	Region	1	2	3	4	5	6
1	A	Ventricles		1	1	<0.001	<0.001	<0.001
2		Cortex	1		1	<0.015	<0.001	<0.001
3		Septum	1	1		0.185	<0.002	<0.02
4	B	Ventricles	<0.001	<0.015	0.185		1	1
5		Cortex	<0.001	<0.001	<0.002	1		1
6		Septum	<0.001	<0.001	<0.02	1	1	
7	C	Ventricles	1	1	1	<0.001	<0.001	<0.001
8		Cortex	1	1	1	0.088	<0.001	<0.01
9		Septum	1	1	1	1	<0.025	0.167
10	D	Ventricles	0.297	1	1	1	<0.005	0.24
11		Cortex	<0.001	<0.01	0.142	1	1	1
12		Septum	<0.015	0.127	0.57	1	1	1
			7	8	9	10	11	12
1	A	Ventricles	1	1	1	0.297	<0.001	<0.015
2		Cortex	1	1	1	1	<0.01	0.127
3		Septum	1	1	1	1	0.142	0.57
4	B	Ventricles	<0.001	0.088	1	1	1	1
5		Cortex	<0.001	<0.001	<0.025	<0.005	1	1
6		Septum	<0.001	<0.01	0.167	0.24	1	1
7	C	Ventricles		1	1	0.187	<0.001	<0.01
8		Cortex	1		1	1	0.062	0.528
9		Septum	1	1		1	1	1
10	D	Ventricles	0.187	1	1		1	1
11		Cortex	<0.001	0.062	1	1		1
12		Septum	<0.01	0.528	1	1	1	

Statistically significant results indicated in black. A: Mock-infected i.c. PPS; B: Mock-infected No i.c. PPS; C: Scrapie-Infected i.c. PPS; D: Scrapie-Infected No i.c. PPS.

Table 38. MRI Slice 7 Group x Region Comparison at 47 dpi.								
Group/Region ID			p values					
	Group	Region	1	2	3	4	5	6
1	A	Ventricles		0.256	0.547	<0.001	<0.001	<0.001
2		Cortex	0.256		1	<0.001	<0.001	<0.001
3		Septum	0.547	1		<0.015	<0.001	<0.005
4	B	Ventricles	<0.001	<0.001	<0.015		0.596	0.999
5		Cortex	<0.001	<0.001	<0.001	0.596		1
6		Septum	<0.001	<0.001	<0.005	0.999	1	
7	C	Ventricles	0.426	1	1	<0.001	<0.001	<0.001
8		Cortex	<0.001	0.644	0.892	0.378	<0.002	0.136
9		Septum	<0.01	0.877	0.96	0.759	0.052	0.415
10	D	Ventricles	<0.001	0.281	0.719	0.208	<0.001	0.07
11		Cortex	<0.001	<0.001	<0.001	0.92	1	1
12		Septum	<0.001	<0.001	<0.01	1	0.989	1
			7	8	9	10	11	12
1	A	Ventricles	0.426	<0.001	<0.01	<0.001	<0.001	<0.001
2		Cortex	1	0.644	0.877	0.281	<0.001	<0.001
3		Septum	1	0.892	0.96	0.719	<0.001	<0.01
4	B	Ventricles	<0.001	0.378	0.759	0.208	0.92	1
5		Cortex	<0.001	<0.002	0.052	<0.001	1	0.989
6		Septum	<0.001	0.136	0.415	0.07	1	1
7	C	Ventricles		0.446	0.757	0.137	<0.001	<0.001
8		Cortex	0.446		1	1	<0.015	0.291
9		Septum	0.757	1		1	0.143	0.611
10	D	Ventricles	0.137	1	1		<0.002	0.191
11		Cortex	<0.001	<0.015	0.143	<0.002		1
12		Septum	<0.001	0.291	0.611	0.191	1	

Statistically significant results indicated in black. A: Mock-infected i.c. PPS; B: Mock-infected No i.c. PPS; C: Scrapie-Infected i.c. PPS; D: Scrapie-Infected No i.c. PPS.

Table 39. MRI Slice 7 Group x Region Comparison at 61 dpi.								
Group/Region ID			p values					
	Group	Region	1	2	3	4	5	6
1	A	Ventricles		1	1	<0.001	<0.001	<0.001
2		Cortex	1		1	<0.025	<0.001	0.051
3		Septum	1	1		0.325	<0.05	0.363
4	B	Ventricles	<0.001	<0.025	0.325		1	1
5		Cortex	<0.001	<0.001	<0.05	1		1
6		Septum	<0.001	0.051	0.363	1	1	
7	C	Ventricles	1	1	1	0.053	<0.005	0.105
8		Cortex	0.273	1	1	1	0.156	1
9		Septum	1	1	1	1	0.936	1
10	D	Ventricles	1	1	1	<0.005	<0.001	<0.025
11		Cortex	<0.001	0.98	1	1	1	1
12		Septum	<0.025	1	1	1	1	1
			7	8	9	10	11	12
1	A	Ventricles	1	0.273	1	1	<0.001	<0.025
2		Cortex	1	1	1	1	0.98	1
3		Septum	1	1	1	1	1	1
4	B	Ventricles	0.053	1	1	<0.005	1	1
5		Cortex	<0.005	0.156	0.936	<0.001	1	1
6		Septum	0.105	1	1	<0.025	1	1
7	C	Ventricles		1	1	1	1	1
8		Cortex	1		1	1	1	1
9		Septum	1	1		1	1	1
10	D	Ventricles	1	1	1		0.644	1
11		Cortex	1	1	1	0.644		1
12		Septum	1	1	1	1	1	

Statistically significant results indicated in black. A: Mock-infected i.c. PPS; B: Mock-infected No i.c. PPS; C: Scrapie-Infected i.c. PPS; D: Scrapie-Infected No i.c. PPS.

Table 40. MRI Slice 7 Group x Region Comparison at 75 dpi.								
Group/Region ID			p values					
	Group	Region	1	2	3	4	5	6
1	A	Ventricles		1	1	<0.001	<0.001	<0.001
2		Cortex	1		1	<0.005	<0.001	<0.001
3		Septum	1	1		0.32	<0.005	0.051
4	B	Ventricles	<0.001	<0.005	0.32		1	1
5		Cortex	<0.001	<0.001	<0.005	1		1
6		Septum	<0.001	<0.001	0.051	1	1	
7	C	Ventricles	1	1	1	0.176	<0.001	<0.025
8		Cortex	<0.002	0.133	1	1	1	1
9		Septum	0.076	1	1	1	1	1
10	D	Ventricles	1	1	1	<0.02	<0.001	<0.005
11		Cortex	<0.002	0.188	1	1	0.11	1
12		Septum	<0.02	0.76	1	1	0.559	1
			7	8	9	10	11	12
1	A	Ventricles	1	<0.002	0.076	1	<0.002	<0.02
2		Cortex	1	0.133	1	1	0.188	0.76
3		Septum	1	1	1	1	1	1
4	B	Ventricles	0.176	1	1	<0.02	1	1
5		Cortex	<0.001	1	1	<0.001	0.11	0.559
6		Septum	<0.025	1	1	<0.005	1	1
7	C	Ventricles		1	1	1	1	1
8		Cortex	1		1	0.613	1	1
9		Septum	1	1		1	1	1
10	D	Ventricles	1	0.613	1		0.883	1
11		Cortex	1	1	1	0.883		1
12		Septum	1	1	1	1	1	

Statistically significant results indicated in black. A: Mock-infected i.c. PPS; B: Mock-infected No i.c. PPS; C: Scrapie-Infected i.c. PPS; D: Scrapie-Infected No i.c. PPS.

Table 41. MRI Slice 7 Group x Region Comparison at 89 dpi.								
Group/Region ID			p values					
	Group	Region	1	2	3	4	5	6
1	A	Ventricles		1	1	<0.001	<0.001	<0.001
2		Cortex	1		1	<0.002	<0.001	<0.001
3		Septum	1	1		0.119	<0.005	<0.02
4	B	Ventricles	<0.001	<0.002	0.119		1	1
5		Cortex	<0.001	<0.001	<0.005	1		1
6		Septum	<0.001	<0.001	<0.02	1	1	
7	C	Ventricles	0.31	1	1	1	0.121	0.613
8		Cortex	<0.001	<0.02	0.274	1	1	1
9		Septum	<0.025	0.371	1	1	1	1
10	D	Ventricles	1	1	1	0.929	<0.025	0.145
11		Cortex	<0.002	0.078	0.598	1	1	1
12		Septum	0.072	0.79	1	1	1	1
			7	8	9	10	11	12
1	A	Ventricles	0.31	<0.001	<0.025	1	<0.002	0.072
2		Cortex	1	<0.02	0.371	1	0.078	0.79
3		Septum	1	0.274	1	1	0.598	1
4	B	Ventricles	1	1	1	0.929	1	1
5		Cortex	0.121	1	1	<0.025	1	1
6		Septum	0.613	1	1	0.145	1	1
7	C	Ventricles		1	1	1	1	1
8		Cortex	1		1	1	1	1
9		Septum	1	1		1	1	1
10	D	Ventricles	1	1	1		1	1
11		Cortex	1	1	1	1		1
12		Septum	1	1	1	1	1	

Statistically significant results indicated in black. A: Mock-infected i.c. PPS; B: Mock-infected No i.c. PPS; C: Scrapie-Infected i.c. PPS; D: Scrapie-Infected No i.c. PPS.

Table 42. MRI Slice 7 Group x Region Comparison at 103 dpi.							
Group/Region ID			p values				
	Group	Region	1	2	3	4	5
1	A	Ventricles		0.776	0.916	<0.01	<0.001
2		Cortex	0.776		1	0.591	<0.001
3		Septum	0.916	1		0.851	<0.025
4	B	Ventricles	<0.01	0.591	0.851		0.068
5		Cortex	<0.001	<0.001	<0.025	0.068	
6		Septum	<0.001	<0.02	0.109	0.466	1
7	C	Ventricles	<0.001	<0.001	<0.002	<0.005	0.335
8		Cortex	<0.001	<0.001	<0.001	<0.001	<0.001
9		Septum	<0.001	<0.001	<0.002	<0.01	0.171
			6	7	8	9	
1	A	Ventricles	<0.001	<0.001	<0.001	<0.001	
2		Cortex	<0.02	<0.001	<0.001	<0.001	
3		Septum	0.109	<0.002	<0.001	<0.002	
4	B	Ventricles	0.466	<0.005	<0.001	<0.01	
5		Cortex	1	0.335	<0.001	0.171	
6		Septum		0.29	<0.001	0.144	
7	C	Ventricles	0.29		0.738	0.996	
8		Cortex	<0.001	0.738		1	
9		Septum	0.144	0.996	1		

Statistically significant results indicated in black. A: Mock-infected i.c. PPS; B: Mock-infected No i.c. PPS; C: Scrapie-Infected i.c. PPS.

Table 43. MRI Slice 7 Group x Region Comparison at 117 dpi.								
Group/Region ID			p values					
	Group	Region	1	2	3	4	5	
1	A	Ventricles		<0.001	<0.001	<0.001	<0.001	
2		Cortex	<0.001		1	0.988	<0.002	
3		Septum	<0.001	1		1	0.119	
4	B	Ventricles	<0.001	0.988	1		<0.005	
5		Cortex	<0.001	<0.002	0.119	<0.005		
6		Septum	<0.001	<0.015	0.24	<0.05	1	
7	C	Ventricles	<0.001	0.441	0.834	0.761	1	
8		Cortex	<0.001	<0.005	0.055	<0.015	0.909	
9		Septum	<0.001	<0.05	0.172	0.117	0.953	
			6	7	8	9		
1	A	Ventricles	<0.001	<0.001	<0.001	<0.001		
2		Cortex	<0.015	0.441	<0.005	<0.05		
3		Septum	0.24	0.834	0.055	0.172		
4	B	Ventricles	<0.05	0.761	<0.015	0.117		
5		Cortex	1	1	0.909	0.953		
6		Septum		1	0.917	0.952		
7	C	Ventricles	1		0.868	0.905		
8		Cortex	0.917	0.868		1		
9		Septum	0.952	0.905	1			

Statistically significant results indicated in black. A: Mock-infected i.c. PPS; B: Mock-infected No i.c. PPS; C: Scrapie-Infected i.c. PPS.

Table 44. MRI Slice 7 Group x Region Comparison at 131 dpi.								
Group/Region ID			p values					
	Group	Region	1	2	3	4	5	6
1	A	Ventricles		<0.001	<0.002	0.334	<0.001	<0.001
2		Cortex	<0.001		1	<0.01	1	1
3		Septum	<0.002	1		<0.05	1	1
4	B	Ventricles	0.334	<0.01	<0.05		<0.001	<0.01
5		Cortex	<0.001	1	1	<0.001		1
6		Septum	<0.001	1	1	<0.01	1	

Statistically significant results indicated in black. A: Mock-infected i.c. PPS; B: Mock-infected No i.c. PPS.

Appendix 3 – Certificate of Permission to Use Copyrighted Material

Appendix 4 – Certificate of Analysis of Pentosan Polysulphate

Appendix 5 – Full Size Images of Hamster Histology

The enclosed CD contains un-cropped, full size, un-cropped, images corresponding to those that may be found in Figure 16. The images were collected as described in the Materials and Methods section, with Leica FireCam 1.2.0 software and a Leica DMLD light microscope fitted with a DFC digital camera. The resulting TIF files may be viewed with any image viewing software. These images are only examples of the images that were evaluated; in each region of interest in each hamster, a number of images were collected and evaluated. The naming system of the files is self-explanatory. Briefly, files are named according to control or scrapie-infected hamster; then brain region; and finally staining (either H and E, for Haematoxylin and Eosin; GFAP for evaluation of gliosis; or PrP, for evaluation of PrP^{Sc} deposition). The following is a complete list of image files on the CD:

- Control Cortex GFAP
- Control Cortex H and E
- Control Cortex PrP
- Control Hippocampus GFAP
- Control Hippocampus H and E
- Control Hippocampus PrP
- Control Hypothalamus GFAP
- Control Hypothalamus H and E
- Control Hypothalamus PrP
- Control Thalamus GFAP
- Control Thalamus H and E

- Control Thalamus PrP
- Scrapie Cortex GFAP
- Scrapie Cortex H and E
- Scrapie Cortex PrP
- Scrapie Hippocampus GFAP
- Scrapie Hippocampus H and E
- Scrapie Hippocampus PrP
- Scrapie Hypothalamus GFAP
- Scrapie Hypothalamus H and E
- Scrapie Hypothalamus PrP
- Scrapie Thalamus GFAP
- Scrapie Thalamus H and E
- Scrapie Thalamus PrP